Phase Diagram and Phase Transformations in Ti-Al-Si System* .

Cesar R. de Farias Azevedo - BSc(Eng), MEng
Department of Materials,
Imperial College of Science, Technology and Medicine.

February, 1996.

---

* A thesis submitted for the degree of Doctor of Philosophy of the University of London and the Diploma of Membership of the Imperial College.

to my parents

"YOU RUN ON AHEAD?
DO YOU DO SO AS A HERDSMAN OR AS AN EXCEPTION?
A THIRD POSSIBILITY WOULD BE AS A DESERTER...
FIRST QUESTION OF CONSCIENCE."

F. NIETZSCHE
(TWILIGHT OF THE IDOLS)

• Abstract

Phase Diagram and Phase Transformations in Ti-Al-Si System

The phase equilibria between titanium, Ti-β(bcc) and Ti-α(hcp), titanium aluminide, Ti_3Al-α2(hcp), and titanium silicide, Ti_5Si_3(hcp), have been investigated in the temperature range of 973 to 1473K. The ternary titanium alloys containing 14 to 22at% aluminium and 1 to 3.5at% silicon, and additional quaternary alloys containing 1at% niobium or zirconium were produced by arc melting. The as-cast samples were then homogenised at 1573K, quenched and isothermally heat treated at temperatures between 973 and 1373K. The as-cast, as-quenched and isothermally heat treated microstructures have been characterised by light and analytical electron microscopy, and X-ray diffractometry. The effect of alloying elements on the morphology of allotropic transformation, Ti-β(bcc)->Ti-α(hcp), was studied using the quenched samples. The morphologies observed have been correlated with the possible types of reaction for the allotropic decomposition of Ti-β(bcc) phase. Quantitative chemical analyses of the phases identified in the isothermally heat treated samples were carried out by analytical electron microscopy equipped with X-ray energy dispersive analysis (EDX). The experimental results for the ternary system were then used for the thermodynamic modelling of the Ti-rich corner of the Ti-Al-Si phase diagram. The sublattice model was used to describe mathematically the phases under investigation. Finally, a calculated version of a portion of the ternary phase diagram has been proposed.

• List of Tables

• List of Figures

Chapter 4

Chapter 1

Introduction

Silicon is an important alloying element for developing creep resistance near–α alloys which have been progressively developed over the past thirty years. Alloys such as the British IMI 685, 829 and, most recently, 834 have been developed and have increased the maximum temperature of service in gas turbine engines to about 600°C. Most recently alloys based on the aluminides Ti_3Al and TiAl have been the subject of intense development effort in the hope of further increasing the service temperature to between 700 and 900°C. Silicon is again viewed as important in the Ti_3Al based alloys for improving creep resistance and in TiAl for enhancing oxidation resistance. Furthermore, in the development of titanium based metal matrix composites containing SiC fibres the reaction between matrix and fibres to produce titanium silicides is of considerable concern because of the deleterious effect of the reaction.

In all these cases the constitution of titanium alloy–silicon systems is of central importance but has not been systematically studied. In the present work the Ti-rich corner of the ternary Al–Si-Ti system is examined over the composition range of interest for the development of near–α and aluminide alloys.

Chapter 2
Literature Review

2.1. General aspects of titanium and titanium alloys

Titanium is the fourth most abundant metal on earth and the prevalent processes for the production of titanium sponge is the reduction of titanium tetrachloride by magnesium or sodium (Kroll and Hunter processes). The energy requirement for the production of the primary titanium is rather high when compared to steel (approximately 15 times) or aluminium (approximately twice), but there is considerable room for to improve the energy efficiency of the refinement process [JAF 80].

The proportionate share of titanium usage in the military aerospace industry fell from 94% in 1955 to 13% in 1992 [JAF 80][PEA 95b]. In contrast to this fall, the non-aerospace sector grew to approximately 42% of the world market in 1992 [PEA 95b]. Efforts are still being made to develop new large non-aerospace markets to overcome a serious overcapacity worldwide in the titanium industry, caused by the shrinkage of both military and commercial aerospace markets [PEA 95]. There is still growing use of Ti alloys in the oil and gas industry, petrochemicals, power generations, civil engineering & building construction [NUR 95] and even the automotive market is considered to be a strong candidate [BAN 93]. For instance, temperature resistant materials dictate breakthroughs in the thermal efficiency of power generation industry by allowing an increase of the firing temperature of gas turbines (~1500°C) and compressors (~500°C), so that titanium alloys might be found useful for parts exposed up to 600°C [GIL 95][PET 95]. The search for alternative markets is, however, not new. Potentially large markets have been pursued for decades but only with limited success and one possible explanation for this scenario is the attempt to fit expensive aerospace alloys into non-aerospace applications, where cost is by far the number one obstacle. Development of low cost alloys would stand a better chance of opening such a large new market for titanium [PEA 95]. The same approach should be applied to develop cost-effective processing of Ti alloys and casting technology might be a route to be considered. Casting products might replace, with advantages, forged and machined parts (hot isostatic pressing is said to make castings technically competitive with forgings but 40% cheaper) [NUR 95][PET 95]. Furthermore, Ti castings of valve and pump components for chemical plants have been reported elsewhere [NUR 95][PET 95].

Chapter 2
Literature Review

2.1. General aspects of titanium and titanium alloys

Titanium is the fourth most abundant metal on earth and the prevalent processes for the production of titanium sponge is the reduction of titanium tetrachloride by magnesium or sodium (Kroll and Hunter processes). The energy requirement for the production of the primary titanium is rather high when compared to steel (approximately 15 times) or aluminium (approximately twice), but there is considerable room for to improve the energy efficiency of the refinement process [JAF 80].

The proportionate share of titanium usage in the military aerospace industry fell from 94% in 1955 to 13% in 1992 [JAF 80][PEA 95b]. In contrast to this fall, the non-aerospace sector grew to approximately 42% of the world market in 1992 [PEA 95b]. Efforts are still being made to develop new large non-aerospace markets to overcome a serious overcapacity worldwide in the titanium industry, caused by the shrinkage of both military and commercial aerospace markets [PEA 95]. There is still growing use of Ti alloys in the oil and gas industry, petrochemicals, power generations, civil engineering & building construction [NUR 95] and even the automotive market is considered to be a strong candidate [BAN 93]. For instance, temperature resistant materials dictate breakthroughs in the thermal efficiency of power generation industry by allowing an increase of the firing temperature of gas turbines (~1500°C) and compressors (~500°C), so that titanium alloys might be found useful for parts exposed up to 600°C [GIL 95][PET 95]. The search for alternative markets is, however, not new. Potentially large markets have been pursued for decades but only with limited success and one possible explanation for this scenario is the attempt to fit expensive aerospace alloys into non-aerospace applications, where cost is by far the number one obstacle. Development of low cost alloys would stand a better chance of opening such a large new market for titanium [PEA 95]. The same approach should be applied to develop cost-effective processing of Ti alloys and casting technology might be a route to be considered. Casting products might replace, with advantages, forged and machined parts (hot isostatic pressing is said to make castings technically competitive with forgings but 40% cheaper) [NUR 95][PET 95]. Furthermore, Ti castings of valve and pump components for chemical plants have been reported elsewhere [NUR 95][PET 95].

The principal virtues of Ti and its alloys are high strength/weight ratio, good corrosion resistance, high service temperature and non-toxicity (body implant market) [NUR 95]. Pure titanium has a high melting point (1660°C), low density (4.5 g/cm^3) and undergoes an allotropic transformation at 882.5°C: Ti-α(hcp) <=> Ti-β (bcc). Titanium is a transitional metal with an electronic structure represented as $3d^2\ 4s^2$. This structure enables Ti to form solid solutions and compounds with metallic, covalent and ionic chemical bonds, depending on the similarity or difference of the atomic radii and the electronic structure of the alloying elements [KOR 70]. This wide range of chemical bonds causes the alloying elements to affect Ti differently: Elements like Al, O, N, C and Ga tend to stabilise the α phase; the β stabilisers are generally the transition metals, which can be further divided into β isomorphous elements (V, Zr, Hf, Re, Nb and Ta) and β eutectoid elements (W, Cr, Mn, Fe, Co, Ni and Cu). Figure 2.1.1 shows five types of systems formed by binary Ti–alloys systems.

Commercial alloys are usually classified in three groups: near α, metastable β, and α+β alloys. α phase (hcp) is less ductile and more difficult to deform than the non close-packed β phase. Additionally the diffusion coefficient of α phase is about two orders of magnitude lower than that of β, favouring creep and oxidation resistance, so that near α alloys are preferred elevated temperature materials. Metastable β alloys can be processed at much lower temperature due to its cubic structure (some can be formed at room temperature). They can be hardened to the overall highest strength levels of Ti alloys and still reveal high toughness. α+β alloys present well balanced mechanical properties. The microstructures of Ti-alloys are usually a result of thermo-mechanical treatments, which might be separated into three steps: deformation, solution heat treatment and ageing. The various microstructures substantially influence mechanical behaviour: equiaxed microstructures have a potential for high strength, ductility, fatigue strength and super plasticity; lamellar microstructures have better creep and fatigue crack growth resistance and reveal higher toughness; while bimodal microstructures, consisting of equiaxed primary α in a lamellar α+β microstructure, show a well balanced set of engineering properties [PET 95]. Although oxidation and hot salt stress corrosion may limit the service temperature of a Ti alloy in some applications, the mechanical limitation is generally imposed by high–temperature creep [COL 84]

There are, however, many more microstructural possibilities for the development of new Ti alloys and they might include the presence of: aluminide phases such as α2 and γ; ordered β2 phase; and second phase precipitation of other intermetallics and or silicides. Titanium aluminide

alloys might push the temperature limit from 600 to 800°C. The operative strengthening mechanisms in more complex alloys include: solid solution; second phase precipitation; short and long–range ordering strengthening. More specific challenges to be overcome for the development of new commercial Ti–aluminide alloys are the room temperature brittleness of TiAl and Ti_3Al; and the poor oxidation resistance of Ti_3Al.

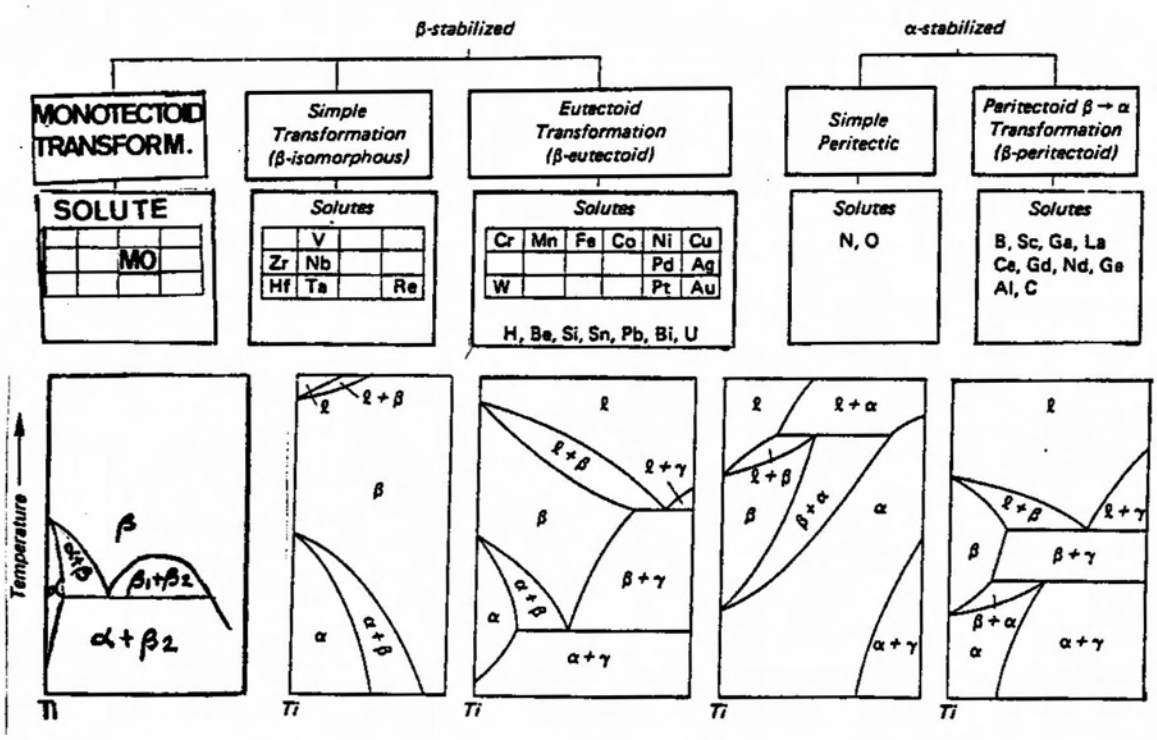

FIGURE 2.1.1. CLASSIFICATION FOR BINARY TI–ALLOY [TER 82][COL 84].

2.2 The Ti-rich corner of the Al-Ti system

More than 40 years on from the pioneering works of H.R.Ogden et al. [OGD 51] and E.S.Bumps et al. [BUMP 52] there are still some uncertainties concerning the nature of the phase relationships in the Al-Ti system. Figure 2.2.1 shows the most recent version of the Al-Ti phase diagram. The phases present are the solution phases: Ti(α)-hcp, Ti(β)-bcc and Al-fcc; the ordered intermetallic phases: Ti_3Al(α2)-hcp, TiAl(γ)-fcc and $TiAl_3$; the stoichiometric phases: $TiAl_2$-fcc and Ti_2Al_5-fcc; and the liquid phase. The invariant equilibria of Ti-rich corner of the Al-Ti system are given in the table 2.2.1.

T(°C)	reaction
~1490	Peritectic: Liquid + β(Ti)–> α(Ti)
~1462	Peritectic: Liquid + α (Ti)–> γ(TiAl)
~1165	Congruent: α (Ti)–> α2(Ti_3Al)
	or
~1200	Peritectoid: β(Ti) + α (Ti)–> α2(Ti_3Al)
~1150	Peritectoid: β(Ti) + α2(Ti_3Al) –> α(Ti)
~1120	Eutectoid: α(Ti) –> α2(Ti_3Al) + γ(TiAl)

Table 2.2.1. Invariant equilibria of the Ti-rich corner of the Al-Ti System [KAT 92].

Ever since the first investigation [OGD 51] there have been numerous attempts to explore the phase equilibria in this system. The existence of the intermetallic ordered phase Ti_3Al, also known as α2, was first observed and confirmed around 1960, and from then on much research has been concentrated on determining the position and extent of the α2 phase field. R.D.Shull et al. [SHU 84] mentioned that the problem, which has remained the same for more than 40 years, has been how to add the ordered phase α2 into Bump's diagram. They listed some of the difficulties faced by investigators to determine the exact position and extent of the α2 phase field: the phase coherency and composition similarity between α and α2 make metallography unreliable; α2 phase sometimes forms during quenching while low temperature equilibrium between α and α2 phases is sometimes difficult to obtain; the ease with which Ti-alloys are contaminated by gases causes large phase boundary shifts, resulting in inaccurate comparisons of results from different investigators.

Oxygen and nitrogen are both α-stabilisers and therefore affect the shape and the position of the phase fields in the Al-Ti system. Contamination by gases can occur during production and heat treatment of

Ti-alloys. The presence of even small amounts of these contaminants may lead: to a broadening of the $\alpha+\beta$ phase field; to a rise of the β-transus; to a reduction of the solubility of aluminium in α phase; and finally to the formation of $\alpha 2$ phase [CRO 69] [ARD 95]. Most of the investigations, up to the revolutionary paper by M.J.Blackburn [BLA 67_b] seem to be the result of suspect or inadequate methods of investigation, which indicated, for instance, the presence of more than one intermetallic phase in the Ti-rich corner of the phase diagram or a miscibility gap within Ti_3Al phase field. Table 2.2.2 presents a historical survey over the papers dealing with the Ti–rich corner of the Ti–Al phase diagram prior 1966 while figure 2.2.2 shows some of the phase diagrams proposed over this period.

M.J.Blackburn [BLA 67_b] criticised the rather infrequent use of thin foils during previous investigations and the limitations of the investigation techniques used up to that point:

- X–ray diffraction: This technique is limited by the low intensity of the superlattice reflections of Ti_3Al. An additional question arises when these superlattice reflections are observed: Whether the ordered phase Ti_3Al was stable at the heat treatment temperature or its formation occurred during quenching.
- Light microscopy: This technique is limited: by the spatial resolution of this equipment; by the coherency and composition similarity between Ti_3Al and α; and by the hydrogen contamination of the samples during etching. Titanium hydride is responsible for certain types of striated lamellar structures observed under light and electron microscopy [MAR 68];
- Measurements of physical properties: Changes indicate the presence of phase transformations, but are usually inadequate to identify the transformations.

Blackburn [BLA 67_b] used transmission electron microscopy and electron diffraction techniques to study the ordering reaction of Ti_3Al. The structure of the Ti_3Al phase was confirmed as ordered hexagonal, $D0_{19}$ type, with a and c parameters varying with Al content. He showed that care must be taken during thin foil preparation to avoid hydride formation, as these hydrides completely obscure the true microstructure in thin foils.

The ordering reaction might occur either during isothermal heat treatment, long range ordering, or during quenching, short range ordering. When the ordering reaction cannot be suppressed by rapid quenching from

single phase α or β, one observes the presence of small domains of ordered phase (from 30 to 70 A in diameter) [BLA 67_b].

Finally M.J.Blackburn [BLA 67_b] presented his version for the Ti-rich corner of the Al-Ti phase diagram between 0-25at% Al and 500–1100°C (see figure 2.2.3.). The boundaries between the α/α+α2 phase fields have been taken as the limit of resolvable α2 particles by the dark field technique. A resolvable thickness of disordered material between ordered domains has been taken as the boundary between α2/α+α2. He considered the possibility of the existence of a peritectoid reaction (β+α2–>α), as proposed by T.Tsujimoto et al. [TSU 66] but he stated that this reaction had not been specifically investigated. Two years later, M.J.Blackburn [BLA 70] extended his investigation to 45at%Al in order to study the continuity of the α+α2 boundaries. He could not find evidence for the existence of the peritectoid reaction (α2+β–>α). He detected instead the presence of the disordered α phase field between α+β and α+α2 fields.

P.J.Ash [ASH 73] three years later examined the Al-Ti system between 22 and 50at%Al. He proposed a peritectoid reaction (α+γ–>α2) at about 1200°C and 42at%Al as the invariant reaction in which α2 is formed (figure 2.2.4.). At that stage all the efforts had been directed to solve the uncertainties related to the shape and extent of the α+α2 phase field.

The position of the α/α+α2 and α+α2/α2 boundaries were investigated again by E.W.Collings [COL 79] who studied the Al-Ti system between 30 and 57at%Al. He employed a different technique, magnetic susceptibility, to distinguish more clearly the position of the boundaries. His results were in reasonable agreement with Blackburn's data [BLA $67_{a,b}$] despite the use of highly contaminated Al alloy for the production of his binary alloys (wt%Cu+wt%Si+wt%Fe=5). Additionally, he proposed and estimated the temperature (~1325°C) of another peritectoid reaction (β+γ–>α) occurring at ~45.2at%Al(see figure 2.2.5).

L.J.Swartzendruber et al. [SWA 81] applied similar technique to study the extension of α+α2 boundaries in the Al-Ti system. Their results show that :

$$x^{\alpha}_{Al} = 0.11 \text{ and } x^{\alpha 2}_{Al} = 0.20 \text{ at } 500°C; \text{ and}$$

$$x^{\alpha}_{Al} = 0.18 \text{ and } x^{\alpha 2}_{Al} = 0.255 \text{ at } 1100°C.$$

where x^{α}_{Al} and $x^{\alpha 2}_{Al}$ are, respectively, the mole fraction of aluminium soluble in α and α2 (see figure 2.2.7.).

These values were in good agreement with the results of T.Tsujimoto et al. [TSU 66] but showed, when compared to M.J.Blackburn's results, a wider $\alpha+\alpha 2$ phase field at above 700°C. Work by J.Y.Huh et al. [HUH 90] studied the coherent and incoherent $\alpha+\alpha 2$ phase equilibria in a Ti-16.64at%Al using analytical electron microscopy. They obtained the composition, in weight percent, of the coexisting α matrix and $\alpha 2$ particles at 800°C for both coherent and incoherent states:

$$w_{Al}^{\alpha} = 14.15 \pm 0.32 \text{ and } w_{Al}^{\alpha 2} = 19.80 \pm 0.61 \text{ for coherent particles; and}$$
$$w_{Al}^{\alpha} = 14.79 \pm 0.32 \text{ and } w_{Al}^{\alpha 2} = 20.82 \pm 0.42 \text{ for incoherent particles}$$

Both the matrix and precipitate compositions were shifted to the Ti-rich side of the diagram as a result of the coherency stresses (see figure 2.2.6.). The results for the incoherent precipitation agree with the previous work of M.J.Blackburn [BLA 67b]. It is believed that some of the disagreement in the literature concerning the $\alpha+\alpha 2$ region in the Al-Ti phase diagram could also be due to coherency effects.

In 1984 R.D.Shull et al. [SHU 84], employing TEM and DTA; and taking extra care to avoid gaseous contamination, determined a very important experimental version of the binary phase diagram (see figure 2.2.8) showing that the α phase field extends continuously into aluminium contents greater than 37.5at%Al at temperatures of approximately 1200°C. They proposed the existence of a congruent transformation ($\alpha 2 \rightarrow \alpha$) at approximately 1180°C for 30at%Al; and an eutectoid transformation ($\alpha \rightarrow \alpha 2+\gamma$) at approximately 1160°C and 39.5at%Al. The latter disagreed with Ash's proposal of a peritectoid reaction ($\alpha+\gamma \rightarrow \alpha 2$) at about 1200°C and 42at%Al [ASH 73]. Shull's contributions for the Al-Ti phase diagram concerning the existence of both congruent and eutectoid transformations have remained unchallenged since then.

In 1987, J.L.Murray [MUR 88] published an optimised version of the Ti–Al phase diagram using thermodynamic modelling to fit the selected experimental data [BUM 52][COL 79][SHU 84][BLA 67b]. Some uncertainties were still present in the published diagram (see figure 2.2.9), such as the position of the $\alpha 2/\alpha 2+\gamma$ boundary and the existence of an eutectoid reaction ($\alpha \rightarrow \alpha 2+\gamma$) at approximately 1125C and 39.5at% Al. Additionally, her calculated version of the binary diagram indicated the presence a peritectic reaction (liquid$+\beta \rightarrow \gamma$) at 1470°C for 35at%Al and a peritectoid reaction ($\beta+\gamma \rightarrow \alpha$) at 1125°C for 45at% Al. The existence of these two reactions was, however, challenged almost simultaneously. J.J.Valencia et al. [VAL 87] used TEM, SEM and XRD to examine the morphological features of a shrinkage

cavity of a binary alloy with 50at% Al cooled at modest cooling rates. They observed that the dendritic arms were not orthogonal, as one would expect for Ti(β)-bcc (this phase had been considered stable during solidification by Murray's diagram [MUR 88]). They noticed instead that the dendrites generally lay at 60 degrees with respect to each other, resembling very much dendrites of a hcp crystal. This observation was interpreted as an evidence of the presence of primary dendrites of α phase. Finally, á "new" phase diagram, based on a previous version [WIL 73] showing two peritectic reactions (liquid+β->α and liquid+α->γ) was proposed (figure 2.2.10.).

In 1988 J.J.Valencia et al. [McC 88] published another investigation employing extra experimental techniques such as containerless solidification and high temperature X-ray diffraction to establish the nature of the reactions occurring during solidification. This work confirmed the presence of a peritectic reaction (liquid+β->α) and suggested the existence of a second peritectic reaction (liquid+α->γ). The latter (liquid+α->γ) was confirmed subsequently by J.J.Valencia et al. [VAL 89] using electromagnetic levitation melting to study the effect of supercooling and cooling rate on the microstructural evolution of Ti–Al alloys with Al content between 45 and 55at%Al. These same reactions, liquid+β->α and liquid+α->γ, were latter observed by J.C.Mishurda et al. [MIS 89] using DTA and light microscopy. Their new calculated version of the binary phase diagram (see figure 2.2.11), obtained by thermodynamic modelling featured the two cascading peritectics (liquid+β->α and liquid+α->γ) between 30 and 55at%Al. Additionally, they proposed: a discontinuous α single phase field; a peritectoid reaction (β+α ->α2) at ~ 1230°C for 34at%Al; a peritectoid reaction (β+α2->α) at ~1080°C for 21at%Al; and a eutectoid reaction (α->α2+γ) at ~ 1140°C for 41at%Al. Another investigation by J.C.Mishurda et al. [PER 93] established the phase boundaries for the α+γ phases field by using DTA analysis and diffusion couple experiments (see figure 2.2.12). These results were in good agreement with the data obtained by C.McCullough et al. [McC 89].

In 1992, H.A.Lipsitt et al. [BAR 93] investigated the central region of the Ti-Al phase diagram and confirmed the eutectoid reaction at 1115°C (α->α2+γ) for 39,6at%Al. His version of the central part of the binary is shown in figure 2.2.13. The same eutectoid reaction had been previously confirmed by A.Hellwig et al. [HEL 92] as shown in figure 2.2.14.

Finally, U.R.Kattner et al. [KAT 92] published his new calculated version of the Al-Ti phase diagram. The proposed diagram agrees well with the experimental data within the given experimental uncertainties and it does not show the α phase field as discontinuous. However, they admitted that effort is still needed to define the type of the invariant reaction in which

Ti_3Al is formed: either congruent (α->$\alpha 2$), as shown in his optimised version, or peritectoid ($\beta+\alpha$->$\alpha 2$). The latter would produce a second peritectoid reaction ($\beta+\alpha 2$->α) at lower temperatures, as shown in the calculated phase diagram proposed by J.C.Mishurda and J.H.Perepezko [MIS 89].

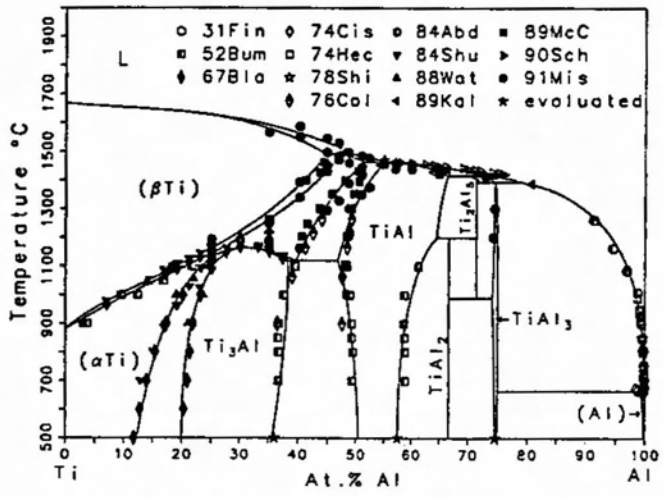

Figure 2.2.1. Assessed Ti-Al Phase Diagram by U.R.Kattner [KAT 92].

source	range		experimental techniques**	contribution
	at%Al	T(°C)		
[OGD51]	0 - 64	700-1000	XRD, DTA, LM	-first study on Ti-rich corner; -effect of O,N,C on α/β transus.
[BUM52]	0 - 75	700-1400	XRD, LM, HARD	-study on higher temperatures.
[VAN54]	0 - 10	900-1100	XRD, OM	-effect of O,N,C
[ENC57]	0 - 37	1000	XRD	-proposes existence of Ti_2Al(hcp) between 12-25 wt% Al.
[CRO57]	6 - 10	200-800	XRD, Tensile + Charpy Tests	-confirms presence of Ti_2Al(hcp).
[AND57]	-	-	-	-finds out presence of superlattice reflections based on Ti_3Al
[SAU59]	7 - 15	600-1000	EM, Electron Diff.	-confirms presence of Ti_3Al(hcp) Mg_3Cd type with a=5.77 and c=4.65 A.
[ENC61]	0 - 34	800-1450	XRD, LM, HARD	-confirms presence of Ti_3Al(hcp) with a=11.52 and c=4.65 A, formed by a peritectoid reaction: $\beta + Ti_2Al \rightarrow Ti_3Al$.
[GOL61]	25		XRD	-identifies ordered phase as Ti_3Al(hcp), $D0_{19}$ type structure with a=5.77 and c=4.65 A, and isomorphous with Ni_3Sn.
[CLA62]	0 - 40		XRD, LM, Resistometry	-suggests presence of a miscibility gap inside Ti_3Al phase field containing 2 ordered α2 phases.
[TSU66]	13 - 20	600-1200	LM	-denies existence of miscibility gap; -suggests peritectoid reaction: $\alpha_2(Ti_3Al) + \beta(bcc) \rightarrow \alpha(hcp)$
[CRO66]	0 - 35	600-1200	LM, EM, DTA, XRD, Dilatometry Resistometry	-denies existence of more than one ordered phase at low Al content; -suggests that Ti_3Al has virtually no solubility range; -explain microstructural artefacts caused by homogenisation of α+β alloys at low temperatures.

** LM= light microscopy; XRD= X-ray diffraction; HARD= hardness test; EM= electron microscopy.

Table 2.2.2. Chronological investigation summary on the Al-Ti phase diagram prior 1967.

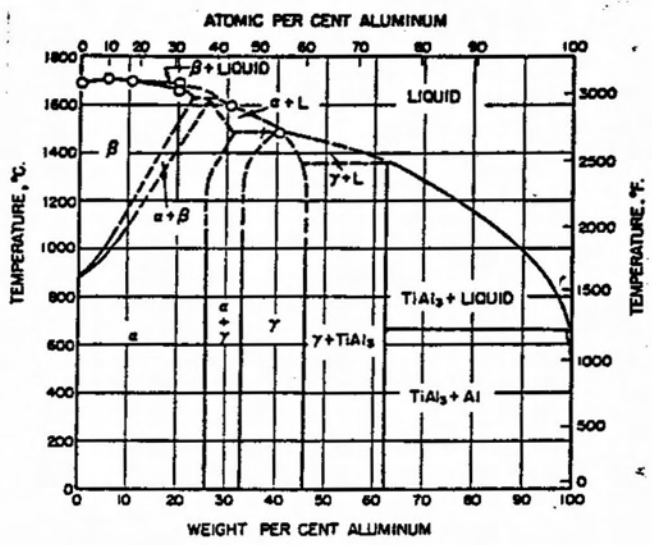

FIGURE 2.2.2.A. TI-AL PHASE DIAGRAM BY H.R. OGDEN ET AL. [OGD 51].

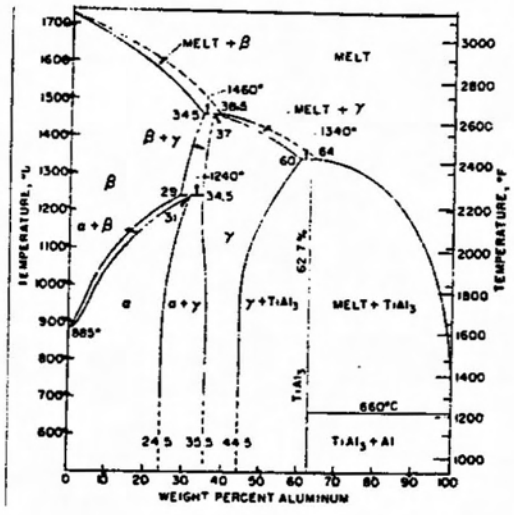

FIGURE 2.2.2.B. PORTION OF THE TI–AL PHASE DIAGRAM BY E.S. BUMPS [BUM 52].

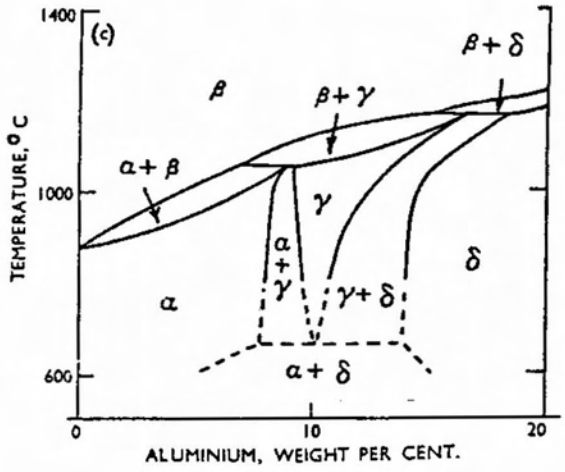

FIGURE 2.2.2.C. PORTION OF THE TI–AL PHASE DIAGRAM BY E. ENCE [ENC 61].

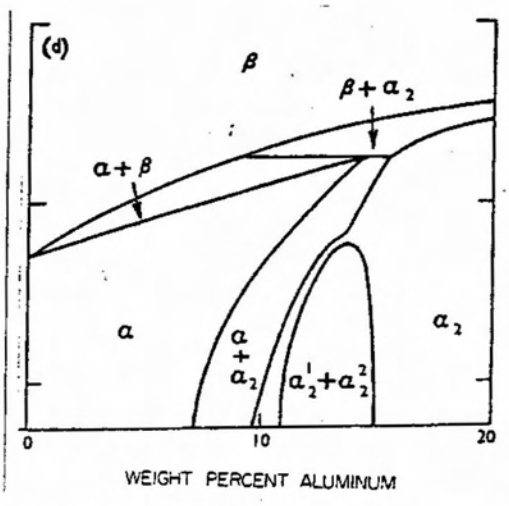

FIGURE2.2.2.D. PORTION OF THE TI–AL PHASE DIAGRAM BY D.CLARK [CLA 62]

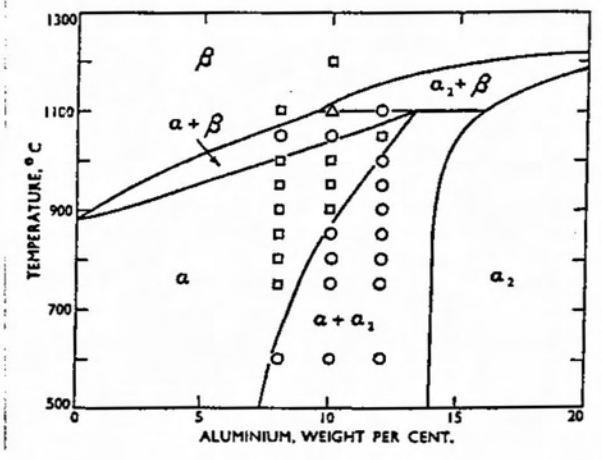

FIGURE 2.2.2.E. PORTION OF THE TI–AL PHASE DIAGRAM BY T.TSUJIMOTO ET AL. [TSU 66]

FIGURE2.2.2. HISTORICAL EVOLUTION OF TI–AL PHASE DIAGRAM BETWEEN 1951-66.

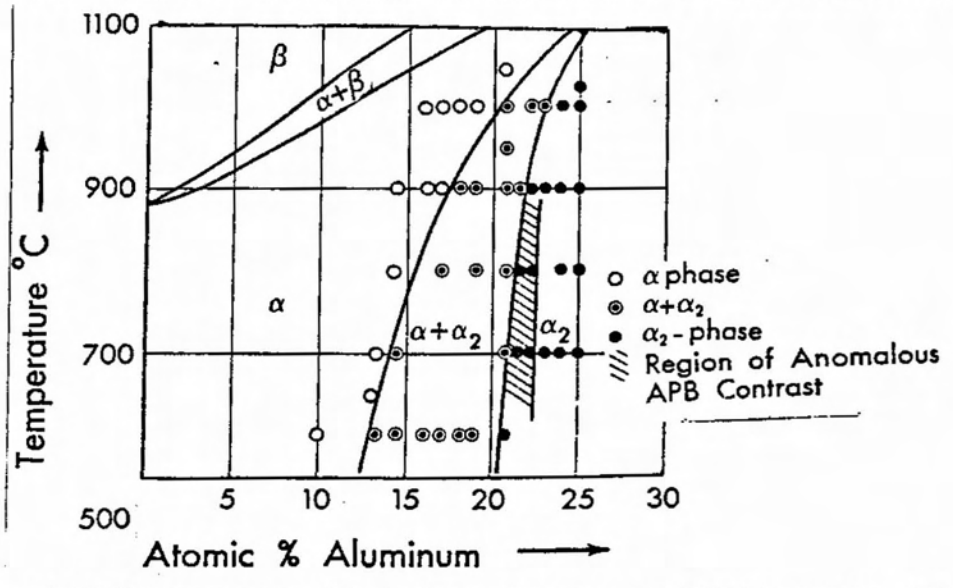

FIGURE2.2.3. PORTION OF THE TI–AL PHASE DIAGRAM BY M.J. BLACKBURN [BLA 67B].

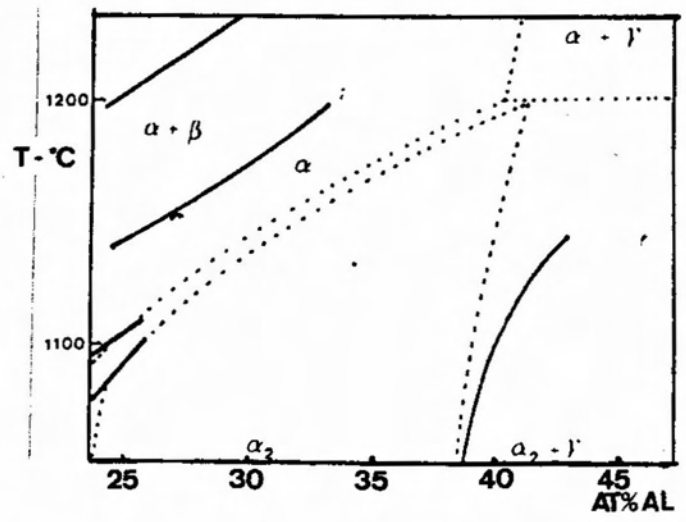

FIGURE 2.2.4. PORTION OF THE TI–AL PHASE DIAG. BY P.J. ASH [ASH 73] - (DOTTED LINES).

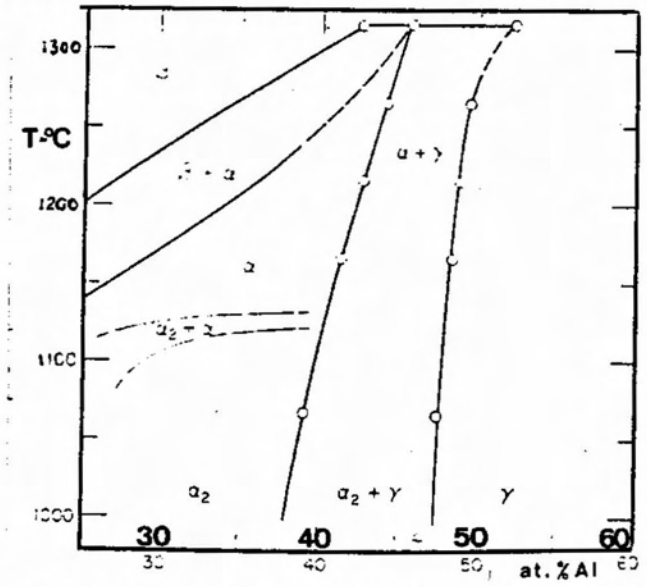

FIGURE 2.2.5. PORTION OF THE TI–AL PHASE DIAGRAM BY E.W. COLLINGS [COL 79].

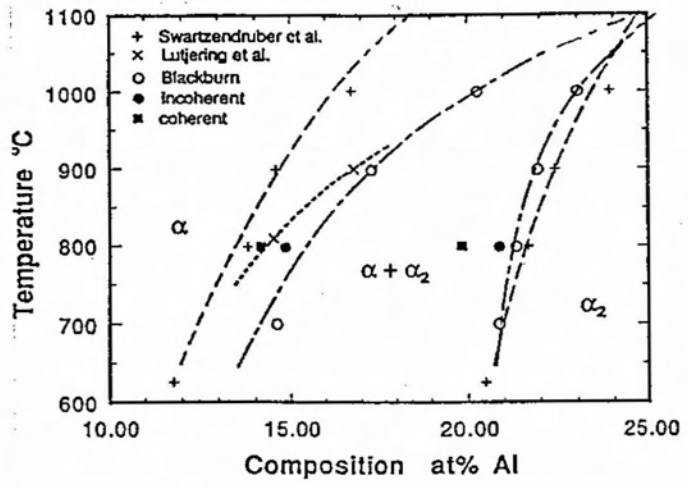

FIGURE 2.2.6. PORTION OF THE TI–AL PHASE DIAGRAM BY J.Y. HUH ET AL. [HUH 90].

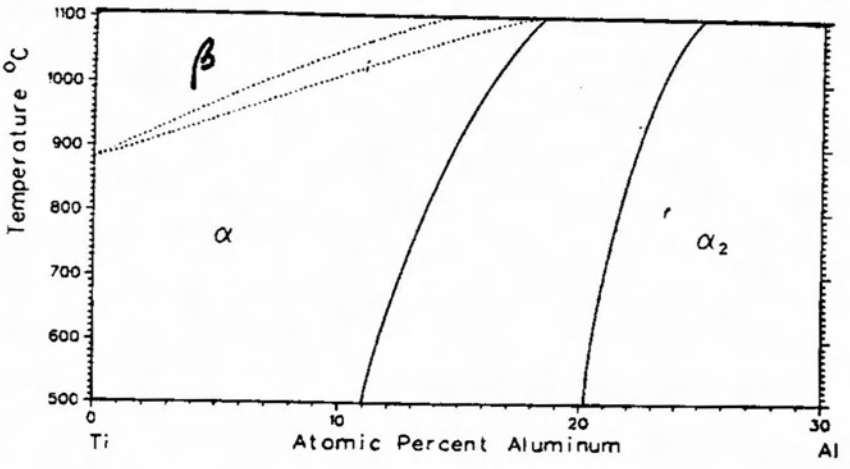

FIGURE2.2.7. PORTION OF THE TI–AL PHASE DIAGRAM [SW A84]

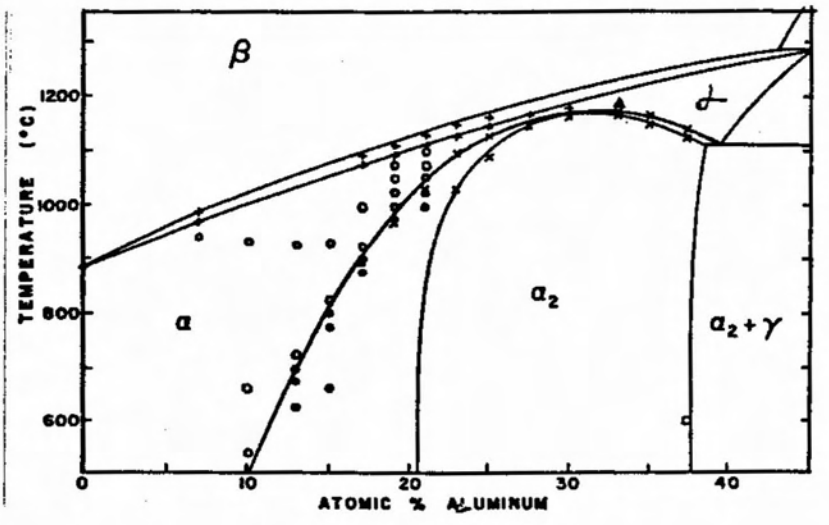

FIGURE2.2.8. PORTION OF THE TI–AL PHASE DIAGRAM BY R.D. SHULL ET AL. [SHU 84]

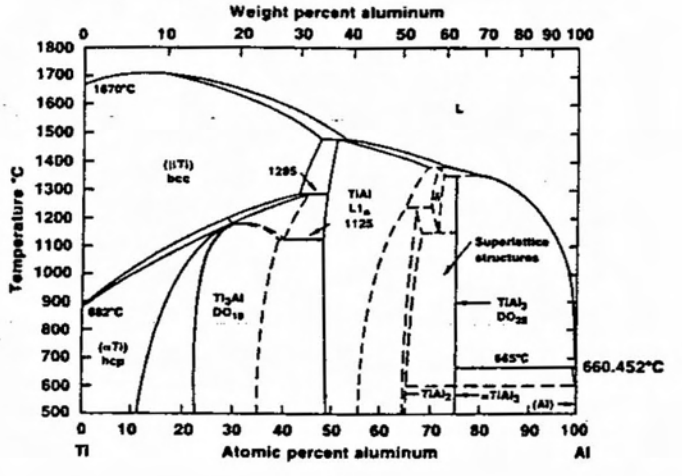

FIGURE2.2.9. ASSESSED PHASE DIAGRAM BASED ON EXPERIMENTAL DATA [MUR 88]

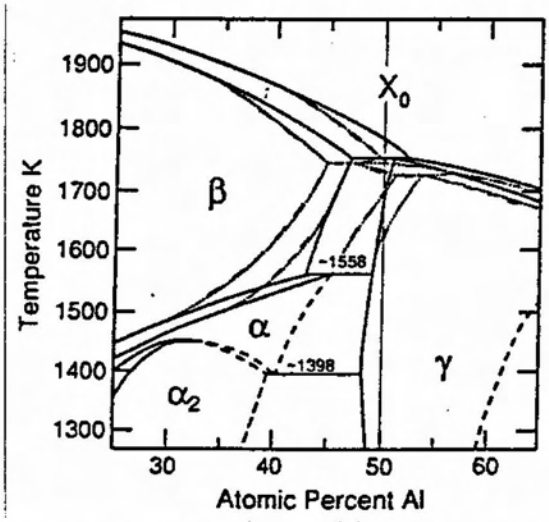

FIGURE2.2.10. PORTION OF THE TI–AL PHASE DIAGRAM BY J.J.VALENCIA ET AL. [VAL87]

*SOLID LINES [MUR88]; DOTTED LINES [WIL73].

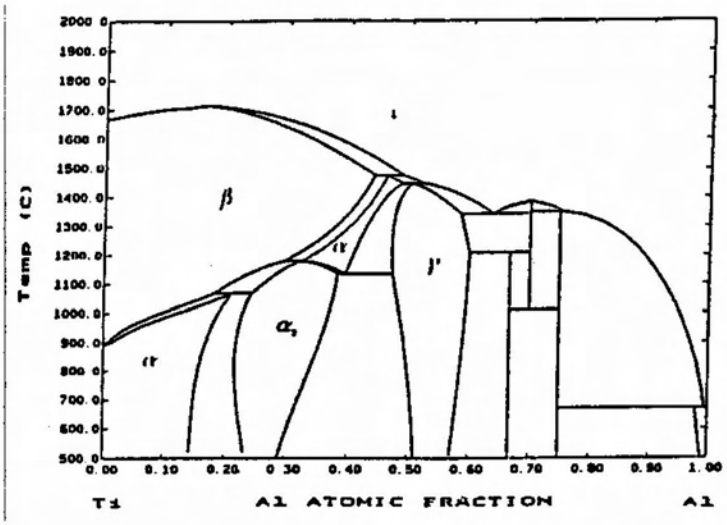

FIGURE2.2.11. CALCULATED PHASE DIAGRAM BY J.C.MISHURDA ET AL. [MIS 89].

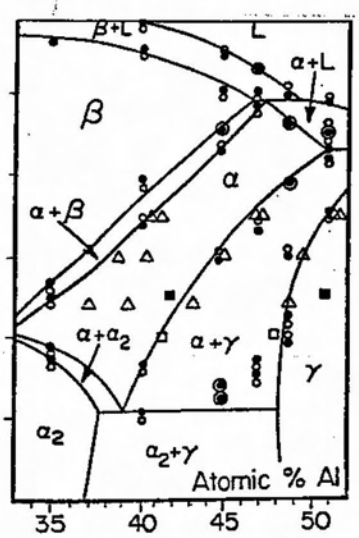

FIGURE2.2.12. PORTION OF THE TI–AL PHASE DIAGRAM BY J.H.PEREPEZKO ET AL. [PER 93].

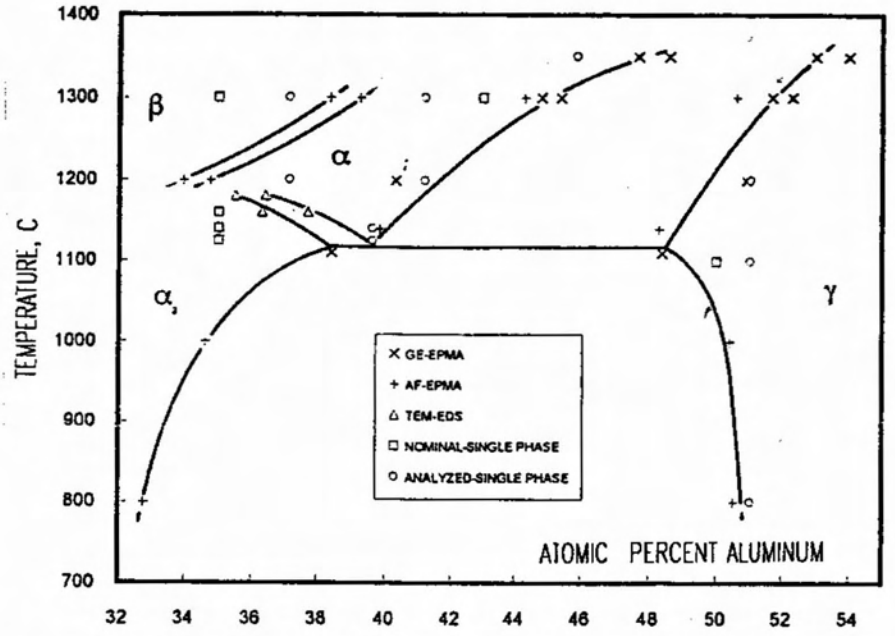

FIGURE2.2.13. PORTION OF THE TI–AL PHASE DIAGRAM BY H.A.LIPSITT ET AL. [BAR 93]

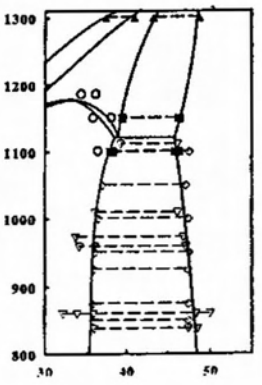

FIGURE2.2.14. INVARIANT REACTION α->γ+α2 [HEL 92]

2.3. The Ti-rich corner of the Si-Ti system

The Si-Ti phase diagram has been investigated since 1952, when M.Hansen et al. [HAN 52] first studied this system by using incipient melting detection, thermal analysis, metallography and X-ray diffraction (figure 2.3.1).

Almost 20 years later V.N.Svechnikov et al. [SVE 70] made another comprehensive study of the Si-Ti system by using thermal analysis, metallography and X-ray diffraction. Their proposed phase diagram (see figure 2.3.2), when compared to the previous one, contained three extra intermetallic phases: Ti_3Si, Ti_6Si_5 and Ti_5Si_4. The intermetallic Ti_3Si was first observed by W.Roβteutscher et al. [ROS 65].

Additionally, the two phase diagrams predicted different phases appearing in as–cast and heat treated alloys over a wide temperature and

composition range [MUR 87b]. For instance, V.N.Svechnikov et al. [SVE 70] indicated the following cascades of peritectic reactions: at 1920°C (L+Ti_5Si_3->Ti_5Si_4); at 1760°C (L+Ti_5Si_3->TiSi); and at 1570°C (L+Ti_5Si_4->TiSi), while M.Hansen et al. [HAN 52] presented only one peritectic reaction, at 1760°C (L+Ti_5Si_3->TiSi).

In 1979, L.Kaufman [KAU 79] published his first thermodynamic assessment of the Ti-Si system, complementing an earlier version [KAU 73] of a portion of this binary (see figure 2.3.3.). His version was based on Hansen's experimental data [HAN 52] and the silicide Ti_3Si is not considered in his calculation. The silicide Ti_5Si_3 was treated as a stoichiometric compound, so the diagram does not show the solubility range of Si.

In 1987 J.L.Murray [MUR 87b] published a calculated version of the Si -Ti phase diagram (see figure 2.3.4). On her critical survey of past experimental data, she concluded that:

- There was good agreement ($\Delta T_{eut} \simeq 15$°C) among all studies on the position of the eutectic reactions, (Liq-> β(Ti) + Ti_5Si_3; Liq -> TiSi + $TiSi_2$; and Liq-> $TiSi_2$ + Si);
- Concerning phase equilibria, there was some disagreement involving the existence of the intermetallics Ti_3Si and Ti_5Si_4 [HAN 52][SVE 70].

J.L.Murray [MUR 87b] decided to base her assessment on Svechnikov's data [SVE 70]. J.L.Murray assumed, for the thermodynamic calculation of the phase diagram, the intermetallic phases Ti_3Si, $TiSi_2$, Ti_5Si_3 and Ti_5Si_4 as stoichiometric compounds without any solubility range. Table 2.3.1 lists the crystal structure and chemical composition of the equilibrium solid phases of the Ti-rich corner of the Si-Ti system.

phase	composition at.% Si	crystal structure
Ti(α)	0 to 0.5	hcp
Ti(β)	0 to 3.5	bcc
Ti_3Si	25	tetragonal [Sve70] a= 1.0206 nm c= 0.5069 nm
Ti_5Si_3	35.5 to 39.5	hcp a= 0.7431 nm c= 1.2977 nm

Table 2.3.1. Phases of the Ti-rich corner of the Si-Ti system [MUR 87b]

C.Vahlas et al. [VAH 89] also produced a calculated version of the Si-Ti phase diagram. The fit between this optimised version and the selected experimental results was considered satisfactory, except for the temperature

of invariant reaction Ti(β)+Si3Ti5 ->SiTi3, calculated at 1506°C while the experimental data [SVE 70] pointed it at 1443±10°C. C.Vahlas et al. [VAH 89] considered the accuracy given by the experimental result "too weak", but it seemed rather difficult to understand what they exactly meant by that. Figure 2.3.5 shows their calculated version, which does not present any significant difference from the previous version proposed by J.L.Murray [MUR 87b].

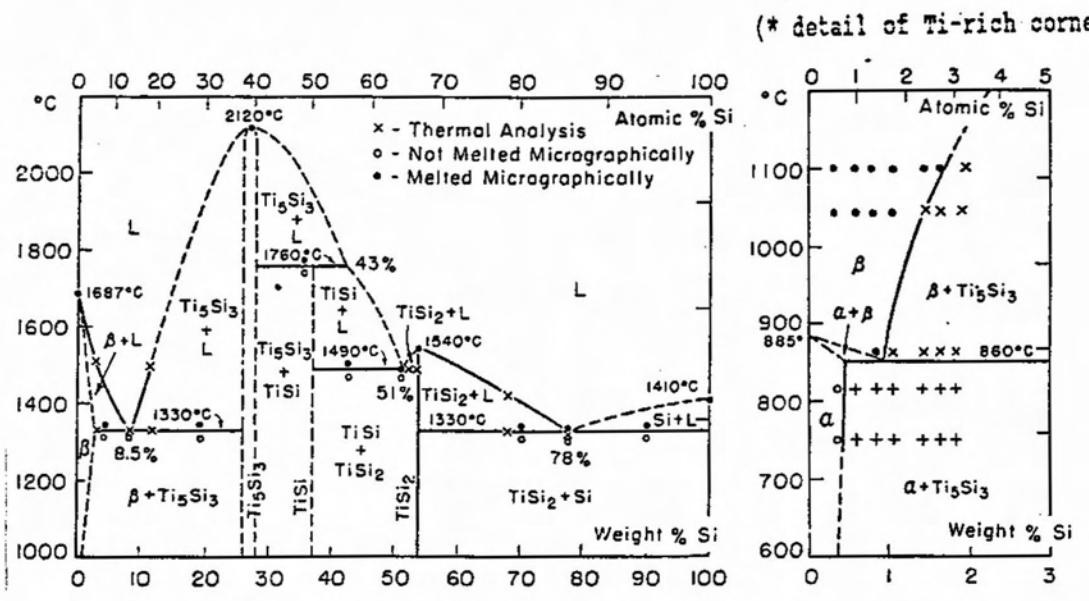

FIGURE2.3.1. EXPERIMENTAL SI-TI PHASE DIAGRAM BY M.HANSEN [HAN 52].

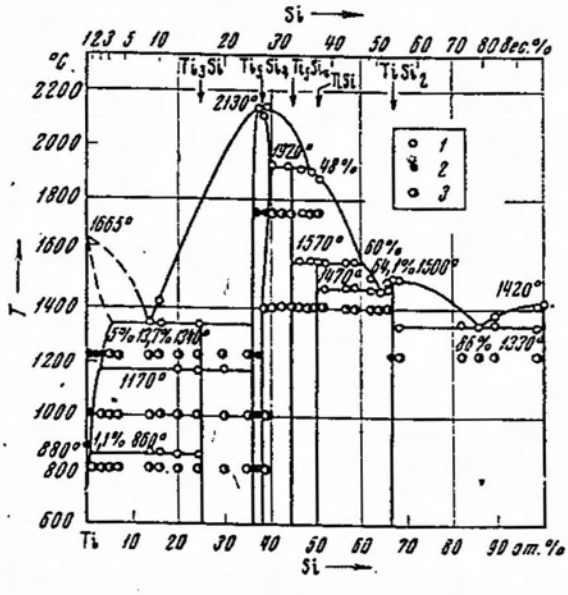

FIGURE2.3.2. EXPERIMENTAL SI-TI PHASE DIAGRAM BY V.N.SVECHNIKOV ET AL. [SVE70].

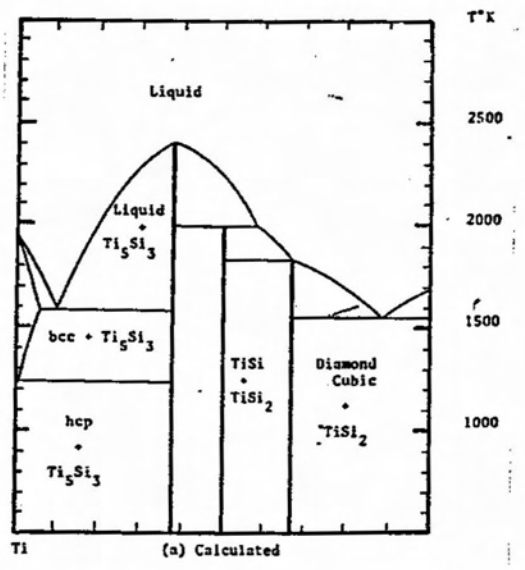

FIGURE2.3.3. ASSESSED SI-TI PHASE DIAGRAM BY L.KAUFMAN [KAU 77].

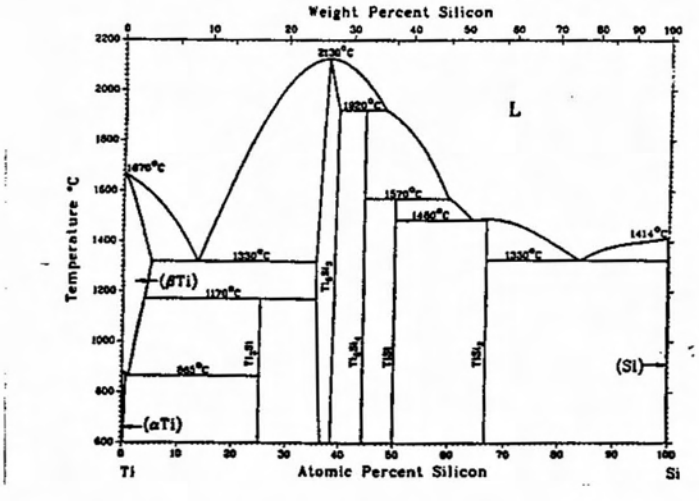

FIGURE2.3.4. ASSESSED SI-TI PHASE DIAGRAM BY J.MURRAY [MUR 87B]

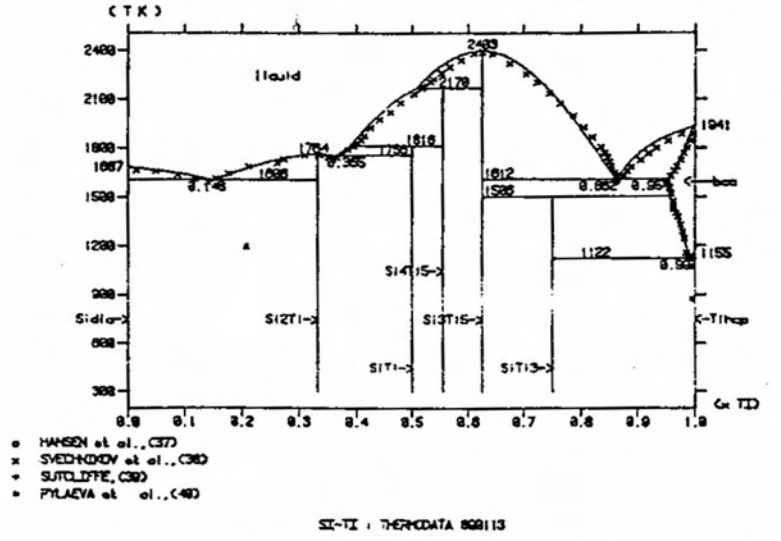

FIGURE2.3.5. ASSESSED SI-TI PHASE DIAGRAM BY C.V.AHLAS ET AL. [VAH 89].

2.4. The Ti-rich corner of the Al–Si-Ti system

The understanding of the Al–Si-Ti system is of vital importance for the development of new intermetallic alloys based on Ti_3Al and TiAl with silicon additions [WU 90]. However, there are only very few investigations published up to now [CROS 53][CROS 58][SCH 62][WU 90] and most of them are either based on outdated versions of the binaries Ti–Al and Ti–Si or do not deal with the Ti–rich corner of the ternary system.

F.A.Crossley [CRO 55][CRO 58] studied the Ti–Al–Si system between 600-1200°C, 2-8wt%Al and 0.1-2.0wt%Si by means of light metallography along with extrapolations of the binaries Al-Ti [BUM 52] and Si–Ti [HAN 52]. The isothermal and vertical cross sections are shown in figure 2.4.1. He observed that aluminium decreased the solubility of silicon in β phase but had little effect on the solubility in α phase.

In 1962, Von O.Schob et al. [SHC 62] published an isothermal at 1200°C of the Ti–rich corner of the ternary system (see figure 2.4.2). In this version, it is shown that Si addition reduces the solubility of Al in intermetallic $Ti_{3-2}Al$ (Mg_3Cd type also called Ni_3Sn type and equivalent to the structure type of Ti_3Al). Other important observation is that Si presents higher solubility in the intermetallic phase than in β. The ternary diagram also proposes the existence of a two phase field β+ $Ti_{3-2}Al$.

J.S.Wu et al. [WU 90] studied the eutectic reaction in the Ti–Al–Si system. The microstructure and phase relationships were characterised by metallography, X–ray diffraction and electron microscopy (SEM and TEM). Matrix compositions were determined by point analysis using an EDX-SEM. The phase transformations were obtained via DTA. They proposed the existence of a eutectic reaction (L->β+Ti_5Si_3). The course of the eutectic line across the two phase region [α2-Ti_3(Al,Si) + Ti_5(Si,Al)$_3$] is shown in figure 2.4.3. projected over Schob's isothermal at 1200°C. They also observed that the melting points of the eutectic alloys decreased, in general, along the direction of the arrow in figure 2.4.3 (lower Al and higher Si content). For the alloy Ti-30at%Al-6.5at%Si, they suggested the following solidification sequence:

eutectic: Liq. -> β-Ti(Al,Si) + Ti_5(Si,Al)3 at 1515°C
allotropic: β–Ti(Al,Si) –> α–Ti(Al,Si) at 1218°C
ordering: α –Ti(Al,Si) –> α2–Ti_3(Si,Al) at 1172°C

This sequence, however, did not agree with the isothermal at 1200°C [SCH 62], which suggested the existence of a [α2–Ti_3(Si,Al) + Ti_5(Si,Al)$_3$] instead of [α+Ti_5(Si,Al)$_3$] two phases field

Z.Zhang et al. [ZHA 91] observed that addition of 5at%Al coarsened the eutectic silicides; slowed the precipitation of secondary silicides ; and, due to solid solution of Al in Ti_5Si_3 phase, reduced the Si content in the silicide. The effect of Al on the morphology of the eutectic silicide was not discussed, but the coarsening of Ti_3Si_5 might indicate that the addition of 5at%Al increases the eutectic temperature. This outcome agrees with the previous observation by J.S.Wu et al [WU 90].

D.J.Arrell et al. [ARR 93] proposed that Si acts as an eutectoid forming element (β->α+Ti_5Si_3) in the binary Ti-Si and that the addition of Al transforms this into a ternary peritectoid (β+Ti_5Si_3->α) at Al contents greater than 2wt%. Their investigation of quaternary alloys Ti-20Al-11Nb-XSi, provided evidence that this effect remains the same when α2 replaces Ti(α). As a whole, Si was suggested to replace Al in the intermetallic and to increase the fraction of α2 in the quaternary alloys on an isothermal basis.

S.H.Manesh et al. [MAN 94] published a partial liquidus projection of the Ti-Al-Si ternary system (see figure 2.4.4.). They suggested the following reactions along the lines TP, POP and ON:

Liq->β+Ti_5(Si,Al)$_3$
Liq->α+Ti_5(Si,Al)$_3$
Liq->γ+Ti_5(Si,Al)$_3$

It was also suggested the existence of a maximum point on the eutectic line around 30at%Al. At points P and O they suggested, respectively, two peritectic reactions:

Liq+β–>α+Ti_5(Si,Al)$_3$
Liq+α–>γ+Ti_5(Si,Al)$_3$

Their results were qualitatively consistent with the calculated portion of the Ti-Al-Si phase diagram (Thermo Calc Data-Bank). It should be noted that the thermodynamic data available for the calculation treated Ti_5Si_3 as a line compound and did not consider substitution of Al for Si in the silicide. Other factors not taken into account in the calculated portion were the binary Al-Si and ternary interactions in α and β phases; and Si solution in γ-TiAl phase. The authors pointed, however, that these factors were unlikely to materially alter the calculated partial diagram, at least in the temperature and chemical composition range investigated.

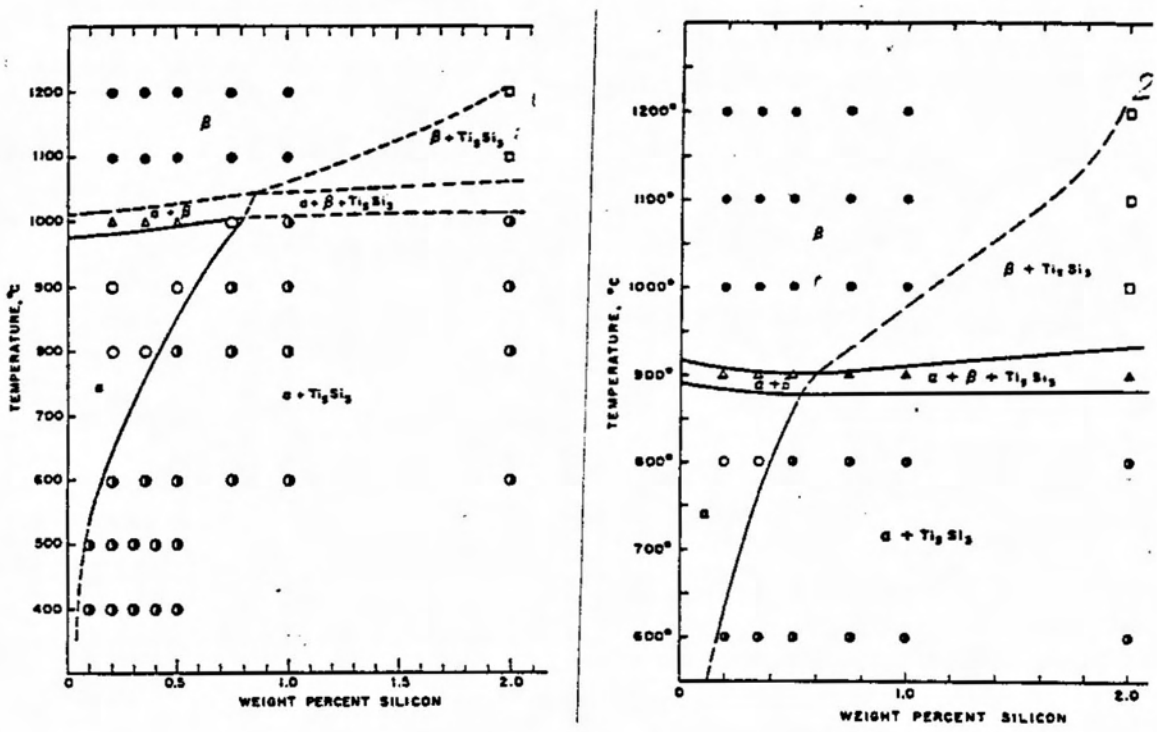

A) 6WT%AL; B) 2WT%AL.

FIGURE2.4.1. PARTIAL VERTICAL SECTION OF THE SYSTEM TI–AL–SI [CRO58].

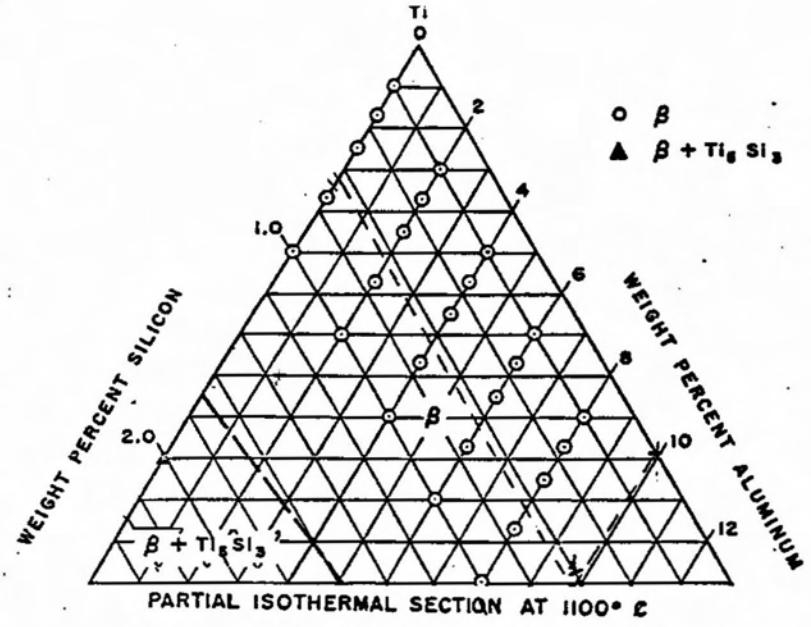

FIGURE2.4.1.C. PARTIAL ISOTHERMAL SECTION OF TI–AL–SI SYSTEM AT 1100° C [CRO55].

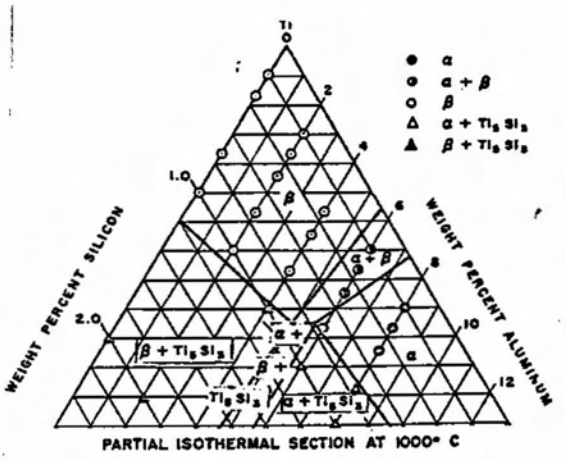

FIGURE 2.4.1.D. PARTIAL ISOTHERMAL SECTION OF TI–AL–SI SYSTEM AT 1000° C [CRO 55].

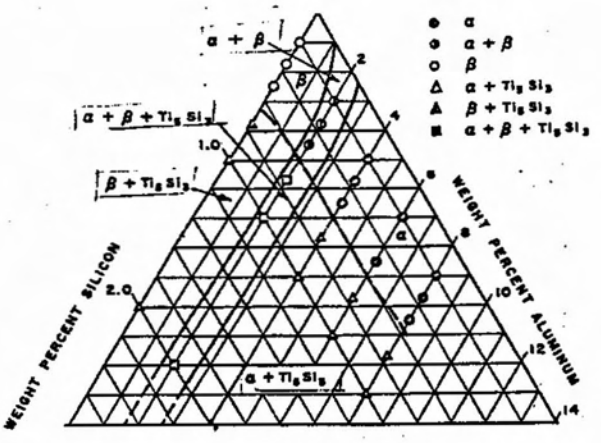

FIGURE 2.4.1.E. PARTIAL ISOTHERMAL SECTION OF TI–AL–SI SYSTEM AT 900° C [CRO 55].

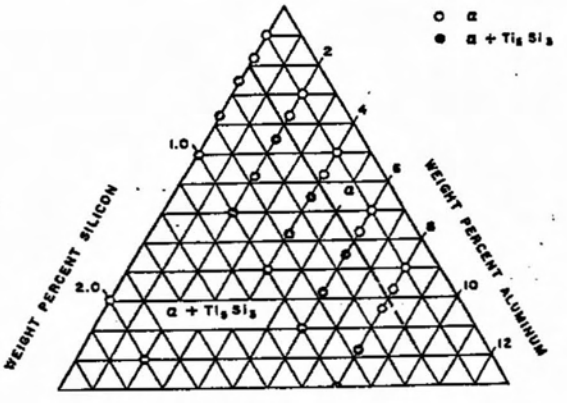

FIGURE 2.4.1.F. PARTIAL ISOTHERMAL SECTION OF TI–AL–SI SYSTEM AT 800° C [CRO 55].

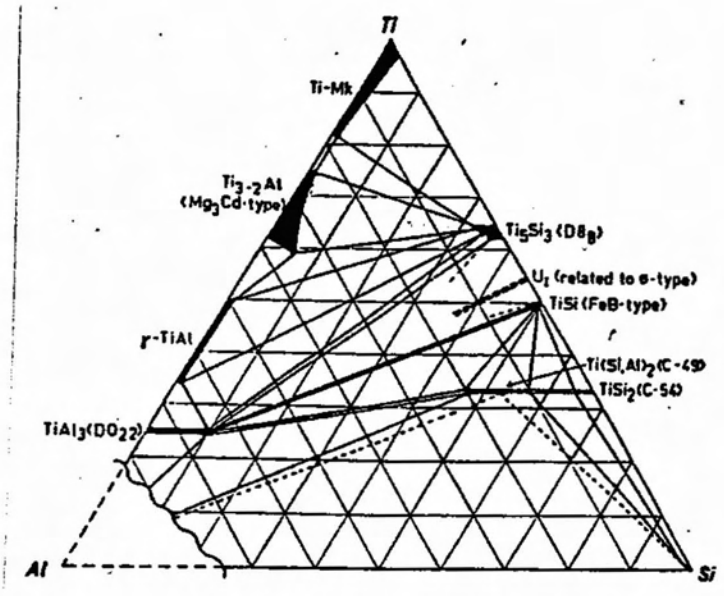

FIGURE 2.4.2. PARTIAL ISOTHERMAL SECTION OF TI–AL–SI SYSTEM AT 1200° C [SCH 62].

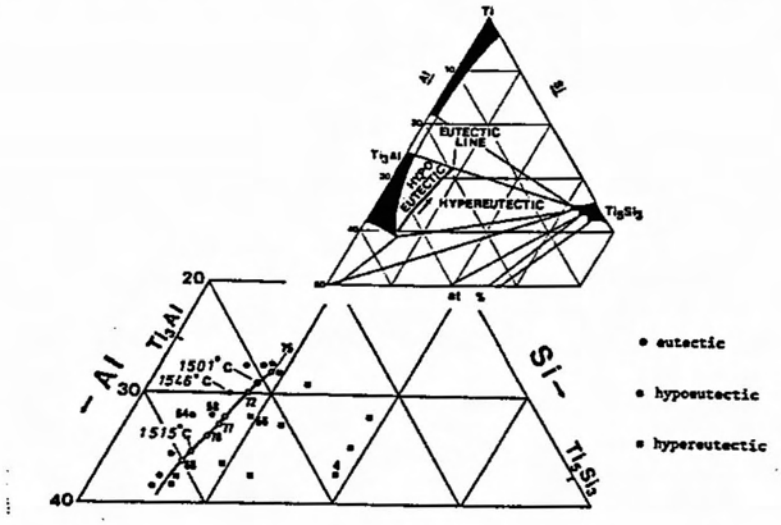

FIGURE 2.4.3. PROJECTION OF THE EUTECTIC LINE ON THE 1200° C ISOTHERMAL SECTION OF THE TI–AL–SI SYSTEM [WU 90].

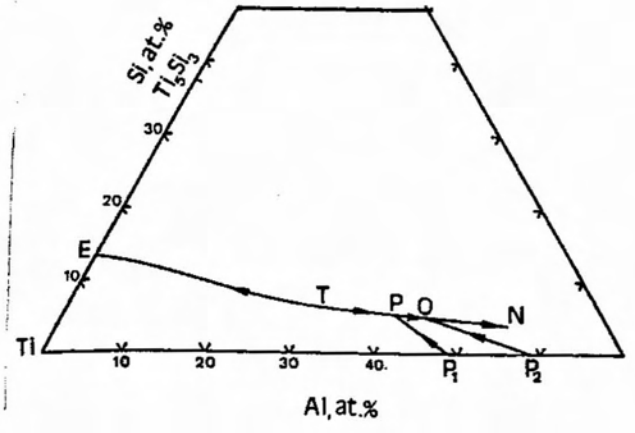

FIGURE 2.4.4. LIQUIDUS PROJECTION BY S.H.MANESH ET AL. [MAN 94].

2.5. Phase transformations in the Ti-rich corner of the Ti-Al-Si system

The understanding of the various reactions, which occur in the Ti-rich corner of the Ti-Al-Si system such as decomposition of β phase during quenching, silicide precipitation and ordering of Ti_3Al titanium, is very important for the study and determination of the ternary phase diagram. This assists the correct metallographic characterisation of the quenched samples, allowing, for instance, the identification of the transformed β from the phases, which were stable at the heat treatment temperature, and the distinction between Ti_3Al stable and Ti_3Al formed during quenching.

2.5.1. Decomposition of β-phase

Besides the study of phases diagram, the understanding of the possible mechanisms for the decomposition of β-phase might also be helpful for the microstructural control and optimisation of as-cast Ti-aluminide based alloys. For example H.B.Aanon and H.I.Aaronson [AAN 71] studied the effect of the type of nucleation sites of the prior microstructure on the morphology of the precipitation of ferrite, and they concluded that modifications on the quantity and structure of the boundaries of the prior microstructure alter both the kinetics and the morphology of precipitation during posterior heat treatment. In this sense, the transformed β microstructure produced by the allotropic reaction Tiβ(bcc)->Tiα(hcp) during quenching, seems to be one of the variables available for the microstructural design of (α+α2) alloys, as α2 may present heterogeneous nucleation under certain heat-treatment and chemical composition conditions.

However, the full comprehension and control of the morphology of transformed β is not an easy task, specially in Ti-Al based alloys. These alloys present (β/β+α) and (β+α/α) transus, T_0 and Ms temperatures very close to each other and at considerably high temperatures. So, in practice, a clear boundary separating nucleation and growth and martensitic process is generally not possible and a series of quenching structures extending from lath martensite through acicular martensite and massive to the Widmanstätten structure can be observed [COL 84].

Furthermore, investigators [BHA 90][AAR 90][HAL 94][AAR 94][CHR 94][DAH 94][FUR 95] are still discussing the roles of shear and diffusion on the formation of plate-like precipitates in systems where the temperature range for the occurrence of different types of morphology during quenching is comparatively much wider. G.R.Purdy and M.Hillert [PUR 84]

following this approach, emphasised that the lower the reaction temperature, the more significant the effect of the lattice strain energy on the kinetics of nucleation and growth. In this sense, the martensitic reaction was defined just as a lower limit where diffusion is inoperative. J.W.Christian [CHR 94] has recently proposed a new category of phase transformations, designated as "diffusional-displacive", for reactions where composition changes do not exclude concomitant shape changes. So, it seems very unlikely, for the case of Ti-Al "martensites", that diffusion is inoperative. The same discussion on nature of reaction seems to apply for the massive transformation.

2.5.1.1. Massive transformation

Transitions between phases in the solid state may occur by a number of different mechanisms. One apparently simple class includes those transformations such as martensitic reactions, order-disorder transitions and massive transformations, which involves change in crystal structure without changes in composition. The present debate on the massive transformation is related to: the type of interface between parent and daughter phases (coherent versus incoherent); the presence of an orientation relationship (OR) between matrix and massive product; the mechanism of growth of the massive product (ledge mechanism versus random transfer of atoms across interfaces); the possible presence of sub-boundaries; to the presence of invariant plane strain surface relief; and finally to the semantics of massive product.

H.I.Aaronson and co-workers [MEN 88][PLI 84] suggested that growth by the ledge mechanism is a reasonable possibility for the massive transformation and that invariant plane strain surface relief can be generated during massive transformation when reaction occurs at sufficiently large undercoolings so that anisotropic growth, involving large areas of partially coherent interphase boundary with a constant boundary orientation, is feasible. Under this view, for instance, many other morphologies, such as plate-shaped and other anisotropic forms, resulted from a no-composition change reaction have been defined as massive. Following this approach, the transition between massive and martensite can also become very unclear indeed.

T.Massalki [MAS 84] does not completely disagree with the possible existence of OR between parent and daughter phases massively transformed, but he states that " Thus, it seems that while massive transformations are composition invariant at least on macroscopic scale, all composition invariant (diffusional) transformations should not be regarded as massive. The problem is, and remains, one of arbitrary definitions". Massalki and co-

workers [PLI 77][PER 84][MAS 84] observed that the massive transformation can be fundamentally defined by a combination of characteristic features such as: absence of compositional differences between parent phase and massive product (composition invariance); crossing of the grain boundaries of the parent phase; preferential formation at the grain boundaries of the parent phase; and presence of irregular interfaces with the parent phase (either very irregular; smoothly curved; or strongly faceted).

J.H.Perepezko [PER 84] mentioned that during the massive transformation a new structure forms and grows through a noncooperative transfer of atoms across relatively high energy incoherent interfaces. A single massive grain can grow at speeds exceeding 10 mm/s and absorb several parent phase grains during transformation. Massive transformations exhibit nucleation and growth characteristics and are thermally activated. T.Massalki [MAS 84] mentioned that "in the past" the massive transformation presented sufficient distinctive features to make it distinguishable from other types of transformation. He added that with increased new data, improved methods of investigation and changing emphases, some of the distinguishing features have become somewhat blurred. He pointed out that disputes can arise depending "on how one regards the massive transformation features such as the speed of the transformation interfaces, its ability to cross prior parent grain boundaries, the appearance of the resulting microstructure, the nature of the nucleation, the mechanism of atomic transfer at the interfaces, and the details of possible orientation relationships".

For instance, it has been long accepted that the thermodynamic condition that must be satisfied for the occurrence of a massive transformation is that the free energy of the new phase must be lower than the parent phase, both phases having the same composition, and this condition is satisfied for temperatures below T_0* [PER 84][PLI 78]. M.Hillert [HIL 84], however, reported that a review of the experimental information available indicates strongly that the solvus line, rather than the T_0 line, is the natural limit condition for the massive mode of growth. This observation reinforced previous observations that massive transformation occurs inside two-phase fields at temperatures much closer to the solvus than T0.

M.Hillert [HIL 84] explained that when a transformation takes place at the solvus temperature, the α phase can grow with the same composition of the parent phase (β). However, there will be a local solute redistribution in front of the advancing interface according to the local equilibrium concept

* The To temperature is defined as the temperature at which two stress-free phases with same composition are in unstable equilibrium with each other; each phase thus has the same free energy.

and all the driving force available for the transformation would then be absorbed by the process of diffusion, so that the rate of composition-invariant reaction would be negligible. By reducing the temperature into the α one-phase field, some net driving force would then be available for the composition invariant transformation itself. Hillert introduced another factor which might also affect the driving force available for the transformation and explain the observation of massive products inside the two-phase fields: the coherency strains in the solute concentration spike formed by solute redistribution into the parent phase ahead of the growing disordered interface. Providing that the region of β phase presenting the concentration profile, called the spike (see figure 2.5.1.1.1.), is coherent with the rest of the parent phase, the spike would present coherency strains caused by the difference in atomic sizes of the two components. By including this strain energy in the Gibbs energy, Hillert obtained a new equilibrium between α and β. The coherency strains were shown: to increase solute solubility in the daughter phase (α); to decrease solute solubility in the parent phase (β); and to displace slightly the α/α+β transus to higher temperatures. This would explain the occurrence of massive transformation inside "two phase field". He concluded that the solvus line is the natural limit for the massive transformation and that the condition of local equilibrium may be established very well during the massive transformation. Menon et al. [MEN 88] arrived to the same conclusion on the role of solvus temperature on the massive transformation, but they added that this transformation can occur inside a two-phase fields when the ratio between T_0 and the solvus temperature is sufficient low so that solute distribution cannot occur during growth.

Concerning the nature of nucleation, T.Massalki and co-workers [MAS 84][HAW 70] indicated that nucleation of massive grains most likely occurred at heterogeneous sites without any obvious low index orientation relationship between the parent and the product phase (incoherent nuclei). This explained the fact that massive grains could grow at high speeds and across several parent grains, as the growth involved incoherent interfaces and no OR. H.I.Aaronson and co-workers [PLI 84][PLI 80], however, proposed the formation of coherent nuclei at parent grain boundaries to explain the high nucleation frequency under conditions of rather low activation energy (ΔG^*) present in Ti-X alloys. T.Massalki [MAS 84] counter-argued by stating that coherent faceting would imply an orientation relationship of the massive product with the parent grain, which would constitute an impediment to subsequent grain growth across many parent grains. He added that in Ti-based systems, the very large nucleation rate observed for the fine

massive grains, of the order of 10^0 to 10^1 nuclei/mm^2 inside fairly large parent grains [PLI 78][PLI 80] might suggest that many of the nuclei may have formed through volume nucleation and without association with the grain boundary. Nevertheless, T.Massálki [MAS 84] agreed that it is possible to envisage a growing massive crystal as being bounded in some areas by disordered interfaces, and in the remaining areas, by ledged, partially coherent interfaces. Clearly, more detailed work on OR and nucleation is needed [MAS 84][PLI 84].

Other example of disagreement concerns the definition of the massive product in numerous (macroscopically) composition-invariant transformations: The ordering reaction CuAu->CuAuII requires atomic diffusion, its transformation process is slow and involves strictly crystallographic relationships; and the precipitates present a plate like microstructure with coherent interfaces and invariant plain strain relief [MAS 84]. H.I.Aaronson et al. [AAR 77] argued that since the CuAuII phase formation "does not involve a change in composition and yet cannot take place by shear" it must be termed massive transformation. Following the same approach, E.S.K.Menon et al. [MEN 88] stated that it would seem more appropriate to identify bainitic ferrite, present in almost pure iron, as simply a different morphology of ferrite such as equiaxed and massive ferrite. These morphological variations seem to be products of the same massive transformation of austenite to ferrite and they should develop from the orientation-dependencies of growth kinetics, which themselves vary with reaction temperature.

The main point behind all this discussion about the definition of massive transformation is very similar to the debate on the roles of shear and diffusion on the formation of plate-like precipitates. Is the spectrum for phase transformations continuous or not? As the transformation temperature decreases, the anisotropy of the interfacial and strain energies, and the activation energy for the diffusion across the interphase boundary occupy a more decisive role on the nucleation and growth of a precipitate. Supposing that the spectrum is continuous, it seems very straightforward to assume that those variables will also act on the massive transformation and affect its nucleation and growth. Following this approach, it is not difficult to hypothesise the existence of transitional microstructures between "typical" massive grains and martensite plates presenting. A semantic question, however, seem to arise in this hypothetical situation: How to classify this microstructure?. In this sense, Massalki [MAS 84] was very "perceptive" in his remark "The problem is, and remains, one of arbitrary definitions". This problem would be partially solved by classifying the microstructure by its morphology

without imposing any mechanism of formation. The dispute on the roles of T_0 and solvus temperature on the thermodynamics of massive reaction demonstrates how much development is still needed for better understanding of this transformation. Furthermore, the operating mechanisms at atomic level (composition invariant versus local solute redistribution; and type of reacting interface) are not clear and experimental evidence is still very limited and conflicting.

Few investigators [PLI 77][PLI 78][PLI 79][PLI 80][RUC 90][WAN 92] have studied the occurrence of massive transformations in Ti-based alloys. M.R.Plitcha and H.I.Aaronson [PLI 77][PLI 78] studied and confirmed the existence of massive transformation in three Ti–based eutectoid systems, Ti–Ag; Ti–Au; and Ti–Si, out of the fourteen Ti-X systems examined. Among other possible Ti-based systems presenting massive transformation, they suggested Ti-Al and Ti-V. TEM examination showed that the massive product presents low dislocation density and does not present internal boundaries as those associated with the individual laths in the martensite. They reported that three basic requirements must be satisfied to make a massive transformation possible:

- The massive transformation can only take place when the T_0 temperature is high enough so that atomic jumps across the interface are still feasible at reasonable rates (note that this early investigation is considering T_0 and not solvus temperature as parameter);
- The kinetics of any competing precipitation reaction must be relatively slow. In this context, it was deduced that a narrow interval between the transus and the T_0 temperature, i.e., a narrow nearly horizontal two phase field in the phase diagram, is favourable to massive transformation. This results in the small driving force for precipitation at T_0 temperature. The massive reaction tends to be inhibited as the two–phase field becomes wider and more nearly parallel to the temperature axis;
- The product phase must have a reasonably wide range of existence to favour the massive transformation.

Metallographic examination [PLI 78][PLI 77] revealed that the predominant constituent of samples cooled at rates less than about 800°C/s is massive α. In Ti-Si and Ti-Au alloys, the massive product was found to be replaced by martensite as the cooling rate and solute content were increased. In addition, the massive grains were observed to decrease in size with increasing cooling rate and their boundaries to become more irregular in appearance. The martensite morphology in these alloys is that of "packet" martensite, also known as lath martensite. The martensite plates were separated by small angle boundaries and the dislocation density in the

interiors of these plates was relatively high. In the Ti–Si system, the massive reaction was observed only in hypo–eutectoid alloys (Si< 1.3 at%) and the critical cooling rate for martensite formation was estimated around 10^3°C/s.

West et al. [ABB 91] observed the presence of massive product in the Ti-Al system. This system showed an increase in the proportion of massive product with increasing Al content from 17 up to 36 at%. The authors explained the increase in the proportion of massive product by the increase in the Ms temperature caused by Al addition.

Massive transformation from α to γ phase has been reported in quenched Ti–48at%Al alloys [WAN 92]. This study indicated that γ phase forms from α in three different morphologies depending on the cooling rate. At low rates, a lamellar morphology prevailed; at slightly higher rates, the Widmanstätten structure appears; and at very high rates, the massive morphology was prevalent. This investigation suggests that typical massive morphology occurs at higher undercoolings than Widmanstätten structure. Additionally, the presence of massive morphologies was favoured by the refinement of the prior grain size. Widmanstätten morphology is favoured in relation to massive and martensitic products when solute diffusion coefficient is large, either because of the intrinsically large frequency factor, Do; or because the reaction takes place at high temperatures, where long–range diffusional process competes with short-range diffusional and diffusionless transformations during the quenching of β–Ti-alloys [COL 84].

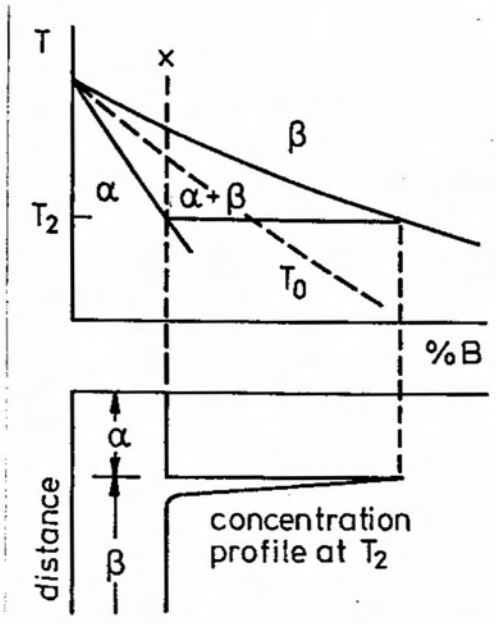

FIGURE 2.5.1.1.1. COMPOSITION INVARIANT β–>α TRANSFORMATION UNDER LOCAL PARAEQUILIBRIUM AT T_2 [HIL 84].

2.5.1.2. Martensitic transformation

Martensitic transformation presents cooperative movement of atoms resulting in a microscopically homogeneous transformation of one crystal lattice into another. The ideal martensitic process itself is not thermally activated and takes place at high speeds, which are independent of temperature. The phenomenological theory of martensite crystallography is based on the observation that the habit plane is an invariant plane in which all lines in it are neither distorted nor rotated by the displacement vector of the invariant plane strain [WAY 94]. The invariant plane-strain surface-relief effect formed where a plate-shaped transformation product intercepts a free surface polished flat prior to transformation has long been accepted as a defining characteristic of shear or martensitic phase transformation, but it has been noted in the literature that diffusional transformations are also capable of producing such relief [HAL 94][HOW 94]. U.Dahmen [DAH 94] stated that "in fact, a number of common precipitation systems forms plate-shaped inclusions, similar to those of martensitic transformation products, which offer themselves readily to application of the concepts of martensite crystallography, regardless of its formation mechanism". Recently, J.W.Christian [CHR 94] introduced a new category of transformation called "diffusional-displacive" to deal with such transformations.

In practice, for Ti-alloys a clear boundary separating displacive and diffusional transformations are generally not possible, and a series of quenching structures extending from lath martensite through acicular martensite and massive grains to the Widmanstätten structure can be observed [COL 84]. There are two types of Ti martensites, the hexagonal α', which is the most prevalent type and is generally presented in two different types of morphology: lath and acicular; and the orthorhombic α''[WIL 70]. The lath martensite consist of colonies of approximately parallel platelets, all of which belonging to the same variant of the orientation relationship. The plates are separated by small angle boundaries and present internal distribution of dislocations [FLO 72]. With increasing solute concentration, the coherence between the plates of the lath martensite is lost. The result of this is an array of individual platelets referred as acicular martensite [COL 84]. The acicular martensite occurs as an intimate mixture of individual plates, each having a different variant of the orientation relationship.

M.K.McQuillan [McQ 63] mentioned in his review on phase transformations in Ti and its alloys that "although Widmanstätten morphology can be readily distinguishable from the inter-woven needles of a "typical" martensite structure, transformed β can shade imperceptibly from one morphology to the other without it being possible to observe a change in

the mechanism involved". He suggested that this wide range of morphologies of α obtained after quenching, including retained β between parallel α plates, could be explained by the initial formation of α plate via shear mechanism plus the subsequent operation of atomic diffusion. He evoked then an analogy between the martensitic reaction in Ti-alloys and the bainitic reaction in steels to explain the surface rumpling associated with atomic diffusion. He finally proposed that the martensitic transformation in Ti-alloys is a mixed athermal-isothermal transformation.

G.Parr and M.Bibby [BIB 63] showed that, for pure Ti, the Ms temperature was dependent on the cooling rate. They defined the presence of martensitic transformation by the presence of a rumpled surface on the pre-polished faces of the quenched samples (surface-relief-criterion). For pure Ti they established the critical cooling rate for the occurrence of martensitic transformation as 200°C/sec . This value when compared to ~10^2 C/sec suggested for Ti-Si alloys [PLI 77][PLI 78] is paradoxical as it goes against the general principle that increasing the solute content reduces the critical cooling rate [JEP 70]. G.Parr and M.Bibby [BIB 63] observed that, even for cooling rates faster than 200°C/sec., the effective $T_{\beta->\alpha'}$ decreased with faster cooling rates. The transformation temperature vs. cooling rate curve obtained was continuous, not showing therefore the onset of the martensitic transformation. K.S.Jepson et al. [JEP 70] stated that the concepts of martensitic transformation lead to the presence of some discontinuity in a transformation temperature vs. cooling rate curve. This discontinuity should characterise the onset of the martensitic transformation . Using the surface-rumpling-criterion and varying the cooling rate for Ti-Nb and Ti-Al alloys, they observed that the Ms temperature decreased with the increase in the cooling rate. They concluded then that the martensitic transformation in the alloys studied appeared to be thermally activated. Schematic C-curves for the martensitic transformation were then proposed for Ti-Nb alloys.

It should be noticed that all the studies mentioned above used the surface-rumpling-criterion for identifying the martensite. Some recent studies [HOW94][HAL 94][DAH 94] on the roles of shear and diffusion on the formation of plate products proved that surface relief effects can be associated with diffusional transformations. H.Lee and H.I.Aaronson [LEE 88] observed for Ti-Cr alloys surface relief effect in the transformation $\beta->\alpha+TiCr_2$ at temperatures above T_0. Furthermore, E.S.K.Menon et al. [MEN 88] mentioned that the absence of invariant plane strain surface relief effects is not general during massive transformation and does not seem to be a fundamental characteristic of this reaction. They added that investigations of surface relief effects associated with massive transformation are needed in

alloys where growth is not uncontrollably rapid and pronouncedly anisotropic massive morphologies are able to develop. Assuming that a surface relief criterion cannot be used to identify uniquely the operation of a shear transformation mechanism, it is suggested that some of the above studies were not dealing with a martensitic transformation at all.

Changes in the morphology of α' with increasing cooling rates have been observed in the literature. K.S.Jepson et al. [JEP 70] showed evidence for the alloy Ti-5at%Nb of a morphological change from colony of parallel plates to acicular with an increase on the cooling rate (from 1500°C/sec. to 52000 °C/sec). This variation on the morphology of α' was neither mentioned nor discussed in this work. S.Banerjee et al. [BAN 73] observed the same morphological change in α' between the surface (acicular) and the interior of (lath) a quenched sample (Ti-5at%Zr). Once more no discussion on the possible effect of the cooling rate on the morphology of the martensitic reaction was presented.

H.M.Flower et al. [FLO 72] suggested that the transition in α' morphology with the addition of alloying elements is due to shear interactions. Lath martensite would form when slip occurs in the β-phase ahead of the α'-plate to reduce the shape strain. When solid-solution strengthening and lowering of the Ms sufficiently strengthen the β-phase to prevent slip, plate like martensite is obtained. H.M.Flower et al. [FLO 74] suggested that diffusion may contribute to the reduction of the shape strain during water quenching from the β-field of very dilute Ti-Mo alloys. This effect of diffusion could also explain the transition from lath to acicular martensite with increasing cooling rates. R.Davies et al. [DAV 79] observed the presence of secondary α' plates with lath morphology located between primary acicular α' plates. The formation of lath morphology was explained by the local decrease in the cooling rate due to the release of latent heat as the primary plates were formed.

In 1973, H.M.Flower et al. [NIC 73] showed for quenched samples that the addition of 0.5 and 1.0at%Mo to a Ti1at%Si resulted in retention of a thin discontinuous layer of β-phase between the α'crystals and that this β-phase was enriched in Mo. In 1974, H.M.Flower et al. [FLO 74] proposed a mechanism to explain the formation of retained β-phase, using dilute Ti-Mo alloys quenched from β-phase field at different cooling rates. For the highest cooling rate, the quenched microstructure presented predominantly large primary acicular martensite α'-plates, which presented uniform surface tilts, high internal dislocation density, and OR between adjacent plates consistent with the Burgers relationship. These features were considered and the allotropic transformation β–>α was assumed to be of displacive-type. At

smaller cooling rates [FLO 74] the amount of colony product (lath martensite) increased and larger amounts of retained β were associated with the boundaries between adjacent plates. Since no β-retention occurred in association with large acicular martensite α'-plates, but only within lath martensite, it was assumed that a change of mechanism (shear->diffusional) occurred during quenching. Additional evidence for a change in growth mechanism was afforded by the observation that some primary acicular plates broke up into colony structures (lath martensite), maybe due to local decrease in cooling rate due to release of latent heat as the primary plates were formed [DAV 79]. The presence of β layers between the α' plates present in the colony product [FLO 74][DAV 79] clearly demonstrated that diffusion occurred, at some stage, during their growth. These β phase layers were formed as a result of Mo segregation to the β-phase ahead of the advancing α' plate interface, stabilising the β-phase. The colony areas of lath martensite exhibited extensive surface tilting, but the tilting was much less regular than in acicular martensite α' plates. It was also proposed that diffusion following the initial growth by shear of the acicular martensite plates relieved the shape strain and resulted in low dislocation density in the colonies, fact which was observed experimentally. Since it is well established [FLO 74][DAV 79] that the α' formed in β by shear or diffusion both have the same orientation relationship, $(0001)_{\alpha'}//(011)_{\beta}$ and $<11\bar{2}0>_{\alpha'}//<11\bar{1}>_{\beta}$, and habit plane, near $\{334\}_{\beta}$}; it is possible that the transition from shear to diffusional growth, and vice-versa, is not sharply defined and the relative contributions of shear and diffusion to the growth of α' plates cannot be distinguished. The precise effect of the diffusional component on the martensite transformation is not known, but must play a part in the nucleation and growth when the diffusional curve is crossed first. For slightly faster cooling rates, the Ms is crossed first, but the diffusional curve may be crossed before Mf is reached, so there would be a diffusional component of the transformation following the martensite nucleation (see figure 2.5.1.2.1). Increasing the Mo content decreases both the Ms and the critical cooling rate and, therefore, completely shear transformations can happen.

C.Jourdan et al. [JOU 91] studied, in situ, the nucleation, variant selection and the orientation memory effect during the β <=> α martensitic transformation in pure Ti. They observed, via synchrotron X-ray topography, the presence of shape deformation for the α<=>β transformation . At the onset of the α->β transformation β crystals are isolated in the parent phase. As the transformation progresses, new β crystals appear between the original ones. The nucleation of new β crystals induces deformation of the β phase initially formed. They conclude that this deformation might be induced by mutual

shape deformation (between α/β) and by the fact that adjacent little β crystals have nearly the same orientation (the common grain boundaries are low angle grain boundaries which possess long range stress field). For β–>α, they deduced that the development of α phase follows a similar procedure, so that one would expect deformation of both the α' plates and of the β phase. Additionally, they did not observe either the presence of homogeneous or autocatalytic nucleation, and they defined the nucléation of martensite as heterogeneous. In previous papers [JOU 87][JOU 89] they had showed that the nucleation of martensite was induced by the stress field associated with crystalline defects. After nucleation, the growth of a new phase involves the deformation of the surrounding matrix and, generally, this shape deformation is relaxed by the nucleation of new variants so that the mutual deformations are self compensating [JOU 91]. In pure Ti this effect seemed inoperative as they observed the presence of only one α single crystal after a α<=>β cycle (the β(bcc)–>α(hcp) transformation can produce 12 variants, while the reverse reaction hcp->bcc can generate 6 variants). One of the possible explanations given by the authors [JOU 91] to explain this severe selection of variants is that the stability of the crystal lattice seems to be closely related to its elastic anisotropy. The large softening of the shear elastic constants at the transformation temperature (Ms) along certain preferential directions should induce the martensitic transformation. It has been shown, for instance, that the C_{66} shear modulus in the α phase, which represents the active shear system $\{10\bar{1}0\}\langle 11\bar{2}0\rangle$ in the α–>β transformation, is the most temperature sensitive. The structural forces (shape deformation and interfacial surface energy) opposing to a phase transformation are directly related to the shear moduli and they are expected to decrease rapidly around Ms. This differential dependence of the shear moduli with the temperature was also observed for β –> α transformation [FIS 69].

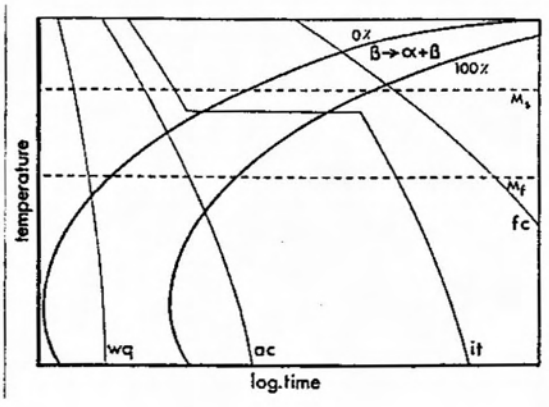

FIGURE 2.5.1.2.1- SCHEMATIC TTT CURVE FOR DILUTE TI-MO ALLOY [FLO 74].

2.5.1.3. Formation of α plates by diffusion

At only modest undercoolings (~10°C) below transus β/α+β temperature, the pro-eutectoid reaction in Ti-X alloys produces α sideplates, and, at somewhat larger undercoolings, intragranular plates also appear. Far more so than in the proeutectoid ferrite reaction in steel, sideplates and intragranular plates are the predominant morphology during the proeutectoid reaction in Ti-X alloys at all but the smallest undercoolings [FUR 90].

H.I.Aaronson et al. [FUR 90] analysed the interfacial structures of proeutectoid α plate formed by diffusion. They investigated the interfacial structure of α plates formed from a β matrix in Ti-Cr, Ti-Fe and Ti-Co. Partially coherent α/β interphase boundaries were shown to be present at both the broad faces and the edges of α plates. The OR between α and β was given by:

$$(0001)_\alpha // (0\bar{1}1)_\beta, [11\bar{2}0]_\alpha // [111]_\beta.$$

Ledges and misfit dislocations were observed on the broad faces of α plates in Ti-7.2wt%Cr alloys (T_0 between 200-340°C) and Ti-5.2wt%Fe (T_0 smaller than 100°C) reacted at respectively 585°C and 550°C, so that the isothermal reactions took place above T_0. They concluded that there are increasing indications that the migration of the α/β interface in the diffusional proeutectoid transformation takes place by means of the formation and lateral spreading of growth ledges.

Two works tried to prove that growth by diffusion can also occur at temperatures lower than T_0. Enamoto et al. [ENO 90] analysed the composition of α plates formed isothermally in Ti-binary alloys. They reported for a Ti-5.4at%V alloy (T0~730-735°C and Ms~630-700°C) and a Ti-2.6at%Fe alloy (T0~580-660°C and Ms~510-630°C) that solute partitioning occurred between α plates and the β matrix during the growth of α plates in a wide temperature range, even at temperatures more than one hundred degrees below T_0, the maximum temperature at which the composition invariant transformation is thermodynamically possible.

The solute concentration in the α plates was measured using a STEM (Hitachi 700H equipped with KEVEX X-ray analyser at 200KV, with beam diameter not larger than 50 nm and presenting a lower detectable limit of solute concentration between 0.3 and 0.4at%). They observed that the

solute concentration in the α plates was already close to equilibrium* after very short reaction times at temperatures below T_0 and even below Ms, as for instance:

- after 30 seconds at 680°C and after 3 minutes at 540°C : Ti-5.4V alloy
- after 20 seconds at 540°C and after 2 minutes at 340°C: Ti-2.6Fe alloy.

No evidence of partial partitioning of solute, i.e., the partitioning halfway toward equilibrium, was observed along α plates, suggesting diffusional nucleation and growth.

In other work, following a similar fashion, M.Enomoto et al. [ENO 91] studied the solute partitioning during the proeutectoid α transformation in ternary Ti-5at%Al-(2.5at%Fe or 2.5 at%Cr) and Ti-4at%V-(2.5at%Fe or 2.5at%Cr). Isothermal heat treatment following solution treatment in the β field, with no quenching in between, was applied to the samples. The alloying element concentration in the α grain boundary allotriomorph, α sideplates and intragranular α plates formed from the β matrix between 500 and 700 °C was measured by STEM-EDX. The Ti-5at%Al-2.5at%Fe alloy (T_0=583°C and Ms~560-680°C) reacted for 30 seconds at 500°C presented a microstructure composed of thin long intragranular α plates lying in one or two crystallographic directions and presenting a small amount of retained β between the plates. The alloying elements concentration in the α particles were observed to be close to the α/(α+β) phase boundary composition. On the other hand, the concentrations in the β matrix were mostly within the (α+β) two phase region. They explained that this is obviously because the measurements were made before the final equilibrium was achieved and that these data points for the matrix are seen to move towards β/(β+α) boundary as the reaction time is increased. If these α particles were formed with the full supersaturation of solute, α phase would present concentration gradient perpendicular to α/β interface. They concluded that the massive or martensitic transformation is unlikely to be the major transformation mode in the substantial temperature range below T_0 in these alloys.

At the end of this section on decomposition of β phase , it is worth quoting Z.Nishyiama [NIS 78] "Although the martensitic transformation

* In the diffusionless mechanism of plate formation, it is postulated that plates are formed with supersaturation of solute (in a extreme case with a composition identical to the matrix) and, subsequently, solute atoms are drained from the plates by diffusion.

occurs by the rearrangement of atoms by cooperative motion, some atoms involved in the transformation may move independently. There remains the question how to combine the cooperative motions with the independent movements of atoms in the theoretical treatment of the transformation. If we succeed in answering more detailed crystallographic observations in the thermomechanical and kinematic treatment, a more complete theory of martensitic transformations will have been established". Some recent progress has been made on the roles of shear and diffusion on the formation of plate-shape precipitates. Christian [CHR 94] remarked that even when atomic mobility is high, some ordered products or precipitates still exhibit shape changes with appreciable shear components. He suggested the existence of a new category of transformations, called diffusional-displacive, to deal with this transitional situation. It seems worth mentioning that this model would help to establish a thermomechanical treatment for the martensitic reaction itself. His recent suggestion very much resembles the comments made by M.K.McQuillan [McQ 63] in 1963 about the morphologies of α' formed during quenching of Ti-alloys. Diffusion seems to occupy indeed a very important part in the thermodynamics of $\beta \rightarrow \alpha$ transformation in Ti-alloys either by changing the conditions for further nucleation and growth of α' plates by shear or by controlling the nucleation and growth of α' plates. This appears to make Ti-alloys a fruitful class of alloy to study as a source of further important developments in the theory of phase transformation.

2.5.2. Ordering reaction of Ti_3Al

In a binary solid solution AB which presents preferential atomic bonds, the heat of mixing of the system is primarily due to the bond energies between adjacent atoms. If the heat of mixing is endothermic, the atoms in solution will prefer to be surrounded by atoms of the opposite type, generating, therefore, a certain degree of ordering in the system in order to maximise the number of A–B bonds. Furthermore, a parameter **s** (short–range order) can be defined to quantify the degree of ordering achieved in a particular system. If each kind of atom in the solution ideally occupies only predetermined sites of a particular lattice, the solution is considered to be a ordered phase and a long–range order parameter (**L**) can then be defined to quantify the degree of order of this phase, whose lattice is defined as a superlattice [POR 81]. Increase in temperature causes a continuous decrease of the long–range order until, above a certain critical temperature, there is no long–order at all. This phenomena occurs because the effect of entropy on free energy becomes increasingly more important at higher temperatures. In order to increase the entropy of mixing, some atoms interchange positions and end up located on wrong sites [BRA 34].

There are two possible mechanisms for creating an ordered superlattice from a disordered solution: either by a continuous increase in short–range order by local rearrangements occurring homogeneously throughout the crystal, which finally leads to long–range order (in a mechanism equivalent to spinodal decomposition and operative in second order transformations or at very high supercoolings below Tc), or by the formation of ordered domains in a process of nucleation and growth. The second mechanism is believed to be most common. When domains meet during growth, their respective sublattice occupancies are either in phase or out of phase. The latter defines the existence of a boundary called thermal antiphase boundary (APB), which presents an APB energy associated with "wrong" nearest neighbour bonding.

The Al-Ti system presents four ordered aluminide phases[GOL 61][GEH 70] [MUR 87a]: **Ti_3Al**, an ordered $D0_{19}$ hexagonal structure based on Ti(α), and also designated α2 with a P63/mmc space group ; **TiAl**, an ordered $L1_0$ fcc phase of homogeneity range approximately 48 to 68at%Al; **$TiAl_2$**, an ordered fcc phase ; and **$TiAl_3$ -(α2)**, a stoichiometric phase with DO_{22} ordered fcc structure.

The ordering reaction α->Ti_3Al was studied by M.J.Blackburn [BLA 67b] and by S.M.L.Sastry and H.A.Lipsitt [SAS 77]. In both studies the reaction was found to be by nucleation and growth. The reaction is so rapid that sometimes, depending on chemical composition, it cannot be suppressed

during quenching from a disordered single phase field (α or β), generating small ordered domains of α2,whose diameter varies from 30 to 70A [WIL 72][BLA 67b][SAS 77]. Isothermal treatment in the α+α2 phase region produces a microstructure consisting of ordered α2 phase dispersed in a disordered α matrix. The size, distribution and morphology of the ordered phase depend strongly on the heat treatment, on the type of nucleation sites (heterogeneously nucleated α2 particles have diameters two to three times larger than average) and aluminium content (the size and volume fraction of the α2 particles increase with Al content) [WIL 72][BLA 67b][SAS 77].

In duplex α+α2 alloys, the microstructure consists of either a uniform dispersion of coherent α2 precipitates, homogeneously nucleated, or a heterogeneous dispersion of larger α2 precipitates, nucleated at grain boundaries and sub-boundaries, and smaller α2 precipitates, formed intergranularly [WIL 72]. The type of precipitation is controlled by the chemical composition and heat treatment temperature, so that, if the ageing temperature is higher than the coherent solvus, the precipitation is heterogeneous [LUT 70] (see figure 2.5.2.1). The morphology of α2 particles varies from spherical to ellipsoidal as the particles become larger. The major axes of the ellipsoids are seen along $[0001]_\alpha$ while the minor axes lie in the basal plane. The faces of these ellipsoids tend to be parallel to the $(10\bar{1}0)_\alpha$ and $(11\bar{2}0)_\alpha$ planes. Up to a size of ~ 120nm these particles are still coherent with the matrix and strain contrast can be observed [BLA 67b].

The isothermal heat treatment of the small domains obtained on quenching in the single α2 field produces domain growth, separated by a metastable array of APB's. The size of these small ordered domains increases with the square root of the annealing time. With prolonged ageing it is possible to reach a situation where each grain becomes a single ordered domain. As the Al content is reduced, the APB's become more stable [BLA 67b]. For a constant ageing temperature, the higher the Al content, the higher the ordering temperature. So, it seems reasonable to assume that both the long range order parameter and the APB energy increase with the Al content for a given temperature. As the driving force for the growth of ordered domains is determined by the APB energy, it is not surprising that binary alloys containing lower Al present more stable APB's. The growth of the small ordered domains minimise the APB energy per unit volume, while the morphological change from spherical to ellipsoidal, caused by the preferential growth of the particle along $[0001]_\alpha$ direction, occurs to minimise the elastic strain energy related to the α/α2 interface [WIL 72][BLA 67][SAS 77]. The α2/α misfit is 0.35% parallel to [0001] and 0.83% perpendicular to [0001]. Ternary additions can alter the morphology of α2 precipitation, more

specifically the precipitate aspect ratio and particle size. For instance, Sn causes the α2 misfit to become more isotropic whereas Ga causes it to become more directional and larger along [0001]. As a result, the former promotes a nearly equiaxed precipitation, with some precipitates showing irregular semi-coherent α/α2 interfaces [WIL 85].

J.C.Williams [WIL 85] mentioned that in the Ti-Al system containing from 22 to 27at%Al, since the nucleation of α2 during quenching is homogeneous, there appears to be little or no effect of the martensitic substructure on the α–>α2 ordering reaction or subsequent domain coarsening. In contrast, the ternary addition of β-stabilising elements such as Mo, Nb and W results in a significant gradient in antiphase domain size from edge to centre of the martensite plates. In addition, the domains near the boundaries are elongated, which suggests heterogeneous nucleation of α2. He also pointed out, in a rather generic way, that increasing amounts of ternary alloying elements leads to a reduction in the volume fraction of the α2-phase in quenched alloys. He proposed that this effect could be understood by the decrease in Ms, so that the disordered α-phase would exist for less time at temperatures where atomic mobility is high enough to permit the short range diffusion. He obviously ignored the effect of ternary addition on diffusion coefficients and also the hypothetical situation where the ternary addition promotes a peritectoid reaction (β+α2–>α), which would allow α2 to form during quenching at temperatures higher than Ms. Additionally, ternary additions may favour heterogeneous nucleation of α2, enabling the reaction to occur at lower undercoolings.

The Ti-aluminides are being considered as potential replacement materials for Ni-superalloys and conventional Ti-alloys [ARR 93] . Low ductility and fracture toughness properties near room temperature are the main obstacle to the use of Ti_3Al based Ti-alloys. Other major problem for α2 based alloys is their relative poor oxidation resistance at temperatures of 650°C and above [PEN 93]. Although better than conventional titanium alloys, the α2 titanium aluminide alloys do not have the required oxidation resistance to challenge the supremacy of Ni-based super-alloys in the hotter parts of a gas turbine engine [CHA 93]. H.A.Lipsitt [LIP 85] stated that intermetallics are particularly suited to high temperature application due to the modulus retention with temperature and the high activation energy required for diffusion. Both properties derive from the ordering of the structure, caused by the strong chemical bond between unlike atoms. However, in many intermetallics this strong bond also causes the low ductility at room temperature.

Many studies have been carried out to identify the deformation mechanisms of Ti_3Al and to explain why the ductility of Ti_3Al at low temperatures is rather low when compared to others hcp systems. Generally, the hcp systems slip on {0001} (basal), $\{10\bar{1}0\}$ (prism), and $\{11\bar{2}1\}$ (pyramidal) planes in directions $<11\bar{2}0>$, <0001> and $<11\bar{2}3>$ respectively [HUL 81]. DO19 systems are expected to slip on the same planes and directions (care must be taken once one of the lattice parameters of DO19 system is twice the hcp, $a_{DO19} \sim 2xa_{hcp}$, and although the indexes are the same, the directions and planes are not always equivalent). Activity of dislocations having Burgers vector other than $1/3<11\bar{2}0>$ for hcp systems, or $1/6<11\bar{2}0>$ for hcp-$D0_{19}$ systems, is necessary to satisfy the requirement of five independent slip systems for complete slip transmittal across arbitrary grain boundaries [KER 84]. Deformation studies on Ti_3Al have shown that the brittleness of Ti_3Al at low temperatures (T<700°C) is explained by the inactivity of $1/6<11\bar{2}3>$ and 1/2<0001> dislocations [KER 84]:

- The $<11\bar{2}0>\{10\bar{1}0\}$ slip system is the dominant mode of deformation [SAS77][LIP 80][LIP 85]. H.A.Lipsitt [LIP 85] explained that the highest density of dislocations was on the prism planes because such movement produced no wrong first near neighbours;
- The transition brittle->ductile of Ti_3Al, occurring around 700°C, is due to the presence of $1/6<11\bar{2}3>$ dislocations on the pyramidal planes [SAS 77][LIP 80].

H.A.Lipsitt [LIP 85] suggested that the first step on the development of α2-based alloys must focus on lowering the temperature at which the "non-basal" slip appeared in quantity. A.Khataee et al. [KHA 88] noted that enhanced ductility may be achieved through modification of slip systems by using alloying elements, and/or the production of fine scale microstructures to disperse the slip. Several possibilities for this refinement were listed by P.L.Martin et al. [MAR 80]: grain refinement by cold working; microstructural control via heat treatment; and precipitation of second phase particles. The ideal aluminide alloy should present room temperature ductility; microstructural stability at working temperatures besides its usual properties of strength and creep resistance at high temperatures.

G.Lütjering et al. [LUT 70] studied the interaction between moving dislocations and the ordered particles in $\underline{\alpha+\alpha 2}$ alloys mechanically tested at room temperature. They showed that:

- For samples heat treated at temperatures below the coherent solvus (see figure 2.5.2.1), the interaction mechanism between dislocations and ordered particles was by a cutting mechanism, which caused premature failure. The slip was shown to be predominantly of $<11\bar{2}0>\{10\bar{1}0\}$ type.

Shearing of grain boundaries resulting from the high stress concentration at the head of dislocation pile–ups were also observed;

• For alloys heat treated shortly below line B in figure 2.5.2.1, the particles were by–passed by dislocations, which formed loops around the particles. The distribution of dislocations in these samples was remarkably homogeneous. The slip systems operating for this condition were identified as $<11\bar{2}0>\{10\bar{1}0\}$ and {0001} and the samples presented better elongation to fracture;

• The highest increase in elongation was obtained for the alloy Ti–16.5at%Al–1.5%Si, which after an annealing treatment at 900°C for 100h showed a total plastic elongation of about 7% at room temperature (see table 2.5.2.1). The slip systems operating in all alloys which presented a total plastic elongation higher than 2% were identified as $(0002)\ 1/3<11\bar{2}0>$; $\{10\bar{1}0\}\ 1/3<11\bar{2}0>$; $\{10\bar{1}1\}\ 1/3<11\bar{2}0>$; and $\{10\bar{1}0\}\ 1/3<11\bar{2}3>$. No evidence of the presence of silicides particles was observed.

alloy (at%)	ageing treatment	α2 diameter (nm)	α2 length (nm)	interparticle distance (nm)	volume fraction of α2 (%)	elongation ε(%)
Ti-18Al	900°C-100h	130	600	200	20	3.0
Ti-18Al-1Zr	"	140	400	200	20	5.8
Ti-16.5Al-1.5Si	"	160	550	225	18	7.0

Table 2.5.2.1. Relationship between size and distribution of α2 particles & the total plastic elongation at room temperature for α+α2 alloys [LUT 70].

It is concluded that the influence of the dislocation–particle interaction on the strength properties of these alloys did not appear to depend on the type of slip system which is operative, but on the type of dislocation distribution. A more uniform distribution could be achieved by controlling the particle size and distribution in order to induce a dislocation by–pass mechanism. It can be suggested from the results shown above that a smaller length/diameter ratio might cause a more uniform dislocation distribution. Other suggestion is that Si is more effective than Zr, as a ternary addition, in increasing the stress field (around the α2 particles) which interacts with the dislocations.

S.M.L.Sastry and H.A.Lipsitt [SAS 77] studied the influence of Nb on the microstructure and properties of Ti_3Al alloys. They showed that the addition of Nb induced a change of morphology on the quenched samples from lath martensite to a very fine acicular martensite refining therefore the slip length. The alloying with Nb also slowed down the domain growth kinetics, promoting a more refined domain size after ageing in the single

phase α2 field. The analysis of dislocation structures of unalloyed and alloyed specimens deformed at 700°C showed that:

- A high degree of planarity of slip and the absence of extensive slip with vectors other than <11$\bar{2}$0> are responsible for the limited ductility observed in unalloyed specimens;
- There was an indication of the presence of "c+a" dislocations in alloyed samples, but no detailed dislocation analysis could be carried out. The decrease in the degree of planarity of slip and the significant activity of non–basal slip vectors were considered responsible for the improved ductility of these samples.

P.L.Martin et al. [MAR 80] reported a similar study, but adding W along with Nb. The quenched sample showed a rather refined martensitic microstructure. Annealing the quenched sample at 900°C caused heterogeneous nucleation of β phase, which is stabilised due to the partitioning of Nb and W. Tensile tests showed a modest increase in ductility and a significant increase in strength for the quaternary alloy. They concluded that additional slip length refinement can be obtained through the secondary precipitation of stable β phase. The design of alloys with some room-temperature ductility has centred around stabilising the ductile high temperature phase β, into equilibrium with the α2 structure [THO 93]. Nb has found favour as a β-stabiliser, since it also increases the non-basal slip activity in the α2 phase. Additionally, Nb enhances oxidation resistance of Ti_3Al [VER 93][CHA 93]. So, it is not surprising the fact that Ti_3Al-Nb alloys form the basis of current research into α2-based titanium aluminides. Two commercial alloys have been produced: Ti-24Al-11Nb, and Ti-25Al-10Nb-3V-1Mo (Super α2). They show a good balance of elevated temperature rupture strength and room temperature ductility [CHA 93]. The addition of β-stabilisers leads to the formation of a two phase microstructure consisting of the ordered phases α2 and β2(bcc). In this case of super-α2 alloys, bi-modal microstructures, consisting of equiaxed primary α2 in a lamellar matrix of α2 and β2, are supposed to present the best combination of strength, room temperature ductility and creep resistance [PRO 93].

Deviation from stoichiometry is another one of the parameters that may enhance the plasticity of α2 ordered phase, as the introduction of lattice defects may change the deformation mechanism and therefore the fracture behaviour. The improvement in ductility of sub-stoichiometric Ti_3Al+V α2+β2 alloys was mainly attributed to an increased activity of "c+a" dislocations on {11$\bar{2}$1} pyramidal planes. It was assumed that deviation from perfect order in sub-stoichiometric Ti_3Al+V may reduce lattice frictional

stresses thereby enhancing dislocations mobility and improving plasticity [EHR 93].

D.J.Arrell et al. [ARR 93] studied the role of silicon in Ti_3Al+Nb based alloys. They concluded that addition of 0.9at%Si to the Ti-20Al-11Nb alloy significantly enhanced its ductility at room temperature. This result was explained by the formation of an orthorhombic phase (O phase) replacing the ordered bcc phase (β0). At silicon levels of 1.2at% and above, the precipitation of titanium silicide particles produced degradation in both tensile strength and ductility [ARR 93]. Finally, Thomas mentioned that the determination of the α2+β(β2)/β(β2) transus in Ti_3Al-based alloys with increasing Nb content from 5 to 17at%Nb has been very useful for determining both the thermochemical and heat treatment conditions required to optimise the microstructure. For a successful development of new Ti_3Al based alloys, the knowledge of the phase boundaries should be extended to Ti-Al-X (X=Mo, V, Ta, Fe, etc.) alloys systems other than Ti-Al-Nb.

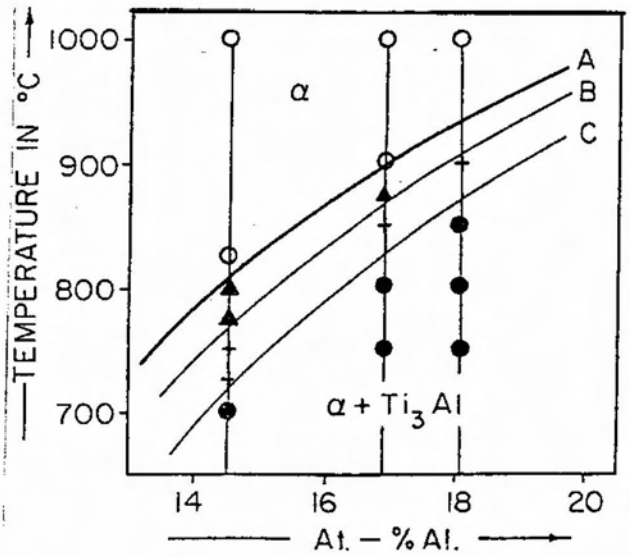

FIGURE 2.5.2.1. SECTION OF TI–AL PHASE DIAGRAM SHOWING THE NUCLEATION BEHAVIOUR OF THE α2 PHASE [LUT 70]:

- Region A–B: only on dislocation and boundaries;
- Region B–C: preferred on dislocation and boundaries, later throughout the matrix;
- Region below C: simultaneously on dislocation and boundaries and throughout the matrix.

2.5.3. Precipitation of silicides

Silicon is a common alloying addition to Ti–alloys destined for elevated temperature applications. It is an effective strengthening agent in solid solution and, at high temperatures, it appears to segregate to mobile dislocations, reducing their mobility and improving creep resistance [CHU 88]. Additionally, the precipitation of silicides from the supersaturated matrix may result in dispersion strengthening and microstructural stability at elevated temperatures [CHU 88].

H.M.Flower et al. [FLO 71] studied silicide precipitation during ageing of quenched samples the Ti–Si, Ti–Al–Si, Ti–Zr–Si, Ti–Zr–Al–Si and Ti–Zr–Al–Mo–Si systems. The silicide precipitation of the binary alloy was extremely slow and entirely heterogeneous. The titanium silicides seemed to nucleate preferentially on [0001] dislocations and in martensite plate boundaries, and to grow as rods along the $<11\bar{2}0>$ directions. The silicide distribution was found to be basically two dimensional. The silicides were identified, through electron diffraction, as Ti_5Si_3 (hcp with **a**=4.29A and **c**=5.139A) with the following orientation relationship:

$$(01\bar{1}0)\alpha' \,//\, (01\bar{1}0)Ti_5Si_3$$
$$(2\bar{1}\bar{1}0)\alpha' \,//\, (2\bar{1}\bar{1}\bar{1})Ti_5Si_3$$

Increasing ageing temperature, from 550 to 650°C, produced coarser precipitation of Ti_5Si_3 particles, which were formed more rapidly. Increasing silicon content increased the nucleation of Ti_5Si_3 particles and produce more homogeneous distribution of precipitates. The latter was explained by the increase of supersaturation of the matrix, which caused an increase in both the dislocation density of the quenched samples and the driving force for Ti_5Si_3 precipitation [FLO 71]. They also observed that ternary addition of Al slowed down the kinetics of silicide precipitation and accentuated the nucleation heterogeneity. Ageing the alloy Ti-5Al-1Si at 550°C for two weeks produced the precipitation of very few silicide particles confined almost entirely to grain boundaries. Some hypotheses were considered to explain the effects of aluminium on silicide precipitation:

- Aluminium would increase the solubility of silicon in α phase.
- Aluminium would reduce the atomic mobility, either by being incorporated into the precipitate or by reducing the atomic mobility of silicon in the matrix.

Finally, they observed that the ternary addition of zirconium (Ti-5Zr-1Si alloy) produced a finer and more tridimensional dispersion of $(TiZr)_5Si_3$, which grew more slowly. The Zr addition changed the orientation

relationship between silicide and matrix and induced the precipitation of a second silicide precipitate (hcp with a=7.0A and c=3.6), which was present together with $(TiZr)_5Si_3$ in the ternary alloy. At temperatures below 550°C, this ternary addition produced a homogeneous nucleation of coherent precipitates.

The presence of Ti_5Si_3 instead of Ti_3Si (the stable phase in the Ti–Si phase diagram, see figure 2.3.4) seems to be caused by the rather slow precipitation of the latter. M.Pajunen et al. [PAJ 89] made some thermodynamic and kinetics considerations of Ti–Si diffusion couples. He observed the formation of Ti_3Si, in a sample made of commercial purity titanium, after 32 hours annealing at 1100C. For samples made of high purity titanium, Ti_3Si phase could not be observed even after 100 hours annealing. N.H.Salpadoru et al. [SAL 95] observed formation of Ti_3Si in Ti-Si binary alloys after 99 days at 800°C, while Svechnikov et al [SVE 70] observed Ti_3Si precipitation after 115h at 1000°C, but not after 200h at 800°C. These results show that the precipitation of Ti_3Si is sluggish and dependent on the presence of impurities

L.S.Chumbley et al. [CHU 88] studied the crystallography of Ti_5Si_3 in Ti–Si alloys over the range of ageing temperatures. He observed two morphologies of "stable" silicides: rod like, as reported by H.M.Flower [FLO 71] for temperatures above 700°C; and hexagonal–shaped plates at lower temperatures (500–600°C). The latter showed:

- An orientation relationship differing from that responsible for the rod morphology;
- Preferred heterogeneous nucleation on $c[0001]_{\alpha'}$ and $a/3\langle\bar{1}2\bar{1}0\rangle_{\alpha'}$ dislocations, both within the tempered martensite α'; and at both lath and grain boundaries.

They concluded that the lattice parameter ratio $\mathbf{a/a_0}$ (a= lattice parameter of silicide; a_0= lattice parameter of α' matrix) determines the extent of the lattice misfit along key parallel directions in precipitate and matrix lattices. Figure 2.5.3.1. shows that a large initial value of $\mathbf{a/a_0}$ would favour the adoption of the hexagonal plate morphology, while lower values of this ratio would favour precipitate rods.

So, in order to optimise the creep resistance of aluminide alloys, it seems that a coherent–type silicide precipitation, completely homogeneous and widely dispersed, with a rather sluggish coarsening rate would be tempting. To achieve this ideal precipitation, it is likely that additions of Nb and Zr should be used.

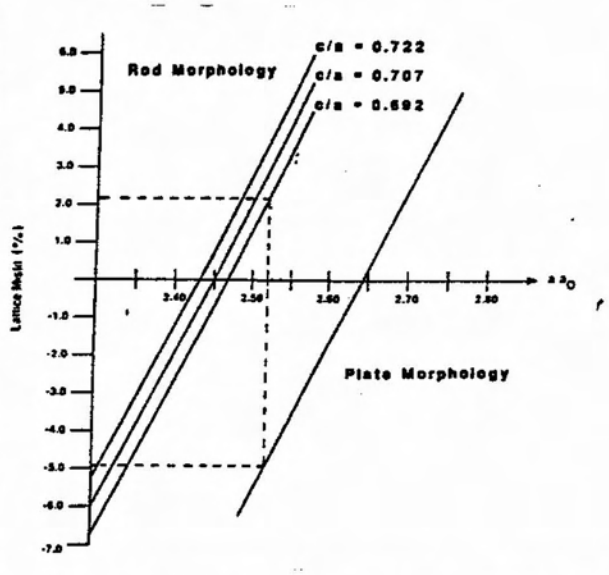

FIGURE 2.5.3.1. PLOT OF LATTICE MISFIT vs. THE RATIO a/ao FOR TWO MORPHOLOGIES OF Ti_5Si_3 [CHUM 88].

2.6 Thermodynamic modelling of phase diagrams

Thermodynamic calculations of phase diagrams have become a very useful tool for checking the validity of proposed phase boundaries, or for predicting portions or whole phase diagrams of many systems. As computer programs become more sophisticated and accessible, thermodynamic modelling is performed more often. This leads to attempts to adjust or check experimental phase boundary data [OKA 91]; and even to construct a general thermodynamic data bank to produce phase diagrams and a large variety of thermodynamic quantities [HIL 86]. These computer techniques also allow a more rational way of devising sets of critical experiments for the accurate determination of phase diagrams. It must be realised that the complete experimental investigation of even a simple ternary system may cost several man-years. Hence, a combination of computation and critical experiments is crucial in the determination of ternary and higher order phase diagrams [LUP 83].

Computer programs permit the derivation of thermodynamic functions of phases by optimising the input data of some of their measured thermodynamic properties available in the literature; and/or by making use of experimental data of portions of the phase diagram[OKA 91]. It is not rare, however, to find thermodynamic models that involve functions with parameters of inconceivable magnitude. Such functions would not be appropriate if they were used for purposes other than phase diagram modelling, as, for example kinetic calculations or prediction of

thermodynamic properties [OKA 91]. M.Hillert [HIL 86] warns that one should be cautious when using the adjustable parameters of a particular model for the prediction of thermodynamics properties. He explains that, for instance, it is possible that sometimes more than one model can successfully describe the experimental information on a certain system. This situation would not produce any insight in the physical nature of the solution. Nevertheless he points that it is legitimate to use a purely "mathematical" model opposed to a physical model as long as it is capable of describing the experimental information and it can be used to predict further information under conditions not studied directly by experiments.

H.Okamoto [OKA 91] emphasises that the simpler the thermodynamic model, the easier the examination of the thermodynamic and physical properties associated with the system under examination will be. M.Hillert [HIL 86] concludes that the sounder the physical model underlying the mathematical model, the safer the predictions will be. The essential property of the models is the ability to describe experimental information and allow extrapolation from these data. In a not so recent review of alloys modelling, B.Sundman [SUN 90] stated that a large number of thermodynamic models have been developed for alloys and related systems. He adds that these models are, however, very similar to each other, and that in the near future the number of models used will be quite small. This would improve the cooperation towards a generally applicable thermodynamic database and would allow the development of new materials with better properties and at a lower cost.

Among the difficulties found for the formation of a general thermodynamic data bank, M.Hillert [HIL 86] reported: the definition of the thermodynamic function to be used for the data storage; the self-consistency of all information contained in the database in order to assess higher order systems; the compatibility of mathematical models so that it is possible to combine them in order to describe a higher order system; the choice of a simple but effective model which does not grow very complex for higher order systems; and finally the fact that any new information or improvement of a model may justify the revision of a lower order system, and, as a consequence, the reassessment of all the higher order systems. There are, however, few thermodynamic data banks and software available at the market at the moment that were constructed with a high degree of generality in mind to deal with computer modelling of phase diagrams or, more appropriately defined computer modelling of thermodynamic properties of phases. These softwares and databases are available for use

either on on-line access through modem or on a personal computer version. Among the software and database packages one could mention:

- ChemSege, developed by the Institute of Theoretical Metallurgy, Technical University, Aachen;
- LUKAS [LUK 77] developed by Hans Leon Lukas, Max-Planck-Institute, Stuttgart;
- THERMO-CALC [SUN 85] developed by the Département of Materials Science, Royal Institute of Technology, Stockholm, Internet home page address- http://balrog.met.kth.se/tc/;
- FACT [PEL 86] developed by the Centre de Researche en Calcul Thermodynamique, Ecole Polytechnique, Montreal;
- MTDATA, developed by the Division of Materials Metrology, National Physical Laboratory, Middlesex.

There is also a consortium of centres, Scientific Group Thermodata Europe (SGTE), engaged in the development of thermodynamic data banks in Europe. One of the aims of the SGTE group is the cooperation in a broader international effort to unify thermodynamic data and assessment methods.

Once all the selected experimental data have been inputted into the programme and all the parameters of the thermodynamic functions of the phases under investigation have been calculated and optimised, one must decide when the assessment of a particular phase diagram is finished. B.Sundman [SUN 90] concluded that there are no finished assessments in the literature and that all the results presented from such practice represent the situation when the assessor had to stop work either through lack of funding or interest.

2.6.1. Thermodynamic models for solid solution

Theoretical methods for the prediction of phase diagrams mean, in a rigorous sense, the quantum mechanical calculation of thermodynamic functions on the basis of well-defined parameters of the constituent elements. However, even for binary system, there is no way to use such theoretical methods for every binary combination of elements. So, the theoretical methods must be used more in a sense of qualitative and quantitative representation of measured data for extrapolation procedures [HEN 79]. These analytical representations may be based on models, such as regular solution, sub-regular solution and cluster variation method, or on purely mathematical expressions using different kinds of power series. Differences in representations are not really in the physical meaning of the coefficients but more in the prior limitation of the number of coefficients used [HEN 79]. In the development of a model, many assumptions have to be made. A model with too many simplifying assumptions may not represent

the data adequately. On the other hand, a model that is too realistic is often mathematically intractable or introduces too many parameters, so it seems that a compromise is usually necessary [LUP 83]

During modelling, each phase of a system must be modelled separately as well as each compound. As most solid solution phases are stable only within a limited composition range, it is often necessary to make assumptions of its properties outside its stability range [SUN 90]. Once one or more models have been chosen to describe thermodynamically each phase and component of the system, one starts the calculation by applying a set of arbitrary values for the parameters of the Gibbs free energy of each phase. These parameters should then be optimised by means of iterative techniques, such as least-square method, to give the best fit between the calculated equilibrium and all the experimental information available [HIL 79][HEN 79].

The first model to be investigated is the ideal solution one. This model corresponds to a statistical model in which the atoms are distributed at random on lattice sites and there is no energy change associated with a rearrangement of the atoms [LUP 83]. So, using this model one may describe any particular ideal solution phase as shown by equation 2.6.1. The first term of the equation corresponds to a mechanical mixture of components and it can also be defined as the Gibbs free energy of reference, as it defines a level of reference (line, plane or surface) according to the order of the system. The second term corresponds to the ideal entropy of mixing [PEN 93][HIL 86]. In the ideal solution there is neither heat nor change of volume during the mixing process [LUP 83].

$$G(\text{phase}) = \sum_{i=1}^{m} x_i \cdot G_i^0 + RT \sum_{i=1}^{m} x_i \cdot \ln x_i \quad \text{..... eq.2.6.1}$$

Where: m is the number of components; G(phase) is the Gibbs free energy of mixing of the a particular phase; G^0 is the Gibbs free energy of the pure component i in the same structure as that of the phase under consideration; x_i is the mole fraction of the component i ; T is the temperature; and R is the universal gas constant.

In order to account for the interaction between elements one must use a model that considers the existence of a so called excess Gibbs energy. The excess contribution is the difference between the real and the ideal solution and its value depends on the chosen model. For binary systems, however, all these excess models produce the same result. The Gibbs free energy of mixing of a particular solution phase can be described as shown in equation 2.6.2. [SUN 90].

$$G(\text{phase}) = \sum_{i=1}^{m} x_i \cdot G_i^0 + RT \sum_{i=1}^{m} x_i \cdot \ln x_i + G\text{excess} \quad \text{eq.2.6.2}$$

So, it seems worthwhile to start describing some of the models which regard the excess term. The first one to be considered is the regular solution model. This model tries to account for the non-ideality of a phase by introducing terms in the excess Gibbs free energy that depend on mole fractions. The model assumes the atoms are distributed at random on the sites of a three-dimensional lattice (S_{excess} = zero); there are no vacancies; the energy of the system may be calculated as a sum of pairwise interactions [LUP 83]. The excess term is mathematically described as a function of concentration and it depends on the model used to describe the thermodynamic properties. The simplest description is by a polynomial of the concentration. Table 2.6.1 shows some polynomials which are often used to describe the excess term. Redlich Kister has the advantage that it can be more easily handled [LUK 82]

type of polynomial	analytical expression for the binary excess term **
Margules	$G_{excess}^{1,2} = x_1 \cdot x_2 \cdot \sum_{i=0}^{n} L_{1,2}^{(i)} \cdot (x_2)^i$
Redlich and Kister	$G_{excess}^{1,2} = x_1 \cdot x_2 \cdot \sum_{i=0}^{n} L_{1,2}^{(i)} \cdot (x_1 - x_2)^i$
Borelius	$G_{excess}^{1,2} = x_1 \cdot x_2 \cdot \sum_{i=0}^{n} L_{1,2}^{(i)} \cdot (x_1)^{(n-1)} \cdot (x_2)^i$

** $L_{1,2}^{(i)}$ is the coefficient of binary interaction of order n; and n is the degree of the polynomial.

Table 2.6.1. Types of polynomials for binary excess terms [LUK 82].

The number of terms in the polynomial can be arbitrary high and the greater the number of coefficients, the higher the fit to the experimental data. It is appropriate, however, to point out that increasing the number of coefficients will decrease the significance of each coefficient and that there is an advisable limit. If it is not possible to obtain fit within this limit one should reconsider the model used to describe the phase. In multicomponent systems, for instance, one can introduce an interaction between each pair of constituents and the excess free energy can be obtained as the sum of all binary contributions as shown by the following equation using the Redlich and Kister polynomial [SUN 90]:

$$G\,excess = \sum_{i=1}^{m-1}\sum_{j>i}^{m} x_i \cdot x_j \cdot \{\sum_n (x_i - x_j)^n . L^n_{i,j}\} \quad \text{.....eq.2.6.3.}$$

Where n is the degree of the polynomial, $L_{i,j}$ is the coefficient of binary interaction between the constituents i and j and m is the number of components.

When the species or atoms are different in size, shape, electronegativity, etc., it may be a good approximation to assume non-random mixing of the atomic species and, as consequence, the solution will not have an ideal entropy of mixing. For instance, the quasi-regular solution model [LUP 83] retains the simplicity of the regular model but no longer assumes that the excess entropy is equal to zero, so that the constituents are not mixed randomly. This assumption leads to an equation of the following type:

$$Gexcess = \sum_{i=1}^{m-1}\sum_{j>1}^{m} x_i \cdot x_j \cdot \{\sum_n (x_i - x_j)^n \cdot L^n_{i,j} \cdot [1 - (T/\tau ij)]\} \quad \text{.....eq.2.6.4.}$$

Where T is temperature and τ_{ij} is a parameter linking enthalpy and entropy contributions.

A practical example of phase description seems very useful at this stage. U.R.Kattner et al. [KAT 92] used a regular solution-type model the Redlich and Kister polynomial to describe the disordered solution phases: liquid, Ti-β, Ti-α and Al of the Al-Ti binary system (equation 2.6.5).

$$G(phase) = x_{Ti} * G^0_{Ti} + x_{Al} * G^0_{Al} + RT\{x_{Ti} \ln x_{Ti} + x_{Al} \ln x_{Al}\} + x_{Ti} * x_{Al}\{G_0 + G_1 * (x_{Ti} - x_{Al})\} \quad \text{.....eq.2.6.5.}$$

Where X_i is the mole fraction of i; G^0_i is the reference state of i; and G_0 and G_1 are coefficients of the excess Gibbs energy.

As discussed in the beginning of this section, differences in representations of regular-type solutions are not really in the physical meaning of the coefficients but more in the limitation of the number of coefficients used for the optimisation [HEN 79]. The equation 2.6.5 uses the coefficients, G_0 and G_1, as adjustable variables. These variables can be represented by either a constant or a function of temperature. Table 2.6.2 displays the values of the coefficients, G_0 and G_1,to show how regular solution-type models differ only on the number and type of adjustable variables.

model	coefficient values
Quasi-subregular	$G_0 \neq 0$ and $G_1 \neq 0$; G_0 and $G_1$are represented by a function.
Quasi-regular	$G_0 \neq 0$ and $G_1 = 0$; G_0 is represented by a function.
Subregular	$G_0 \neq 0$ and $G_1 \neq 0$; are both represented by a constant.
Regular	$G_0 \neq 0$ and $G_1 = 0$; G_0 is represented by a constant.

Table 2.6.2. Regular solution-type models.

In the modelling of a ternary solution phase, the description of the adjacent binary solution phases must appear, so it seems useful to consider the properties of the ternary solution as the sum of binary and ternary contributions. Very often it is necessary to modify the binary subsystems when assessing a ternary system. However if a binary subsystem has been used in other ternary assessments, one may not change it without reassessing also these systems, specially when one is developing a general thermodynamic database [SUN 90]. One may describe qualitatively the excess Gibbs free energy for ternary regular-type solutions, as:

$$G\,excess = \sum_{i=1}^{2} \sum_{j>i}^{3} x_i \cdot x_j \cdot L_{i,j} + x_1 \cdot x_2 \cdot x_3 \cdot L_{1,2,3} \quad \text{.....eq.2.6.6.}$$

Where $L_{i,j,k}$ and $L_{i,j}$ are, respectively, the ternary and the binary interaction parameters.

There are many ways to develop the description of ternary and higher order systems, and among them there are two formalisms which seems worth mentioning: Muggianu's and Kohler's. In a ternary solution with A,B and C-neighbours, Kohler's treats the C-neighbours like A (if A-neighbours are predominant), otherwise they are treated like B. Muggianu's treats C-neighbours like an equal mixture of A and B. H.L.Lukas [LUK 82] however, admitted that there is no strong reason to prefer one or other formalism. So, considering the Redlich and Kister polynomial, the two different formalisms when applied for binary systems are shown in table 2.6.3.

formalism	mathematical expression
Kohler's	$G_{excess}^{binary} = x_1 \cdot x_2 \sum_{i=0}^{n} L_{1,2}^{(n)} \cdot ((x_1 - x_2)/(x_1 + x_2))^i$
Muggianu's	$G_{excess}^{binary} = x_1 \cdot x_2 \sum_{i=0}^{n} L_{1,2}^{(n)} \cdot (x_1 - x_2)^i$

Table 2.6.3. Muggianu's and Kohler's formalism for a binary system [LUK 82].

For the description of ordered intermetallic compounds, a more sophisticated approach is usually needed. The Bragg-Williams approximation uses the bond-energy model and has been widely used for description of ordering. In the bond-energy model it is usually assumed that the total energy of the system may be regarded as the sum of the energies of bonds between atoms. W.L.Bragg and E.J.Williams [BRA 34][BRA 35] applied the bond-energy model to ordering by using sublattices and assuming that each sublattice presents random mixing of atoms. The configurational entropy is calculated for each sublattice and the total entropy is then calculating by summing up the contributions of each sublattice multiplied by its site fraction. The site fraction gives the fraction of each component on each sublattice and the fraction of each sublattice in the phase. Only the interaction of species within the same sublattice is usually considered, but interaction between species on different sublattices is also possible and can be described [LUK 82]. The distribution of atoms amongst the sublattices may vary continuously without change of phase, from being random at high temperatures to being partially regular at low temperatures [BRA 34].

Difficulties with the Bragg-Williams approximation arise when this model is applied to a case where the atoms in the two sublattices have a different coordination number [AND 86]. J.O.Andersson et al. [AND 86] concluded that the bond-energy model must be modified in some way. It has also been argued elsewhere [KAT 92] that difficulties also arise when this approximation is used for modelling ordering based on close-packed structures. In fcc ordering reactions, for instance, the Bragg-Williams approximation (considering near neighbour pair-wise interactions) gave a completely unrealistic phase diagram, which remained unaltered by considering higher neighbour pair-wise energy [CAH 79]. To overcome these difficulties with the Bragg-Williams approximation, M.Hillert et al.[AND 86] developed a new model, called compound-energy, which assumes that the energy of a system is mainly given by a weighted average of the energy of compounds. This model when applied to a case with sublattices presenting a constant coordination number, is formally identical to the bond-energy

model under the assumption of random mixing within each sublattice [AND 86]. The basic free Gibbs energy expression for a phase presenting several constituents and sublattices is then given by [SUN 90]:

$$G(\text{phase}) = \sum_I P_I(Y)*G_I^0 + RT\sum_s a_s \sum_i y_i^s * \ln(y_i^s) + G_{excess} \quad \text{.....eq.2.6.7.}$$

Where I is a constituent array which specifies one constituent in each sublattice; Y is the matrix with all constituent site fractions. $P_I(Y)$ is the product of the site fractions of the constituents specified by I, one from each sublattice, so that $P_I(Y) = \prod_i y_i^s$; y_i^s is the fraction of constituent i on sublattice s. G_I^0 is the Gibbs energy of a compound with the constituents given by I. a_s is the relative number of sites on sublattice s.

The first term of the equation 2.6.8 is the state of reference for the Gibbs energy and it might include the energy of formation of hypothetical compounds like B_aA_b. Because of the existence of such compounds in this term, M.Hillert and co-workers [HIL 86][AND 86] referred to this sublattice model as a compound-energy model. The second term expresses the ideal entropy of mixing, which is due to the random mixing on each sublattice, and the last term represents the excess Gibbs energy. The excess Gibbs energy (G_{excess}) in this model is mainly composed of the interaction energy between different components in the same lattice. The interactions between neighbouring atoms in different sublattices are essentially described by the first term of the equation 2.6.8. B.Sundman [SUN 80] defines mathematically the excess Gibbs energy as:

$$G_{excess} = \sum_{Z>0} \sum_{IZ} P_{IZ}(Y)*L_{IZ} \quad \text{..... eq.2.6.8.}$$

Where IZ are high order component arrays and L_{IZ} is the interaction parameter.

It is appropriate to exemplify at this stage the thermodynamic modelling of an ordered phase using sublattices. J.P.Gros et al. [GRO 88] calculated the Ti-rich corner of the Al-Ti binary using a computer-operated optimisation procedure called PARROT and developed by B.Jansson [JAN 84] and an optimisation procedure developed by H.L.Lukas et al. [LUK 77]. The liquid and Ti-β phases were described as quasi-regular solutions, where:

$$G_{excess} = x_{Al}.x_{Ti}.L_{(Al,Ti;0)}$$

Ti-α (hcp) and Ti_3Al(hcp) were described with the sublattice model developed by M.Hillert et al [AND 86] as one single phase undergoing an order-disorder transition. J.P.Gros et al. [GRO 88] considered the Al-Ti system as: having two sublattices (1 and 2); presenting site fractions given by 0.75

and 0.25 respectively; and with the components Ti and Al randomly mixed in each lattice, so that this solution phase could be represented as (Ti,Al).75(Ti,Al).25. They finally described the ordered phase Ti_3Al and the disordered phase Ti-α as:

$$
\begin{aligned}
G(Ti_3Al) = \quad & y^1_{Ti} \cdot y^2_{Ti} * G^0_{Ti_{.75}Ti_{.25}} + y^1_{Al} \cdot y^2_{Al} * G^0_{Al_{.75}Al_{.25}} + \\
& + y^1_{Ti} \cdot y^2_{Al} * G^0_{Ti_{.75}Al_{.25}} + y^1_{Al} \cdot y^2_{Ti} * G^0_{Al_{.75}Ti_{.25}} + \\
& + R.T.\{ 0.75*(y^1_{Ti}.\ln y^1_{Ti} + y^1_{Al}.\ln y^1_{Al}) + 0.25*(y^2_{Ti}.\ln y^2_{Ti} + y^2_{Al}.\ln y^2_{Al}) \} + \\
& + y^1_{Al} \cdot y^1_{Ti} * \{ y^2_{Ti} \cdot L_{(Al,Ti:\,Ti)} + y^2_{Al} \cdot L_{(Al,Ti:\,Al)} \} + \\
& + y^2_{Ti} \cdot y^2_{Al} * \{ y^1_{Ti}\ L_{(Ti:\,Al,Ti)} + y^1_{Al} \cdot L_{(Al:\,Ti,Al)} \} + \\
& + y^1_{Ti} \cdot y^1_{Al} \cdot y^2_{Ti} \cdot y^2_{Al} \cdot L_{(Ti,Al:\,Ti,Al)} \quad \text{.....eq.2.6.9.}
\end{aligned}
$$

Where y^s_i is the site fraction of component i on sublattice s and $L_{A,B:C}$ is the interaction between components A and B of the first sublattice in relation to the component C of the second sublattice. Notice that: the component array is written with a comma "," between components in the same sublattice and a colon ":" between components on different sublattices; a component must not be contained more than once for the same sublattice.

Additionally, the interaction parameters, $L_{(A,B:C)}$ can vary with the temperature and may be given different kinds of composition dependency (Redlich and Kister polynomial under Muggianu's formalism).

$$L(A,B:C) = L(A,B:C;0) + L(A,B:C;1)*(y^1_A - y^1_B) + L(A,B:C;2)*(y^1_A - y^1_B)^2 \quad \text{eq.2.6.10.}$$

Where $L_{(A,B:C;n)}$ is the term of $n^{\underline{th}}$ order of the polynomial expansion.

The same equation (2.6.9) was used for the disordered hcp phase, just assuming that the site fractions of Al and Ti on the sublattices was the same. The equation became identical to a regular solution formed by only "one sublattice". In order to favour the stability of the disordered phase in certain temperature or composition ranges it was necessary to impose some constraints on the interaction coefficients shown in equation 2.6.9. Such constraints can be derived either by considering nearest and next-nearest bond energies or by mathematical considerations [ANS 88]. J.P.Gros et al. [GRO 88] found reasonable agreement between experimental and calculated values for the Ti-α and Ti_3Al phase boundaries (see figure 2.6.1.1.). The authors also verified that the congruent transformation of the Ti-α(hcp)->Ti_3Al would be substituted by a peritectoid reaction {Ti-β(bcc)+Ti_3Al->Ti-α(hcp)} if the Gibbs energy for the Ti-α(hcp) phase had been decreased by 170J/mole. Another possibility for the modelling is to describe Ti_3Al and Ti-α(hcp) separately as proposed by M.Hillert [HIL 86].

U.R.Kattner et al. [KAT 92] also thermodynamically assessed and calculated the binary Al-Ti using the optimisation and calculation program developed by H.L.Lukas et al. [LUK 77]. The disordered solution phases β and α were described as, respectively, quasi-regular solution and quasi-subregular solution (equation 2.6.5 and table 2.6.2). As the ordered intermetallic compound Ti_3Al exhibits an appreciable wide range of homogeneity, it was considered to consist of two sublattices. Random mixtures of Ti and Al on each lattice was assumed, and the analytical description given by:

$$G(Ti_3Al) = x_{Ti}*G^0_{Ti} + x_{Al}*G^0_{Al} + \Delta G^f + n^2_{Ti}*G^2_{Ti} + n^1_{Al}*G^1_{Al} +$$
$$+ RT*\{ n^1_{Ti}\ln n^1_{Ti} + n^1_{Al}\ln n^1_{Al} + n^2_{Ti}\ln n^2_{Ti} + n^2_{Al}\ln n^2_{Al} - N^1\ln N^1 - N^2\ln N^2\} +$$
$$+ n^1_{Ti}*n^1_{Al}\{ G^1_0 + G^1_1*(n^1_{Ti} - n^1_{Al})\} + n^2_{Ti}*n^2_{Al}\{ G^2_0 + G^2_1*(n^2_{Ti} - n^2_{Al})\}$$
$$+ n^2_{Ti}*n^1_{Al}*G^{12} \quad \text{eq.2.6.11}$$

with: $x_{Ti} = n^1_{Ti} + n^2_{Ti}$, $x_{Al} = n^1_{Al} + n^2_{Al}$, $N^1 = n^1_{Ti} + n^1_{Al}$ and $N^2 = n^2_{Ti} + n^2_{Al}$

Where $n^1_{Ti}, n^1_{Al}, n^2_{Al}$ and n^2_{Ti} are mole fractions of Ti and Al atoms on sublattices 1 and 2, and N^1 and N^2 are the site fractions of sublattices 1 and 2; G^0_{Ti} and G^0_{Al} are the reference states; ΔG^f is the Gibbs energy of perfectly ordered phase at stoichiometric composition, referred to one mole of atoms, G^2_{Ti} and G^1_{Al} are the Gibbs energy of formation of one mole of substitutional Ti or Al atoms on sublattice 2 and 1, respectively, and G^1_0, G^1_1, G^2_0 and G^2_1 are coefficients of polynomial interaction between atoms on the same sublattice, and G^{12} is the coefficient of an interaction term between the substitutional atoms on the different sublattices. The quantities $n^1_{Ti}, n^1_{Al}, n^2_{Al}$ and n^2_{Ti} are calculated by minimising the Gibbs energy for given x_{Ti} and x_{Al}.

In the literature [SUN 81][LUK 82] eq,2.6.11 is often called sublattice model. This equation can also be used for the Bragg-Williams approximation. In this case, constraints for the numerical values of $\Delta G^f, G^2_{Ti}, G^1_{Al}, G^1_0, G^1_1, G^2_0, G^2_1$ and G^{12} must be derived from summing the nearest-neighbour interactions of the ordered and disordered structures in question. In the analytical description of the ordered intermetallic compounds, substitution of both elements was assumed to occur on both sublattices, allowing these compounds to exist over the entire composition range. At complete substitution, the degree of order in these compounds must be zero, and the Gibbs energy of these compounds must be equal to the Gibbs energy of the pure elements with the corresponding crystal structure, so that the Gibbs energy of formation of substitutional Ti and Al atoms cannot be adjusted independently and:

$$G^2_{Ti} = -\Delta G^f / N^2 \text{ and } G^1_{Al} = -\Delta G^f / N^1$$

The calculated phase diagram obtained by U.R.Kattner et al. [KAT 92] agreed well with the critically evaluated data from literature (see figure 2.2.1). The optimisation process revealed that the phase relationships obtained from the calculation of the Al-Ti phase diagram were extremely sensitive to small changes in the Gibbs energy. The fact that small changes in Gibbs energy result in different phase relationships may help to explain the experimental difficulties in determining an accurate phase diagram for the Al-Ti system. For instance, at ~1100°C for 25at%Al the differences in the calculated relative Gibbs energy for Ti_3Al, Ti(α) and Ti(β) were very small and very likely to be smaller than the uncertainties usually found in experimentally determined thermodynamic data. This might explain the uncertainty of the existence of two peritectoid reactions: $\beta(Ti) + \alpha(Ti) \rightarrow \alpha2(Ti_3Al)$ at~1200°C and as $\beta(Ti) + \alpha2(Ti_3Al) \rightarrow \alpha(Ti)$ at~1150°C; as proposed by J.C.Mishurda et al. [MIS 89] instead of the congruent reaction: $\alpha(Ti) \rightarrow \alpha2(Ti_3Al)$.

In contrast to the compound-energy model proposed by M.Hillert et al. [AND 86] and described by equation 2.6.10, the sublattice model used by U.R.Kattner et al. [KAT 92] does not present any term representing the Gibbs energy of hypothetical compounds (see equation 2.6.12). At the same time, a closer look at the mathematical formalism of these models reveals that they are, in general, mathematically identical and differ only in the number of independently adjustable parameters [KAT 92]. These models have both ignored the short range order contribution for the Gibbs free energy, underestimating, thus, the stability of the disordered phase [SUN 90]. M.Hillert [HIL 86] mentioned that the modelling of the critical temperature for ordering is still difficult and that the SGTE group has not been able to make any suggestion for a unified treatment of the ordered and disordered states in a system. He concluded that it seems better to describe the two states (ordered and disordered) as two completely different phases.

A more elaborate model for ordering, called the cluster variation method (CVM) has been developed by R.Kikuchi [KIK 51]. In this model one does not only take pairwise bonds into account, but also "clusters" containing more than three atoms. Each of these clusters will have a Gibbs energy of formation from the number of AB bonds it contains. The entropy expression has a correction term to take into account the fact that clusters share surfaces, edges and corners. This method has been shown to be a very convenient

approach to study long and short range in binary and multicomponent systems [CAH 79][KIK 74].

J.L.Murray [MUR 88] pointed out that in CVM calculations, attention had been paid primarily to the order-disorder equilibrium, and not so much to the consistency of the Gibbs energies with those of the other structurally dissimilar phases of the systems. On her calculation of the Al-Ti phase diagram, she sacrificed the greater accuracy of CVM for the ordered states to make use of optimisation techniques for fitting Gibbs energies to experimental data. So she applied the sublattice model as treated by H.L.Lukas at al [LUK 77] to the ordered phases. Ti(α)-hcp was described as a quasi-regular solution (equation 2.6.5 and table 2.6.2). The predicted Ti-α(hcp) plus Ti_3Al phase field was considerably narrower than observed and had a lower congruent point. Besides this minor discrepancy, her assessed version was in good agreement with the available experimental data.

Although CVM approximation is supposed to have better accuracy than other models, as it can calculate the probabilities of atom configurations affected by interactions between atoms in the same and different sublattices, recent modelling [ONO 94][AST 93] of the Ti-Al phase diagram using this method have shown rather unsatisfactory results (see figure 2.6.1.2.), suggesting that there is still a lot of refinement to be performed. However, Asta et al. [AST 93] where studying first-principles of phase stability of Ti-Al intermetallic compounds (heat of formation and other zero-temperature properties of intermetallic compounds as well as of elemental fcc and hcp Ti and Al) to calculate thermodynamic and structural properties and to perform an abinitio study of phase stability. As a first attempt, it must be agreed that the general topology of the phase diagram at lower Al is in reasonable agreement with Kattner's version [KAT 92], specially if one ignores the temperature axis and recognises that they did not include β phase in the calculations). Almost the same observation applies for Onodera et al. [ONO 94], suggesting that CVM approximation might be a useful tool for a more fundamental modelling the Ti-Al system. It is hoped that in near future, one can use the basic information available for instance for pure A and B, such as electronic structure, bulk modulus, melting points and allotropic transition temperatures, to construct the corresponding A-B phase diagram with no additional alloy data, in other words, an interpolating scheme for predicting stable and metastable alloy equilibria using as input only pure element parameters [KUM 90].

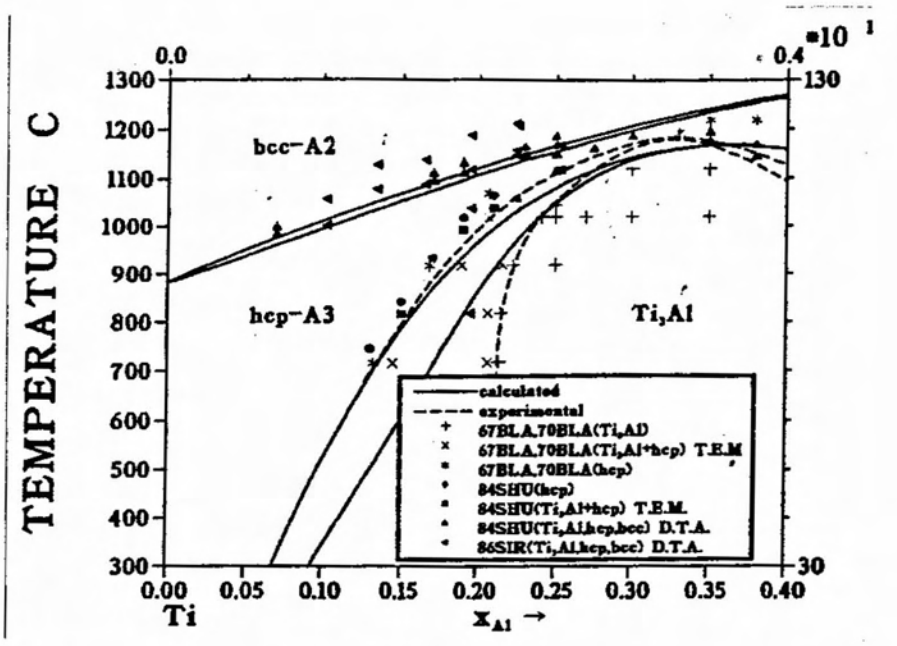

FIGURE 2.6.1.1. TI-AL PHASE DIAGRAM CALCULATED VIA REGULAR-SUBLATTICE MODEL [ANS 88].

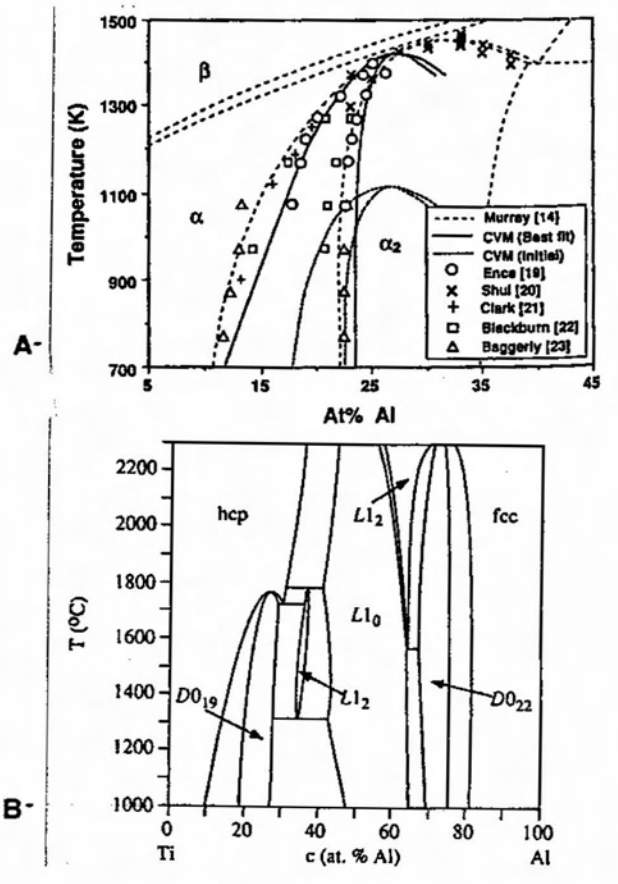

FIGURE 2.6.1.2. TI-AL PHASE DIAGRAM CALCULATED VIA CVM: A)H.ONODERA ET AL.[ONO 94]; B) M.ASTA ET AL. [AST 93].

Chapter 3

Experimental Procedure

3.1 Alloys preparation

The alloys used in this study (see nominal chemical compositions in table 3.1.1.) were prepared from high purity melted titanium sponge (99.7%), high purity silicon granules (99.9999%), electrolytic aluminium (99.99%), niobium powder (99.9%, 40mesh) and zirconium sponge (99.7wt%). The melted titanium buttons had their hardness measured to monitor the interstitial content. Low interstitial content was assured by choosing buttons whose measured hardness were between 94 and 115 VHN [AHM 92]. Aluminium was washed in dilute sodium hydroxide solution to remove scale.

The raw materials were, in order: weighed; washed in acetone and dried (to avoid contamination); and then loaded into an argon arc furnace. A titanium getter was also loaded into the furnace. The argon arc furnace was equipped with a water cooled copper hearth, a non–consumable tungsten electrode, a device for injection of gases and a vacuum pump. After loading the raw materials, the furnace was evacuated and flushed with high purity argon four times before melting the raw materials in a low pressure argon atmosphere.

alloy code	nominal composition				
	at%Al (±0.1)	at%Si (±0.01)	at%Nb (±0.01)	at%Zr (±0.01)	at%Ti
1	16.0	0	-	-	balance
2	16.5	0.97	-	-	"
3	16.5	3.5	-	-	"
4	22.1	0	-	-	"
5	22.1	0.97	-	-	"
6	22.1	3.5	-	-	"
2N	14.2	0.88	0.89	-	"
2Z	14.4	0.87	-	0.90	"
5N	20.4	0.86	0.87	-	"
5Z	20.3	0.86	-	0.87	"

Table 3.1.1. Nominal compositions of alloys prepared

The melting process consisted of the initial melt of the titanium getter, which would be melted again during the melting of the raw materials to pick up residual oxygen and nitrogen still present in the atmosphere of the furnace. Following this initial step, the arc was brought in contact with the raw materials, causing them to melt. After approximately 3 minutes of fusion, the alloy produced was allowed to solidify into a button by moving the electrode back to the getter. The alloy button was turned over and melted again. This procedure was repeated four times to ensure chemical homogeneity. The button was then moved into the rod-shaped mould, where the melting procedure was applied twice, producing the final ingot (length =5cm vs. diameter =1cm). The ingot was then weighed, so that the weight losses could be obtained. If the weight loss was more than 1%, the alloy had to be reprepared.

3.2 Heat treatment

Both extremities of the rod-shaped ingots were cut off to examine the as-cast structures and to ensure that the remaining material was macroscopically homogeneous in terms of microstructure. The ingots were then: ground using lubricating SiC paper to remove any oxide layer, which could cause contamination of the alloys during heat treatment; wrapped in molybdenum foil and put inside silica glass tubes. The Molybdenum foil prevents the alloy from reacting with the silica tube. The silica tubes containing the alloys were then evacuated and flushed with high purity argon several times. The pressure of argon (~0.3 atm at room temperature) inside the silica tube was chosen so that the internal pressure at the heat treatment temperature would slightly higher than 1 atm to avoid vaporisation of aluminium and contamination by oxygen and nitrogen.

All alloys were homogenised at 1300°C for 4 hours and quenched. The samples were quenched into an ice–water bath, and care was taken to make sure that the silica tube had been broken as soon as they reached the bath. The homogenised alloys were then cut into samples, whose thicknesses were kept around 8mm, descaled, encapsulated (using the same procedure previously described) and, finally, isothermally heat treated following the cycles shown table 3.2.1 . Heat treatments above 1000°C were carried out under a high purity argon atmosphere and in a vertical furnace.

code	temp. (°C) ± 5°C	time (h)	comment
A	1300	4	-initial condition: as-cast; -quenched in iced water
B	1200	24	-initial condition: A -quenched in iced water
C	1100	42	-initial condition: A -quenched in iced water
D	1000	72*	-initial condition: A -quenched in iced water
E	900	8 days*	-initial condition: A -quenched in iced water
F	800	14 days*	-initial condition: A -quenched in iced water
G	700	36 days*	-initial condition: A -quenched in iced water

*calculated from $\sqrt{(D_{\alpha}^{Al} * t)} \sim 15\mu m$

Table 3.2.1. Heat treatment cycles used.

code*	hardness (VHN) ± 30	oxygen content in solid solution (ppm)
1	327	-
1A	348	1700
2	310	-
2A	339	1400
2Z	310	-
2ZA	358	-
2N	343	-
2NA	350	1450
4	325	-
4A	343	1800
5	360	-
5A	381	1600
5Z	346	-
5ZA	421	1200
5N	333	-
5NA	418	2150

*code=XXY, where XX is the chemical composition (table 3.1.1.) and Y is the heat treatment (table 3.2.1.)

Table 3.3.1. Hardness and oxygen in solid solution

3.3. Hardness

Hardness measurements of as-cast and as-quenched were used to monitor the interstitial content, which was aimed below 2200ppm. Hardness was measured by using Vicker diamond pyramid indenture on flat and parallel surfaces of polished samples. An average of six readings were considered for the calculations of the average value and standard deviation. Some of the homogenised alloys were sent to Inco Test to have their oxygen checked by LECO analyser. Table 3.3.1. shows the values for hardness and oxygen content. The results for hardness were considered satisfactory and the alloys were generally assumed as having oxygen content between 1200 and 2200ppm.

3.4 Metallographic characterisation

Metallographic characterisation was carried out in the following microscopes: light microscopy using a Nikon EPIPHOT, scanning electron microscopy in JEOL JSM-T200 and JSM-35CF, transmission electron microscopy in a JEOL TEMSCAN 120CX (100KV) and JEOL 2000FX (200KV)

Heat treated samples were descaled and mechanically ground with water lubricated 220 to 1200 grit SiC papers. The samples for light and scanning electron microscopy were either electropolished or mechanically polished and etched. The latter was carried out with 14, 6, 3 and 1 μm diamond paste using lubricant. The polished samples were then lightly etched with Kroll's reagent, consisting of 3% HF and 10% HNO_3 in distilled water by volume. Electropolished samples were mechanically polished up to 3 μm diamond paste and then electropolished at temperatures between -40 and -30°C, voltage between 10 and 20V, and using a solution of 10% sulphuric acid in methanol by volume. Electropolished samples that did not present any contrast under either light or scanning electron microscope (BEI mode) had to be lightly etched with Kroll's reagent.

The preparation of thin foils for the transmission electron microscopy should be carried out very carefully to avoid unwanted reactions such as hydride formation and spontaneous transformations [AHM 92][BLA 67_a][MAR 68][BAN 88]. Heat treated samples were cut into 1-2 mm thick slices, which were ground to 250 μm thick using water lubricating SiC papers. Discs presenting diameter of approximately 3 mm were spark eroded from these 250 μm thick slices. The discs were then ground from 250 to approximately 100 μm using 1200-grit SiC paper, washed with water and then methanol, and finally placed on a holder for the electrochemical thinning.

The electrochemical thinning was carried out by Struers Tenupol twin jet apparatus with an electrolyte composed of either 10% sulphuric acid in methanol by volume or 6% perchloric acid and 35% n-butanol in methanol by volume. The electrolyte temperature was kept within the range of -50 to -40°C and the voltage was selected from the range of 10 to 30V. Some of the thin foils prepared had to be further ion-milled for various times to improve the amount of thin area available.

3.5 Microanalysis

Microanalysis using energy dispersive x-ray (EDX) spectroscopy was employed to determine the chemical composition of equilibrated phases. Depending on the size of the precipitates, either scanning (JEOL JSM35-CM attached to a Link Systems ZAF4 software) or transmission electron microscopy (JEOL 2000FX equipped with a Link Systems AN10000 analytical software) was employed. The former presented a spatial resolution limit for X-ray analysis around 2μm, while the latter presented a spatial resolution around 10nm. In both cases, correction factors between experimental and nominal composition for each element had to be determined by analysing the chemical composition of standard samples, whose nominal composition had been previously obtained by classical wet analytical chemistry.

For SEM-EDX analysis, depending on the contrast, unetched samples in BEI mode and slightly etched samples in SEI mode were used for EDX readings. A minimum of ten EDX readings on each phase was adopted and a life time of 100 seconds was used. Most of the measurements were carried out in the spot mode (~1μm). Only six results for each element were considered for the calculation of average and standard deviation (the two highest and two lowest values were discharged). Care was taken to analyse precipitates larger than the spatial resolution limit for titanium (~2μm).

For TEM-EDX analysis, conditions of the microscope had to be optimised to obtain adequate x-ray counting statistics (several thousand counts each peak!) to analyse small α2 particles, specially concerning silicon content, whose concentration was around 1 at% in some alloys. A compromise between beam spot size, x-ray collection time and x-ray output had to be made. The following working conditions were chosen for the analytical work: condensor aperture number one, lifetime =300s, tilt angle = zero, spot size either number four (160 nm) or five (70 nm).

The analysed composition in Ti-Al alloys can be affected by absorption (mass absorption coefficients for the Al-K_α peak are much larger than those for the Ti-K_α peak in Ti-Al alloys) even when conditions such as

the setting of the microscope and the take-off angle are kept constant through out the analysis. So, to correct for mass absorption, it was necessary to obtain the value of the foil thickness of each analysed point. There are various methods available to measure the foil thickness [KEL 75][HEI 64][AHM 92][HUH 90], but considering the errors involved, the stereographic analysis of the misfit dislocations present at some $\alpha/\alpha 2$ interfaces seemed to be the most reliable technique to measure the foil thickness (trace method). Initially, 4 points were chosen and had their thickness measured. These initial measurements were then used for the calibration of thickness against the total x-rays out-put, so that the thickness could be obtained onwards by indirect measurement [HUH 90]. Foil thickness measurements were carried out in a JEOL TEMSCAN 120CX (100KV). The four $\alpha 2$ precipitates used for the measurement of foil thickness were marked by the contamination spot technique and also by photographic recording. These areas were later localised in a JEOL TEM 2000FX, and had their x-ray out-put count analysed (total area) against diverse working conditions such as condensor aperture, spot size, phase. Equations (eq.3.4.1.) were obtained using the chosen working conditions. After calibration, for each point analysed the total area (A) was read and converted into foil thickness (t). This value was then inputted into the software, which corrected the mass absorption and gave corrected values for the concentrations of Al, Si and Ti.

• <u>spot size 4</u>:	phase-$\alpha 2$: t(nm) = 46.5 + 1.7e-04xA	eq.3.4.1.
	phase-α : t(nm) = 52.8 + 1.2e-04xA	
• <u>spot size 5</u>:	phase-$\alpha 2$: t(nm) = 49.2 + 6.2e-04xA	
	phase-α : t(nm) = 49.1 + 4.9e-04xA	

Samples 2A, 2NA, 2ZA, 5A, 5NA and 5ZA whose nominal composition were obtained by classical wet analytical chemistry, were used to obtain the scaling factor (K_X) between nominal and experimental results. The scaling factors were checked regularly. Some of the values are shown below:

- SEM: $K_{Al}^{\alpha} = 1.07$; $K_{Al}^{\alpha 2} = 1.11$; $K_{Si}^{\alpha} = 0.97$; $K_{Si}^{\alpha 2} = 0.97$;
- TEM: $K_{Al}^{\alpha} = 1.24$; $K_{Al}^{\alpha 2} = 1.26$; $K_{Si}^{\alpha} = 0.77$; $K_{Si}^{\alpha 2} = 0.77$; $K_{Nb}^{\alpha,\alpha 2} = 1.0$; $K_{Zr}^{\alpha,\alpha 2} = 0.70$;

Other important precaution that should be taken in quantitative X-ray analysis of a precipitate phase dispersed in a matrix is to ensure that the precipitate extends through the thickness of the foil. For the case of coherent $\alpha 2$, most of the analyses were performed near $[0001]_{\alpha 2}$. For $\alpha 2$ precipitates wrapped by misfit dislocations, this condition was assured by observing these

dislocations being cut by both foil surfaces [HUH 90]. For the chemical analysis of Ti_5Si_3 care was taken to ensure that the readings were performed on very thin areas of the precipitate. Unfortunately the analysed spots could not have their thickness measured. The trace method did not seem to account for the strong thickness gradient observed within a silicide particle (sometimes a small perforation of the foil was observed within a precipitate) and the error in the foil thickness by the spot contamination method can be greater than 100%. So, for the Ti_5Si_3 analysis, the thickness was considered invariable and equal to 100nm.

3.6. X–ray diffraction

Polished samples were examined in a Philips X–ray diffractometer (CuK–α radiation at 40 KV and 40 mA, graphite monochromator, sample spinner and connected to a Philips PC-APD software) to identify the phases present and calculate their lattice parameters. The diffractometer was calibrated by using a polycrystalline silicon standard, which was scanned five times at the beginning of each session. Titanium alloys were scanned at a rate of 0.033 degrees per second, using a sampling interval time of 1.50 seconds and examined in the range from 24 to 124 degrees. In some special cases a different scan velocity (0.016 degrees per second), sampling interval (3.00 seconds) and scan range (from 10 to 68 degrees) were employed to obtain a more detailed analysis of the silicides.

Additionally, step scan mode using step size ($^\circ 2\theta$) = 0.020, time per step = 12 s, start angle ($^\circ 2\theta$) =25 and end angle ($^\circ 2\theta$) =95 was used to calculate the lattice parameters of α and $\alpha 2$ phases. These two phases have the same hcp structure, with **c** parameter very close to each other and $\mathbf{a}_{\alpha 2} \sim 2 \times \mathbf{a}_{\alpha}$, so that it can be very difficult to differentiate most of α and $\alpha 2$ peaks. Partitioning of ternary and quaternary alloying elements between α and $\alpha 2$, however, is known to alter the lattice parameters of these phases and might enable a better distinction of these peaks. Low scan rate was therefore used in order to detect possible presence of double peaks ($\alpha+\alpha 2$) very close to each other.

The peaks and related planes were identified by comparison of the results with the JCPDS powder diffraction file and Diffract.v.1.2 software. For the calculation of lattice parameters (**a** and **c**), the procedure described elsewhere [CUL 59] for the precise lattice parameter measurements was used. Firstly, all the planes of the type (h,k,0) of a particular phase were used for the determination of the parameter **a**. As the true value of **a** occurs at 180°(2θ), plots of **a** versus f(2θ) were employed to extrapolate the value of **a** at

180°(2θ). Using the calculated value of **a**, the remaining planes (h,k,l) with l >> (h and k) could have their values of **c** calculated employing similar extrapolation procedure.

3.7. Thermo.Calc databank

The Thermo.Calc [SUN 85] databank was developed at Division of Physical Metallurgy of The Royal Institute of Technology, Sweden, and it is an attempt to provide a single software system for all thermodynamic calculations. The software is interactive and operated by sets of commands. The system is composed of several application programs, modules, which cooperate through defined software interfaces and utilise a database of assessed thermochemical parameters. One of the application programs is called Therm-Optimiser (TOP). This program was first released in 1988 and its different modules, including PARROT, allows: the creation of an experimental data file; the thermodynamic description of the phases under investigation and the calculation of the parameters used to describe the phases through a mathematical optimisation method. The former employs the sublattice model, where the excess term is expressed by a Kister-Redlich polynomial developed under Muggianu's formalism.

The assessment procedure follows an interactive process. It allows one: to introduce start values for the parameters used for the thermodynamic description of a particular phase; to edit, read, select and set weight to the experiments; to calculate equilibria on selected experiments; to perform optimisation (via least-square method [LUK 77]) on the initial values for the parameters and to produce optimised values for them.

The relative standard deviation of the parameters should be as low as possible. A high value implies that the uncertainty is too high, so it is possible that either there is not enough data to describe the phase or that too many parameters have been used. The sum of squares and the reduced sum of squares are used to compare the calculated and experimental values for the equilibria. A value equal to one for the reduced sum of squares is usually satisfactory and to decrease this value one has to increase the number of parameters. A constant compromise between number of variables, number of selected experimental equilibria, weight of each equilibrium and error analysis is needed for a good fit between experimental and calculated values.

When the optimisation is finished, the phase diagram can be calculated by the Newton Raphson technique [LUK 82]. This iterative method needs for starting a set of approximate values of all the parameters to be calculated. The better the approximation, the faster is the interaction. Also,

the possibility to jump to another metastable branch of the same equilibrium is diminished by a better approximation. The equilibria between specified phases are calculated, regardless whether they are stable or not. Afterwards the different equilibria are compared and the stable one can be defined.

The phases identified in the ternary Ti-Al-Si alloys in the present work and considered for the thermodynamic modelling were: Ti(α); Ti(β), Ti_3Al(α2) and Ti_5Si_3. The next step was the choice of a suitable database, which described accordingly the binary phase diagrams (Ti-Al and Ti-Si). For compatibility reasons, the same database should be used for both binaries. The choice (SSOL versus KP database) was based on the Ti-Al binary: KP proposed the existence of a peritectoid reaction β+α2->α, which has not been confirmed [KAT 92]; SSOL proposed the conventional congruent reaction α ->α2. Additionally, KP presented for the Ti-Si diagram the eutectoid reaction β -> α + Ti_5Si_3, while SSOL indicated β -> α+ Ti_3Si. SSOL was selected as a database for the calculation of the ternary diagram.

As one of the stable phases (Ti_3Si) present in the Ti-Si binary had not been identified in the present work, it had to be suspended from the calculations. A metastable phase diagram (Ti-Ti_5Si_3) was then calculated using the selected database (SSOL). This version of the binary diagram, however, was not considered satisfactory (the solubility of Si in Ti-α was rather low) and this binary had to be reassessed. This new assessment used, for compatibility reasons, the phase descriptions as proposed by SSOL database but considered, as experimental input, the Ti_5Si_3/β and Ti_5Si_3/α phase boundaries as obtained by KP's database.

In the assessment of the ternary diagram, few binary interaction parameters between Al and Si in the first sublattice and the vacancies described in the second sublattice were missing, such as L(bcc,Al,Si:Va), L(hcp,Al,Si:Va). In this notation "," separates elements in the same sublattice and ":" separates the different sublattices. Additionally, few other interaction parameters had to be considered to account for the solid solution of Si in Ti_3Al such as L(Ti_3Al,Ti:Al,Si), L(Ti_3Al,Al,Ti:Si), L(Ti_3Al,Ti:Al,Si,Ti) and L(Ti_3Al,Al:Al,Si,Ti). The phase equilibria data produced in the present work were used as input so that these parameters could be determined and the ternary phase diagram finally calculated. No solid solution of Al in Ti_5Si_3 has been considered in the present modelling to simplify this initial calculation of the ternary diagram. Although simplistic, this assumption is not realistic: Al is known to be soluble in this phase [ZHA 91][MAN 94][WU 90], so it is suggested that at some stage this contour condition should be relaxed.

Chapter 4
Results & Discussion

4.1. As-cast samples

The as–cast microstructures are shown in figure 4.1.1.a-k. The micrograph of alloy 1 (Ti16Al) shows large grains (~400μm) of transformed β (figure 4.1.1.a). The grains have a rather irregular shape presenting straight, serrated and curved boundaries, which strongly resembles decomposition via a massive type transformation [PLI 77][RUC 90]. Some grains presented elongated colonies of parallel α plates. The microstructure of alloy 2 (Ti16Al+1.0Si) shows the same features of alloy 1 except that it appears more refined (massive grains ~200μm) (figure 4.1.1.b). Precipitation of silicides has not being observed in this ternary alloy, indicating either complete solubility of silicon due to the rapid cooling or the presence of very fine precipitation of silicides, unresolvable under SEM.

Alloy 3 (Ti16Al+3.5Si) shows a (ghost) dendritic structure composed of primary phase, probably β, and a lamellar structure, present interdendriticaly and composed of primary phase and silicides (figure 4.1.1.c-d). In some other areas the presence of silicides along grain boundaries of β phase (figure 4.1.1.e) suggests both recrystallisation of β phase and precipitation of silicides along previous β grain boundaries. The matrix is mainly composed of elongated colonies of parallel α plates. Additionally, some featureless and irregular shaped grains, resembling a massive product (grain size ~20μm), could also be observed. The observation of massive product in this ternary hypo-eutectic alloy suggests that Al promotes the massive transformation. Plitcha et al. [PLI 77] did not observe formation of massive product in Ti-Si hypo-eutectic alloys. Further precipitation of silicide along α/α interfaces, caused by the supersaturation of the α matrix in silicon during cooling, would be expected but no evidence has been found, suggesting that α phase is supersaturated in solute.

Alloy 4 (Ti22Al) shows the same features as alloy 1 (Ti16Al): large grains (~500μm) presenting irregular and faceted boundaries (figure 4.1.1.g); and sporadic presence of colonies of parallel α plates (figure 4.1.1.f). Alloy 5(Ti22Al+1.0Si) does not present any evidence of silicide precipitation. The matrix is composed of two different types of transformed β: irregular–shaped grains (~120μm) (figure 4.1.1.h), principally observed in the middle of the

specimen and along previous β grains ; and small colonies of parallel α plates.

Alloy 6 (Ti22Al+3.5Si) shows a (ghost) dendritic structure similar to alloy 3, but presenting a higher volume fraction of lamellar eutectic product (figure 4.1.1.i). This feature enabled a better analysis of the solidification path for this alloy, and consequently for alloy 3. The angle between secondary branches and primary dendrites is very close to 90°, suggesting that the primary phase for ternary alloys containing up to 22at%Al and 3.5at%Si is β(bcc) and not α(hcp). X ray diffraction of samples 3 and 6 identified the silicide as Ti_5Si_3. Table 4.1.1. presents the calculated lattice parameters for Ti_5Si_3. The addition of Al slightly increased the lattice parameters of Ti_5Si_3, confirming previous work by Z.Zhang and H.M.Flower [ZHA 91].

	Ti_5Si_3	
alloy	a (±0.004A)	c (±0.005A)
3	7.458	5.158
6	7.468	5.169

Table 4.1.1. Lattice parameters for Ti_5Si_3.

The lamellar interdendritic product (figure 4.1.1.j-k) indicates the existence of an eutectic reaction given by ($L \rightarrow \beta + Ti_5Si_3$), confirming solidification path proposed by S.H.Manesh and H.M.Flower [MAN 94]. Additionally, the eutectic microstructure of alloy 6 was observed to be coarser than alloy 3, suggesting an increase of the eutectic temperature with the increase in Al content. This observation is in agreement with works by S.H.Manesh et. al. [MAN 94] and J.S.Wu et al. [WU 90]. The transformed β matrix is apparently composed of elongated and equiaxial α grains, suggesting that Al addition promotes the formation of "more diffusional" microstructures. The next section will study with more detail and under more controlled cooling rates the effect of alloying elements on the morphology of the product of allotropic reaction β–>α.

Figure 4.1.1. As-cast microstructures for binary and ternary alloys:

a) alloy 1 (Ti-16Al): massive grains; SEM (scanning electron microscope) - SEI (secondary electrons image);
b) alloy 2 (Ti-16Al-1.0Si): massive grains; SEM-BEI (backscattered electrons image);
c) alloy 3 (Ti-16Al-3.5Si): dendritic microstructure; SEM-BEI;

d) alloy 3 (Ti-16Al-3.5Si): eutectic microstructure; SEM-BEI;

e) alloy 3 (Ti-16Al-3.5Si): transformed β microstructure; LM (light microscope);
f) alloy 4 (Ti-22.0Al-3.5Si): massive grains
and colony of parallel α plates; SEM-SEI;

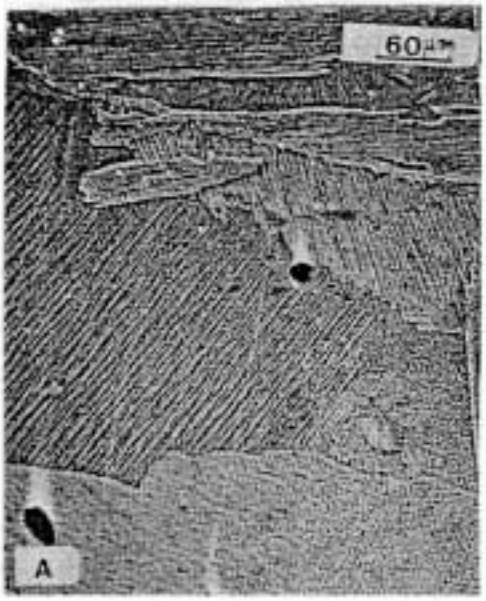
60 µm
A


60 µm
B

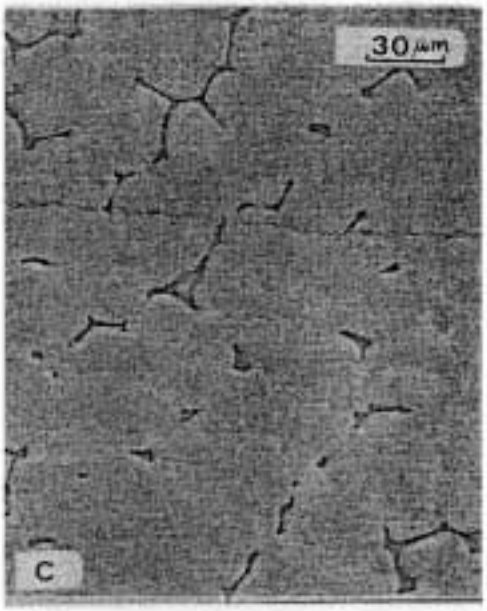
30 µm
C

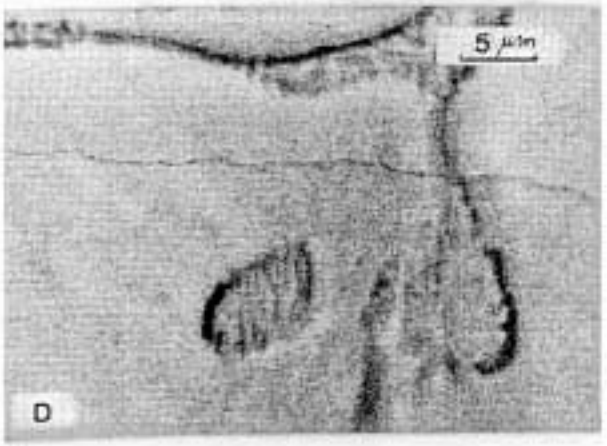
5 µm
D

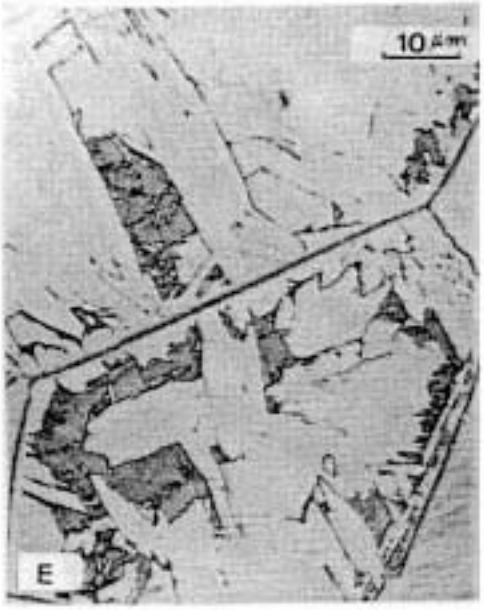
10 µm
E

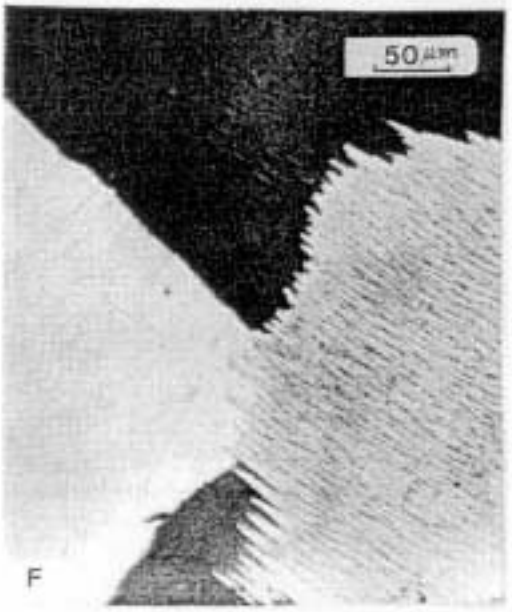
50 µm
F

Figure 4.1.1. As-cast microstructures for binary and ternary alloys:

g) alloy 4 (Ti-22.0Al): massive grains; LM;

h) alloy 5 (Ti-22.0Al-1.0Si): massive grains
and colonies of parallel α plates; LM;

i) alloy 6 (Ti-22.0Al-3.5Si): dendritic microstructure; LM;

j) alloy 6 (Ti-22.0Al-3.5Si): dendritic microstructure; SEM-BEI;

k) Alloy 6 (Ti-22.0Al-3.5Si): eutectic microstructure SEM-BEI.

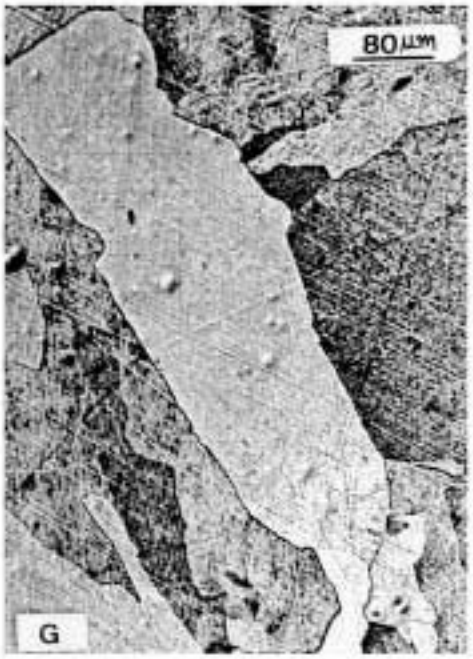
80 µm
G


80 µm
H

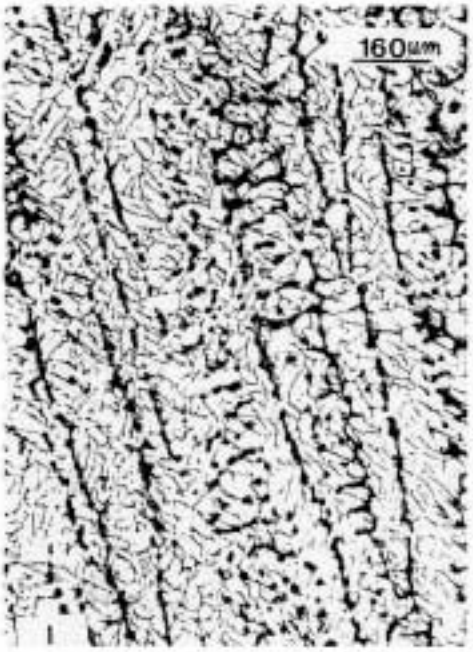
160 µm
I

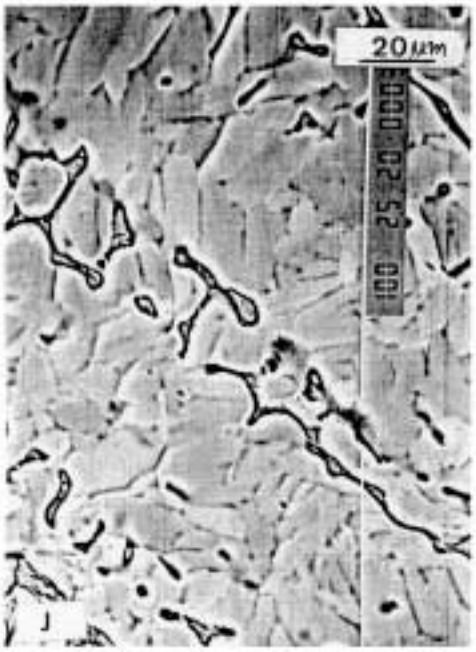
20 µm
J

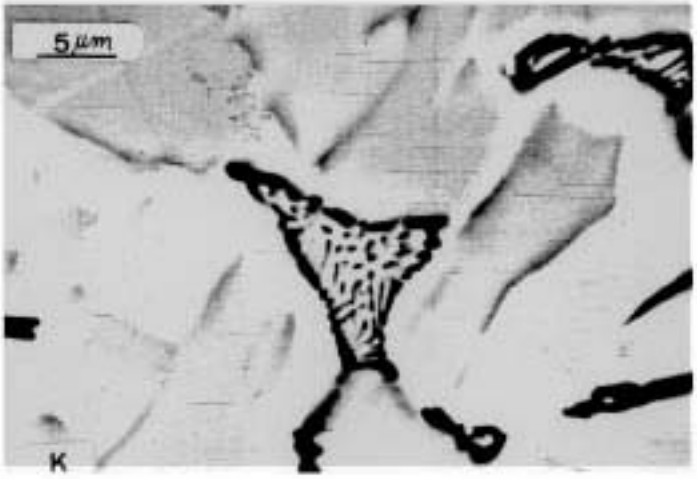
5 µm
K

4.2. As-quenched samples

The samples were held at 1300°C for four hours and then water quenched following the procedure described in chapter 3. Light and electron microscopy examinations showed at least four microstructural features of transformed β which were morphologically "distinct". These include:

- massive α: Featureless grains presenting irregular interfaces under light microscopy. TEM observation of some of these areas showed absence of sub-boundaries and presence of dislocations and stacking faults. SEM-microanalysis established that there was no detectable difference in chemical composition between massive grains and colonies of parallel plates, usually the morphology adjacent to massive grains.
- colonies of parallel α plates: Presence of colonies observed under light microscopy, TEM observation of these areas showed that one singular plate may be composed of many aligned sub-units (sheaves);
- primary α plates: Larger isolated plates, usually presenting two variants of growth. Between adjacent primary plates there were usually found colonies of parallel secondary α plates. Another possibility is the presence of a zig-zag microstructure (3 variants of growth). Primary plates showed internal presence of dislocations and a faceted boundary.
- secondary α plates: They were usually found either as colonies of parallel α plates or as a zig-zag microstructure (3 variants of growth).

The microstructure of sample 1A (Ti16Al) (figure 4.2.1.a) shows large grains (~600μm) of transformed β. The grains have a rather irregular shape with boundaries presenting various forms such as irregular curves or numerous facets (figures 4.2.1.a and 4.2.1.c), resembling strongly a decomposition via massive type transformation [PLI 77][PLI 78][PLI 79][PLI 80][MAS 84][RUC 90][WAN 92]. The massive grains when examined under TEM, presented a low density of dislocations (figure 4.2.1.e). In some areas of the sample the presence of 2 variants of colonies of parallel plates is observed (see figure 4.2.1.b), suggesting the existence of at least two competing mechanisms for the formation of α phase. Figure 4.2.1.d. shows that the parallel plates are composed internally of parallel subunits, and the arrows point at the possible presence of ledges, suggesting that the growth of colonies of parallel plates occurs by ledge mechanism. Observation of the areas near the surface of the samples, exposed to higher cooling rates, showed predominant presence of colonies of parallel α plates, which indicates that this morphology is formed under higher undercoolings. It is suggested that

during quenching the morphological transition for the allotropic product is: massive α -> colonies of parallel α plates. SADP and XRD of sample 1A did not show any α2 superlattice reflections, suggesting that there is no resolvable formation of ordered phase α2 during quenching from β field.

The microstructure of sample 2A (Ti16Al+1.0Si) resembles very much the microstructure of sample 1A, but the former shows more refined massive grains of approximately 200μm (figure 4.2.2.a.). The boundary between two adjacent massive grains seemed much more irregular, with the formation of acicular facets along one preferential direction (figure 4.2.2.b.). The decrease of both T_0 and solvus temperature with silicon addition indicates that the allotropic transformation occurred at lower temperatures, suggesting that OR might play a more important role on the massive transformation at lower temperatures. Areas presenting a higher proportion of colonies of parallel α plates were also observed in this alloy (figure 4.2.2.c). Small colonies of parallel secondary α plates, formed between the primary plates, were noticed in some of these areas (figure 4.2.2.d). The secondary plates presented another variant of growth when compared to the primary ones. SAPD and XRD of sample 2A did not show any α2 superlattice reflections suggesting that there is no resolvable formation of ordered phase α2 during quenching. Precipitation of silicides was not observed in XRD/SEM/TEM work.

In the sample 2ZA (Ti14Al+1.0Si+1.0Zr), the addition of Zr inhibited completely the formation of large massive grains. The microstructure presented grain boundary α sideplates (figure 4.2.3.a) and primary α plates presenting 3 variants of growth at 60° from each other (figure 4.2.3.b). The secondary plates are present either as colonies of parallel plates or in zig-zag microstructure. The former was presented in areas adjacent to two primary α plates (figure 4.2.3.c). Additionally, this micrograph shows that the primary plates present a faceted interface with the colony of parallel plates. The primary α plates presented high density of dislocations (figure 4.2.3.d.). XRD and SADP examination of sample 2ZA did not show any α2 superlattice reflections, suggesting that there is no resolvable formation of ordered phase α2 during quenching. Very scattered precipitation of a hexagonal-shaped silicide (~1.5 μm diameter) was observed in TEM work, although its identity will be discussed only during studies of aged quaternary alloys (figure 4.2.3.e.)

In the sample 2NA (Ti14Al+1.0Si+1.0Nb), the addition of Nb inhibited the massive transformation. Compared to sample 2ZA, this microstructure presents a much smaller proportion of grain boundary α sideplates and larger portions of colonies of parallel α plates. Additionally, some former β grain boundaries presented a product which resembles very much either a GB allotriomorph or a massive grain (as it seems to cross β grain boundaries) (figure 4.2.4.a). TEM examination showed the presence of primary faceted α plates with colonies of secondary parallel α plates (figure 4.2.4.b) and presence of colonies of parallel α plates (figure 4.2.4.c). Additionally, the presence of retained β along the internal boundaries of the colonies of parallel α plates (but not along the boundaries of primary α plates) was observed (figures 4.2.4.d). TEM-EDX analysis confirmed the chemical stabilisation of β phase by partitioning of solute between α and β (see table 4.2.1.), with β-stabiliser elements distributing preferentially into the β phase and α-stabiliser into α phase. These partitioning coefficients were, however, underestimated because the EDX-analysis of the thin layer of β phase was very likely to contain a contribution from the matrix (used spot size ~70nm). Furthermore, the plates belonging to the colonies of parallel plates appear to be composed of smaller plates, defined in this work as sub-units.

alloy	T(°C)	EDX-analysis	phase	chemical composition			
				at%Si	at%Al	at%Nb	at%Ti
2NA	1300	TEM	α	1.0±0.2	14.8±0.6	0.9±0.2	balance
			β	1.1±0.2	10.6±0.5	2.8±0.3	"

Table 4.2.1. Solute partitioning in as-quenched Ti-14Al-1Si-1Nb alloy.

Sample 3A (Ti16Al+3.5Si) shows colonies of parallel α plates formed during quenching and the presence of eutectic and secondary silicides, the latter heterogeneously precipitated along previous β grain boundaries and during quenching along α/α plate boundaries (figure 4.2.5.a-b). The eutectic silicides presented in the as–cast condition seem to have undergone a process of spheroidisation to minimise the Ti_5Si_3/β interfacial area. XRD and electron SADP indicated the presence of α2 superlattice reflections (figure 4.2.5.d-e) and confirmed the presence of Ti_5Si_3-type silicides.

Sample 4A (Ti22Al) presents large grains with irregular and faceted boundaries, characteristic of a massive type decomposition of β occurred during quenching (figure 4.2.6.a.). Some of these boundaries presented a

ledge-like structure, indicating the existence of preferential OR and possible growth by ledges (figure 4.2.6.b.). Additionally, there is a noticeable presence of colonies of parallel α plates presenting the same variant of growth (figure 4.2.6.c-d). Figures 4.2.6.e-f. present boundaries between massive grains and indicated by arrows. Besides the presence of internal dislocations, one can notice the variety of boundaries: planar and curved. One of the massive grains (grain pointed by arrow A in figure 4.2.6.e.) resembles a large primary α plate, suggesting that the transition of mechanism from massive to martensite might be very blurred indeed for this alloy. Additionally, massive grains are shown to present internally stacking faults (figure 4.2.6.g.). Small APDs formed during quenching are seen in figure 4.2.6.h.

Sample 5A (Ti22Al+1.0Si) did not present any evidence of silicide precipitation. The microstructure is composed of two different morphologies of transformed β: massive type irregular shaped grains along prior β grain boundaries and colonies of parallel α plates (see figure 4.2.7.a-b). Figures 4.2.7.c-d shows 2 variants of growth for the colonies of parallel α plates. The chemistry and hardness of the two areas mentioned above has been checked by microanalysis and no measurable differences have been found.

massive α grains: Al =20.5±0.7 at%; Si =1.0±0.1 at%; Ti = balance
hardness = 380 VHN
colony of parallel α plates: Al =20.9±1.1 at%; Si =1.0±0.2 at%; Ti = balance
hardness = 400 VHN

TEM examination (figures 4.2.7.e-f.) showed that the large primary plates contain a moderate dislocation density. Additionally some areas of the primary plates are composed of aligned sub-units along $(10\bar{1}0)_\alpha$. Figure 4.2.7.g shows in more details the interfacial structure of the sub-units where ledges of growth can be observed (see arrows A and B in figures 4.2.7.g). XRD indicated the presence of α2 superlattice reflections and TEM examination confirmed the presence of small APB domains formed during quenching (figure 4.2.7.h.).

Sample 5ZA (Ti20Al+1.0Si+1.0Zr) is composed mainly of coarser faceted primary α plates, some of them presenting mid-ribs (figure 4.2.8.b). The facets present an angle of approximately 120° and the primary plates present 3 variants of growth lying 60° of each other. Along previous β boundaries featureless areas resembling massive grains are observed (see crossing of prior β grain boundaries indicated by arrows A and B); and grain

boundary sideplates (figure 4.2.8.a). Figure 4.2.8.c. shows a primary α plate and colonies of α plates. The boundaries between these two distinct morphologies are less faceted and more irregular than the ones seen before (figures 4.2.3.c. and 4.2.4.b.), resembling massive interfaces observed previously (see figures 4.2.6.f. and 4.2.1.c.). Secondary α plates are usually presented as colonies of parallel plates and they also present aligned sub-units (see arrows in figure 4.2.8.d). Figure 4.2.8.e. shows a large α plate (or an acicular massive grain) adjacent to a featureless area presenting α2 APDs. Once more it is suggested that the morphological transition between massive and martensitic products is very blurred.

Sample 5NA (Ti20Al+1.0Si+1.0Nb) is composed of grain boundary α sideplates (figure 4.2.9.a.); primary α plates with faceted interfaces and colonies of secondary parallel α plates (figures 4.2.9.b); and some massive grains (see arrows in figure 4.2.9.c.). Figure 4.2.9.d shows faceted (arrow A) and curved (arrow B) boundaries between two massive grains. Figure 4.2.9.e. shows the boundary between a massive grain and a colony of parallel plates. Note the presence of facets. Figure 4.2.9.f shows irregularly faceted almost-curved boundaries of a primary α "plate", which resembles a small massive grain. The plates belonging to the colony are composed of parallel sub-units presenting low-angle sub-boundaries (figure 4.2.9.g). The presence of retained β along the boundaries of parallel α plates, but not along the primary α "plates", was observed (figures 4.2.9.h.). Additionally no β phase was found along the plate internal sub-boundaries, which might suggest that the subunits are formed with supersaturation of solute. TEM-EDX analysis showed partitioning of solute between α and β (see table 4.2.2.), with β-stabiliser elements distributing preferentially into β phase, while α-stabiliser into α phase. The partitioning coefficients are, however, underestimated because the EDX-analysis of the thin layer of β phase was very likely to contain a contribution from the matrix (used spot size ~70nm). Finally, small α2 domains were observed (figure 4.2.9.i.)

alloy	T(°C)	EDX-analysis	phase	chemical composition			
				at%Si	at%Al	at%Nb	at%Ti
5NA	1300	TEM	α	1.1±0.2	20.3±0.6	1.0±0.2	balance
			β	1.1±0.2	15.9±0.5	3.2±0.3	"

Table 4.2.2. Solute partitioning in as-quenched Ti-22Al-1Si-1Nb alloy.

Sample 6A(Ti22Al+3.5Si) is composed of colonies of parallel α plates and eutectic plus secondary silicides (figure 4.2.10.a-b). The parallel plates found in this sample seem comparatively coarser than the ones observed in sample 3A, and additionally they are composed of elongated subunits oriented along the same direction (figures 4.2.10.d-e). The silicides present in the as–cast condition appear to have undergone a process of spheroidisation. A few secondary silicides were formed during the homogenisation heat treatment and quenching (figure 4.2.10.c) to relieve the supersaturation of the matrix in silicon, but preferential precipitation of silicides along α/α boundaries has not been as widespread as observed in sample 3A. XRD confirmed the presence of Ti_5Si_3 type silicides. The precipitation of silicides has a much coarser distribution than the one found in sample 3A. XRD also indicated the presence of α2 superlattice reflections. TEM examination of this sample confirmed the presence of small APDs formed during quenching. These small α2 domains are shown to present heterogeneous nucleation (or preferential growth) at certain α plate boundaries and sub-boundaries (figure 4.2.10.f-j.). In some cases, these elongated domains are shown to grow normal to the interface and along $(1\bar{2}10)_{\alpha 2}$ and $(10\bar{1}0)_{\alpha 2}$. The intragranular precipitation of α2 is shown to be equiaxial and more refined and it is interesting to point out that the sub-unit plate boundaries also promoted formation of elongated α2 APDs .

Figure 4.2.1. Ti-16Al alloy as-quenched from 1300°C-4 hours:

a) massive grains; LM;

b) colonies of parallel α plates; SEM-SEI;

c) irregular interface between massive grains; TEM (transmission electron microscope) -BFI (bright field image);
(arrows A and B point at the interface);

d) detail of a colony of parallel α plates; SEM-SEI;
(arrows A and B show presence of ledges of growth);

e) low density of dislocations inside a massive grain;
TEM-BFI and SADP (selected area diffraction patern): B=$[1\bar{2}10]\alpha$
(SADP given below)

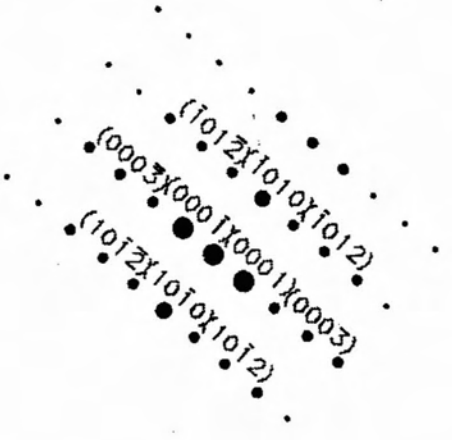


160 μm
A


30 μm
B

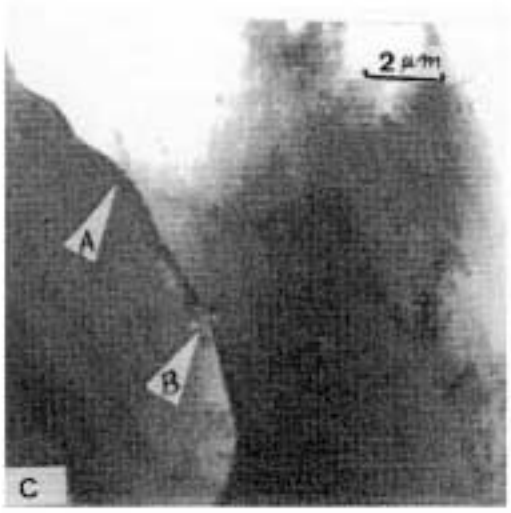
2 μm
A
B
C

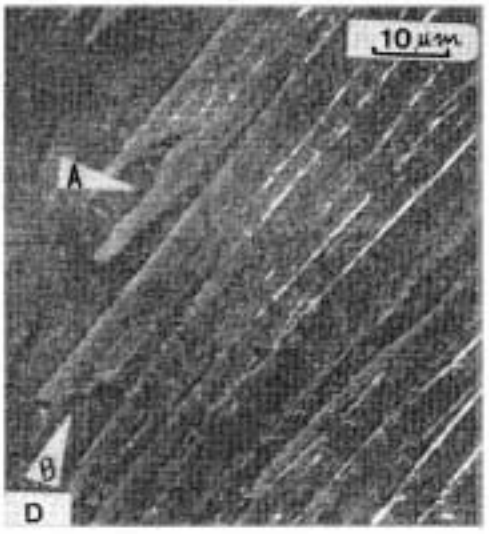
10 μm
A
B
D

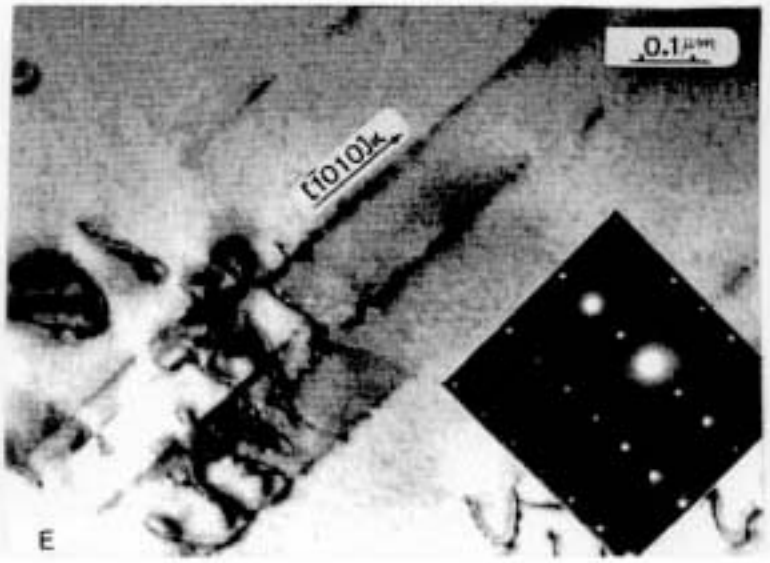
0.1 μm
[10̄10]
E

Figure 4.2.2. Ti-16Al-1Si alloy as-quenched from 1300℃-4 hours.

a) massive grains; LM;

b) detail of interface between massive grains; LM;
(arrows A and B point at preferentially oriented acicular-like facets);

c) colonies of parallel α plates; SEM-SEI;

d) small colonies of secondary α plates; SEM-SEI;


160 µm
A

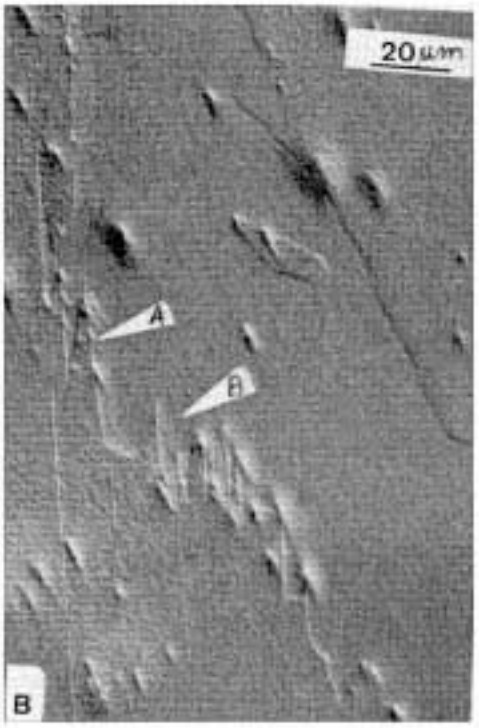
20 µm
A
B
B


20µm
C

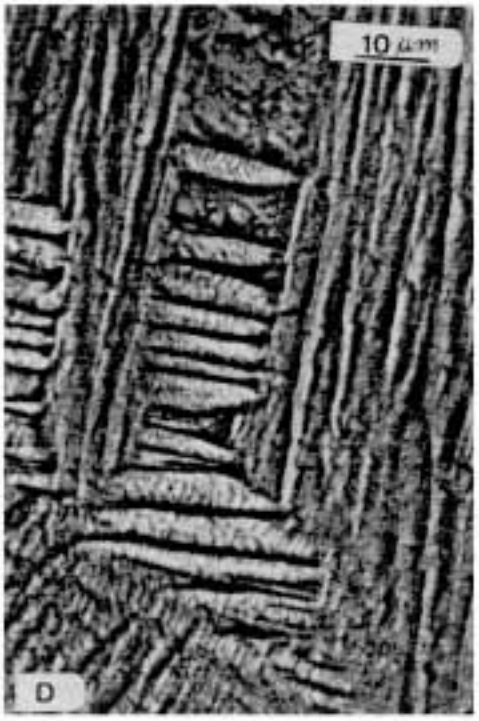
10 µm
D

Figure 4.2.3. Ti-14Al-1Si-1Zr alloy as-quenched from 1300°C-4 hours.

a) grain boundary α sideplates; SEM-SEI;

b) α plates presenting 3 variants of growth; SEM-SEI;

c) detail of the faceted boundary of a primary α plate; TEM-BFI;

d) high density of dislocations inside a primary α plate;
TEM-BFI and SADP: B=$[12\bar{1}0]_\alpha$;

e) hexagonal-shaped silicide; TEM-BFI.

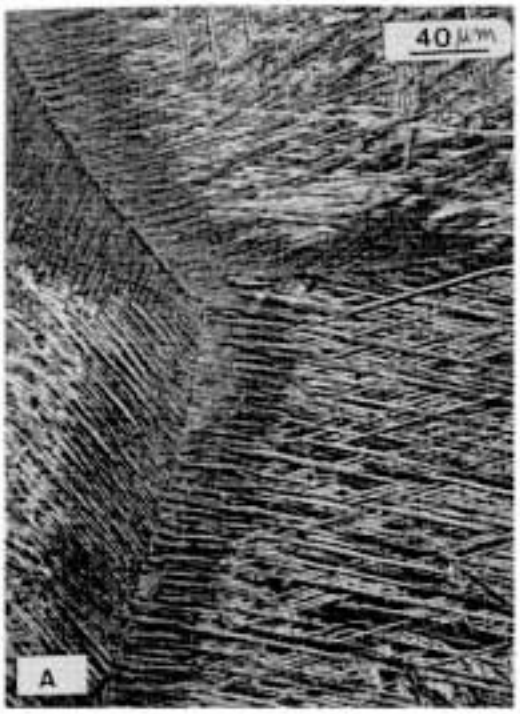
40 μm
A

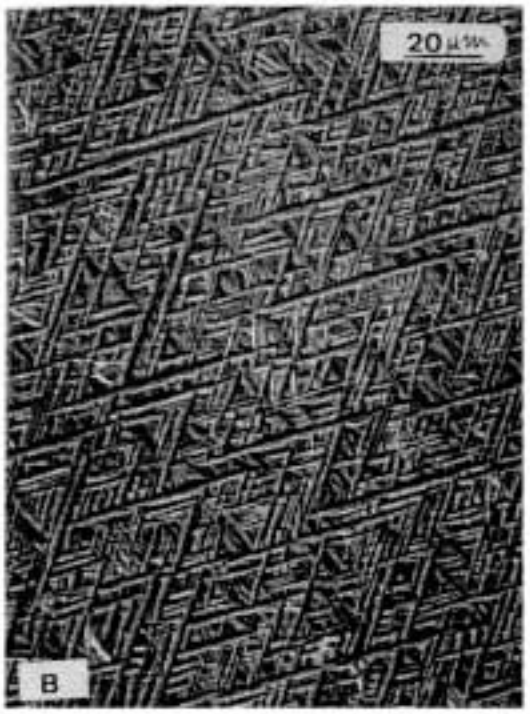
20 μm
B

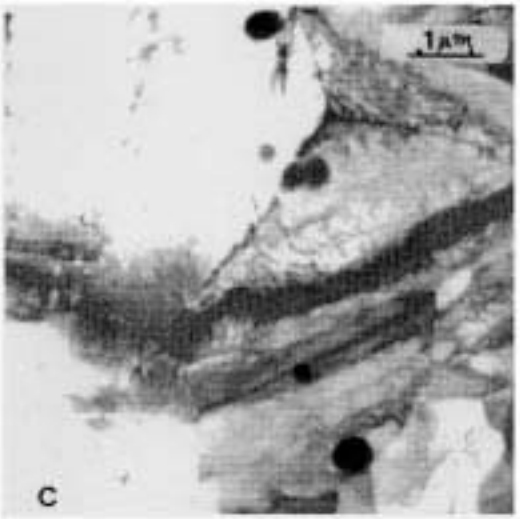
1 μm
C

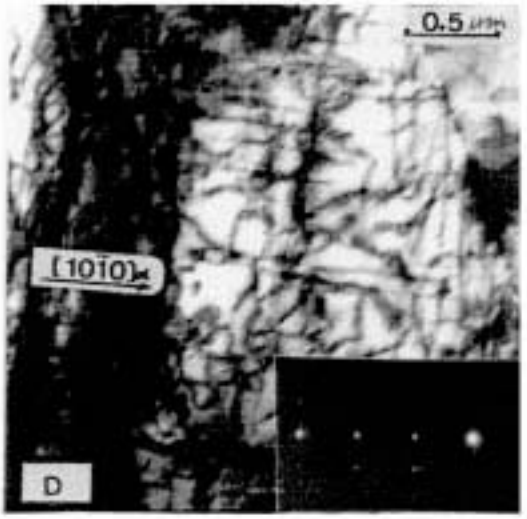
0.5 μm
[10$\bar{1}$0]
D

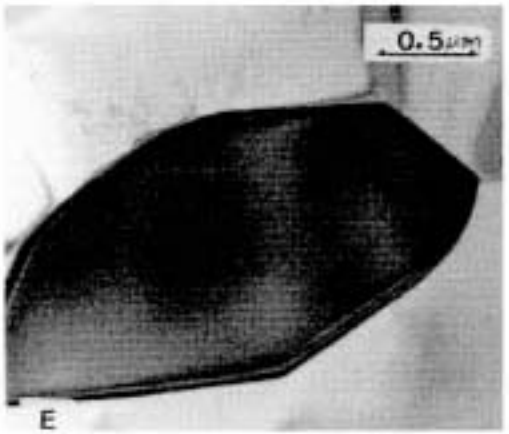
0.5 μm
E

Figure 4.2.4. Ti-14Al-1Si-1Nb alloy as-quenched from 1300°C-4 hours:

a) primary α plates and colonies of parallel plates; SEM-SEI; (arrows A and B point at massive grains crossing prior β grain boundaries);

b) faceted primary α plates and colony of secondary parallel α plates; TEM-BFI;

c) colony of parallel α plates showing retained β; TEM-BFI;

d) retained β along boundaries of parallel α plates; TEM-DFI: B=[001]β and g=(010)β (SADP given below)

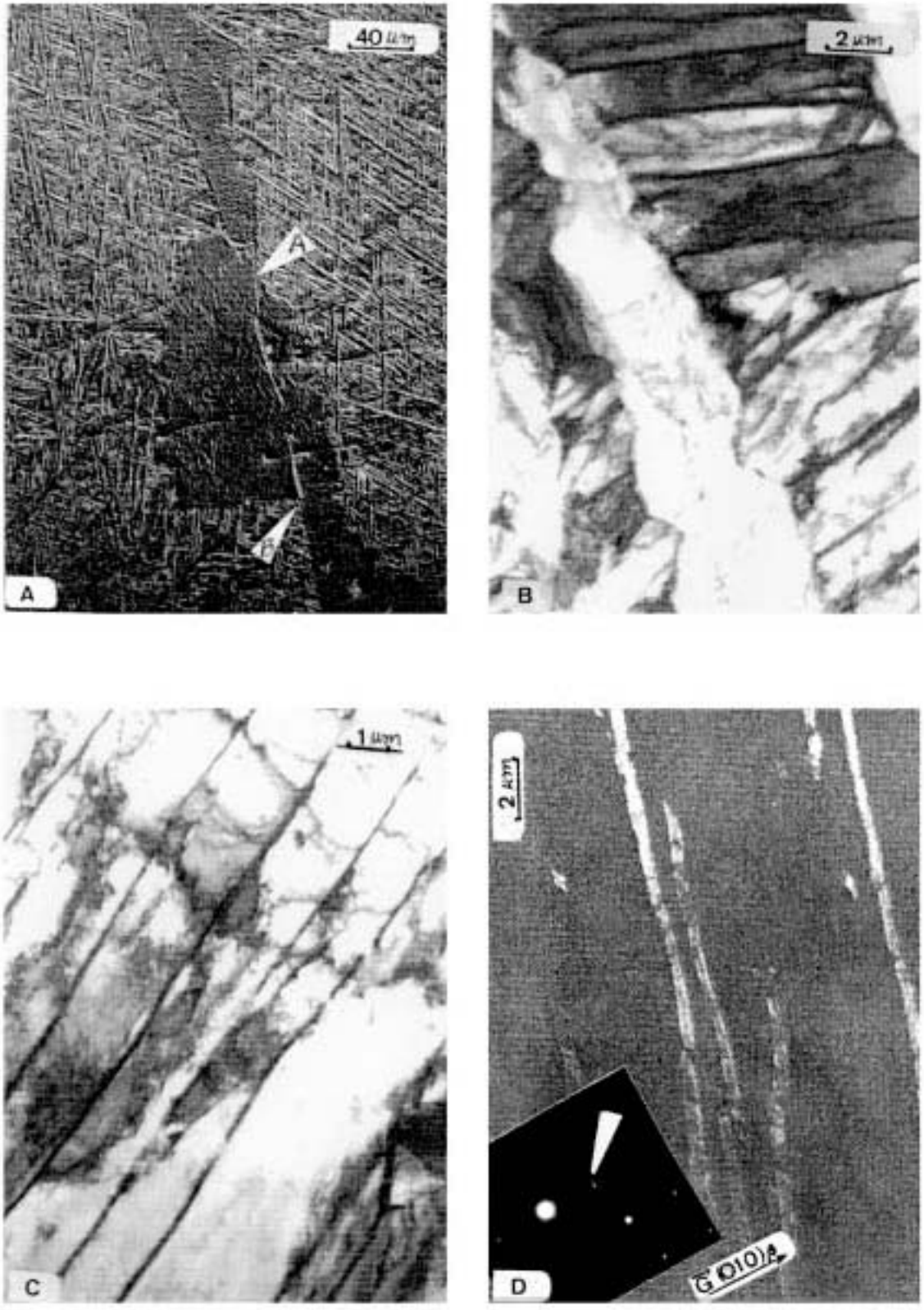
40 μm
A
B
A
2 μm
B
1 μm
C
2 μm
G (010)
D

Figure 4.2.5. Ti-16Al-3.5Si alloy as-quenched from 1300°C - 4 hours.

a) α sideplates and secondary silicides (precipitated along prior β grain boundaries and α plate boundaries); SEM-BEI;

b) detail of α plates and secondary silicides; TEM-BFI;

c) Ti_3Al APDs; TEM-DFI: $B=[\bar{5}416]_{\alpha 2}$ and $g=(10\bar{1}1)_{\alpha 2}$ (SADP given below)

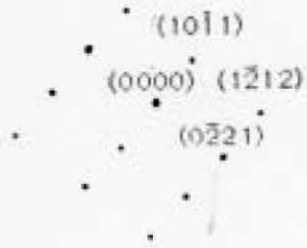

d) TEM-BFI of prior micrograph.


10 µm
A


1 µm
B

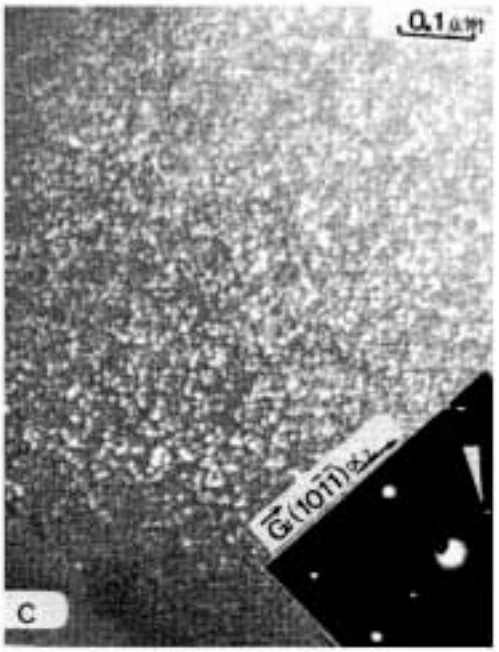
0,1 µm
$\vec{G}(10\bar{1}1)$
C


0,1 µm
D

Figure 4.2.6. Ti-22Al alloy as-quenched from 1300 ℃ - 4 hours.

a) massive grains; LM;

b) detail of the boundary between massive grains; SEM-BEI;
(arrows A and B shows ledges)

c) presence of colonies of parallel α plates; SEM-BEI;

d) detail of the colonies showing parallel α plates; SEM-SEI;


160 µm
A

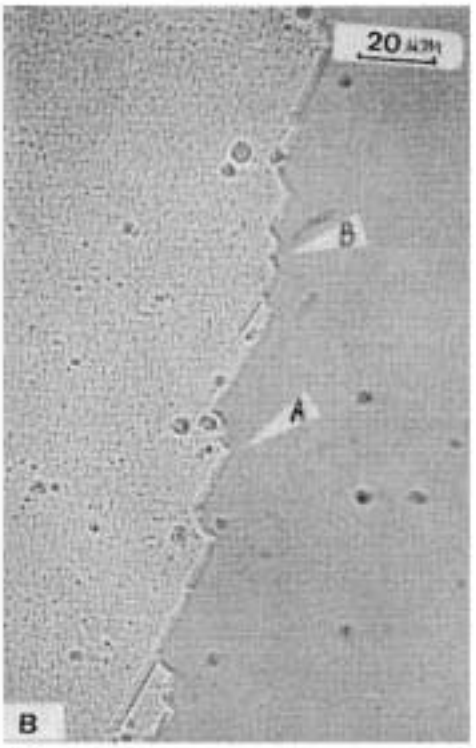
20 µm
B
A
B

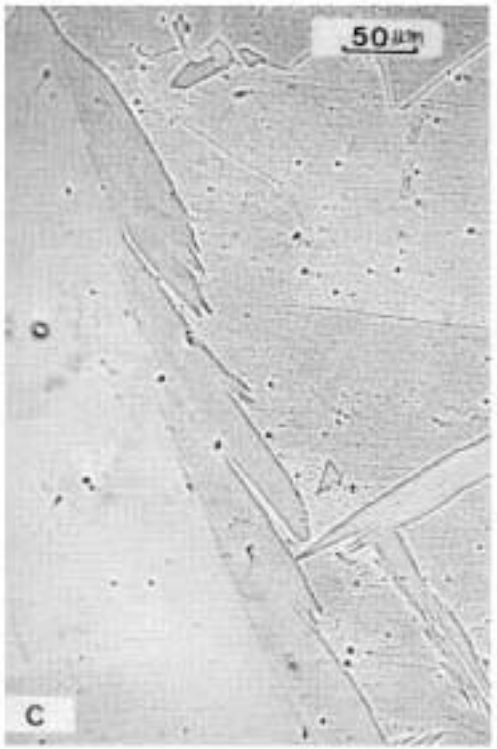
50 µm
A
C

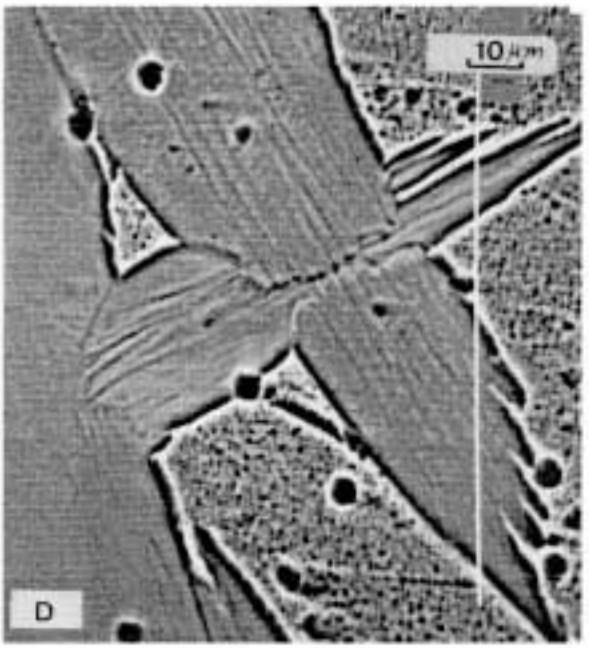
10 µm
D

Figure 4.2.6. Ti-22Al alloy as-quenched from 1300°C-4 hours.

e) presence of "acicular" massive grain (arrow A); TEM-BFI;

f) detail of irregular boundary between massive grains (arrow A); TEM-BFI;

g) stacking-faults present in massive grains; TEM-BFI;

h) Ti_3Al APDs ; DFI of prior micrograph: $B=[\bar{5}416]_{\alpha 2}$ and $g=(10\bar{1}\bar{1})_{\alpha 2}$


1 μm
A
E


1 μm
A
F

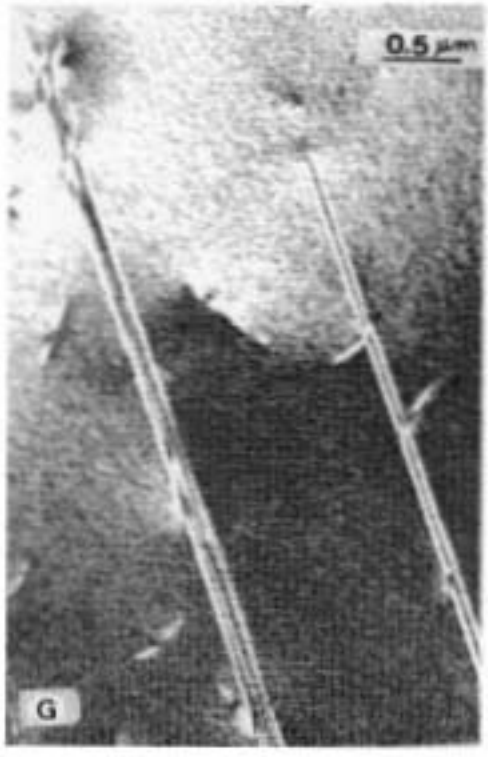
0.5 μm
G

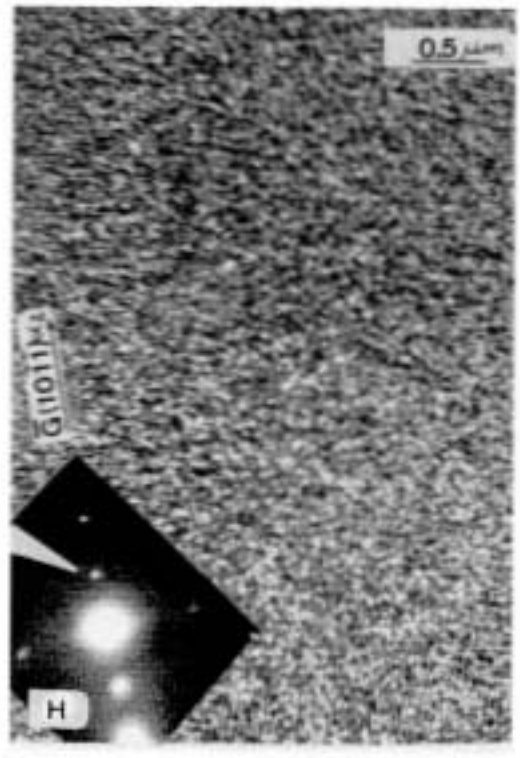
0.5 μm
GIIOIIHI
H

Figure 4.2.7. Ti-22Al-1.0Si alloy as-quenched from 1300°C-4 hours:

a) massive grains precipitated along prior β grains boundary; LM;

b) transition from massive to colony of parallel α plates;
SEM-SEI;

c) colonies of parallel α plates; SEM-SEI;

d) detail of a colony of parallel α plates; SEM-SEI.


160 µm
A

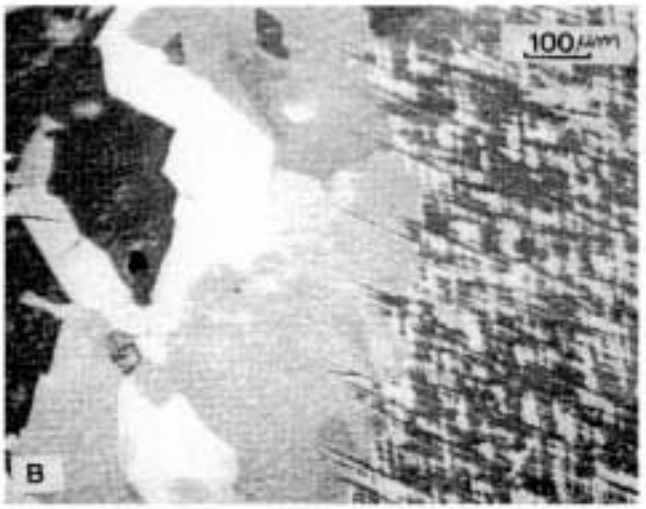
100 µm
B


20 µm
C

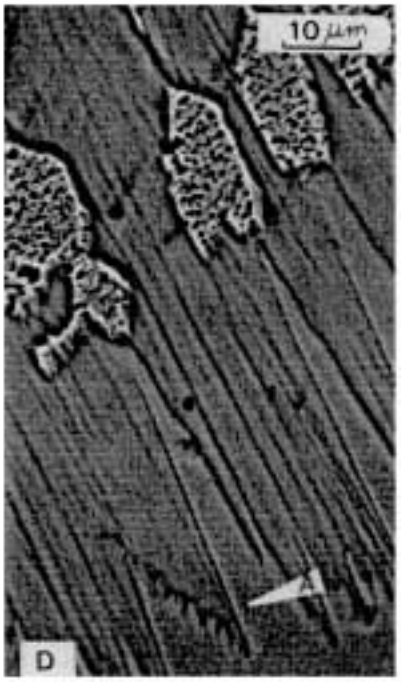
10 µm
D

Figure 4.2.7. Ti-22Al-1.0Si alloy as-quenched from 1300°C - 4 hours:

e) primary α plate (right); adjacent colony of parallel α plates presenting sub-units (centre); and faceted α "grain" (left); TEM-BFI;

f) TEM-DFI of prior micrograph: $g=(02\bar{2}0)_\alpha$; $B=[2\bar{1}\bar{1}3]_\alpha$ (SADP given below);

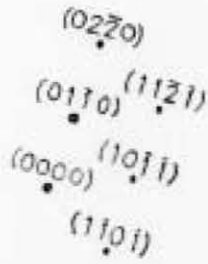

g) interfacial structure of sub-units (arrows A and B point at ledges of growth); TEM-DFI: $g=(10\bar{1}\bar{1})_\alpha$ and $B=[2\bar{1}\bar{1}3]_\alpha$;

h) Ti3Al APD's; TEM-DFI: $g=(10\bar{1}1)_{\alpha 2}$.


1 μm
E


1 μm
$\vec{G}(10\bar{2}0)_\alpha$
F

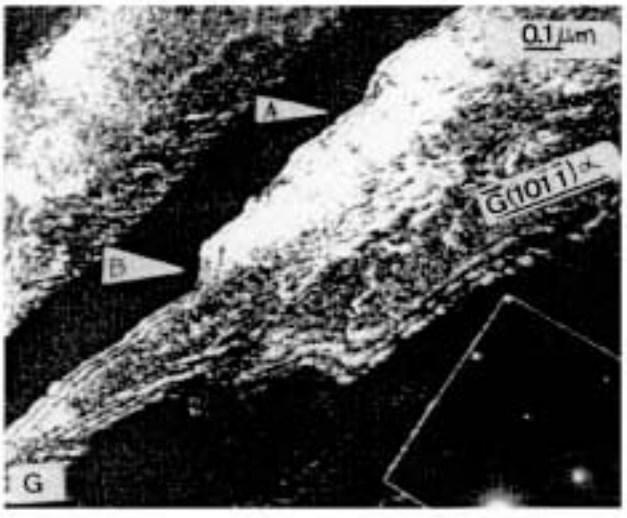
0.1 μm
A
B
$\vec{G}(10\bar{1}1)_\alpha$
G

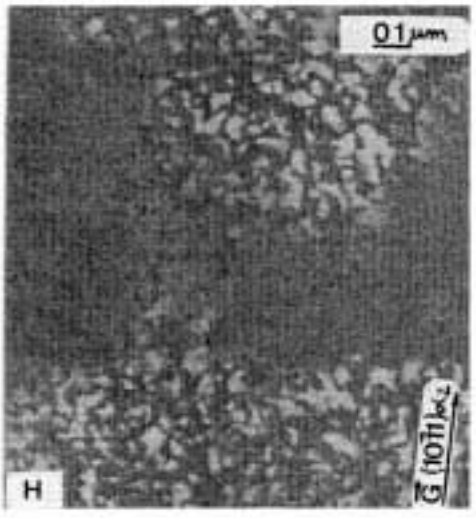
0.1 μm
$\vec{G}(10\bar{1}1)_{\alpha_2}$
H

Figure 4.2.8. Ti-20Al-1Si-1Zr alloy as-quenched from 1300°C-4 hours:

a) presence of massive grains (arrows A and B); primary α plates (upper left); and grain boundary α sideplates (lower centre); SEM-SEI;

b) detail of primary α plates and colonies of secondary parallel α plates; SEM-SEI;

c) detail of primary α plates and colonies of secondary parallel α plates (arrows A and B point at irregular interfaces); TEM-BFI;

d) detail of a colony of secondary parallel α plates (arrows A and B point at sub-units); TEM-BFI;

e) "acicular" massive grain presenting Ti_3Al APD's;
TEM-DFI: $g=(1\bar{2}10)_{\alpha 2}$ and $B=[10\bar{1}0]_{\alpha 2}$ (SADP given below)

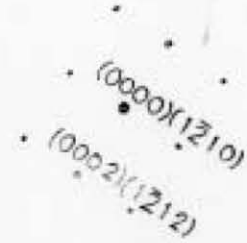


20 µm
A
B
A

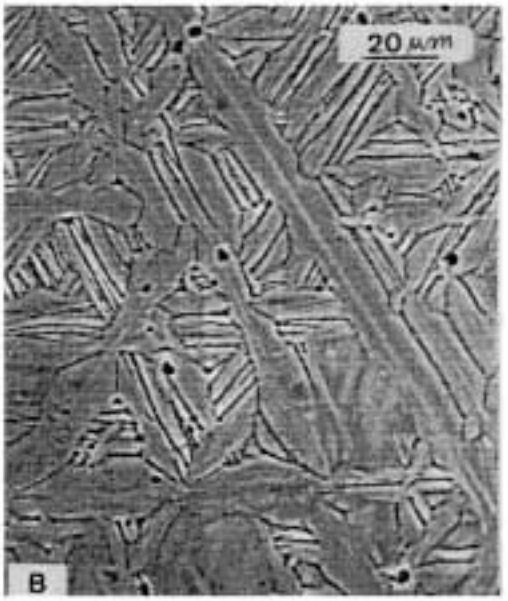
20 µm
B

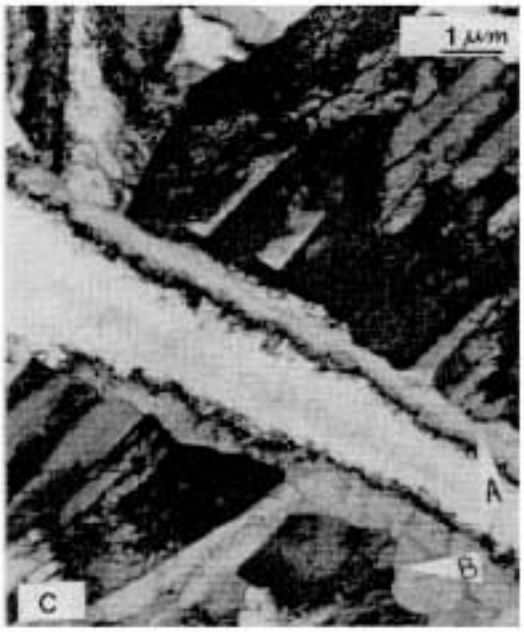
1 µm
A
B
C

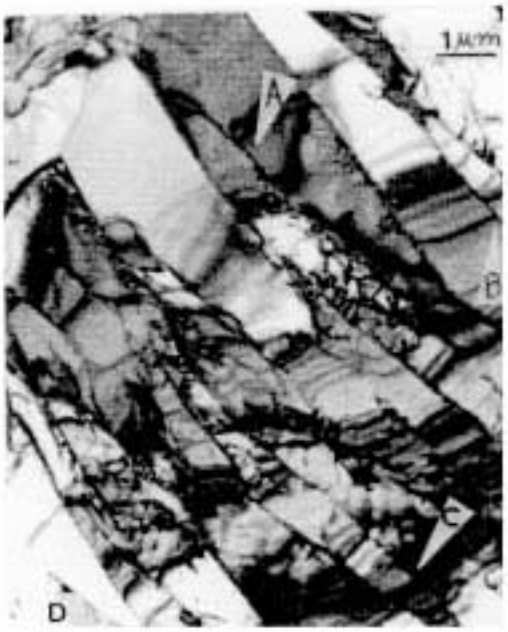
1 µm
A
B
C
D

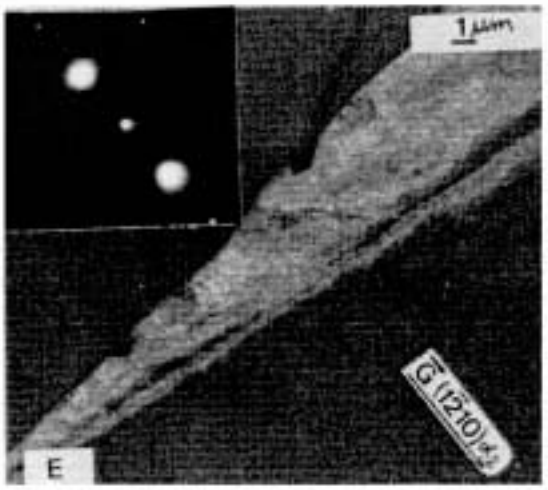
1 µm
G (12$\bar{1}$0)
E

Figure 4.2.9. Ti-20Al-1Si-1Nb alloy as-quenched from 1300°C - 4 hours:

a) grain boundary α sideplates; SEM-SEI;

b) faceted primary α plates and colonies of parallel secondary α plates; SEM-SEI;

c) presence of massive grains; SEM-SEI;

d) faceted (arrow A) and curved (arrow B) boundary between two massive grains; TEM-BFI;


20 µm
A

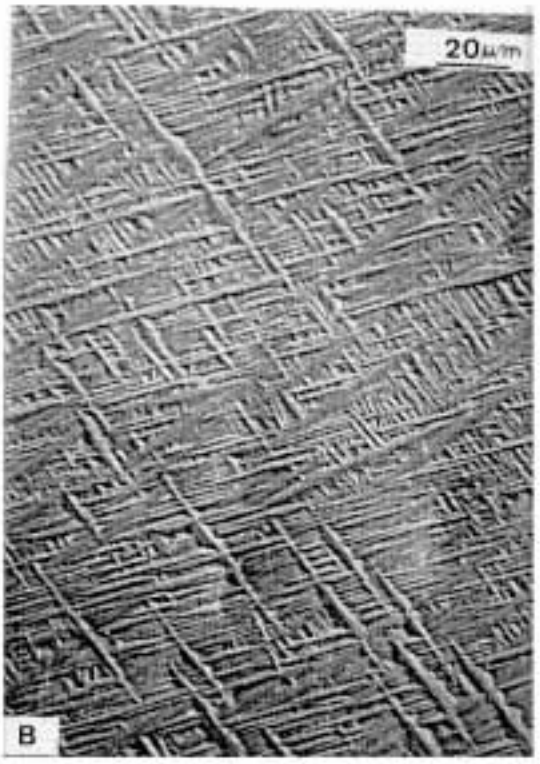
20 µm
B


40 µm
A
B
C
C


1 µm
A
B
D

Figure 4.2.9. Ti-20Al-1Si-1Nb alloy as-quenched from 1300°C-4 hours:

e) faceted boundary between a massive grain and a colony of parallel α plates; TEM-BFI;

f) primary α plate presenting irregular boundary with colonies of parallel α plates, the latter featuring presence of sub-units; TEM-BFI;

g) interfacial structure of the sub-units (arrows A and B); TEM-BFI;

h) presence of retained β along α/α plate boundaries; TEM-DFI: g=(110)β;

i) presence of Ti_3Al APD's; TEM-DFI: g=$(11\bar{2}0)_{\alpha 2}$.


1 μm
E


1 μm
F

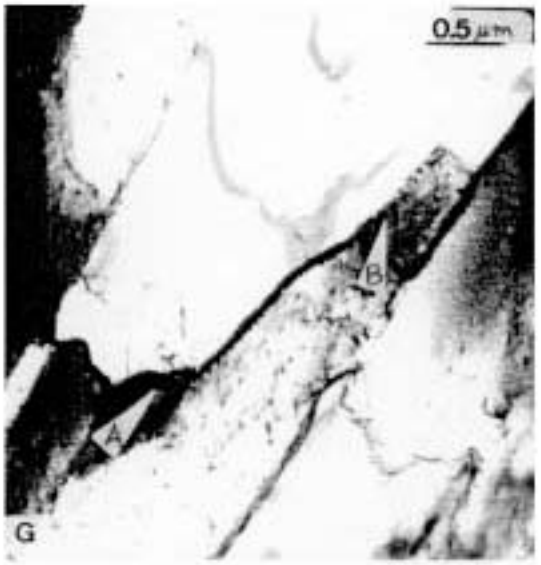
0.5 μm
B
A
G

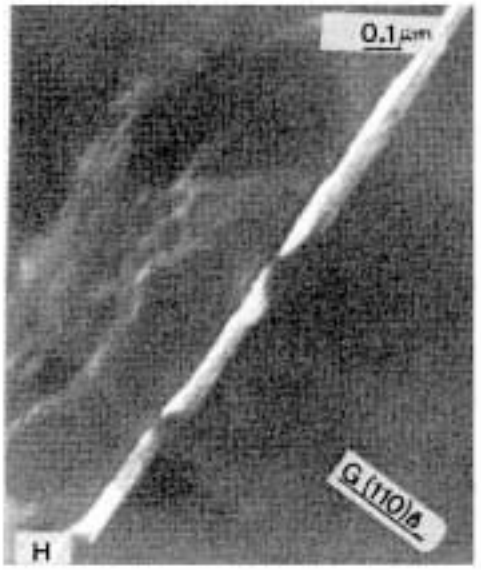
0.1 μm
G (110) α
H

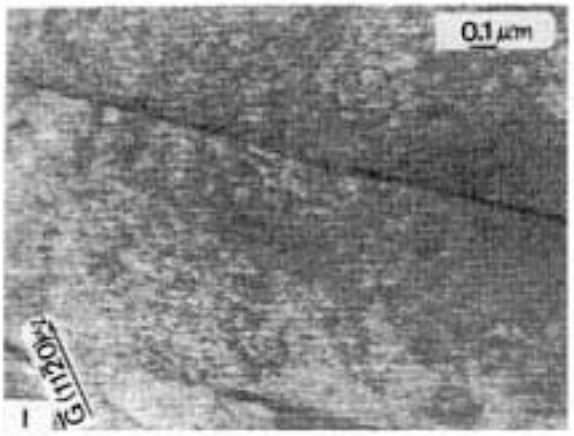
0.1 μm
G (1120) α
I

Figure 4.2.10. Ti-22Al-3.5Si alloy as-quenched from 1300°C-4 hours:

a) silicide precipitation; SEM-BEI;

b) α plates, massive grains (arrow A) and silicide precipitation; LM;

c) hexagonal-shaped silicide; TEM-BFI;

d) elongated sub-units inside an α plate (arrows A and B); TEM-BFI: B=$[1\bar{2}10]_{\alpha 2}$

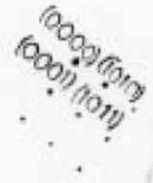


50 μm
A

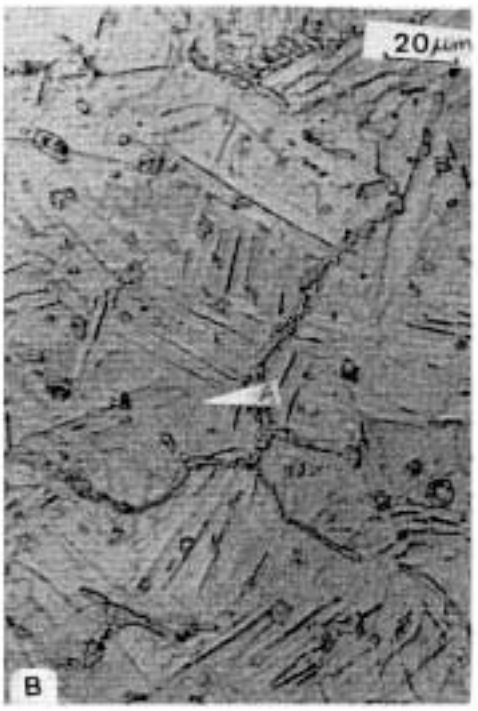
20 μm
B


0.5 μm
C

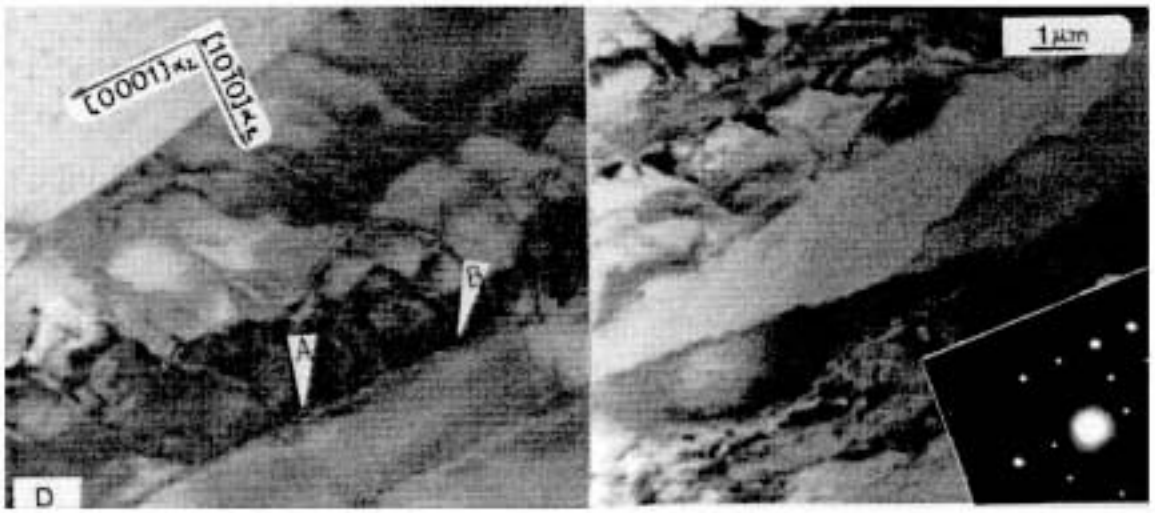
[0001]
[10$\bar{1}$0]
A
B
D
1 μm

Figure 4.2.10. Ti-22Al-3.5Si alloy as-quenched from 1300°C-4 hours:

e) detail of a sub-unit; BFI-TEM;

f) Ti_3Al APD's (arrows A and B point at elongated domains normal to the sub-boundary); TEM-DFI of prior micrograph: $g=(10\bar{1}0)\alpha 2$ and $B=[0001]\alpha 2$

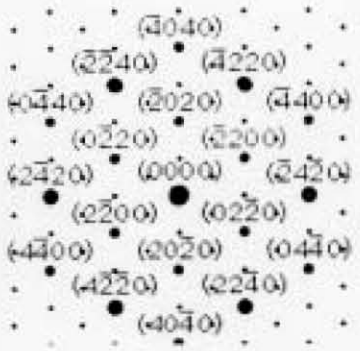

g) elongated Ti_3Al domains; TEM-DFI: $g=(1\bar{2}10)\alpha 2$ and $B=[\bar{1}010]\alpha 2$

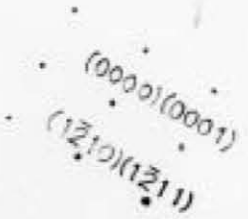


0.1 μm
E

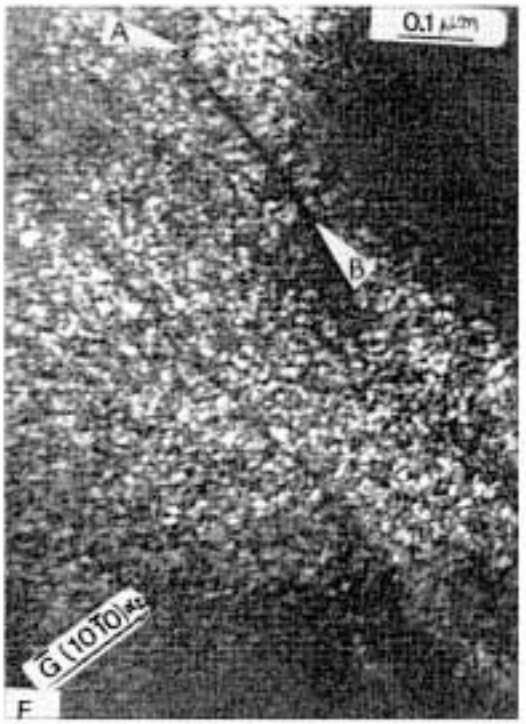
A
0.1 μm
B
G (10$\bar{1}$0)
F

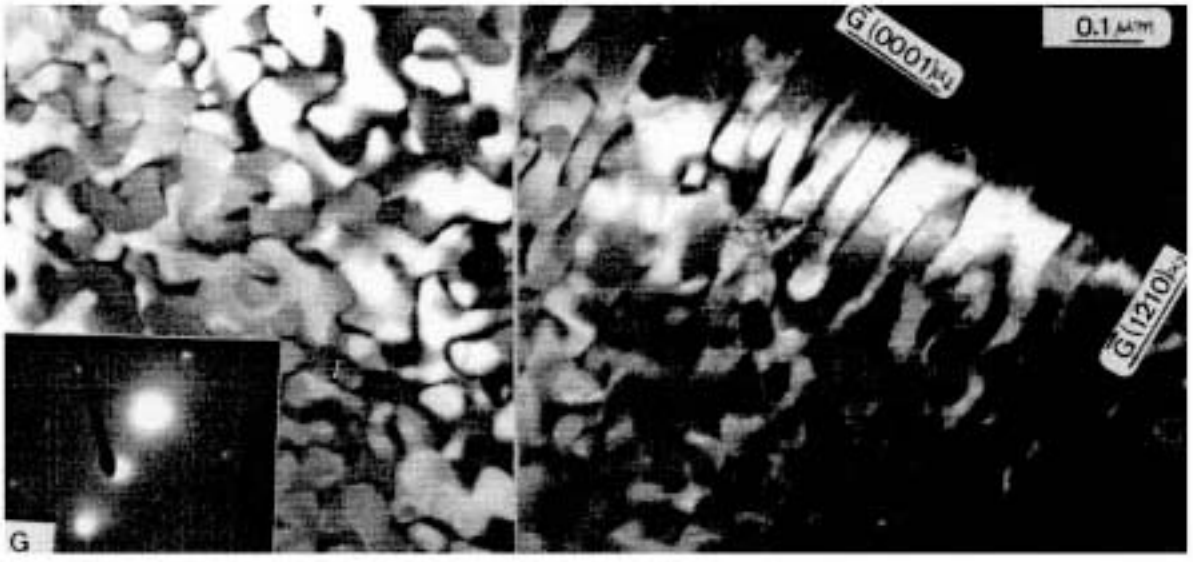
G (0001)
0.1 μm
G (12$\bar{1}$0)
G

Figure 4.2.10. Ti-22Al-3.5Si alloy as-quenched from 1300℃-4 hours:

h) detail of interfacial structure of α plate; BFI-TEM;

i) elongated Ti_3Al APDs; TEM-DFI of prior micrograph: $g=(0\bar{1}11)_{\alpha 2}$ and $B=[1\bar{2}1\bar{3}]_{\alpha 2}$ (SADP given below)

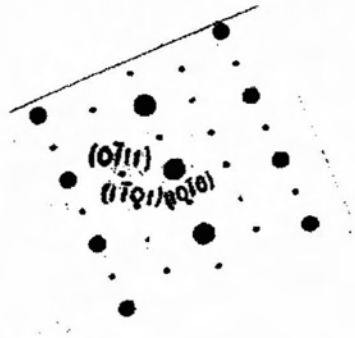

j) elongated Ti_3Al domains; TEM-DFI: $g=(0\bar{1}11)_{\alpha 2}$


0.1 μm
H


0.1 μm
G|0111|α2
[2131]α2
I

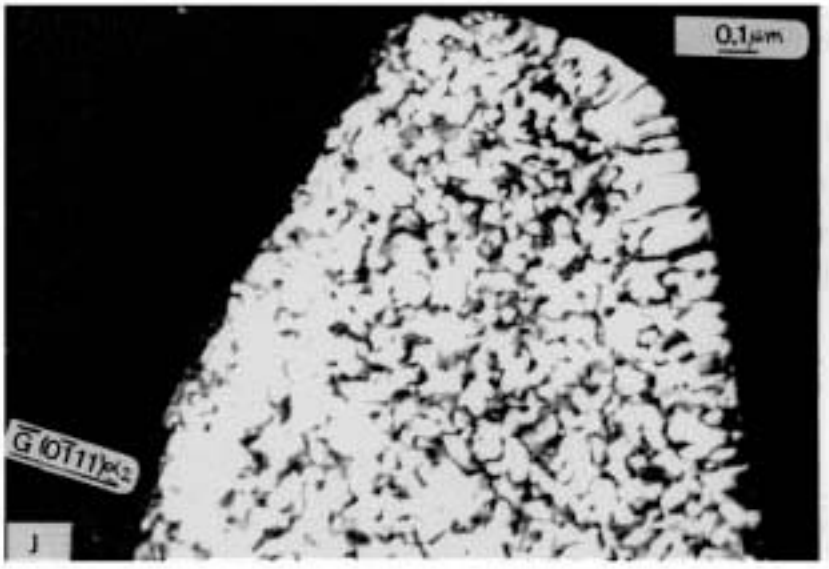
0.1 μm
G|01̄11|α2
J

4.2.1. Discussion on as-quenched alloys

• silicide precipitation

Comparing samples Ti-16Al-3.5Si and Ti-22Al-3.5Si (figures 4.2.5.a. and 4.2.10.a-b.), it is suggested that Al addition promotes less widespread precipitation of silicide along α/α boundaries and coarser secondary silicide precipitation (0.6 μm in sample 3A versus 1.4 μm in sample 6A), in agreement with previous work [ZHA 91]. Additionally, the results of microanalysis of matrix and eutectic silicides (see table 4.2.1.1.) show that:

- the solubility of Si in β phase decreased with Al addition, a fact in agreement with previous work [CRO 58], so that the β matrix of sample Ti-16Al-3.5Si presents more silicon in solution before quenching than sample Ti-22Al-3.5Si;
- addition of Al increases the solubility of Al and decreases the solubility of Si in the silicide, in agreement with previous work [ZHA 91], suggesting that Al replaces Si in the sublattice(s) of Ti_5Si_3.
- addition of Al increases the ratio Ti/(Al+Si) of the silicide from 1.64±.14 to 2.02±0.32, suggesting a possible change in the stoichiometry of the silicide. Such a change is not completely unexpected as Al presents a bigger atomic radius (table 4.2.1.2.); is less electronegative than Si (table 4.2.1.2.) and presents less electrons (+3) in the valence shell than Si (+4) [VAN 70]. Therefore, Al might alter the site occupancy of Ti, Si and vacancies in the different sublattices of the Ti_5Si_3 crystal; decrease the number of covalent (Ti-Si); and increase the number of metallic-type bondings (Ti-Al) in the silicide crystal. The present work, however, did not consider the solubility of Al in Ti_5Si_3 during the thermodynamic modelling of the ternary phase diagram, so that no quantitative information is available. Additionally, it is suggested that a much more precise model than the sublattice model would be needed to deal with the effect of variables such as atomic radius, electronegativity and valence in the stoichiometry of Ti_5Si_3.

alloy	T(°C)	sample	phase	chemical composition		
				at%Si	at%Al	at%Ti
Ti-16Al-3.5Si	1300	SEM	β	1.9±0.1	17.0±0.2	balance
			$Ti_5(Si,Al)_3$	34±1	4±1	"
6A	1300	SEM	β	1.4±0.1	23.7±0.6	"
			$Ti_5(Si,Al)_3$	25±2	9±2	"

Table 4.2.1.1. SEM-EDX analysis of as-quenched alloys.

Considering the partial vertical sections of the Ti-Al-Si system as proposed by Crossley [CRO 58] (figure 2.4.1.), there are two points to be considered to explain the morphological observations. Firstly, Al addition increases the eutectoid temperature, a fact which would explain the coarser silicide precipitation. Secondly, Al addition reduces the solubility of Si in β phase and has very little effect on the solubility of Si in α phase. This fact would promote more intense silicide precipitation during homogenisation heat treatment and reduce, therefore, Si supersaturation in α phase formed from β during quenching, so that precipitation of $Ti_5(Si,Al)_3$ along α/α boundaries would be inhibited. Furthermore, Al addition inhibits silicide precipitation during quenching [FLO 71], so this scarce precipitation of silicides along α/α boundaries would be further inhibited by kinetic reasons.

element (X)	Z(X)	density (g/cm^3)	atomic radius (Å)	valence	crystal structure	electronegativity ratio (e_X/e_{Ti})	melting temp. (°C)
Al	26.98	2.70	1.431	3+	fcc	0.94	660.2
Si	28.09	2.40	1.176	4+	diamond cubic	1.30	1430
Ti	47.90	4.54	1.458	4+	hcp	1.00	1820
Zr	91.22	6.50	1.580	4+	hcp	1.00	1750
Nb	92.91	8.57	1.429	5+	bcc	1.30	2415

Table 4.2.1.2. Table of elements data [VAN 70]

• formation of α2 domains

All binary, ternary and quaternary alloys with Al content close to 22at% presented α2 APD formation during quenching. In the alloys with lower Al content, only the ternary Ti-16Al-3.5Si alloy presented APDs. It is suggested that the addition of 3.5 at% Si favoured α2 precipitation, in contrast to suggestions by J.C.Williams [WIL **] that "increasing amounts of ternary additions lead to a reduction in the volumetric fraction of ordered domains". He related his explanation to the effect of β stabiliser elements on lowering of Ms temperature and, therefore, reducing the ordering temperature and delaying the onset of the ordering reaction. This contrary result obtained for the ternary Ti-Al-Si alloy shows that factors other than Ms temperature should also be considered to explain the kinetics of α2 ordering during quenching. The relative positioning of α, β and α2 phase fields and the effect of ternary additions on the diffusion coefficients seem important parameters to be considered along with Ms for the kinetics of ordering.

The ternary sample Ti-22Al-3.5Si exhibited formation of columnar domains, either formed by heterogeneous nucleation of α2 at low energy α/α boundaries (for instance the α/α sub boundaries observed at the interior of larger primary α plates, see figure 4.2.10.f.) or by the preferential growth of α2 domains adjacent to α/α boundaries and sub-boundaries or α/β interfaces. In the latter, the ordering reaction would occur concomitantly with the migration of α/β interfaces.

The formation of elongated α2 domains was also observed by C.H.Ward [WAR 93] in his review on Ti-Al-Nb α2 intermetallics: in Ti24Al-11Nb columnar α2 domains were shown to be formed, during cooling, from the martensite midribs, which were identified lying approximately parallel to the $\{10\bar{1}0\}_{\alpha 2}$ plane. No explanation for the presence of columnar α2 domains was presented. J.C.Williams [WIL**] observed elongated α2 domains near the martensite plate boundaries in a Ti-25at%Al-5at%Mo-1at%W alloy quenched from 1200°C. He suggested the occurrence of heterogeneous nucleation of ordered domains to explain the presence of this columnar morphology of α2.

In the present work, the elongated α2 domains where observed to grow along different directions such as $<11\bar{2}0>_{\alpha 2}$ (figure 4.2.10.g.), $<10\bar{1}0>_{\alpha 2}$ (see figure 4.2.10.f.) and $<21\bar{3}\bar{1}>_{\alpha 2}$ (see figure 4.2.10.i). The hypothesis of formation of elongated domains by ordering occurring as α/β interface migrates is rejected by the existence of elongated domains on both sides of a sub-boundary (figure 4.2.10.f.). Furthermore, it seems very unlikely that this low-angle boundary would present any lateral growth other than by ledges. The low proportion (high selectivity) of α boundaries presenting elongated domains (figure 4.2.10.j) also rejects the operation of any other mechanism of preferential growth. It is suggested that these elongated domains were heterogeneously nucleated at certain low-angle α/α boundaries, where by balance of interfacial energy it can be expected an anisotropic nucleation and growth of α2 APDs. The exclusive presence of heterogeneous nucleation in the alloy Ti-22Al-3.5Si can be better understood by considering factors other than Ms temperature:

- Si addition changes the relative positioning of α, β and α2 phase fields and promotes a peritectoid reaction β+α2->α in the Ti-Al-Si system at approximately 22at%Al (see figure 4.3.2.4.d.). This change would alter the thermodynamic and kinetic conditions for ordering, increasing the driving force of the reaction α->α+α2 and allowing this reaction to start inside the α+α2 or α+α2+β phase field during quenching;
- Si addition does not decrease the atomic diffusivity;

• Si addition alters the lattice parameters of α and α2 (see table 4.3.1.3.) and increases the misfit along <0001>α2 and <10$\bar{1}$0>α2. This condition would, favour the heterogeneous nucleation of α2 at α/α boundaries and sub-boundaries.

sample	zone axis	reflecting plane	APB size (nm)
Ti-16Al-3.5Si	[5146]	($\bar{1}\bar{1}$01)	10
Ti-22Al	[0001]	(1$\bar{1}$00)	20
"	[10$\bar{1}$1]	(1$\bar{1}$0$\bar{1}$)	28
"	[1$\bar{2}$13]	(1$\bar{1}\bar{1}$)	22
Ti-22Al-1Si	[11$\bar{2}$0]	(1$\bar{1}$00)	22
"	[1$\bar{2}$16]	(10$\bar{1}$0)	17
"	[0001]	(1$\bar{2}$10)	18
"	[10$\bar{1}$2]	(1$\bar{2}$10)	17
Ti-20Al-1Si-1Nb	-	-	15
Ti-20Al-1Si-1Zr	-	-	10
Ti-22Al-3.5Si	[1$\bar{1}$00]	(11$\bar{2}$0)	54
"	"	"	40
"	"	"	48
"	"	"	w= 40 and l= 200 (elongated APD)

Table 4.2.1.3. α2 domain size of as-quenched alloys

The remaining alloys presented only equiaxial APDs. The matrix of the binary Ti-22Al alloy presented stacking faults, where no presence of columnar α2 domains was observed (figure 4.2.5.g-h.). Table 4.2.1.3. shows the measured values of α2 domain size. Although these measurements should not be taken as very precise, it shows qualitatively that intragranular APD did not lie in any preferred plane and that the network is similar to that formed in other superlattices with an isotropic variation of APB energy with orientation [BLA 67b][BLA 67 c]. Quaternary additions of Zr and Nb inhibited the growth of APD's domains as these elements diffuse more slowly than Ti or Al.

This discussion will show how variables which can be obtained through thermodynamic modelling of phase diagrams might help to control the morphology of as-quenched microstructures. Assuming a constant cooling rate and disregarding possible variations on the interstitial contents (C, O, N), it will be shown how $T_{\beta/\beta+\alpha}$, T_0, $T_{\beta+\alpha/\alpha}$ and Ms temperatures and the solute diffusivity control the morphology of α phase, formed by the allotropic reaction β–>α. It is emphasised that these morphologies produced on quenching will control the quantity and quality of the nucleation sites for the subsequent solid state reactions (α2 and silicide precipitation). The control of the amount of α/α interfacial area via heat treatment (without any prior mechanical deformation) along with available data on phase equilibria and microstructure/mechanical properties relationship might enable microstructural design of cheaper titanium aluminide alloys. Two step processing (homogenisation and isothermal heat treatment) is of special importance in the foundry industry, where generally no mechanical work can be used to alter the starting microstructure.

A summary of the morphological observations is given in table 4.2.1.4. Increase in Al content promoted massive-type transformation and the formation of coarser microstructures composed of a transitional massive/martensite primary α plates and colonies of parallel plates presenting sub-units. The addition of Al increases the T_0, $T_{\beta/\beta+\alpha}$, $T_{\beta+\alpha/\alpha}$ and Ms temperatures (see tables 4.2.1.5. and 4.2.1.6.) and these effects, especially on $T_{\beta+\alpha/\alpha}$ [HIL 84][MEN 88] explain the favouring of massive products: the kinetics of diffusional decomposition of β is favoured at higher temperatures, and as long as the ternary addition does not increase the extension of the two phase field (given by $T_{\beta/\beta+\alpha}$ -$T_{\beta+\alpha/\alpha}$) [PLI 77][PLI 78], a larger proportion of massive product will be expected. Under these circumstances isothermal heat treatment between $T_{\beta+\alpha/\alpha}$ and Ms following homogenisation (similar to an austempering) might produce large massive grains. Such transformed β microstructure would promote:

- homogeneous nucleation of α2 during heat treatment inside α+α2 field [ARK 95].
- possible formation of very large α2 grains during treatment inside α2 phase field [BLA 67b].

alloy	morphological observations							
	α_{GBall}	$\alpha_{mas.}$	α_{GB}// plates	$\alpha_{colonies\,of}$ //plates	$\beta_{ret.}$	P(X)α,β	$\alpha_{primary.}$ plate	Suburits
Ti-16Al	-	xxx	-	x	-	-	-	-
Ti-16Al-1Si	-	xx	-	xx	-	-	xx	-
Ti-14Al-1Si-1Nb	x	-	-	xx	x	P	xx	-
Ti-14Al-1Si-1Zr	-	-	xx	xx	-	-	xx	-
Ti-16Al-3.5Si	-	-	xx	xxx	-	–	-	-
Ti-22Al	-	xxx	-	x	-	-	-	-
Ti-22Al-1Si		xx	-	xx	-	-	xx	Y
Ti-20Al-1Si-1Nb	-	x	xx	xx	x	P	xx	Y
Ti-20Al-1Si-1Zr	x	x	xx	xx	-	-	xx	Y
Ti-22Al-3.5Si	-	xx	-	xx	-	-	xx	Y

legend

$\alpha_{GBallot.}$ = grain boundary allotriomorph;
$\alpha_{mas.}$ = massive grains;
$\alpha_{GB//plates}$ = grain boundary parallel sideplates;
$\alpha_{colonies//plates}$ = colonies of parallel plates;
$\beta_{ret.}$ = presence of retained β;
P(X)α,β = solute partitioning between α and β
$\alpha_{prim.plates}$ = α primary plates;
x = morphology observed:
xx = morphology present in substantial area;
xxx = predominant morphology
Subunits = presence of subunits within colony of //α plate.

Table 4.2.1.4 Summary of morphological observations.

Si, Zr and Nb inhibited the massive-type transformation, especially in the alloys with lower Al content. All these alloying elements decreased $T_{\beta+\alpha/\alpha}$ (see tables 4.2.1.5. and 4.2.1.6) and inhibited the formation of massive products. Si is seen to be the weakest massive-type transformation inhibitor, and its addition was shown to decrease the massive grain size and increase the irregularity of the interface, producing a massive product typically formed at higher undercoolings. Figure 4.2.2.b. shows that Si addition promoted a much more faceted and acicular massive interface, suggesting that at higher undercoolings the OR plays an important role on the growth of massive product, in agreement with Aaronson and co-workers [MEN 88][PLI 84]. The observation of a massive product typical of higher undercoolings [PLI 77][PLI 78] agrees with the suggested effect of Si on $T_{\beta+\alpha/\alpha}$ and [$T_{\alpha+\beta/\alpha}$ - Ms] (see table 4.2.1.6.). This widening of [$T_{\alpha+\beta/\alpha}$ - Ms] would allow more time at lower temperature for the massive product to form

before the competing martensitic reaction could occur. Additionally, Si addition did not affect [$T_{\beta/\beta+\alpha}$ -$T_{\beta+\alpha/\alpha}$], which indicates that this addition does not promote β decomposition inside the α+β phase field; and did not decrease the atomic diffusion.

binary alloy (at%)	$T_{\beta->\alpha+\beta}$ (°C)	$T_{\beta+\alpha->\alpha}$ (°C)	T_0 (°C)	Ms (°C)	T_{melt} (°C)
Ti	882 @	882 @	882 @	871 †	1670 @
Ti-16 Al	1090 @	1063 @	1070 ©	1026 &	1710 @
Ti-22 Al	1135 @	1110 @	1120 ©	1078 &	1690 @
Ti-1 Si	867 @	865 @	867 ®	814 @	1660 @
Ti-1 Nb	870 @	780 @	842 ©	830 &	1675 @
Ti-1 Zr	878 @	870 @	872 ©	850 ø	1660 @

Legend

@= data from M.R.Plitcha et al. [PLI 78]

†= data from M.Bibby et al. [BIB 63]

&= data from K.S.Jepson et al. [JEP 70]

®= data from M.R.Plitcha et al.[PLI 78]

©= calculated using available thermodynamic data [MUR 87] and imposing:

$$G(\alpha, X_{Al}) = G(\beta, X_{Al})$$

ø= data from Y.C.Huang et al. [HUA 70]

Table 4.2.1.5. Temperature parameters for some binary Ti-alloys.

The effect of Zr on decreasing $T_{\alpha+\beta/\alpha}$ and widening [$T_{\alpha+\beta/\alpha}$ - Ms] without affecting [$T_{\beta/\beta+\alpha}$ -$T_{\beta+\alpha/\alpha}$] (see table 4.2.1.6.) indicates that this addition would also promote the formation of high undercooling massive α. The experimental results, however, showed otherwise. Zr was very effective, indeed, on inhibiting the formation of massive product, specially in the Ti-14Al-1Si-1Zr, and on promoting the formation of martensitic microstructures. This result shows clearly the effect of the low diffusivity of Zr on inhibiting the diffusional formation of a typical massive product. For Ti-20Al-1Si-1Zr alloy, it is suggested that the increase in Al, which increased both solvus and Ms and shifted [$T_{\alpha+\beta/\alpha}$ - Ms] to higher temperatures, favoured the diffusional decomposition of β and the formation of transitional massive/martensite microstructures.

Ti-Al-Si-X alloy (at%)	$T_1=T_{\beta/\alpha+\beta}$ (°C)	$T_2=T_{\beta+\alpha/\alpha}$ (°C)	Ms (°C)	T_1-T_2 (°C)	T_2-Ms (°C)
Ti-16 Al	1090	1063	1026	27	37
Ti-16Al-1Si	1075	1046	969	29	77
Ti-16Al-1Si-1Nb	1060	944	928	116	16
Ti-16Al-1Si-1Zr	1071	1034	948	37	97
Ti-22 Al	1135	1110	1078	25	32
Ti-22Al-1Si	1120	1093	1021	27	72
Ti-20Al-1Si-1Nb	1108	991	980	117	11
Ti-20Al-1Si-1Zr	1116	1081	1000	35	81

extrapolation method

ternary alloys:

$$T^{(i)}_{Ti\text{-}Al\text{-}Si} = T^{(i)}_{Ti} + \Delta T^{(i)}_{Ti-Al} + \Delta T^{(i)}_{Ti-Si}$$

quaternary alloys:

$$T^{(i)}_{Ti\text{-}Al\text{-}Si\text{-}X} = T^{(i)}_{Ti} + \Delta T^{(i)}_{Ti-Al} + \Delta T^{(i)}_{Ti-Si} + \Delta T^{(i)}_{Ti-X}$$

where

$T^{(i)}_{Ti}$ and various $\Delta T^{(i)}_{Ti-X}$ are given in table 4.2.3.

Table 4.2.1.6. Extrapolated temperature parameters for Ti-Al-Si- X alloys.

Nb addition also decreased $T_{\alpha+\beta/\alpha}$ and Ms (see table 4.2.1.6.) without affecting [$T_{\alpha+\beta/\alpha}$ - Ms]. Additionally, Nb addition showed a singular effect, among the investigated additions: it drastically widened [$T_{\beta/\beta+\alpha}$ -$T_{\beta+\alpha/\alpha}$]. This effect indicates the decomposition of β inside the two phase field would be promoted. This reaction would occur with solute partitioning during nucleation and growth (diffusional mechanism) in case Ms is below $T_{\beta+\alpha/\alpha}$. The experimental work confirmed the solute partitioning and the presence of stabilised β, although no conclusive evidence concerning the mechanism of reaction could be established. Also inconclusive is the fact that the extrapolated value of Ms for Ti-16Al-1Si-1Nb and Ti-20Al-1Si-1Nb (see table 4.2.1.6.) lie below $T_{\alpha+\beta/\alpha}$, suggesting that solute partitioning after nucleation by shear is not thermodynamically feasible for this alloy. The addition of Al also promoted the formation of more diffusional products like GB sideplates and GB allotriomorphs.

The results have shown that the morphology of α formed during quenching can vary profoundly and almost continuously from relatively featureless "massive" grains to a combination of primary and secondary acicular plates presenting dislocations with the addition of Si, Nb and more

effectively Zr. Primary and secondary colonies of parallel plates have also been observed adjacent to the massive grains, primary plates and to transitional massive/martensite microstructures. These colonies may present solute enriched β phase retained along adjacent plates when Nb is added. Additionally each plate within the colony may be composed of parallel sub-units, especially the ternary and quaternary alloys with Al content close to 22at%.

One peculiarity of the allotropic reaction in Ti-alloys is the presence of a very narrow interval of temperature separating all the possible α' morphologies which might result from quenching. Additionally, there is no difference in the crystal structure, orientation relationship and habit plane between the diffusional (hcp) and martensitic (hcp) product in dilute Ti-alloys [DAV 79]. Data from Wilson [WIL 79] for Fe-0.015%C-0.005%N alloy shows, in a schematic TTT curve, that the morphological transition (equiaxed ferrite -> massive ferrite -> bainitic ferrite -> lath martensite -> twinned martensite) for a Fe-0.015%C-0.005%N alloy exists over a temperature interval of approximately 490°C. Following this argument, one would expect that a similar morphological transition would exist for the formation of α' phase in Ti-alloys, but over a much narrower temperature interval ($T_{\beta/\alpha+\beta}$ - Ms) of approximately 60°C for Ti-Al, around 100°C for Ti-Al-Si and around 120°C for Ti-Al-Si-X (X= Nb or Zr) (see table 4.2.1.6.). It is also important to note that diffusion can be a very competitive mechanism around Ms for some Ti-alloys. The formation of α2 APDs during quenching is a good proof of the presence of short range diffusion in these alloys around Ms. Additionally, the ratio between homologous temperatures* can be used as a rough indicator of the atomic diffusivity around Ms. For instance, the recrystallisation temperature is usually within the range 0.33-0.50 [VAN 70]. For the Fe-0.015%C-0.005%N alloy [WIL 79], the massive morphology occurs around 0.48, the bainitic ferrite around 0.43, the lath martensite around 0.35 and finally the twinned martensite, whose appearance defined the Ms temperature, around 0.27. For the Ti-Al-Si-X alloys studied, at Ms the homologous temperature is usually higher than 0.50, reaching values around 0.60 for the binary Ti-Al (see table 4.2.1.7.). This high atomic diffusivity of Ti-Al-Si-X alloys around Ms and the narrow temperature range (see table 4.2.1.6.) available for the morphological transitions resulting from a transition in the mechanism of α' formation (diffusion versus shear) suggest that small variations in the thermodynamic and kinetic conditions in the parent phase might account for changes in the mechanisms of nucleation

*defined as the ratio between T and the solidus temperature.

and growth of α' phase in Ti-Al alloys. This morphological changes in α' formation could be observed, experimentally, not only throughout the quenched samples, but also within a single prior β grain.

alloy (at%)	$M_s/T_{solidus}$
Ti-16 Al	0.60
Ti-16Al-1Si	0.57
Ti-16Al-1Si-1Nb	0.54
Ti-16Al-1Si-1Zr	0.56
Ti-22 Al	0.64
Ti-22Al-1Si	0.61
Ti-22Al-1Si-1Nb	0.58
Ti-22Al-1Si-1Zr	0.60

Table 4.2.1.7. Extrapolated homologous Ms for Ti-Al-Si-X alloys.

Full understanding of the mechanisms involved during these morphological changes is, however, still a big challenge for the theory of phase transformations. As seen in the literature survey, there is still intense debate on the roles of diffusion and shear on the formation of plate-like precipitates; and on the mechanism of growth of massive products: disordered interfaces without any OR controlling the growth versus semi-coherent interfaces respecting OR and presenting ledges of growth, whose riser would present a glissile disordered interface; and the roles of T_0 and solvus temperatures on the thermodynamics of massive transformation. Even semantic discussions on the definitions of a massive product are still happening: is the term massive a type of morphology (irregular interfaces, grain boundary crossing, no OR) or a type of solid state reaction presenting short-range diffusional growth along disordered interfaces [MAS 84][HIL 84][PLI 84][PER 84][MEN 88]. The latter approach does not define a typical massive morphology and does not divide the solid state morphological transitions into spectra.

The present investigation observed few interesting morphological features of massive products which confirm this latter approach, such as: presence of anisotropic growth (figure 4.2.2.b); ledges of growth (figure 4.2.6.b), "acicular" massive grains (figures 4.2.6.e. and 4.2.8.e.), dislocations (figures 4.2.6.e-f), and transitional massive/primary plate morphologies (figures 4.2.8.c. and 4.2.9.e-f). This very blurred transition between massive and primary α plates was observed in some of the Ti-Al-Si-X alloys with higher Al content. It is suggested that the transition between diffusional and

shear mechanism is also diffuse and would account for the transitional massive/primary plates morphologies observed:

- considering initially the transition massive -> martensite, it has been proposed that massive interface moves by individual jumps of atoms across an incoherent interface [HIL 84][MAS 84], but growth by ledges is a reasonable possibility for the massive transformation under increasing undercooling [MEN 88]. Under this circumstances the riser, presenting incoherent interface, would be the moving α/β interface and the resulting massive microstructure would be more anisotropic in character, featuring, for instance, "acicular" massive grains (figure 4.2.6.b. and 4.2.9.c.) and faceted interfaces (figures 4.2.2.b.; 4.2.6.b.; and 4.2.9.d). Furthermore, it is stated that invariant plane strain surface relief can be generated during massive transformation when reaction occurs at sufficiently high undercoolings [MEN 87] due to the larger proportion of partially coherent interface areas.
- considering now the transition martensite -> massive, it has been discussed previously that there is no difference in the crystal structure, orientation relationship and habit plane between the diffusional (hcp) and martensitic (hcp) product in dilute Ti-alloys [DAV 79]. Additionally, the high atomic diffusivity of Ti-Al-Si-X alloys around Ms and the narrow temperature range (see table 4.2.1.6.) available for the morphological transitions suggest that small variations in the thermodynamic and kinetic conditions in the parent phase might account for changes in the mechanisms of nucleation and growth of α' phase in Ti-Al alloys. Under this conditions, an α plate could initially nucleate by shear and grow by diffusion, generating a final plate exhibiting not-so-faceted interfaces (figures 4.2.8.c and 4.2.9.f) and lower dislocation density. The final product would resemble very much a massive products.

In both cases mentioned above, it is possible to produce transitional microstructures resembling the ones observed experimentally. The model proposed by Aaronson and co-workers [MEN 87] for the massive transformation was very useful to explain some of the transitional morphologies observed in the present investigation. The morphological observations agreed with his views on the formation of more anisotropic massive products with increasing undercoolings. Such morphologies, however, have not been observed in alloys with lower Al content, confirming that small variations in the homologous temperatures might

account for changes in the mechanisms of nucleation and growth of α phase in Ti-Al-Si-X alloys investigated.

The previous discussion dealt with the some of the "blocky acicular" morphologies, so the following discussion will concentrate on the roles of diffusion and shear on the formation of colonies of parallel α plates. Far more so than in the proeutectoid ferrite reaction in steel, sideplate and intragranular plate are the predominant morphologies during the proeutectoid reaction in Ti-X alloys at all but the smallest undercoolings [FUR 90]. The experimental results show that colonies of parallel plates formed during quenching presented moderate dislocation density; low-angle α/α plate boundaries; presence of internal aligned subunits presenting small angle sub-boundaries (figures 4.2.7.e., 4.2.7.g., 4.2.8.d., 4.2.9.g., 4.2.10.d and 4.2.10.e) and, in Ti-Al-Si-Nb alloys, the additional presence of retained β (with solute partitioning) along α/α parallel plates boundaries (figures 4.2.4.d and 4.2.9.h. and tables 4.2.1. and 4.2.2.).

The presence of subunits has been described in the literature as an example of sympathetic nucleation [AAR 56][MEN 87][BHA 95]. Clusters of lattice defects, with possible local variations in the chemical composition due to (solute)-(lattice defects) interaction [AAR 56], and heterogeneous nucleation of sub-units on the terraces of plate shaped precipitates (replacing a low energy α/β interface by low energy α/α interface) have been considered to explain the diffusional nucleation of these subunits [MEN 87], although H.Margolin et al. proposed that these sub-units are formed by twinning [MAR 77]. Menon et al. [MEN 87] mentioned in their investigation on the morphology, crystallography and kinetics of sympathetic nucleation in Ti-Cr and Ti-Mn alloys that the strain energy that accompanies the "purely diffusional transformations" considered (Ti-6.6at%Cr reacted at 700°C for 2 hours, T_0 between 200 and 300°C, and Ti-8.6at%Mn reacted at 700°C for 1000 seconds) can play a significant role in the kinetics of sympathetic nucleation. It is also worth mentioning that Bhaskaran et al. [BHA 95] observed these sub-units in some rapidly quenched Ti-eutectoid alloys such as Ti-4%Cu and Ti-2.8%Co. Furthermore, the lack of observation of retained β along these sub-boundaries in the literature and in this experimental work suggest that these subunits are supersaturated in solute, indicating either initial formation by shear or partitioning of solute under paraequilibrium conditions (partitioning of fast diffusers).

Previous investigations on solute partitioning during the proeutectoid α transformation in Ti-alloys [ENO 90][ENO 91] observed that solute concentration in the α plates was close to the α/(α+β) phase boundary composition just after few seconds of isothermal heat treatment above and below T_0. On the other hand, the concentrations in the β matrix were mostly within the (α+β) two phase region. They concluded that the massive or martensitic transformation is unlikely to be the major transformation mode in the substantial temperature range below T_0 in these alloys; and that the plates had been formed by a diffusional. If these α plates were formed with the full supersaturation of solute, α phase would present concentration gradient perpendicular to α/β interface. Considering that the partitioning of solute occurred after the transformation by shear, one can estimate the width of the zone in α phase presenting concentration gradient of solute. This tentative calculation was made for the Ti-16Al-1Si-1Nb alloy to check whether EDX-TEM analysis would be a capable tool to identify the existence of such zones after transformation by shear. For this calculation the following parameters have been employed:

- $T_{\beta/\alpha+\beta}$ and $T_{\alpha+\beta/\alpha}$ temperatures from table 4.2.1.6.; and cooling rate of 200°C/second [DAV 79][FLO 74] have been assumed. Under these circumstances the estimated time available for the solute partitioning (inside α+β phase field) is around 0.6 seconds;
- assuming that the diffusion time is 0.6 seconds and using the diffusion coefficient of Al in Ti-α [OUC 80], the value of $\sqrt{D.t}$ at $T=T_{\beta/\alpha+\beta}=1060°C$ is approximately 30 nm.

This estimated value of 30 nm for the width of the diffusion affected zone indicates that the beam spot size used by the previous works [ENO 90][ENO 91], whose diameter is 50nm [ENO 90], is not small enough to detect possible concentration gradients in α caused by solute partitioning after shear transformation. This suggests that the works by Enomoto and co-workers [ENO 90][ENO 91] concluding that the massive or martensitic transformation is unlikely to be the major transformation mode in the substantial temperature range below T_0 are not conclusive. Also inconclusive is the fact that the extrapolated value of Ms for Ti-16Al-1Si-1Nb (see table 4.2.1.6.) lies below $T_{\alpha+\beta/\alpha}$, suggesting that solute partitioning after nucleation by shear is not thermodynamically feasible for this alloy.

The presence of ledges of growth (figure 4.2.7.g.) appears to be the only evidence of diffusional growth of the colonies of parallel plates in

quenched Ti-22Al-Si alloys. This evidence, however, does not refute the initial formation of the α plate by shear. As the hypothesis of nucleation of α plates by shear followed by solute partitioning is not unrealistic the following discussion will emphasise how diffusion can play a visible role on the nucleation and growth of α' plates via shear.

As mentioned by C.Jourdan et al. [JOU 87][JOU 89][JOU 91], the nucleation of martensite can be induced by residual stresses associated to complex defects. So, as a result of the presence of these crystalline defects induced by the shear transformation, in some areas the stress field might induce further transformation via shear by reducing ΔG^*_{shear}. In other areas the stress field might just oppose such type of transformation by increasing the ΔG^*_{shear} for the nucleation of α' [NIS 78]. Considering now that diffusion and shear mechanisms are competing for the nucleation of α, it does not seem very unlikely that, in some of the areas opposing the shear mechanism, diffusion might become the operative mode for the nucleation of α' ($\Delta G^*_{dif.} < \Delta G^*_{shear}$) and growth of α plates. The release of latent heat during the formation of primary α'plates by shear, under the assumption of martensite formation as an adiabatic process [KAU 92], might as well alter locally the nucleation conditions of secondary plates by increasing temperature of the areas adjacent to this primary plate [DAV 79]. This increase in temperature is expected to increase ΔG^*_{shear} , reduce $\Delta G^*_{dif.}$ and promote diffusional nucleation of α plates.

Additionally, it seems valid to suggest for Ti-Al-Si-X alloys (see table 4.2.1.7.) that the lattice strain energy generated at the start of the allotropic reaction via shear can be relieved by diffusion [FLO 72][FLO74][DAV 79]. Solute partitioning between α and β (if $Ms > T_{\alpha+\beta/\alpha}$) and solute drag phenomenon (such as solute segregation to and away from α/β interfaces and dislocations, and resulting from the interaction of the strain field of solute atoms in the martensite lattice with the stress field of the moving martensitic interface [OWE 92]) are among the diffusional processes which may relieve the strain energy and increase ΔG^*_{shear} (as the nucleation of martensite can be induced by residual stresses associated to defects). The diffusion is likely to, at least, alter locally the thermodynamic conditions for further nucleation and growth of the α' phase via shear. In that sense, M.Hillert and L.Kaufman [KAU 92] suggested that an increase in ΔG^*_{shear} might induce a nucleus formed initially by shear to grow by a diffusion controlled mechanism, such as growth by ledges. This suggestion might explain the morphological change found in figure 4.2.7.e-f, which shows a

colony of parallel α plates presenting sub-units just adjacent to a primary α plate. Note that the parallel plates, in this case, lie almost parallel to the primary plate boundary, suggesting a transition of mechanism during the growth of the primary plate. For a constant cooling rate, the higher the Ms temperature, the more effective the role of diffusion on the nucleation and/or growth of α' plates. This statement is confirmed by the presence of ledges and sub-units in the alloys with higher Al content.

4.3. Isothermally heat treated samples

This section will firstly present the results obtained for the isothermally heat treated ternary alloys regarding the phases identified; EDX-analysis; and experimental Ti-Al-Si phase diagram. The discussion of the ternary diagram will be presented along with the results of the thermodynamic modelling. This section ends with the presentation of the results obtained for the isothermally heat treated quaternary alloys regarding the phases identified and EDX-analysis, followed by a brief discussion on α2 and silicide precipitation in ternary and quaternary alloys.

4.3.1. Ternary alloys

The following section will describe the microstructures in terms of phases in equilibria during the isothermal treatment. So the morphology of precipitation, especially of transformed β microstructures, whose allotropic transformation was discussed in the previous section, will not be taken into account unless it is necessary.

Sample 3B (Ti-16Al-3.5Si – T =1200°C for 24 hours, figure 4.3.1.1.a.) is composed of transformed β and a bimodal distribution of silicides: larger spheroidised eutectic silicides and silicides precipitated during isothermal heat treatment; and smaller silicides precipitated during quenching. XRD and EDX-analysis (see table 4.3.1.1.) identified the silicides as Ti_5Si_3*. Sample 6B (Ti-22Al-3.5Si – T =1200 C for 24 hours, figure 4.3.1.1.b.) shows the same microstructure as sample 3B, but without any evidence of silicide precipitation during quenching. The silicide particles of sample 6B presented, additionally, an increase in the proportion of Al in solution and a small change in the stoichiometry (see tables 4.3.1.1. and 4.3.1.2.). The proportion between Ti and Si plus Al atoms is seen to increase with an increase in Al.

Sample 3C (Ti16Al-3.5Si – T =1100°C for 42 hours), figure 4.3.1.1.c shows silicides finely precipitated during quenching along α plate boundaries. Figure 4.3.1.1.d. shows primary α plates formed during quenching, indicating that the stable phases during isothermal heat treatment were Ti_5Si_3 and β (see table 4.3.1.1. and 4.3.1.2.). By contrast, figure 4.3.1.3.c. shows recovered/recrystallised α grains, which indicate that α (and not β) is one of the stable phases for the alloy Ti-16Al-3.5Si reacted at 1000°C for 42 hours.

* Ti_5Si_3 refers to $Ti_5(Si,Al)_3$ for the ternary alloys.

alloy	T (°C)	EDX sample	phase	chemical composition		
				at%Si	at%Al	at%Ti
Ti-16Al-3.5Si	1200	SEM	β	1.6±0.1	16.7±0.3	"
			Ti_5Si_3	33±2	4±1	"
Ti-22Al-3.5Si	1200	SEM	β	1.4±0.1	23.7±0.3	"
			Ti_5Si_3	27±2	8±2	"
Ti-16Al-3.5Si	1100	SEM	β	1.4±0.1	17.2±0.5	"
			Ti_5Si_3	32±2	5±1	"
Ti-22Al-1Si	1100	SEM/TEM	α2	1.2±0.1	22.9±0.2	"
			β	0.8±0.1	20.1±0.2	"
Ti-22Al-3.5Si	1100	SEM/TEM	α2	1.4±0.1	24.5±0.3	"
			β	1.2±0.1	22.1±0.2	"
			Ti_5Si_3	25±1	8±1	"
Ti-16Al-1Si / Ti-16Al-3.5Si	1000	TEM	α	0.9±0.1	17.2±1.2	"
			Ti_5Si_3	33.7±0.5	2.1±0.4	"
Ti-16Al-1Si / Ti-16Al-3.5Si	900	TEM	α	0.9±0.3	15.2±1.2	"
			α2	1.3±0.3	20.1±1.4	"
			Ti_5Si_3	30.0±0.8	1.5±0.7	"
Ti-16Al-1Si / Ti-16Al-3.5Si	800	TEM	α	0.8±0.3	13.3±1.3	"
			α2	1.2±0.3	19.6±1.2	"
			Ti_5Si_3	29.4±1.3	1.1±0.8	"
Ti-16Al-1Si / Ti-16Al-3.5Si	700	TEM	α	0.7±0.4	11.9±1.4	"
			α2	1.2±0.4	19.3±1.3	"
			Ti_5Si_3	31.6±1.1	3.0±0.7	"
Ti-22Al-3.5Si	1000	TEM	α2	1.4±0.3	24.4±13	"
			Ti_5Si_3	27.2±0.8	3.3±0.9	"
Ti-22Al-3.5Si	900	TEM	α2	1.5±0.3	24.3±1.2	"
			Ti_5Si_3	28.0±0.5	3.0±0.4	"
Ti-22Al-3.5Si	800	TEM	α2	1.3±0.3	24.1±1.2	"
			Ti_5Si_3	28.1+1.2	3.1±0.6	"
Ti-22Al-1Si / Ti-22Al-3.5Si	700	TEM	α2	1.0±0.2	24.1±0.8	"
			Ti_5Si_3	25.6±0.7	4.3±0.7	"

Table 4.3.1.1. EDX analysis of ternary alloys.

alloy	T(°C)	silicide	chemical composition		
			at%Si	at%Al	at%Ti/ (at%Si+ at%Al)
Ti-16Al-3.5Si	1200	Ti_5Si_3	33±2	4±1	1.7±0.3
Ti-16Al-3.5Si	1100	"	32±2	5±1	1.7±0.3
Ti-16Al-1Si/ Ti-16Al-3.5Si	1000	"	33.7±0.5	2.1±0.4	1.8±0.1
"	900	"	30.0±0.8	1.5±0.7	2.2±0.1
"	800	"	29.4±1.3	1.1±0.8	2.3±0.2
"	700	"	31.6±1.1	3.0±0.7	1.9±0.2
Ti-22Al-3.5Si	1200	"	27±2	8±2	1.9±0.3
"	1100	"	25±1	8±1	2.0±0.3
"	1000	"	27.2±0.8	3.3±0.9	2.3±0.2
"	900	"	28.0±0.5	3.0±0.4	2.3±0.2
"	800	"	28.1±1.2	3.1±0.6	2.3±0.3
Ti-22Al-1Si/ Ti-22Al-3.5Si	700	"	25.6±0.7	4.3±0.7	2.4±0.2

Table 4.3.1.2. EDX analysis of ternary silicides.

Sample 5C (Ti-22Al-1.0Si – T =1100°C for 42 hours), figure 4.3.1.2.a. shows a duplex microstructure composed of a transformed β matrix and large precipitates. The latter are presented as large and oriented plates or as a blocky precipitate. TEM-DFI examination (figure 4.3.1.2.b.) reveals that the transformed β matrix is composed of small α2 APD's, while the large precipitates are composed of α2 sub-grains, suggesting that the stable phases are β and α2. XRD and microscopy work did not indicate any presence of Ti_5Si_3. Sample 6C (Ti-22Al-3.5Si – T =1100°C for 42 hours), figures 4.3.1.2.c. to 4.3.1.2.e.) shows a duplex matrix composed of extensive proportion of large precipitates, precipitated either as plates or in a blocky morphology, and transformed β (see detail in figure 4.3.1.2.d. showing primary plate and adjacent colony of parallel α plates). Additionally Ti_5Si_3 particles appear to be heterogeneously distributed throughout the duplex matrix without any visible preferential nucleation site. TEM-DFI examination (see figure 4.3.1.2.e.) reveals that the transformed β matrix is composed of small α2 APD's, while the large precipitates are composed of α2 sub-grains, suggesting that the stable phases are β and α2.

Sample 2D (Ti16Al+1.0Si – T =1000°C for 72 hours, figure 4.3.1.3.a.) shows a matrix composed by large equiaxial grains, which do not characterise a transformed β microstructure, suggesting that α phase is stable instead. Small particles of Ti_5Si_3 are sparsely precipitated along α grain boundaries. XRD and TEM examination did not indicate the presence of ordered α2 phase.

Sample 3D (Ti-16Al-3.5Si – T =1000°C for 72 hours), figure 4.3.1.3.b. shows much additional heterogeneous precipitation of Ti_5Si_3 than sample 3C (see figure 4.3.1.1.c.), but SEM observation did not supply any information concerning the matrix. TEM examination, however, shows that the matrix is composed of recovered/recrystallised grains, suggesting that α phase is stable (see figure 4.3.1.3.c.). No transformed β microstructure could be observed throughout this sample. EDX-analysis of samples 3C (reacted at 1100°C) and 3D (reacted at 1000°C, see table 4.3.1.1) shows that the solubility of Si in β phase is higher than in α, which explains why sample 3D shows much additional silicide precipitation.

Sample 5D (Ti-16Al-1.0Si – T =1000°C for 72 hours) presented a bimodal grain size distribution, larger grains at previous massive grains and smaller grains at prior parallel α plate colonies. Figures 4.3.1.3.d. shows the smaller grains originated at prior parallel α plate colonies. TEM-DFI (see figure 4.3.1.2.e.) showed presence of large α2 sub-grains structure. No APD's were observed in this sample, confirming previous XRD results which did not show α2 double peaks, suggesting that either there is no α phase present in this sample or that the difference in chemical composition between α and α2 is too small to be detected by this technique.

Sample 6D (Ti-22Al-3.5Si – T =1000°C, figure 4.3.1.4.a.) shows silicides precipitated in a single phase matrix which is shown to be composed of α2 sub–grains (see figure 4.3.1.4.b.). No APD's have been found in this sample, confirming previous XRD results that α phase is not stable at this temperature.

Sample 2E (Ti-16Al-1Si - T=900°C for 8 days, figures 4.3.1.4.c. and 4.3.1.4.d) shows heterogeneous silicide precipitation along previous α boundaries. Heterogeneous α2 precipitation at previous α/α boundaries is also observed. XRD and EDX-analysis (see table 4.3.1.1.) indicate the presence of three stable phases: α, α2 and Ti_5Si_3. Sample 3E (Ti-16Al-3.5Si - T=900°C for 8 days, figures 4.3.1.5.a. and 4.3.1.4.d.) also presents three stable phases: α, α2 and Ti_5Si_3. Heterogeneous α2 precipitation might be observed in figure 4.3.1.5.a. Although the exact nature of the preferential nucleation sites is not shown clearly in the micrograph, they are thought to be prior α/α interfaces. Additionally, precipitation of hexagonal-shaped silicides was observed (see figure 4.3.1.5.b.). Figure 4.3.1.5.c. shows that some of the α2 precipitates grow along the interface between Ti_5Si_3 and α. This observation suggests that either this interface acts as a preferential nucleation site for α2 precipitation or as preferential path for the growth of α2 particles. Sample 6E (Ti-22Al-3.5Si - T=900°C for 8 days, figures 4.3.1.5.d. and 4.3.1.5.e.) shows a biphasic microstructure composed of α2 subgrains and silicides.

Sample 2F (Ti-16Al-1Si - T=800°C for 14 days, figures 4.3.1.6.a) shows homogeneous α2 precipitation in an α matrix, while figures 4.3.1.6.b.-c. shows heterogeneous and homogeneous α2 precipitation. The homogeneously nucleated α2 precipitates grow along [0001]α2 (see figures 4.3.1.7.a and 4.3.1.7.b.). The growth of α2 particles along the **c** axis produces a misfit around 0.3% while the misfit for growth along **a** axis would be around 2%. This preferential growth along [0001] minimises the strain energy between α and α2 (see table 4.3.1.3.), and produces extremely elongated α2 precipitates.

alloy	T (°C)	Ti(α) a (Å)	Ti(α) c (Å)		
Ti-16Al	900	2.919	4.665		
"	800	2.925	4.667		
"	700	2.929	4.666		
Ti-16Al-1Si	1000	2.915	4.663		
"	900	2.920	4.666		
"	800	2.921	4.665		
"	700	2.934	4.663		
alloy		Ti_3Al a (Å)	Ti_3Al c (Å)	misfit$_{\alpha/\alpha 2}$ (%) <a>	misfit$_{\alpha/\alpha 2}$ (%) <c>
Ti-16Al	900	-	-	-	-
"	800	5.797	4.652	1.8	0.32
"	700	5.802	4.653	1.9	0.28
Ti-16Al-1Si	900	5.796	4.648	1.5	0.39
"	800	5.789	4.648	1.8	0.36
"	700	5.788	4.645	2.7	0.19

Table 4.3.1.3. Calculated lattice parameters for α and α2 and misfit$_{\alpha/\alpha 2}$.

In sample 3F (Ti-16Al-3.5Si - T=800°C for 14 days, figure 4.3.1.7.c.) the microstructure is also composed of homogeneous and heterogeneous α2 precipitation in an α matrix. Heterogeneously nucleated α2 particles do not present a typical elongated morphology, stressing that the minimisation of strain energy is not a crucial process during the nucleation and growth of heterogeneous precipitates. Silicides have been observed in both samples, and figure 4.3.1.7.d. shows a typical silicide precipitate.

Sample 1G (Ti-16Al - T=700°C for 36 days, , figure 4.3.1.8.a. and 4.3.1.8.c.) shows a duplex α+α2 microstructure, with homogeneous distribution of α2 particles and preferential growth along [0001]α2. These α2 particles are much smaller than the ones present in the ternary alloy (see figures 4.3.1.8.b.), indicating that Si addition alters the conditions of

nucleation and growth of α2 particles. Additionally, figure 4.3.1.8.c. shows that this binary sample did not present heterogeneous nucleation of α2 particles at prior α/α boundaries. It is also observed that the morphology of the α2 particles in this binary sample is less elongated than the ternary one (see figure 4.3.1.8.d.), suggesting that Si addition promotes more elongated particles. This observation is in agreement with the experimental results (see table 4.3.1.3.), which showed that Si addition increases the misfit along a axis and decreases it along c axis at 700°C. Sample 2G (Ti-16Al-1Si - T=700°C for 36 days, figures 4.3.1.8.b. and 4.3.1.8.d.) shows a duplex matrix composed of heterogeneous and homogeneous α2 precipitation in an α matrix. In cross section the elongated α2 precipitates (see figure 4.3.1.8.d.) reveal the presence of sub-boundaries which resemble edge-to-edge and edge-to-face examples of sympathetic nucleation. Additionally, heterogeneous precipitation of rod-like silicide along previous α boundaries was also observed. The homogeneously nucleated α2 precipitates grow along [0001]α2. In sample 3F (Ti-16Al-3.5Si - T=700°C for 36 days, figures 4.3.1.9.a to 4.3.1.9.c) the matrix is composed of heterogeneous and homogeneous α2 precipitation in an α matrix. The homogeneously nucleated α2 precipitates grow along [0001]α2. The micrograph 4.3.1.9.c. shows hexagonal-shaped Ti_5Si_3 precipitates.

Sample 4G (Ti-22Al - T=700°C for 36 days, , figure 4.3.1.10.a.) shows α2 domains, which developed from large massive grains. Sample 5G (Ti-22Al-1Si - T=700°C for 36 days, , figures 4.3.1.10.b.-c.) shows an α2 microstructure developed from previous α plates. α2 domains resemble a sub-grain microstructure, suggesting that the previous microstructure alters the morphology of α2 precipitation/growth. Figures 4.3.1.11.a.-b. show small α2 sub-grains and precipitation of Ti_5Si_3 particles.

Table 4.3.1.4. provides a summary of the identified phases. This table, along with table 4.3.1.1. were used to construct experimental isothermal sections of the Ti-Al-Si system (see figures 4.3.1.12. and 4.3.1.13.). Between 700 and 900°C, tie triangles containing α+α2+Ti_5Si_3 are shown. The variation in Si content in both α and α2 phases with the heat treatment temperature is very small and presents a very large relative error related to this measurement. This error is due to the relatively low Si in solution. Additionally, Si and Al peaks lie very close together to each other, and some superposition of these peaks might contribute to increase the error. Furthermore, the EDX analysis does not allow tilting of the foil, so that some of the very small, in some cases coherent, α2 particles were not analysed under ideal conditions, so it is not surprising that the samples reacted at 700°C present a larger relative error. As mentioned in chapter 3, one important precaution that should be taken in quantitative X-ray analysis of a

precipitate phase dispersed in a matrix is to ensure that the precipitate extends through the thickness of the foil. The variation in Al content, specially in α phase, with heat treatment temperature is well defined and shows that both phases present less Al in solution than shown in the binary phase diagram, suggesting that Si reduces the solubility of Al in both phases.

Concerning Ti_5Si_3 analysis, some solid solution of Al is observed. Table 4.3.1.2. presents a summary of the results of EDX analysis obtained for the silicide phase in the ternary alloys investigated. The results confirm previous result for as-quenched alloys:

- addition of Al decreases the solubility of Si in the silicide, in agreement with previous work [ZHA 91], suggesting that Al replaces Si in the sublattice(s) of Ti_5Si_3.
- in alloys with higher Al content, Al replaces more Si in the silicide.
- addition of Al increases the ratio Ti/(Al+Si) of the silicide suggesting a possible change in the stoichiometry of the silicide.
- decreasing the temperature of isothermal heat treatment decreases the solubility of Al and increases the ratio Ti/(Al+Si).

The results for the equilibria (β+Ti_5Si_3) show that increasing Al content reduces the solubility of Si in β phase, in agreement with previous work [CRO 55]. The equilibrium (α+Ti_5Si_3) at 1000°C suggests that Al addition increases either the eutectoid (β–>α+Ti_5Si_3) or the peritectoid (β+Ti_5Si_3–>α) temperature, as it allows α phase to be stable at temperatures above 865°C, the eutectoid temperature in the Ti-Si binary shown in figure 2.3.4..

Concerning the possible existence of a peritectoid (β+Ti_5Si_3–>α) reaction, the present are not consistent with this: considering the alloy Ti-16Al-3.5Si the equilibria β+Ti_5Si_3 at 1100°C and α+Ti_5Si_3 at 1000°C (see table 4.3.1.1.), the results show that the solubility of Si is higher in β than in α phase, indicating, therefore, the existence of an eutectoid (β–>α+Ti_5Si_3) reaction instead.

The EDX-analysis results for the three phase (β+α2+Ti_5Si_3 at 1100°C) and two phase (β+Ti_5Si_3 at 1200°C) fields (see table 4.3.1.1.), however, might suggest the existence a different peritectoid reaction given by (β+Ti_5Si_3->α2), as the solubility of Si in α2 is higher than β phase.

The existence of a two phase field (β+α2) at 1100°C in the ternary alloy and the phase relationships shown in the Ti-Al binary at 1100°C (see figure 2.2.1.), which shows the presence of (β), (β+α), (α), (α+α2) and (α2) phase fields with increasing Al content, suggest the existence of a three phase field, given by (β+α+α2) for Al content around 22at% and Si content between

0 and 1at%. These results might indicate the existence of a second peritectoid reaction in the ternary Ti-Al-Si given by (β+α2–>α) (see figure 4.3.1.13)..

alloy	T(°C)	phases in equilibria	experimental techniques
Ti-16Al-3.5Si	1200	β+Ti_5Si_3	SEM, XRD, TEM, SADP; EDX-SEM; EDX-TEM
Ti-22Al-3.5Si	"	β+Ti_5Si_3	"
Ti-16Al-1Si	1100	β	"
Ti-16Al-3.5Si	"	β+Ti_5Si_3	"
Ti-22Al-1Si	"	β+α2	"
Ti-22Al-3.5Si	"	β+α2+Ti_5Si_3	"
Ti-16Al-1Si	1000	α+Ti_5Si_3	"
Ti-16Al-3.5Si	"	α+Ti_5Si_3	"
Ti-22Al-1Si	"	α2	"
Ti-22Al-3.5Si	"	α2+Ti_5Si_3	"
Ti-16Al	900	α	"
Ti-16Al-1Si	"	α+α2+Ti_5Si_3	"
Ti-16Al-3.5Si	"	α+α2+Ti_5Si_3	"
Ti-22Al-1Si	"	α2	"
Ti-22Al-3.5Si	"	α2+Ti_5Si_3	"
Ti-16Al	800	α+α2	"
Ti-16Al-1Si	"	α+α2+Ti_5Si_3	"
Ti-16Al-3.5Si	"	α+α2+Ti_5Si_3	"
Ti-22Al-1Si	"	α2	"
Ti-22Al-3.5Si	"	α2+Ti_5Si_3	"
Ti-16Al	700	α+α2	"
Ti-16Al-1Si	"	α+α2+Ti_5Si_3	"
Ti-16Al-3.5Si	"	α+α2+Ti_5Si_3	"
Ti-16Al	"	α2	"
Ti-22Al-1Si	"	α2+Ti_5Si_3	"
Ti-22Al-3.5Si	"	α2+Ti_5Si_3	"

Table 4.3.1.4. Phases identified in ternary alloys.

Figure 4.3.1.1. Isothermally Heat Treated Samples.

a) alloy Ti-16Al-3.5Si reacted at 1200°C for 24 hours; transformed β + silicide; SEM-BEI;

b) alloy Ti-22Al-3.5Si reacted at 1200°C for 24 hours; transformed β + silicide; SEM-BEI;

c) alloy Ti-16Al-3.5Si reacted at 1100°C for 48 hours; transformed β + silicide; SEM-BEI;

d) alloy Ti-16Al-3.5Si reacted at 1100°C for 48 hours; detail of transformed β presenting primary α plates with faceted boundaries; TEM-BFI;

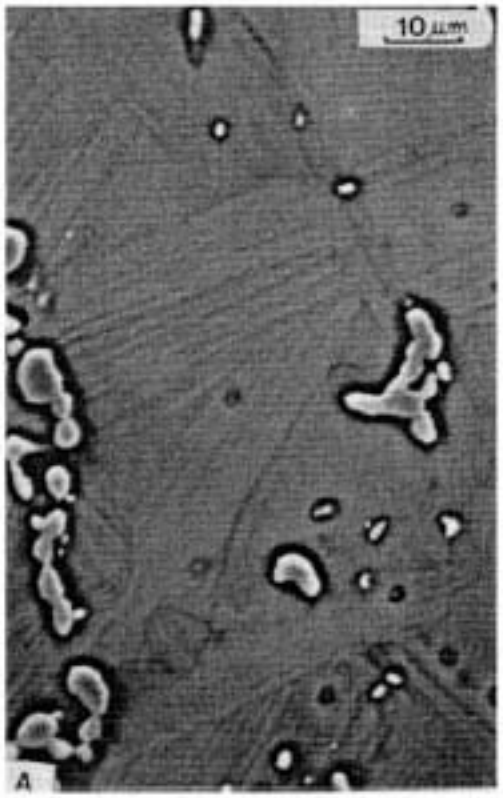
10 µm
A


10 µm
B

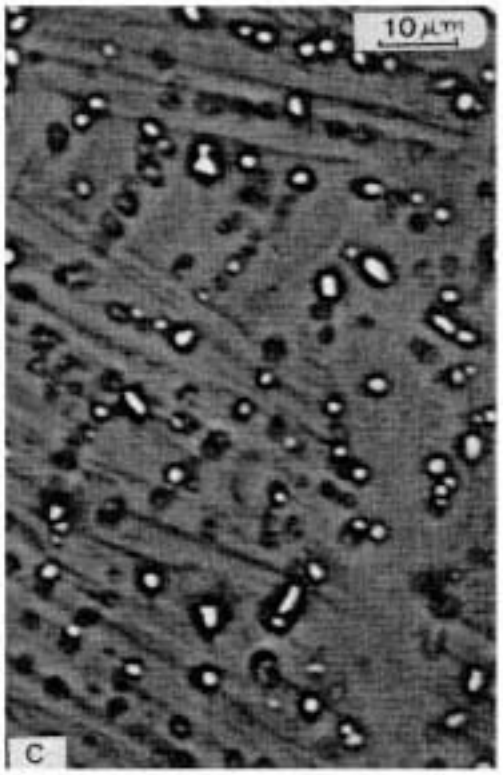
10 µm
C


0.5 µm
D

Figure 4.3.1.2. Isothermally Heat Treated Samples.

a) alloy Ti-22Al-1Si reacted at 1100°C for 48 hours; transformed β + α2; SEM-BEI;

b) alloy Ti-22Al-1Si reacted at 1100°C for 48 hours; detail of transformed β + α2 microstructure, showing respectively small α2 APDs and a large α2 grain; TEM-DFI, $g=(10\bar{1}0)_{\alpha 2}$;

c) alloy Ti-22Al-3.5Si reacted at 1100°C for 48 hours; transformed β + α2; SEM-BEI;

d) alloy Ti-22Al-3.5Si reacted at 1100°C for 48 hours; detail of transformed β microstructure, showing colonies of parallel α plates; TEM-BFI;

e) alloy Ti-22Al-3.5Si reacted at 1100°C for 48 hours; detail of transformed β + α2 microstructure, showing respectively small α2 APDs and a large α2 grain; TEM-DFI, $g=(10\bar{1}1)_{\alpha 2}$;

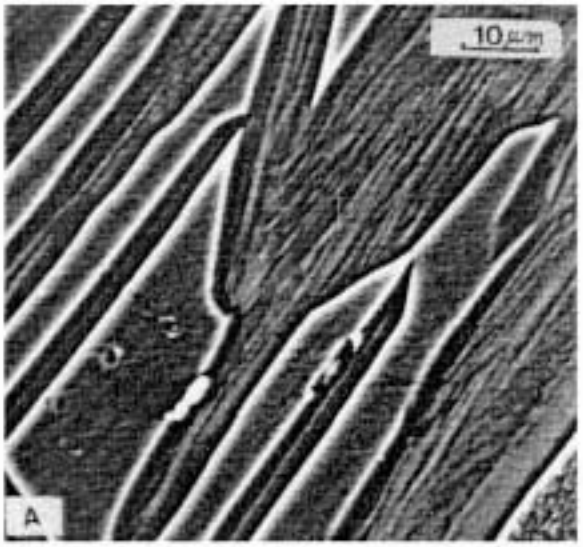
10 μm
A


0.5 μm
G(10$\bar{1}$0)
B


10 μm
C


0.5 μm
D


0.1 μm
G(10$\bar{1}$1)
E

Figure 4.3.1.3. Isothermally Heat Treated Samples.

a) alloy Ti-16Al-1Si reacted at 1000°C for 72 hours; equiaxed α grains and silicide precipitation along α grain boundaries; SEM-BEI;

b) alloy Ti-16Al-3.5Si reacted at 1000°C for 72 hours; recovered/recrystallised α grains and silicide precipitation along α grain boundaries/sub-boundaries; SEM-BEI;

c) alloy Ti-16Al-3.5Si reacted at 1000°C for 72 hours; detail of the recovered/recrystallised α grains showing rearrangement of dislocations; TEM-BFI

d) alloy Ti-22Al-1Si reacted at 1000°C for 72 hours; α2 grain/sub-grains microstructure; SEM-BEI;

e) alloy Ti-22Al-1Si reacted at 1000°C for 72 hours; detail of α2 sub-grains microstructure; TEM-DFI, $g=(10\bar{1}1)_{\alpha 2}$;

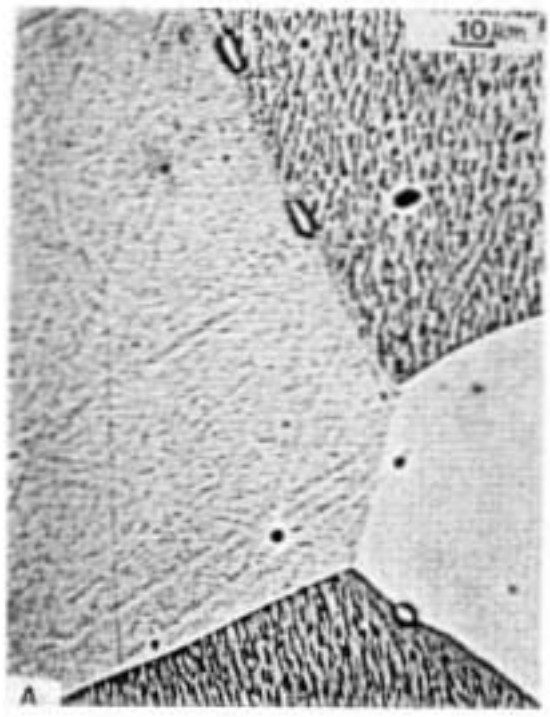
10 µm
A

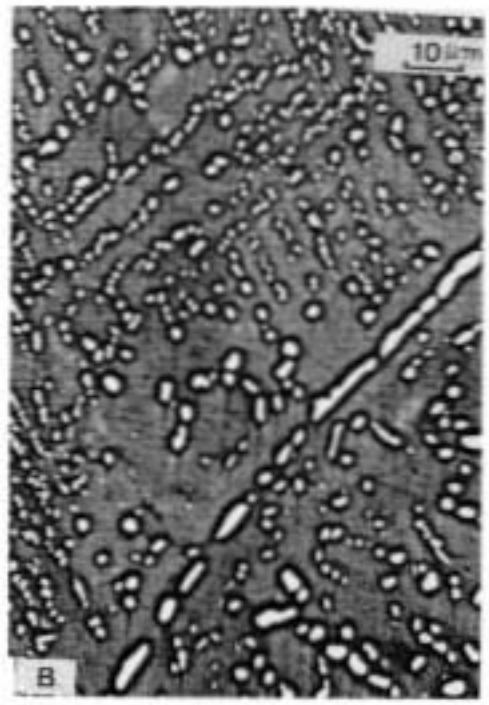
10 µm
B

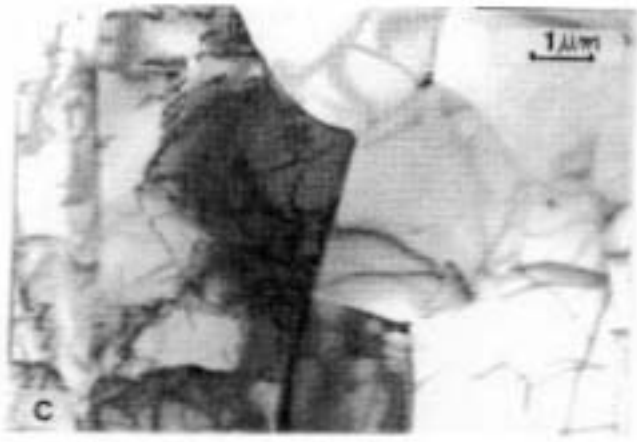
1 µm
C

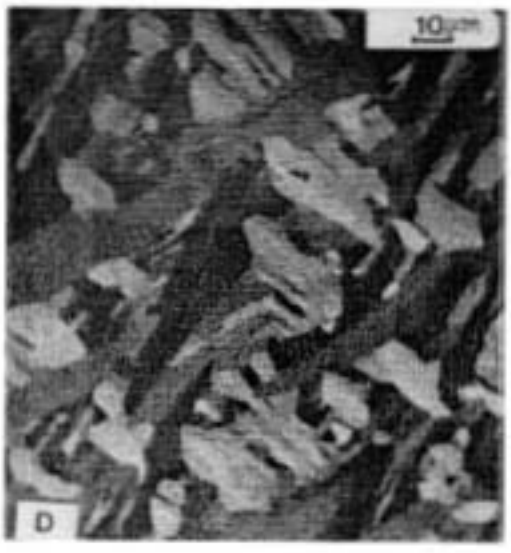
10 µm
D


1 µm
E

Figure 4.3.1.4. Isothermally Heat Treated Samples.

a) alloy Ti-22Al-3.5Si reacted at 1000°C for 72 hours; $\alpha 2$ grain/sub-grains microstructure and silicides; SEM-BEI;

b) alloy Ti-22Al-3.5Si reacted at 1000°C for 72 hours; detail of $\alpha 2$ grain/sub-grains microstructure; TEM-DFI, $g=(11\bar{2}0)_{\alpha 2}$;

c) alloy Ti-16Al-1Si reacted at 900°C for 8 days; heterogeneous silicide precipitation along prior α grain boundaries; SEM-BEI;

d) alloy Ti-16Al-1Si reacted at 900°C for 8 days; heterogeneous $\alpha 2$ precipitation along prior α grain boundaries; TEM-DFI $g=(10\bar{1}1)_{\alpha 2}$.

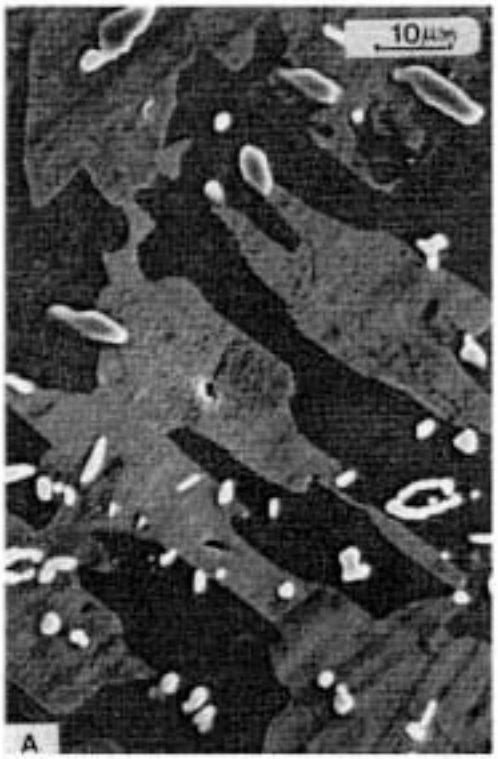
10 µm
A

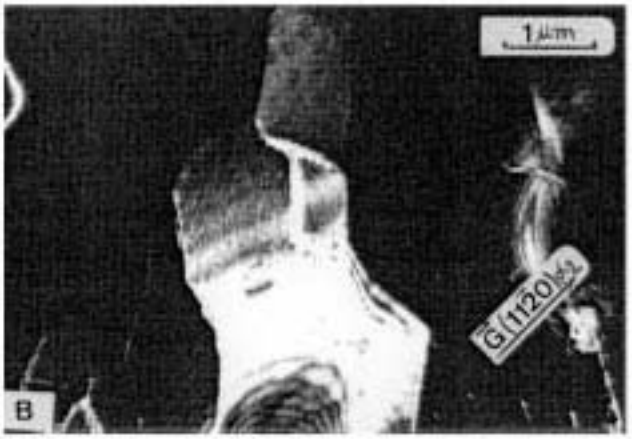
1 µm
G(1120)
B

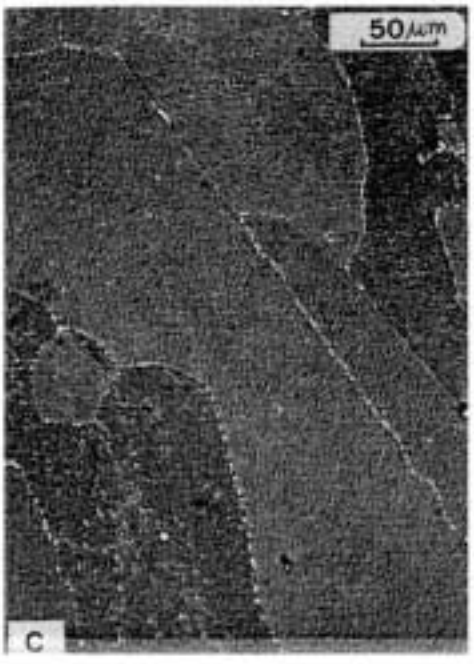
50 µm
C


0,5 µm
G(10ī1)
D

Figure 4.3.1.5. Isothermally Heat Treated Samples.

a) alloy Ti-16Al-3.5Si reacted at 900°C for 8 days; heterogeneous $\alpha 2$ precipitation; TEM-DFI: $g=(\bar{1}01\bar{1})_{\alpha 2}$;

b) alloy Ti-16Al-3.5Si reacted at 900°C for 8 days; Ti_5Si_3 precipitates; TEM-DFI: $B=[\bar{4}5\bar{1}3]Ti_5Si_3$ and $g=(0\bar{1}12)Ti_5Si_3$; (SADP given below);

c) alloy Ti-16Al-3.5Si reacted at 900°C for 8 days; $\alpha 2$ precipitation along prior α/Ti_5Si_3 interfaces; TEM-DFI: $B=[\bar{1}\bar{1}23]_{\alpha 2}$ and $g=(\bar{1}01\bar{1})_{\alpha 2}$;

d) alloy Ti-22Al-3.5Si reacted at 900°C for 8 days; $\alpha 2$ sub-grain; TEM-DFI: $B=[11\bar{2}0]_{\alpha 2}$ and $g=(\bar{1}01\bar{1})_{\alpha 2}$; (SADP given below);

e) alloy Ti-16Al-3.5Si reacted at 900°C for 8 days; Ti_5Si_3 precipitates; TEM-DFI: $B=[0001]Ti_5Si_3$ and $g=(10\bar{1}0)Ti_5Si_3$; (SADP given below);

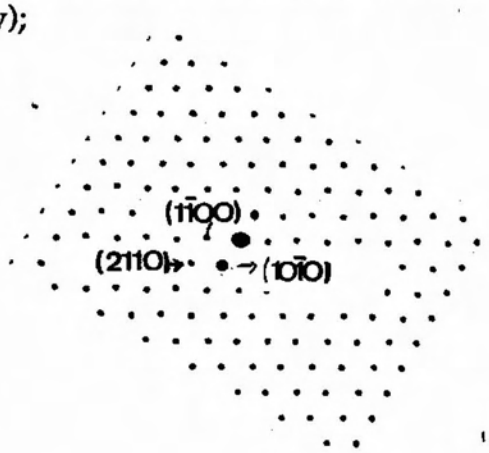


1 μm
G(10$\bar{1}$1)$_{\alpha'}$
A


1 μm
G(01$\bar{1}$2)$_{\alpha'}$
B

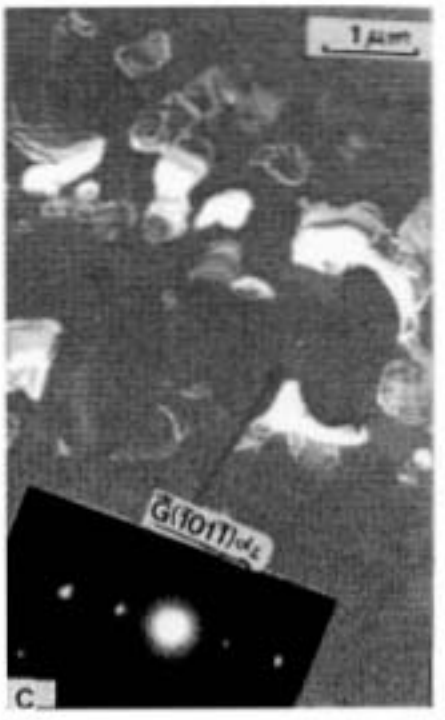
1 μm
G(10$\bar{1}$1)$_{\alpha'}$
C

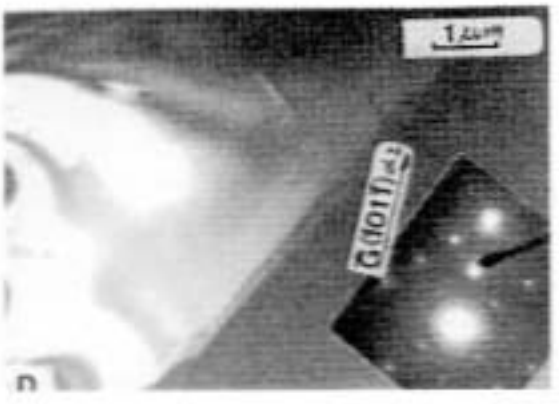
1 μm
G(10$\bar{1}$1)$_{\alpha'}$
D

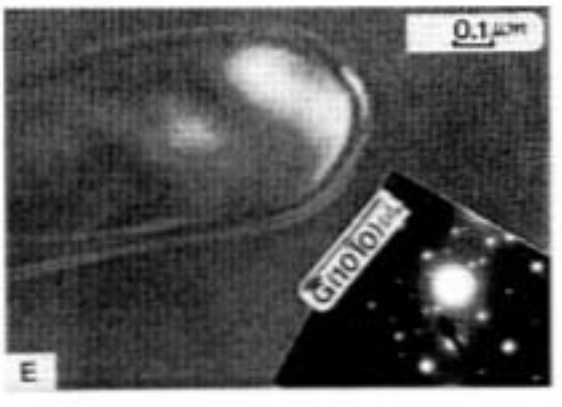
0.1 μm
G(10$\bar{1}$0)$_{\alpha'}$
E

Figure 4.3.1.6. Isothermally Heat Treated Samples.

a) alloy Ti-16Al-1Si reacted at 800°C for 14 days; displacement fringe contrast showing homogeneous α2 particles; TEM-BFI: B=$[1\bar{5}\bar{4}6]_{\alpha 2}$; (SADP given below)

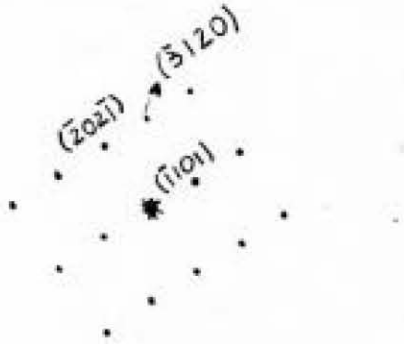

b) alloy Ti-16Al-1Si reacted at 800°C for 14 days; homogeneous and heterogeneous α2 precipitation; TEM-BFI: B=$[0001]_{\alpha 2}$; (SADP given below)

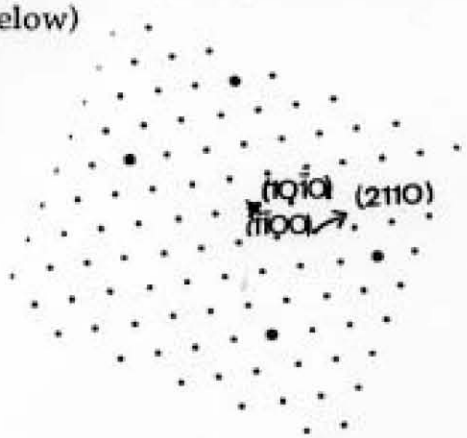

c) alloy Ti-16Al-1Si reacted at 800°C for 14 days; homogeneous and heterogeneous α2 precipitation; TEM-DFI: B=$[0001]_{\alpha 2}$ and g=$(2\bar{1}\bar{1}0)_{\alpha 2}$;

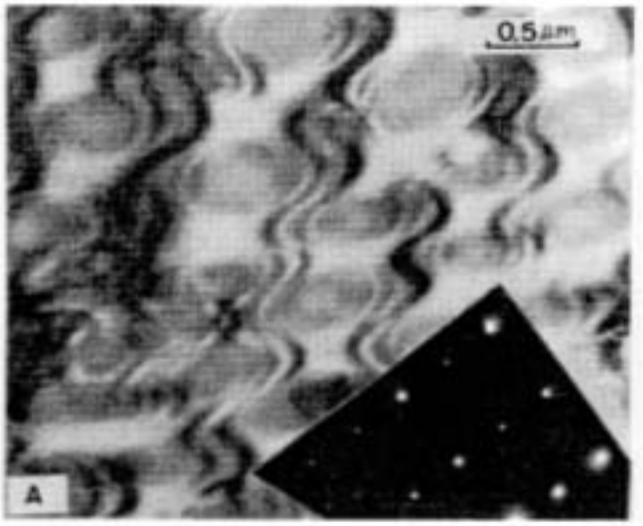
0.5 μm
A


0.5 μm
B


0.5 μm
G2110
C

Figure 4.3.1.7. Isothermally Heat Treated Samples.

a) alloy Ti-16Al-1Si reacted at 800°C for 14 days; detail of homogeneous $\alpha 2$ precipitation; TEM-DFI: $B=[1\bar{1}00]_{\alpha 2}$ and $g=(11\bar{2}0)_{\alpha 2}$; (SADP given below)

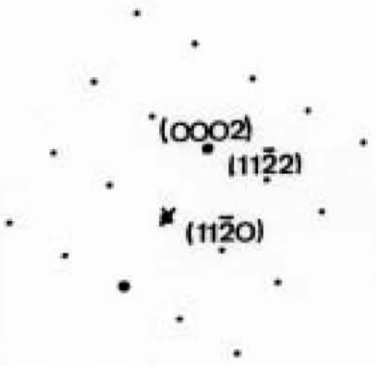

b) alloy Ti-16Al-1Si reacted at 800°C for 14 days; detail of homogeneous $\alpha 2$ precipitation; TEM-DFI: $B=[0001]_{\alpha 2}$ and $g=(11\bar{2}0)_{\alpha 2}$;

c) alloy Ti-16Al-3.5Si reacted at 800°C for 14 days; heterogeneous and homogeneous $\alpha 2$ precipitation; TEM-DFI: $B=[0001]_{\alpha 2}$ and $g=(11\bar{2}0)_{\alpha 2}$;

d) alloy Ti-16Al-3.5Si reacted at 800°C for 14 days; Ti_5Si_3 precipitate; TEM-DFI: $g=(11\bar{2}1)Ti_5Si_3$


0.5 μm
G(1120)
[0001]
A

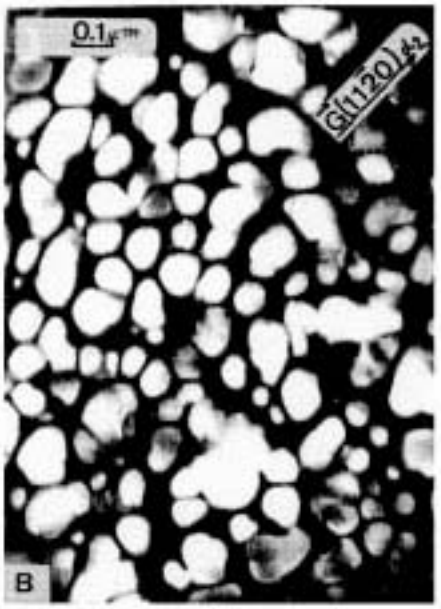
0.1 μm
G(1120)
B

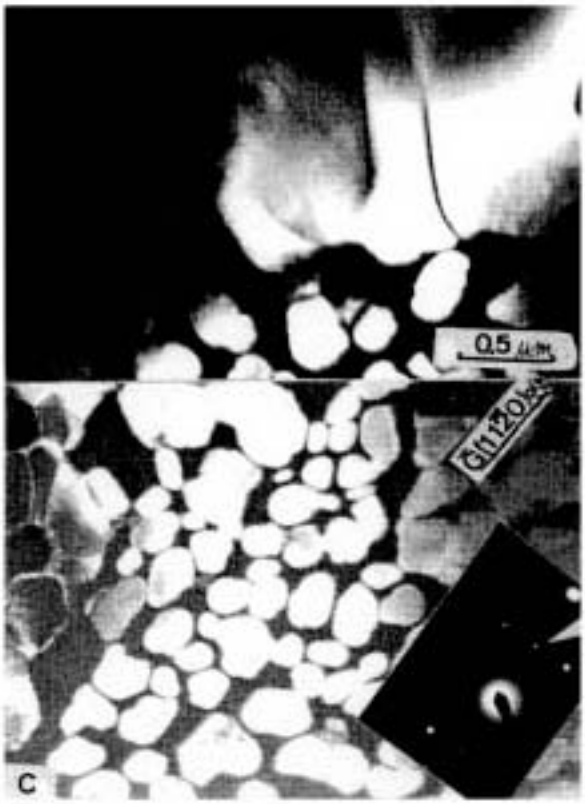
0.5 μm
G(1120)
C


0.5 μm
G(1121)
D

Figure 4.3.1.8. Isothermally Heat Treated Samples.

a) alloy Ti-16Al reacted at 700°C for 36 days; detail of homogeneous $\alpha 2$ precipitation; TEM-DFI: B=$[0001]_{\alpha 2}$ and g=$(2\bar{1}\bar{1}0)_{\alpha 2}$;

b) alloy Ti-16Al-1Si reacted at 700°C for 36 days; detail of homogeneous $\alpha 2$ precipitation; TEM-DFI: B=$[0001]_{\alpha 2}$ and g=$(2\bar{1}\bar{1}0)_{\alpha 2}$;

c) alloy Ti-16Al reacted at 700°C for 36 days; detail of homogeneous $\alpha 2$ precipitation; TEM-DFI: B=$[10\bar{1}0]_{\alpha 2}$ and g=$(\bar{1}2\bar{1}0)_{\alpha 2}$;

d) alloy Ti-16Al-1Si reacted at 700°C for 36 days; detail of homogeneous $\alpha 2$ precipitation; TEM-DFI: B=$[1\bar{2}10]_{\alpha 2}$ and g=$(10\bar{1}1)_{\alpha 2}$;

e) alloy Ti-16Al-1Si reacted at 700°C for 36 days; Ti_5Si_3 precipitate; TEM-DFI: g=$(11\bar{2}0)Ti_5Si_3$

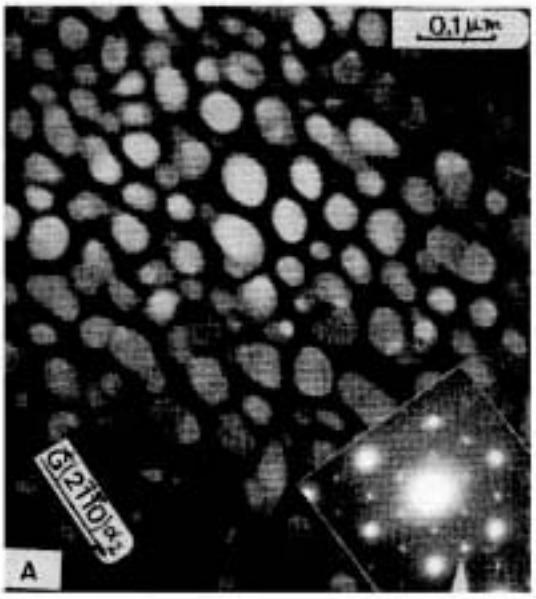
0.1 μm
G(2$\bar{1}$10)$_{\alpha_2}$
A


0.1 μm
G(2$\bar{1}$10)$_{\alpha_2}$
B

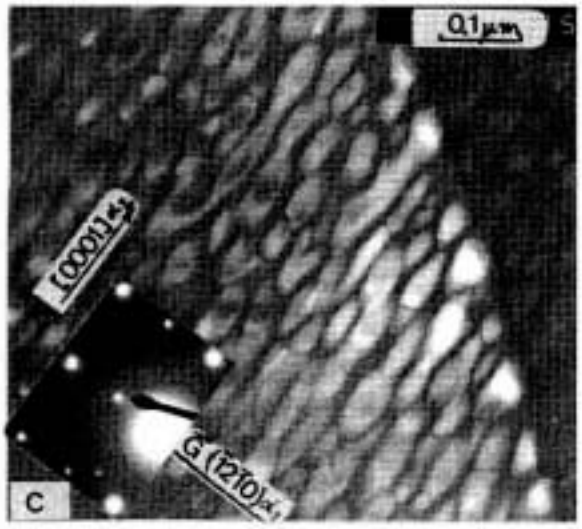
0.1 μm
[0001]$_{\alpha_2}$
G($\bar{1}$210)$_{\alpha_2}$
C


0.1 μm
[0001]$_{\alpha_2}$
G(10$\bar{1}$1)$_{\alpha_2}$
D

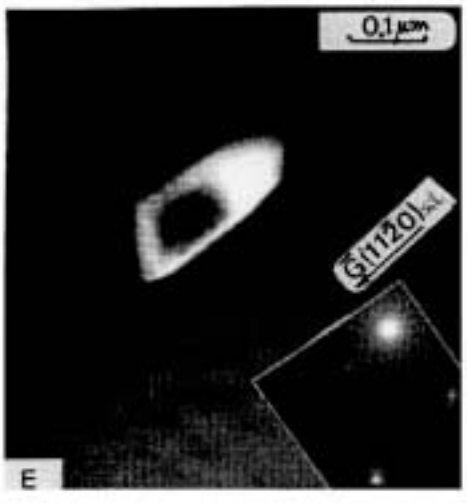
0.1 μm
G(11$\bar{2}$0)$_{\alpha_2}$
E

Figure 4.3.1.9. Isothermally Heat Treated Samples.

a) alloy Ti-16Al-3.5Si reacted at 700°C for 36 days; detail of homogeneous $\alpha 2$ precipitation; TEM-DFI: $B=[1\bar{2}10]\alpha 2$ and $g=(10\bar{1}2)\alpha 2$;

b) alloy Ti-16Al-3.5Si reacted at 700°C for 36 days; heterogeneous and homogeneous $\alpha 2$ precipitation; TEM-DFI: $B=[0001]\alpha 2$ and $g=(21\bar{1}0)\alpha 2$;

c) alloy Ti-16Al-3.5Si reacted at 700°C for 36 days; Ti_5Si_3 precipitate; TEM-DFI: $g=[20\bar{2}1]Ti_5Si_3$

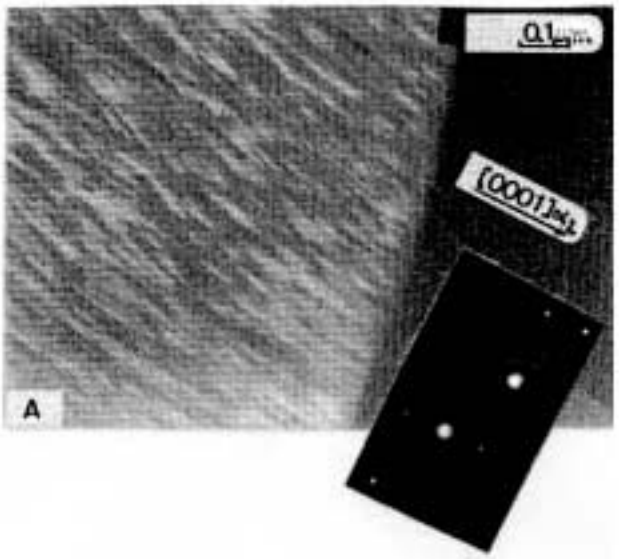
0.1 μm
[0001]hex
A

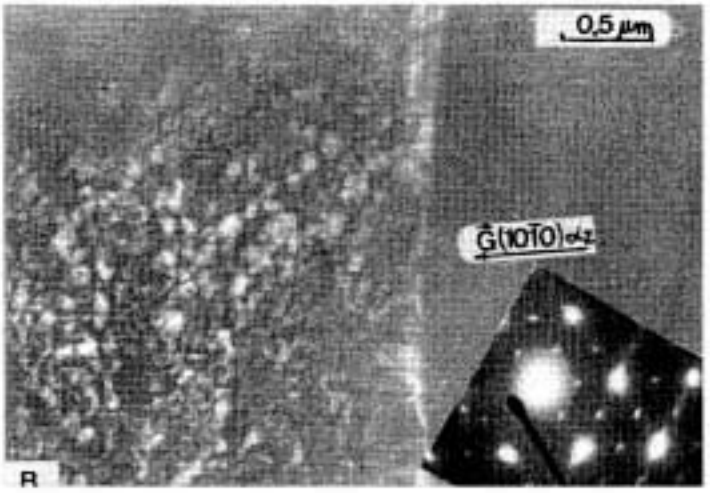
0.5 μm
G(10$\bar{1}$0)α2
B

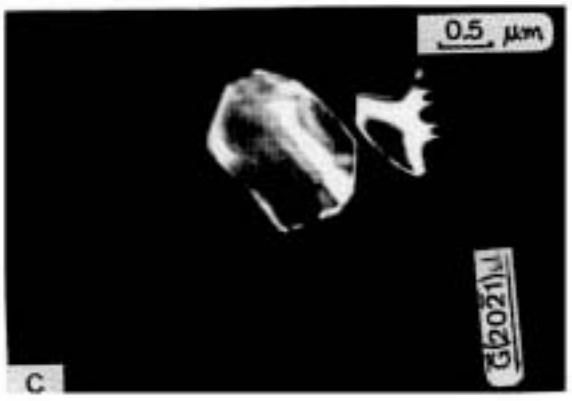
0.5 μm
G(20$\bar{2}$1)L1
C

Figure 4.3.1.10. Isothermally Heat Treated Samples.

a) alloy Ti-22Al reacted at 700°C for 36 days; α2 domains; TEM-DFI: g=$(1\bar{2}10)_{\alpha 2}$;

b) alloy Ti-22Al-1Si reacted at 700°C for 36 days; sub-grain structure; TEM-BFI;

c) alloy Ti-22Al-1Si reacted at 700°C for 36 days; sub-grain structure; TEM-DFI: g=$(10\bar{1}0)_{\alpha 2}$

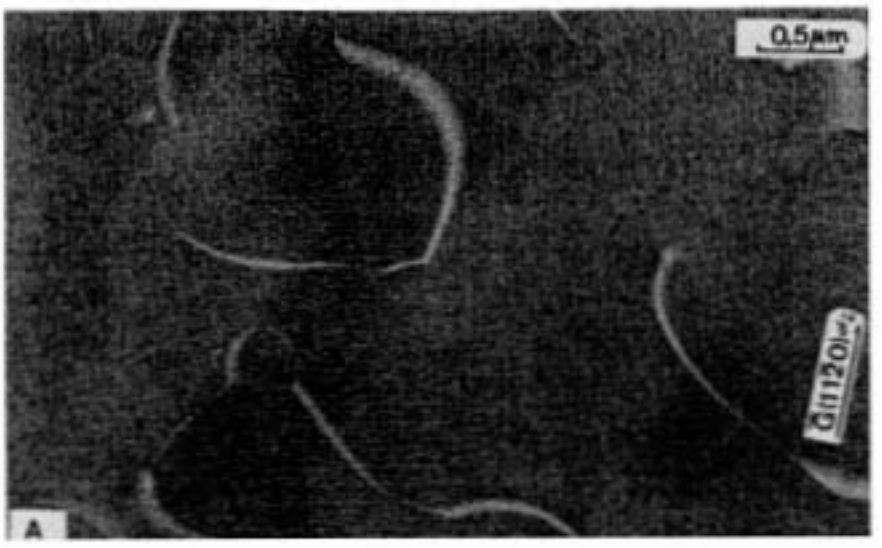
0.5μm
A


0.5μm
B


0.5μm
C

Figure 4.3.1.11. Isothermally Heat Treated Samples.

a) alloy Ti-22Al-3.5Si reacted at 700°C for 36 days; $\alpha 2$ sub-grain; TEM-DFI: $g=(10\bar{1}0)\alpha 2$;

b) alloy Ti-22Al-3.5Si reacted at 700°C for 36 days; silicide particle; TEM-DFI; $g=(10\bar{1}0)Ti_5Si_3$;

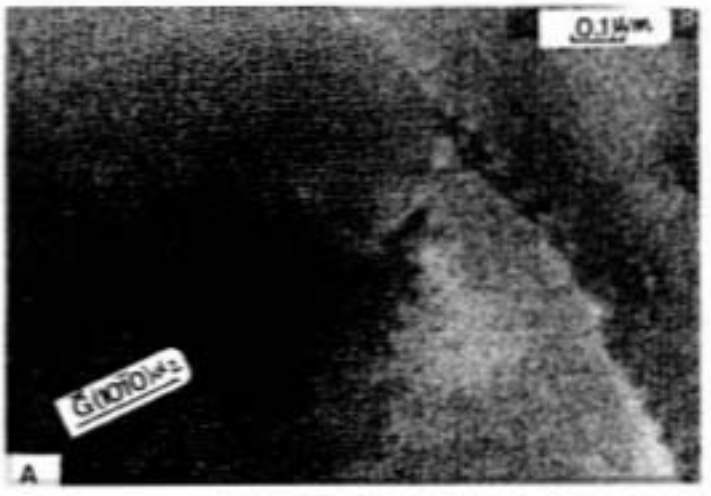
0.1 μm
G(10$\bar{1}$0)
A

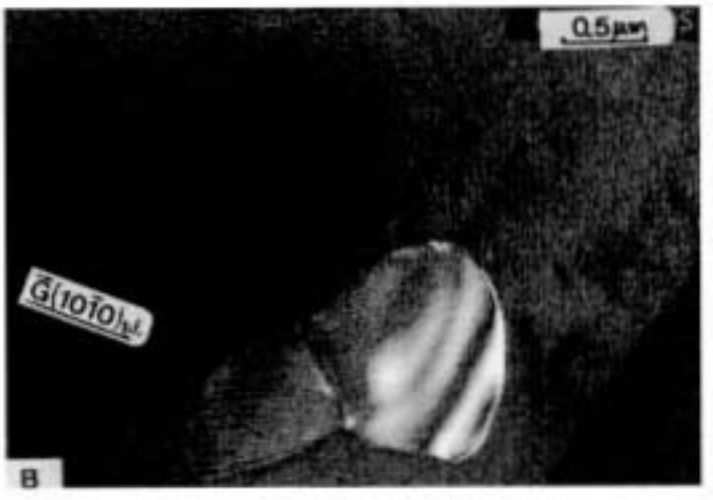
0.5 μm
G(10$\bar{1}$0)
B

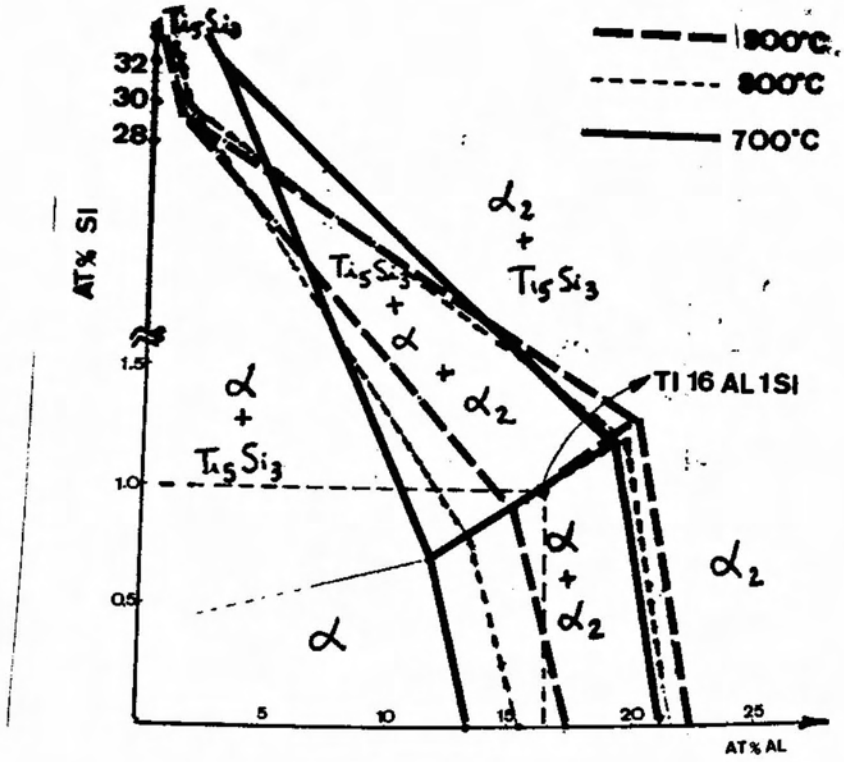

Figure 4.3.1.12. α + α2 + Ti_5Si_3 tie-triangle versus temperature.

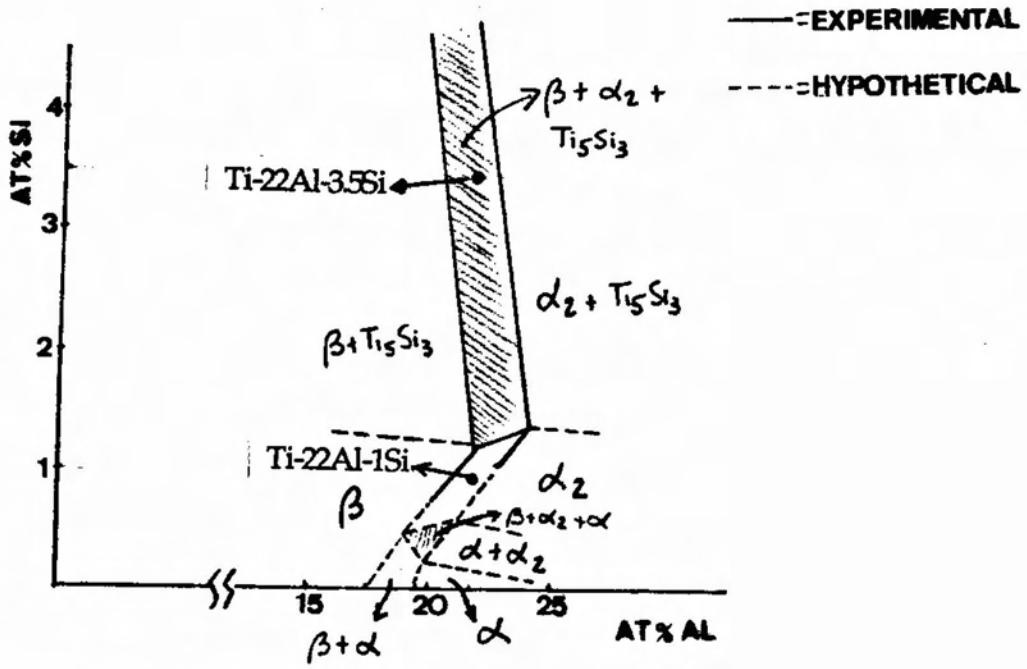

Figure 4.3.1.13. Experimental isothermal at 1100°C.

4.3.2. Thermodynamic modelling of the Ti-rich corner of the Ti-Al-Si system

Figures 4.3.2.1.a-b shows the Ti-Al binary obtained via SSOL (Scientific Group Thermodata Europe - SGTE database) and KP (Kaufman database published in CALPHAD). SSOL database was chosen for the calculation of the Ti-Al-Si system. As mentioned in chapter 3, a new reassessment of the Ti-Si binary diagram using SSOL database had to be made to improve the solubility of silicon in α in metastable equilibrium with Ti_5Si_3 (the stable equilibria is given by α + Ti_3Si at temperatures below 865°C- see figure 2.3.4.); and to maintain the self-consistency of all information contained in the database [HIl 86]. A new and more simple phase description, which considers this phase as a line compound was used:

- previous description (Ti_5Si_3 presenting solubility range):

3 sublattices, sites:	0.375 : 0.25 : 0.375
constituents:	Si,Ti : Si,Ti : Ti

- new description (Ti_5Si_3 as a compound line):

2 sublattices, sites:	0.375 : 0.625
constituents:	Si : Ti

The adoption of a simpler phase description for Ti_5Si_3 agrees with general guidelines found in the literature. H.Okamoto [OKA 91] emphasises that the simpler the thermodynamic model, the easier the examination of the thermodynamic and physical properties associated with the system under examination will be. M.Hillert [HIL 86] mentioned that the choice of a simple but effective model which does not grow very complex for higher order systems is an essential requirement for the formation of a general thermodynamic data bank.

Parameters were optimised following standard procedure described in chapter 3 and figures 4.3.2.2.a-d show respectively the Ti-Si binary obtained via: SSOL; KP; the Ti-Si binary containing the metastable equilibrium Ti(α) + Ti_5Si_3 using previous SSOL database; and finally the reassessed version of Ti-Ti_5Si_3 containing the metastable equilibrium Ti(α) + Ti_5Si_3 using SSOL. The values of the optimised parameters and the description of the phases are given in figures 4.3.2.3.a.-b. The results indicate that a simpler phase description for the silicide phase produced a much better version for the Ti-Ti_5Si_3 phase diagram. Furthermore the optimisation procedure produced very low values for the relative standard deviation of the variables (except for variable 36) and a good value for reduced sum of squares (≤ 1). Both results indicate a successful reassessment. Although the reassessed version provides a much better starting point for the calculation of the ternary system concerning the solubility of Si in α, it must be kept in mind that this

version has been accomplished by adopting an rather simplistic phase description for Ti_5Si_3. The sounder the physical model underlying the mathematical model, the safer the predictions will be [HIL 86], so that this more simple phase description will lead to some misleading predictions, especially during calculation of higher order systems.

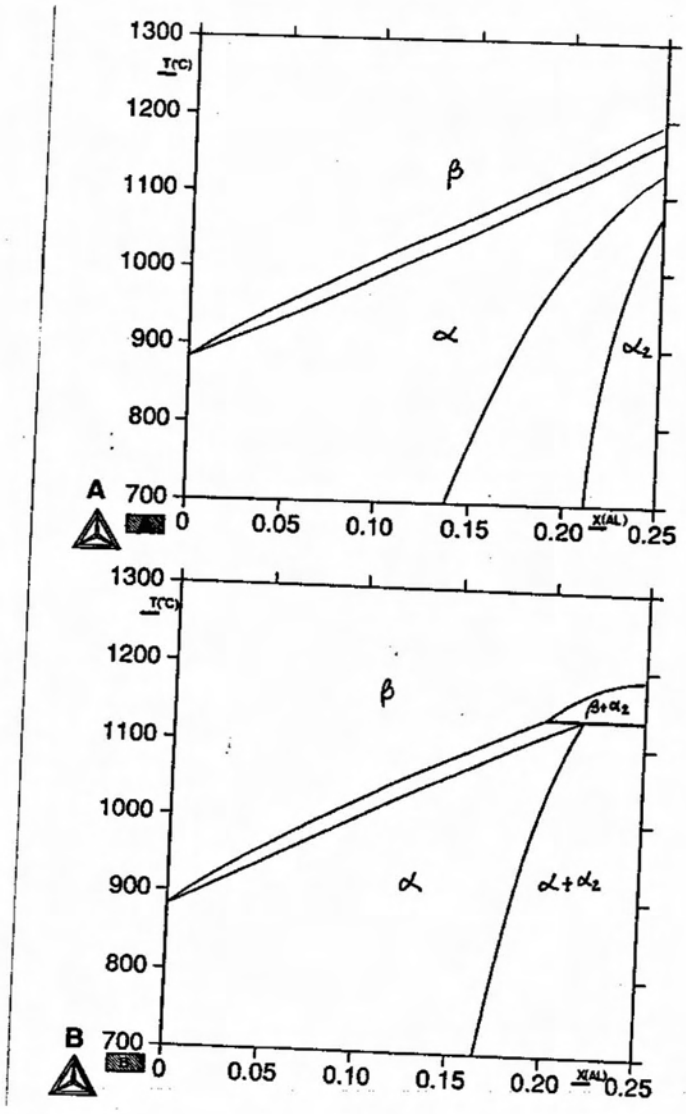

Figure 4.3.2.1. Calculated Ti-Al binary diagrams:
a) SSOL database; b) KP database.

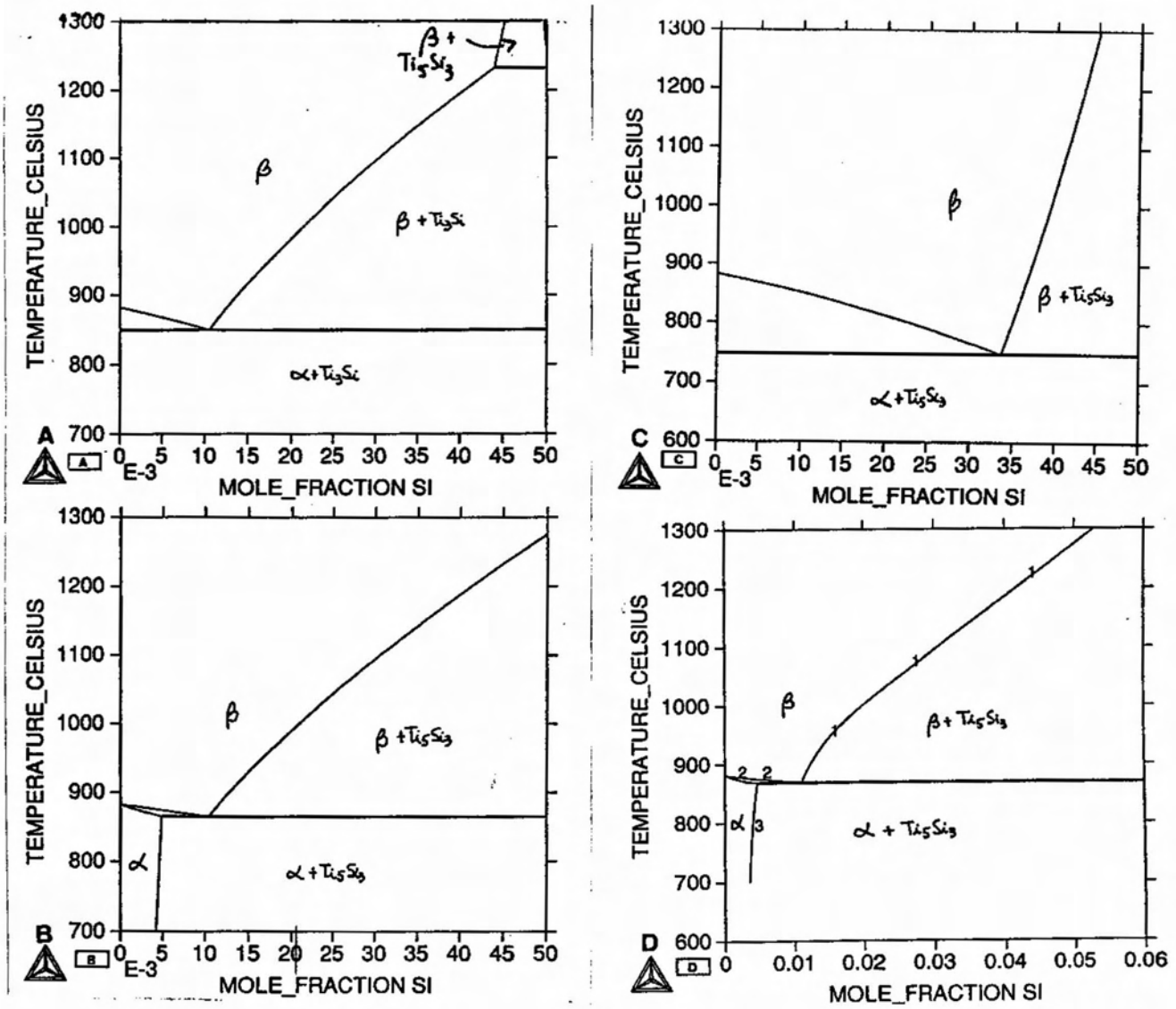

Figure 4.3.2.2. Calculated Ti-Si binary diagrams:
a) SSOL database; b) KP database; c) Ti-Ti_5Si_3 using SSOL database;
d) reassessed Ti-Ti_5Si_3 using SSOL database.

```
SYMBOL          STATUS    VALUE/FUNCTION
  1 R           80000000   8.3145100E+00
  2 RTLNP       20000000 +R*T*LN(9.8692327E-06*P)
  3 GALBCC      20000000 +10083-4.813*T+GHSERAL
  4 GSIBCC      20000000 +47000-22.5*T+GHSERSI
  5 GHSERAL     20000000
      298.14<T<  700.00: -7976.15+137.071542*T-24.3671976*T*LN(T)
    -.001884662*T**2-8.77664E-07*T**3+74092*T**(-1)
      700.00<T<  933.60: -11276.24+223.02695*T-38.5844296*T*LN(T)
    +.018531982*T**2-5.764227E-06*T**3+74092*T**(-1)
      933.60<T< 2900.00: -11277.683+188.661987*T-31.748192*T*LN(T)
    -1.234264E+28*T**(-9)
  6 GHSERSI     20000000
      298.14<T< 1687.00: -8162.609+137.227259*T-22.8317533*T*LN(T)
    -.001912904*T**2-3.552E-09*T**3+176667*T**(-1)
     1687.00<T< 3600.00: -9457.642+167.271767*T-27.196*T*LN(T)
    -4.20369E+30*T**(-9)
  7 GHSERTI     20000000
      298.14<T<  900.00: -8059.921+133.687208*T-23.9933*T*LN(T)
    -.004777975*T**2+1.06716E-07*T**3+72636*T**(-1)

      900.00<T< 1155.00: -7811.815+133.060068*T-23.9887*T*LN(T)
    -.0042033*T**2-9.0876E-08*T**3+42680*T**(-1)
     1155.00<T< 1941.00: +908.837+67.048538*T-14.9466*T*LN(T)-.0081465*T**2
    +2.02715E-07*T**3-1477660*T**(-1)
     1941.00<T< 4000.00: -124526.786+638.878871*T-87.2182461*T*LN(T)
    +.008204849*T**2-3.04747E-07*T**3+36699805*T**(-1)
  8 GHCPAL      20000000 +5481-1.799*T+GHSERAL

 BCC_A2
EXCESS MODEL IS REDLICH-KISTER_MUGGIANU
ADDITIONAL CONTRIBUTION FROM MAGNETIC ORDERING
      Magnetic function below Curie Temperature
      +1-.905299383*TAO**(-1)-.153008346*TAO**3-.00680037095*TAO**9
      -.00153008346*TAO**15
      Magnetic function above Curie Temperature
       -.0641731208*TAO**(-5)-.00203724193*TAO**(-15)
      -4.27820805E-04*TAO**(-25)
  2 SUBLATTICES, SITES  1:  3
    CONSTITUENTS: SI,TI : VA

      G(BCC_A2,SI:VA;0)-H298(DIAMOND_A4,SI;0) = +GSIBCC
      G(BCC_A2,TI:VA;0)-H298(HCP_A3,TI;0) =
            298.14<T< 1155.00: -1272.064+134.78618*T-25.5768*T*LN(T)
          -6.63845E-04*T**2-2.78803E-07*T**3+7208*T**(-1)
           1155.00<T< 1941.00: +6667.385+105.438379*T-22.3771*T*LN(T)
          +.00121707*T**2-8.4534E-07*T**3-2002750*T**(-1)
           1941.00<T< 4000.00: +26483.26-182.354471*T+19.0900905*T*LN(T)
          -.02200832*T**2+1.228863E-06*T**3+1400501*T**(-1)
      L(BCC_A2,SI,TI:VA;0) = +V49+V50*T
      L(BCC_A2,SI,TI:VA;1) = +V47
      L(BCC_A2,SI,TI:VA;2) = +V48

 HCP_A3
EXCESS MODEL IS REDLICH-KISTER_MUGGIANU
ADDITIONAL CONTRIBUTION FROM MAGNETIC ORDERING
      Magnetic function below Curie Temperature
      +1-.860338755*TAO**(-1)-.17449124*TAO**3-.00775516624*TAO**9
      -.0017449124*TAO**15
      Magnetic function above Curie Temperature
       -.0426902268*TAO**(-5)-.0013552453*TAO**(-15)
      -2.84601512E-04*TAO**(-25)
  2 SUBLATTICES, SITES  1:  .5
    CONSTITUENTS: SI,TI : VA

      G(HCP_A3,SI:VA;0)-H298(DIAMOND_A4,SI;0) = +49200-20.8*T+GHSERSI
      G(HCP_A3,TI:VA;0)-H298(HCP_A3,TI;0) =
            298.14<T< 4000.00: +GHSERTI
      L(HCP_A3,SI,TI:VA;0) = +V36+V37*T
      L(HCP_A3,SI,TI:VA;1) = +V38
      L(HCP_A3,SI,TI:VA;2) = +V39


 SI3TI5

EXCESS MODEL IS REDLICH-KISTER_MUGGIANU
  2 SUBLATTICES, SITES  .375:  .625
    CONSTITUENTS: SI : TI

      G(SI3TI5,SI:TI;0)-0.375 H298(DIAMOND_A4,SI;0)-0.625 H298(HCP_A3,TI;0) =
           +V34+V35*T+.375*GHSERSI+.625*GHSERTI
```

Figure 4.3.2.3. Output of Thermocalc showing description of phases, optimising variables; relative standard deviation and reduced sum of squares for the assessed Ti-Si system

OUTPUT FROM P A R R O T. DATE 95. 3.29 15: 1:13

*** OPTIMISATION ERROR. SUM OF SQUARES FAILS TO DECREASE***
NUMBER OF ITERATION: 12

== OPTIMISING CONDITIONS==(DEFAULT)

RELATIVE SATANDARD DEVIATION FOR EXPERIMENTS: N
MINIMUM SAVE ON FILE: Y
ERROR FOR INEQUALITIES = 1.00000000E+00
RELATIVE STEP FOR CALCULATION OF DERIVATIVES = 1.00000000E-04
ARGUMENTS FOR SUBROUTINE VA05AD (HSL)
MAXFUN=*** DMAX = 1.00000000E+02 H= 1.00000000E-04
ACC= (INITIAL SUM OF SQUARES) * 1.00000000E-06

==OPTIMISING VARIABLES===

VARIABLE	VALUE	START VALUE	SCALING FACTOR	REL.STAND.DEV.
V34	-1.64029285E+06	-1.64029285E+06	-1.64029285E+06	6.22182395E-03
V35	7.07374988E+02	7.07374988E+02	7.07374988E+02	2.24298337E-02
V36	2.11541682E+04	2.11541682E+04	2.11541682E+04	4.41804741E 00
V37	1.96378051E+03	1.96378051E+03	1.96378051E+03	1.40745876E-02
V38	1.05760917E+07	1.05760917E+07	1.05760917E+07	1.62762437E-04
V39	6.12698315E+06	6.12698315E+06	6.12698315E+06	9.89722844E-03
V47	4.51506594E+06	4.51506594E+06	4.51506594E+06	5.32119974E-02
V48	2.95092649E+06	2.95092649E+06	2.95092649E+06	1.23349946E-02
V49	-2.87869372E+06	-2.87869372E+06	-2.87869372E+06	9.27718274E-02
V50	1.97204109E+03	1.97204109E+03	1.97204109E+03	3.74761173E-03

NUMBER OF OPTIMISING VARIABLES : 10
ALL OTHER VARIABLES FIX WITH THE VALUE ZERO
THE SUM OF THE SQUARES HAS CHANGED FROM 6.61739057E^{+}00 TO 6.61739057E^{+}00
DEGREES OF FREEDOM 10. REDUCED SUM OF SQUARES 6.61739057E^{-}01

Figure 4.3.2.3.b. Output of Thermocalc showing relative standard deviation and reduced sum of squares for the assessed Ti-Si system.

Figures 4.3.2.4.a to 4.3.2.4.f. present the isothermal sections obtained for the Ti-Al-Si using the experimental data shown in table 4.3.1.1.. Parameters have been optimised following standard procedure described in chapter 3 and figures 4.3.2.5.a.-b. show the values of the optimised variables and the description of the phases. The results indicate low values for the standard deviation, except for variables 12, 13, 14 and 20, which were used to describe the hcp phase, and variable 25, used for bcc phase. Additionally most of the variables presented an unexpectedly high value of order of magnitude. It is not rare, however, to find thermodynamic models that involve functions with parameters of inconceivable magnitude. Such functions would not be appropriate if they were used for purposes other than phase diagram modelling, as, for example kinetic calculations or prediction of thermodynamic properties [OKA 91]. M.Hillert [HIL 86] warns that one should be cautious when using the adjustable parameters of a particular model for the prediction of thermodynamics properties. He explains that, for instance, it is possible that sometimes more than one model can successfully describe the experimental information on a certain system. This situation would not produce any insight in the physical nature of the solution. Nevertheless he points that it is legitimate to use a purely "mathematical" model opposed to a physical model as long as it is capable of describing the experimental information and it can be used to predict further information under conditions not studied directly by experiments. Concerning the Ti_3Al phase description, in order to consider Si solubility in this phase, the following description was used:

2 sublattices, sites:	0.75 : 0.25
constituents:	Al, Ti : Al, Ti, Si

Many combinations of binary and ternary interactions were tried to realistically describe the α2 phase. In the case of binary interactions extra care had to be taken to respect the phase boundaries and phase stability of the binary systems. For instance, few numerical restrictions had to be imposed in the parameter G(Ti_3Al,Ti:Si;0) to avoid the hypothetical compound Ti_3Si(hcp) becoming stable in the Ti-Si binary. Other parameters, such as G(Ti_3Al,Al:Si;0) were shown to have very little effect in the results and their variables were not considered in the final optimisation procedure. The only parameter of ternary interaction considered during the final optimisation procedure was L(Ti_3Al,Ti:Al,Si;0). All the other possible combinations were shown not as effective as L(Ti_3Al,Ti:Al,Si;0) in increasing the fit between experimental and calculated values. The following features of the calculated phase diagram have been observed:

1• Si has a higher solubility in α2 than in α phase (in agreement with Schob [SCH 62] and D.J.Arrell [ARR 92] (see figures 4.3.2.4.a-e);

2• Si decreases the solubility of Al in α in equilibrium with α2 (see figures 4.3.2.4.a-d.), so that Si addition promotes α2 precipitation by increasing the driving force of α–>α+α2. This is in agreement with experimental work (see table 4.3.1.1. and figure 4.3.1.12.);

3• the effect of Si on the solubility of Al in α2 varies with temperature (see figures 4.3.2.4.a-d) and this observation is not consistent with the experimental results (see table 4.3.1.1. and figure 4.3.1.12.), which show that Si always decreases the solubility of Al in α2, suggesting that Si replaces Al in the sublattice(s) of Ti_3Al crystal. It is suggested that the rather simple Ti_5Si_3 phase description, which does not include Al solubility , together with the relative standard deviation obtained for α phase variables, are responsible for this inconsistency in the calculated phase diagram;

4• Al addition decreases the solubility of Si in both α and β phases (see figures 4.3.2.4.a-f). The latter agrees with the experimental results (see table 4.3.1.1. and figure 4.3.1.12.). The observed effect of Si on α phase is , however, more complex, as shown by figures 4.3.2.4.a-b: addition of Al up to 0.02 at%Al increases the solubility of Si in α, but higher levels of Al addition decrease the solubility of Si in α phase. This observation suggests the existence of a peak of solubility of Si in α at around 0.02 at%Al. This prediction does not agree with previous work by Crossley [CRO 58] and might have been caused by the high values of relative standard deviation of variables used to describe the hcp phase in both binary and ternary assessments, (see figures 4.3.2.3.a.-b. and 4.3.2.5.a.-b.);

5• at 900℃ (and not at 1000℃), α phase presents higher Si solubility than β phase, indicating possible presence of a peritectoid reaction β+ Ti_5Si_3 ->α around 0.02at%Al. This prediction, however, should be examined very carefully, as it does not agree with the experimental results (see table 4.3.1.1.) Such positioning is very likely to have been caused by the presence of the peak of solubility of Si in α phase previously discussed;

6• at 1000℃ the boundary α/α+α2 is shown to be discontinuous at around 0.02at%Si. Additionally, the tie-lines show that for Si<0.02at% the same point in α phase is connected to at least two different points in α2 phase. This observation is thermodynamically incorrect and indicates the presence of instabilities in the calculation of α+α2 equilibria. This error might be once more explained by the high values of standard deviation presented for hcp phase, specially for variables 12 and 20, whose weight are enhanced by increases in the temperature (see figures 4.3.2.5.a.b.). Other possibilities to explain the presence of such instabilities would be: the existence of at least

two mathematical solutions, presenting different Al and Si site occupancies in α2, for the equilibrium; and the use of a step size (Δat%Si=0.001) smaller than the calculated error for the solubility of Si in α phase (0.005);

7• Al addition increases the solubility of Si in α2 phase (see boundaries Ti_5Si_3+α2/α2 in figures 4.3.2.4.a.-d. This observation is not supported by the experimental work (see table 4.3.1.1. and figure 4.3.1.12.), and appear contrary to the hypothesis that Si replaces Al sites in sublattice(s) of α2. It is suggested that the rather simple Ti_5Si_3 phase description, which does not include Al solubility is responsible for this inconsistency in the calculated phase diagram;

8• at 1100℃ Si addition promotes a peritectoid reaction: β+α2–>α, in agreement with experimental work (see table 4.3.1.1. and figure 4.3.1.13.), which shows the presence of β+α2+Ti_5Si_3 and β+α2 phase fields (see figures 4.3.1.2.a-e.);

9• at 1100℃ a β+α2 two phase field is present. The experimental results (see table 4.3.1.1. and figure 4.3.1.13.), however, indicate that this phase field extends to lower Si contents than shown in figure 4.3.2.4.e, as alloy 5C (Ti-22Al-1Si reacted at 1100℃) has been identified as α2+β (see table 4.3.1.1.);

10• at 1100℃ α2 phase field is very narrow (more stoichiometric), and Si addition reduces the solubility of Al in α2;

12• at 1100℃ the solubility of Si in α2 is higher than in β phase, indicating the existence of a second peritectoid reaction given by β+Ti_5Si_3->α2, in agreement with experimental work (see table 4.3.1.1. and figure 4.3.1.13.).

Some of the experimental points, concerning the equilibria α2+Ti_5Si_3, had to be excluded during the thermodynamic modelling, as they were introducing instabilities during the optimisation procedure. These situation appears to be caused by the rather simple description used for Ti_5Si_3 phase so that during the the optimisation procedure there were not enough number of variables to describe the experimental points. In order to overcome this problem there were few options to be considered: increase the number of parameters to describe α β and α2 phases; set weight zero to the "troublesome" experimental points; and/or modify Ti_5Si_3 phase description. The presented investigation opted for the second and simplest alternative, so that the calculated phase diagram should not be for the equilibria α2+Ti_5Si_3.

The thermodynamic calculation of the Ti-Al-Si system, although presenting few misleading and/or yet-to-be-checked phase boundaries and using a simple Ti_5Si_3 phase description, was considered to be a useful tool. It proposes two peritectoid reactions and gives a general description of the ternary phase diagram wich agrees qualitatively rather well with the experimental results (see table 4.3.1.1. and figures 4.3.1.12. and 4.3.1.13.). It is

worth pointing out that calculations of the Ti-Al-Si phase diagram performed using the updated COST database did not indicate the presence of these peritectoid reactions [SUN 95]. Some of the isothermals do present uncertainties, which will, however, allow a more rational way of devising sets of critical experiments for a more accurate determination of the Ti-Al-Si phase diagram, especially in composition and temperature ranges not covered by the present investigation. It must be realised that the complete experimental investigation of even a simple ternary system may cost several man-years. Hence, a combination of computation and critical experiments is crucial in the determination of ternary and higher order phase diagrams [LUP 83].

The comparison between experimental and calculated results (see table 4.3.2.1. and figures 4.3.1.12, 4.3.1.13 and 4.3.2.4.a.-f.) shows that both results are qualitatively equivalent. Going down to quantitative details there are few points that should be noted and regarded in case of future developments such as the difference in the solubility of Si, and in some cases Al, in β phase, and the solubility of Al in α2 phase (see table 4.3.2.1.). Such deviations, however, are considered normal and the result of 0.289 (see figure 4.3.2.5.b.) for the reduced sum of squares obtained after the optimisation procedure is below the advisable unity value.

It is interesting to notice that the apparently weak effect of Si as an eutectoid β stabiliser was just enough to promote a peritectoid reaction around 22at%Al: α2+β->α. Although the current investigation did not have access to this more updated database, the suggestion of a peritectoid reaction obtained via modelling agrees qualitatively with previous observations in the Ti-Al system: J.P.Gros et al. [GRO 88] verified that the congruent transformation of the Ti-α(hcp)->Ti_3Al would be substituted by a peritectoid reaction {Ti-β(bcc)+Ti_3Al->Ti-α(hcp)} if the Gibbs energy for the Ti-α(hcp) phase had been decreased by 170J/mole. Furthermore U.R.Kattner et al. [KAT 92] agreed that the phase relationships obtained from the calculation of the Al-Ti phase diagram were extremely sensitive to small changes in the Gibbs energy. The fact that small changes in Gibbs energy result in different phase relationships may help to explain the experimental difficulties in determining an accurate phase diagram for the Al-Ti system. For instance, at ~1100°C for 25at%Al the differences in the calculated relative Gibbs energy for Ti_3Al, Ti(α) and Ti(β) obtained by the authors [KAT 92] were very small and very likely to be smaller than the uncertainties usually found in experimentally determined thermodynamic data. This might explain the uncertainty of the existence of two peritectoid reactions: β(Ti) + α (Ti)-> α2(Ti_3Al) at ~ 1200°C and as β(Ti) + α2(Ti_3Al) -> α(Ti) at~1150°C; as

proposed by J.C.Mishurda et al. [MIS 89] (see figure 2.2.11) instead of the congruent reaction: α (Ti)–> α2 (see figure 2.2.1.).

The solution found for the present calculated ternary diagram resembles very much the ternary Ti-Al-Nb, bearing in mind the differences in solute solubility in α and β phases; and presence of eutectic/eutectoid products. This indicates that the Ti-Al-Si system might become attractive for the production of low-cost α2+β alloys, with Si addition replacing Nb. There are only two commercial β+α2 alloys [PET 95]: alpha 2 (Ti-24Al-11Nb) and super alpha 2 (Ti-25Al-10Nb-3V-1Mo). For instance, low cost alpha 2 alloys could be produced by adding 1at%Si instead of 11at%Nb, with savings of approximately 10% in weight and 2.12£/g of alloy (laboratory prices - Aldrich). Further investigation on the mechanical properties, thermal stability and oxidation resistance of Ti-Al-Si alpha 2 alloys should be carried out.

It appears doubtful, however, that Si will have a similar effect to Nb on the slip mode of Ti_3Al. Nb enhances additional <a> component slip systems, $\{10\bar{1}0\},1/3<11\bar{2}0>\alpha 2$ and $(0001),1/3<11\bar{2}0>\alpha 2$; and the necessary <c+a/2> slip, $\{11\bar{2}1\}$, $1/6<11\bar{2}6>\alpha 2$. Addition of Nb atoms, which are known to occupy Ti lattice sites when in solution, into the α2 lattice promotes less covalent bondings between the Ti atoms, so that the planes containing all Ti atoms would be disrupted. With less covalent bondings the Peierls valleys would be more shallow for dislocations lying perpendicular to formerly all Ti planes. This would allow the activation of additional slip systems [WAR 93]. Si atoms occupy Al lattice sites and should, therefore, increase the number of covalent bonding (Ti-Si), which would replace Ti-Al bondings. Whether or not covalency controls dislocation slip has yet to be proven, so that the effect of Si on the slip mode of Ti_3Al might be unexpectedly beneficial and worth investigating.

alloy	T(°C)	phase	at%Si	at%Al
Ti-16Al-3.5Si	1200	β	1.6±0.1	16.7±0.3
(β+Ti_5Si_3)		β (calc.)	1.54	16.28
Ti-22Al-3.5Si	1200	β	1.4±0.1	23.7±0.3
(β+Ti_5Si_3)		β (calc.)	0.90	21.10
Ti-16Al-3.5Si	1100	β	1.4±0.1	17.2±0.5
(β+Ti_5Si_3)		β (calc.)	1.40	15.41
Ti-22Al-1Si	1100	α2	1.2±0.1	22.9±0.2
(β+α2)		α2 (calc.)	1.25	23.47
		β	0.8±0.1	20.1±0.2
		β (calc.)	0.77	18.55
Ti-22Al-3.5Si	1100	α2	1.4±0.1	24.5±0.3
(β+α2+Ti_5Si_3)		α2 (calc.)	1.66	23.02
		β	1.2±0.1	22.1±0.2
		β (calc.)	1.19	17.97
Ti-16Al-1Si /	900	α	0.9±0.3	15.2±1.2
Ti-16Al-3.5Si		α (calc.)	0.79	15.69
(α+α2+Ti_5Si_3)		α2	1.3±0.3	20.1±1.4
		α2 (calc.)	1.46	22.34
Ti-16Al-1Si /	800	α	0.8±0.3	13.3±1.3
Ti-16Al-3.5Si		α (calc.)	0.74	14.21
(α+α2+Ti_5Si_3)		α2	1.2±0.3	19.6±1.2
		α2 (calc.)	1.26	21.81
Ti-16Al-1Si /	700	α	0.7±0.4	11.9±1.4
Ti-16Al-3.5Si		α (calc.)	0.68	12.89
(α+α2+Ti_5Si_3)		α2	1.2±0.4	19.3±1.3
		α2 (calc.)	1.13	20.97

Table 4.3.2.1. Experimental versus calculated results.

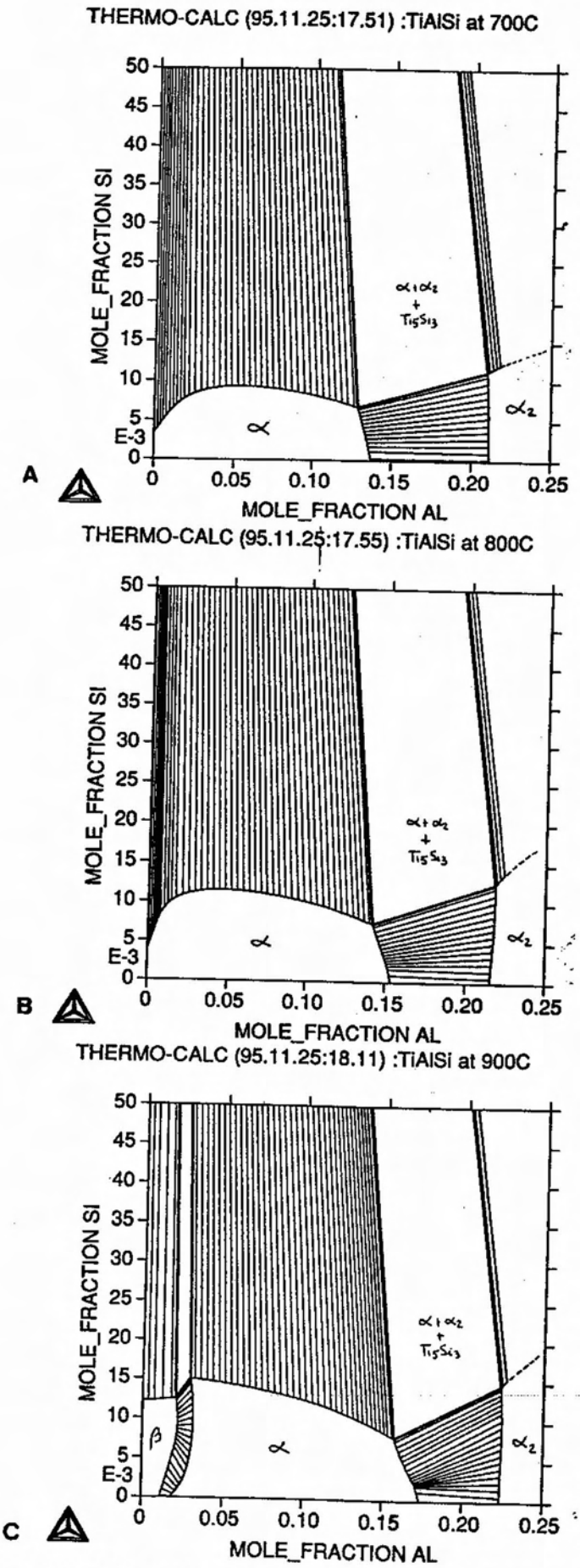

Figure 4.3.2.4. Calculated isothermal sections of the Ti-Al-Si system: a) 700°C; b) 800°C; c) 900°C.

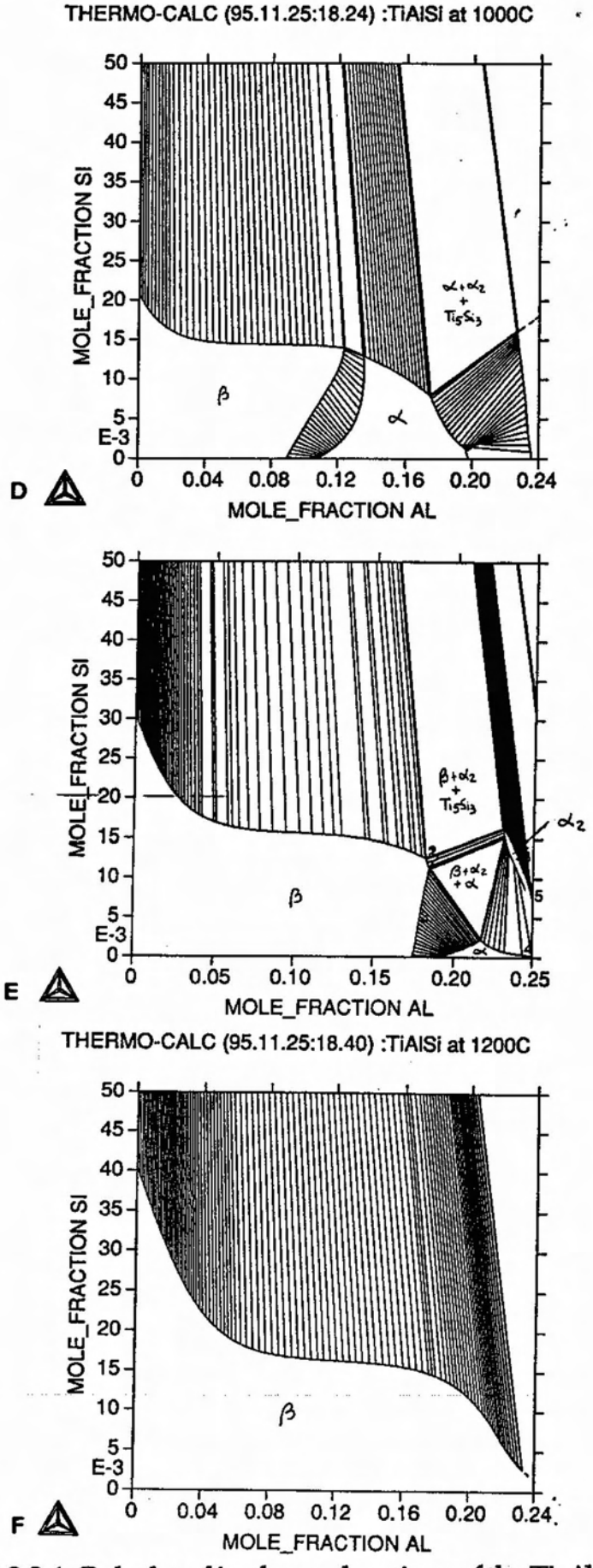

Figure 4.3.2.4. Calculated isothermal sections of the Ti-Al-Si system: d) 1000°C; e) 1100°C; f) 1200°C.

```
BCC_A2
EXCESS MODEL IS REDLICH-KISTER_MUGGIANU
ADDITIONAL CONTRIBUTION FROM MAGNETIC ORDERING
     Magnetic function below Curie Temperature
     +1-.905299383*TAO**(-1)-.153008346*TAO**3-.00680037095*TAO**9
     -.00153008346*TAO**15
     Magnetic function above Curie Temperature
      -.0641731208*TAO**(-5)-.00203724193*TAO**(-15)
     -4.27820805E-04*TAO**(-25)
 2 SUBLATTICES, SITES  1:  3
   CONSTITUENTS: AL,SI,TI : VA

     G(BCC_A2,AL:VA;0)-H298(FCC_A1,AL;0) = +GALBCC
     G(BCC_A2,SI:VA;0)-H298(DIAMOND_A4,SI;0) = +GSIBCC

     G(BCC_A2,TI:VA;0)-H298(HCP_A3,TI;0) =
            298.14<T< 1155.00: -1272.064+134.78618*T-25.5768*T*LN(T)
           -6.63845E-04*T**2-2.78803E-07*T**3+7208*T**(-1)
            1155.00<T< 1941.00: +6667.385+105.438379*T-22.3771*T*LN(T)
           +.00121707*T**2-8.4534E-07*T**3-2002750*T**(-1)
            1941.00<T< 4000.00: +26483.26-182.354471*T+19.0900905*T*LN(T)
           -.02200832*T**2+1.228863E-06*T**3+1400501*T**(-1)
     L(BCC_A2,AL,SI:VA;0) = +V27+V28*T
     L(BCC_A2,AL,SI:VA;1) = +V29
     L(BCC_A2,AL,SI:VA;2) = +V24
     L(BCC_A2,AL,SI,TI:VA;0) = +V25+V26*T
     L(BCC_A2,AL,TI:VA;0) = -128500+39*T
     L(BCC_A2,AL,TI:VA;1) = 6000
     L(BCC_A2,AL,TI:VA;2) = 21200
     L(BCC_A2,SI,TI:VA;0) = +V49+V50*T
     L(BCC_A2,SI,TI:VA;1) = +V47
     L(BCC_A2,SI,TI:VA;2) = +V48


SI3TI5
 2 SUBLATTICES, SITES  .375:  .625
   CONSTITUENTS: SI : TI

     G(SI3TI5,SI:TI;0)-0.375 H298(DIAMOND_A4,SI;0)-0.625 H298(HCP_A3,TI;0) =
           +.375*GHSERSI+.625*GHSERTI+V30+V31*T


TI3AL
EXCESS MODEL IS REDLICH-KISTER_MUGGIANU
ADDITIONAL CONTRIBUTION FROM MAGNETIC ORDERING
     Magnetic function below Curie Temperature
     +1-.860338755*TAO**(-1)-.17449124*TAO**3-.00775516624*TAO**9
     -.0017449124*TAO**15
     Magnetic function above Curie Temperature
      -.0426902268*TAO**(-5)-.0013552453*TAO**(-15)
     -2.84601512E-04*TAO**(-25)
 2 SUBLATTICES, SITES  .75:  .25

   CONSTITUENTS: AL,TI : AL,SI,TI

     G(TI3AL,AL:AL;0)-H298(FCC_A1,AL;0) = +GHCPAL
     G(TI3AL,TI:AL;0)-0.25 H298(FCC_A1,AL;0)-0.75 H298(HCP_A3,TI;0) =
           -27520+5.97*T+.75*GHSERTI+.25*GHSERAL
     G(TI3AL,AL:SI;0)-0.75 H298(FCC_A1,AL;0)-0.25 H298(DIAMOND_A4,SI;0) =
            298.14<T< 2000.00: +V15+V16*T+.75*GHSERAL+.25*GHSERSI
     G(TI3AL,TI:SI;0)-0.25 H298(DIAMOND_A4,SI;0)-0.75 H298(HCP_A3,TI;0) =
            298.14<T< 2000.00: +V17+V18*T+.75*GHSERTI+.25*GHSERSI
     G(TI3AL,AL:TI;0)-0.75 H298(FCC_A1,AL;0)-0.25 H298(HCP_A3,TI;0) =
           -24780+8.07*T+.75*GHSERAL+.25*GHSERTI
     G(TI3AL,TI:TI;0)-H298(HCP_A3,TI;0) = +GHSERTI
     L(TI3AL,AL,TI:AL;0) = -74300+25*T
     L(TI3AL,AL,TI:AL,SI;0) = +V40+V41*T
     L(TI3AL,AL,TI:AL,SI,TI;0) = +V44+V45*T
     L(TI3AL,AL:AL,TI;0) = -24742+8.325*T
     L(TI3AL,TI:AL,TI;0) = +2664-.333*T
     L(TI3AL,TI:AL,SI;0) = +V21+V22*T
     L(TI3AL,TI:AL,SI;1) = +V23
     L(TI3AL,TI:AL,SI;2) = +V33
     L(TI3AL,AL:SI,TI;0) = +V42+V43*T
     L(TI3AL,AL,TI:TI;0) = +8000-T
```

Figure 4.3.2.5. Output of Thermocalc showing description of phases, optimising variables; relative standard deviation and reduced sum of squares for the assessed Ti-Al-Si system

```
HCP_A3
EXCESS MODEL IS REDLICH-KISTER_MUGGIANU
ADDITIONAL CONTRIBUTION FROM MAGNETIC ORDERING
     Magnetic function below Curie Temperature
     +1-.860338755*TAO**(-1)-.17449124*TAO**3-.00775516624*TAO**9
     -.0017449124*TAO**15
     Magnetic function above Curie Temperature
      -.0426902268*TAO**(-5)-.0013552453*TAO**(-15)
     -2.84601512E-04*TAO**(-25)
 2 SUBLATTICES, SITES  1:  .5
   CONSTITUENTS: AL,SI,TI : VA

     G(HCP_A3,AL:VA;0)-H298(FCC_A1,AL;0) =
           298.14<T< 2900.00: +5481-1.8*T+GHSERAL
     G(HCP_A3,SI:VA;0)-H298(DIAMOND_A4,SI;0) = +49200-20.8*T+GHSERSI
     G(HCP_A3,TI:VA;0)-H298(HCP_A3,TI;0) =
           298.14<T< 4000.00: +GHSERTI
     L(HCP_A3,AL,SI:VA;0) = +V11+V12*T
     L(HCP_A3,AL,SI:VA;1) = +V13
     L(HCP_A3,AL,SI:VA;2) = +V14
     L(HCP_A3,AL,SI,TI:VA;0) = +V19+V20*T
     L(HCP_A3,AL,TI:VA;0) = -133500+39*T
     L(HCP_A3,AL,TI:VA;1) = 750
     L(HCP_A3,AL,TI:VA;2) = 17500
     L(HCP_A3,SI,TI:VA;0) = +V36+V37*T
     L(HCP_A3,SI,TI:VA;1) = +V38
     L(HCP_A3,SI,TI:VA;2) = +V39

          ==============================================
          OUTPUT FROM  P A R R O T.  DATE 95.11.25   18:44:34
          ==============================================


*** OPTIMIZATION ERROR. SUM OF SQUARES FAILS TO DECREASE ***
    NUMBER OF ITERATIONS:  107


-- OPTIMIZING CONDITIONS --

  RELATIVE STANDARD DEVIATIONS FOR EXPERIMENTS: N
  MINIMUM SAVE ON FILE: Y
  ERROR FOR INEQUALITIES =  1.00000000E+00
  RELATIVE STEP FOR CALCULATION OF DERIVATIVES =  1.00000000E-04
ARGUMENTS FOR SUBROUTINE VA05AD (HSL)
  MAXFUN = 100    DMAX =  1.00000000E+06    H =  1.00000000E-04
  ACC = (INITIAL SUM OF SQUARES) *  1.00000000E-12



-- OPTIMIZING VARIABLES --

AVAILABLE VARIABLES ARE V1  TO V50

VAR.    VALUE              START VALUE        SCALING FACTOR     REL.STAND.DEV
V11    -1.39128537E+07 -1.39128537E+07   -1.39128537E+07    3.34118353E-01
V12     2.11617164E+03  2.11617160E+03    2.11617164E+03    2.64620868E+00
V13     4.98473302E+06  4.98473305E+06    4.98473302E+06    1.58384605E+00
V14     5.84463658E+06  5.84463688E+06    5.84463658E+06    5.36830134E+00
V17    -1.17724686E+06 -1.17724689E+06   -1.17724686E+06    5.22594179E-02
V18     6.04864946E+02  6.04864940E+02    6.04864946E+02    1.05861119E-01
V19     1.09937735E+07  1.09937722E+07    1.09937735E+07    4.82800781E-01
V20    -2.86714489E+02 -2.86714491E+02   -2.86714489E+02    2.49752703E+01
V21     1.33434017E+05  1.33434018E+05    1.33434017E+05    5.70270505E-01
V22    -1.52148139E+02 -1.52148119E+02   -1.52148139E+02    5.07530143E-01
V24     1.34173666E+07  1.31751415E+07    1.31751415E+07    4.01511798E-02
V25    -1.51543556E+06 -1.51543558E+06   -1.51543556E+06    1.27871066E+00
V26     4.60907066E+03  4.60907061E+03    4.60907066E+03    3.00990516E-01
V27    -3.03877397E+06 -3.03877399E+06   -3.03877397E+06    5.48861976E-01
V28    -1.63628413E+03 -1.63628410E+03   -1.63628413E+03    5.37901170E-01
V29    -1.25633003E+06 -1.21338078E+06   -1.21338078E+06    4.31361654E-02
V30    -1.60018242E+06
V31     7.10077620E+02
V36     3.29238678E+04
V37     1.97021797E+03
V38     1.03674539E+07
V39     6.01515041E+06
V47     5.43297902E+06
V48     3.37369190E+06
V49    -2.25171819E+06
V50     1.95686743E+03

NUMBER OF OPTIMIZING VARIABLES :   2
ALL OTHER VARIABLES ARE FIX WITH THE VALUE ZERO
THE SUM OF SQUARES HAS CHANGED FROM   1.23698502E+01 TO   1.22229743E+01
DEGREES OF FREEDOM   53.  REDUCED SUM OF SQUARES   2.89587580E-01
```

Figure 4.3.2.5. continuation

4.3.3. Quaternary alloys

Sample 2NF (Ti-14Al-1Si-1Nb - T=800°C for 14 days) shows heterogeneous silicide precipitation at prior α/α boundaries (figure 4.3.3.1.a.). Figure 4.3.3.1.b. shows a silicide particle, which has been identified as Ti_3Si by the SADP shown in figure 4.3.3.3.c.. Table 4.3.3.1. shows EDX-analysis confirming the presence of Ti_3Si. Additionally, heterogeneous α2 precipitation at prior α/α boundaries is also observed (figures 4.3.3.1.d-e.).

Sample 2ZF (Ti-14Al-1Si-1Zr - T=800°C for 14 days) shows heterogeneous silicide precipitation at prior α/α boundaries (figure 4.3.3.2.a.). Additionally heterogeneous α2 precipitation at prior α/α boundaries and dislocations is observed (figures 4.3.3.2.b-c.). Figure 4.3.3.1.d shows a DFI for a silicide particle, which has been identified as Ti_3Si. Table 4.3.3.1. shows EDX-analysis confirming the presence of Ti_3Si, while table 4.3.3.2. shows the stoichiometry of the silicides found in the quaternary alloys. Note that Nb and Zr appear to replace Ti, and that the stoichiometry of the silicides fits the results of SADP, which indicate the presence of Ti_3Si.

alloy	T(°C)	sample	phase	chemical composition			
				at%Si	at%Al	at% Zr/Nb	at%Ti
2NF	800	TEM	α	0.8±0.2	14.2±0.1	1.1±0.1Nb	balance
			α2	1.1±0.2	22.0±0.1	1.0±0.2 Nb	"
			Ti_3Si	**23.5±0.6**	**nil.**	**2.8 ±0.3 Nb**	"
2ZF	800	TEM	α	0.6±0.3	15.1±0.5	0.5 ±0.3 Zr	"
			α2	0.9±0.3	20.1±0.7	0.8±0.4 Zr	"
			Ti_3Si	**26.0±2.0**	**nil.**	**24.0±1.5 Zr**	"

Table 4.3.3.1. EDX-TEM analysis for quaternary alloys.

Sample 2NG (Ti-14Al-1Si-1Nb - T=700°C for 36 days) shows heterogeneous silicide precipitation at prior α/α boundaries (figure 4.3.3.3.a.). Figures 4.3.3.3.b-c shows a duplex microstructure composed of heterogeneous and homogeneous α2 precipitation in an α matrix. The homogeneous precipitates present an elongated morphology, which grew preferentially along c axis. This results is in agreement with calculated misfit values shown in table 4.3.3.3, whic shows that misfit along c axis is lower than along a axis.

Additionally, heterogeneous precipitation of rod-like silicide identified as Ti_3Si along previous α/α boundaries was observed (figure 4.3.3.3.d.).

alloy	T(°C)	silicide	ratio = at% (Ti+Nb+Zr) / at% (Si+Al)
Ti-14Al-1Si-1Nb	800	Ti_3Si	3.3±0.1
Ti-14Al-1Si-1Zr	800	Ti_3Si	2.9±0.3

Table 4.3.3.2. Silicides stoichiometry.

Sample 2ZG (Ti-14Al-1Si-1Zr - T=700°C for 36 days) shows heterogeneous silicide precipitation at prior α/α boundaries (figure 4.3.3.4.a.) and heterogeneous silicide precipitation inside prior α plates (figure 4.3.3.4.b.). Figures 4.3.3.4.c shows a duplex microstructure composed of heterogeneous and homogeneous α2 precipitation in an α matrix. The homogeneous precipitates present an elongated morphology, which grew preferentially along c axis. This results is in agreement with calculated misfit values shown in table 4.3.3.3, whic shows that misfit along c axis is lower than along a axis. Additionally, the silicide precipitate has been identified as Ti_3Si (figure 4.3.3.4.d.).

Sample 5NE (Ti-20Al-1Si-1Nb - T=900°C for 8 days), figure 4.3.3.5.a-b. shows an α2 microstructure developed from prior colony of parallel α plates. Presence of α2 subgrains suggest that the previous microstructure controls the morphology of the α2. Neither α2 APD's nor silicides were found in this samples. Sample 5ZE (Ti-20Al-1Si-1Zr - T=900°C for 8 days), figures 4.3.3.5.c-d. show α2 subgrains and additional presence of APD's, indicating a duplex α+α2 microstructure. No silicides were found in this sample.

Sample 5ZF (Ti-20Al-1Si-1Zr - T=800°C for 14 days,), figure 4.3.3.6.a. shows α2 domains, developed from a previous massive α grain. No silicides were found in this sample. Figure 4.3.3.6.b-c (sample 5NG - Ti-20Al-1Si-1Nb - T=700°C for 36 days,) shows small α2 subgrains developed inside a prior α plate. No silicides were found in this sample. Sample 5ZG (Ti-20Al-1Si-1Zr - T=700°C for 36 days) figure 4.3.3.6.d. shows α2 domains developed from previous α plates. Figure 4.3.3.6.e shows heterogeneous silicide precipitation along previous α/α boundaries. These silicides, however, have not been identified.

alloy	T (°C)	Ti(α) a (Å)	Ti(α) c (Å)	
Ti-14Al-1Si-1Zr	900	2.920	4.670	
"	800	2.923	4.673	
"	700	2.926	4.666	
Ti-14Al-1Si-1Nb	900	2.921	4.667	
"	800	2.920	4.664	
"	700	2.923	4.660	

alloy		Ti_3Al a (Å)	Ti_3Al c (Å)	misfit$_{\alpha/\alpha 2}$ (%) <a>	misfit$_{\alpha/\alpha 2}$ (%) <c>
Ti-14Al-1Si-1Zr	900	-	-	-	-
"	800	5.809	4.664	1.1	0.13
"	700	5.812	4.664	1.4	0.04
Ti-14Al-1Si-1Nb	900	-	-	-	-
"	800	5.802	4.655	1.3	0.19
"	700	5.797	4.654	1.7	0.13

Table 4.3.3.3. Calculated lattice parameters for α and α2 and misfit$_{\alpha/\alpha 2}$.

Figure 4.3.3.1. Isothermally Heat Treated Quaternary Alloys (Ti-14Al-1Si-1Nb- T=800℃ for 14 days)

a) heterogeneous silicide precipitation (dark phase) at prior α/α boundaries; SEM/BEI;

b) rod-shaped silicide particle; TEM-BFI;

c) SADP (after unknown tilt) identifying silicide as Ti_3Si; B_{Ti_3Si}=[010]; (SADP given below)

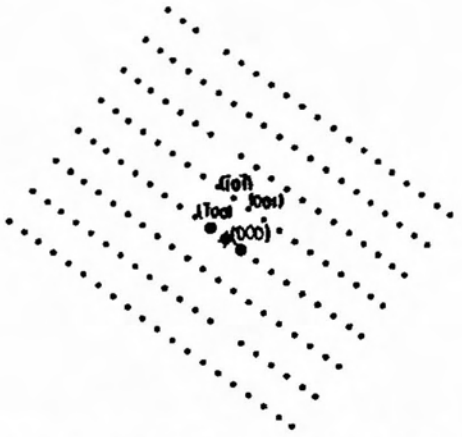

d) heterogeneous α2 precipitation at prior α/α boundaries; TEM-BFI;

e) heterogeneous α2 precipitation at prior α/α boundaries TEM-DFI; $g=(11\bar{2}0)_{\alpha 2}$

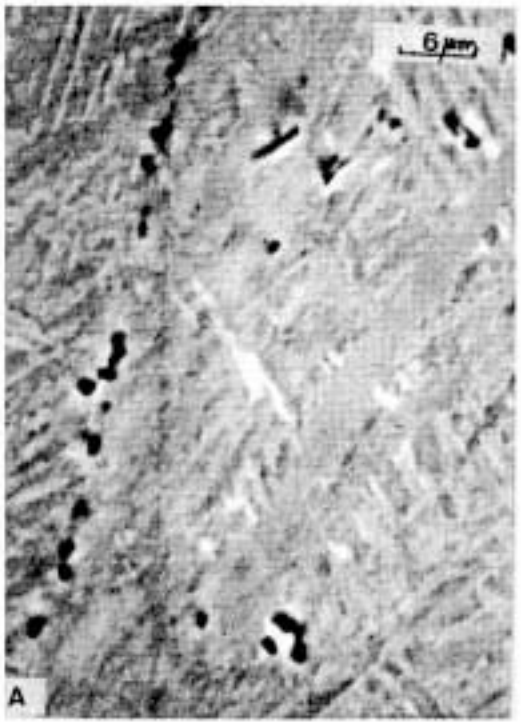
6 µm
A


1 µm
B

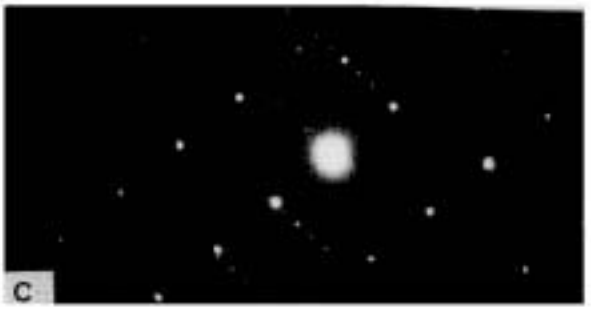
C


0,5 µm
D


0,5 µm
G(1210)
E

Figure 4.3.3.2. Isothermally Heat Treated Quaternary Alloys (Ti-14Al-1Si-1Zr - T=800°C for 14 days)

a) heterogeneous silicide precipitation (bright phase) at prior α/α boundaries; SEM/SEI;

b) heterogeneous $\alpha 2$ precipitation at prior α/α boundaries; TEM-BFI;

c) heterogeneous $\alpha 2$ precipitation at prior α/α boundaries TEM-DFI; $g=(11\bar{2}0)_{\alpha}$;

d) Ti_3Si particle; TEM-DFI; SADP: $g=(\bar{1}01)_{Ti_3Si}$ and $B_{Ti_3Si}=[1\bar{2}1]$; (SADP given below)

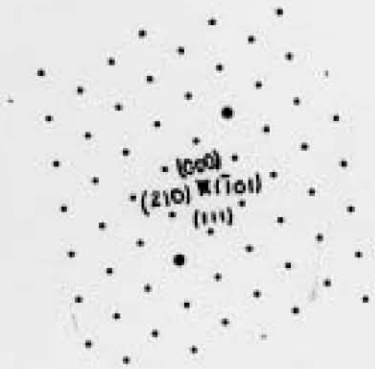


6 µm
A

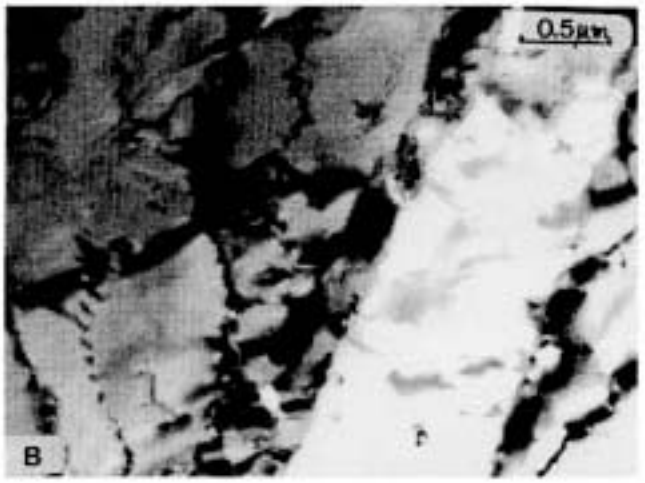
0.5 µm
B

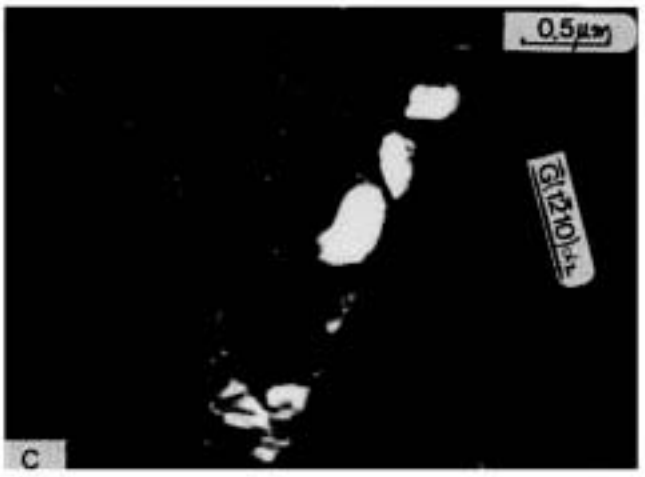
0.5 µm
G(1210)
C

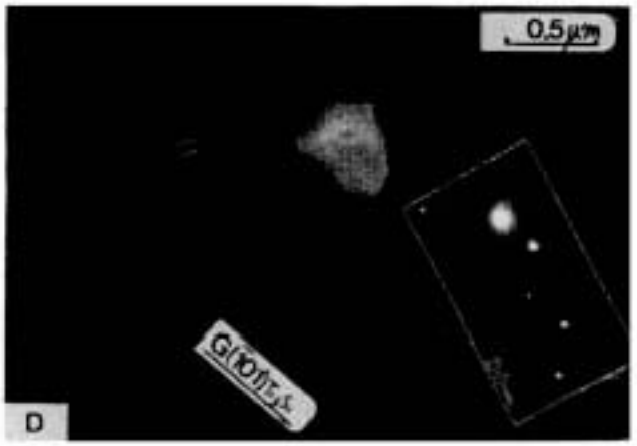
0.5 µm
G(0111)
D

Figure 4.3.3.3. Isothermally Heat Treated Quaternary Alloys
(Ti-14Al-1Si-1Nb- T=700℃ for 36 days)

a) heterogeneous silicide precipitation (dark phase) at prior α/α boundaries; SEM/BEI;

b) homogeneous and heterogeneous $\alpha 2$ precipitation, the latter at prior α/α boundaries; TEM-DFI, $g=(1\bar{2}10)_{\alpha 2}$;

c) detail of homogeneous $\alpha 2$ precipitation;
TEM-DFI; $B=[1\bar{2}10]_{\alpha 2}$ and $g=(10\bar{1}1)_{\alpha 2}$

d) Ti_3Si particle; TEM-DFI; SADP: $g=(33\bar{1})_{Ti_3Si}$ and $B_{Ti_3Si}=[2\bar{1}3]$;

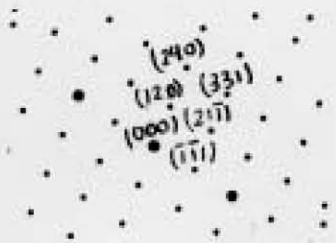

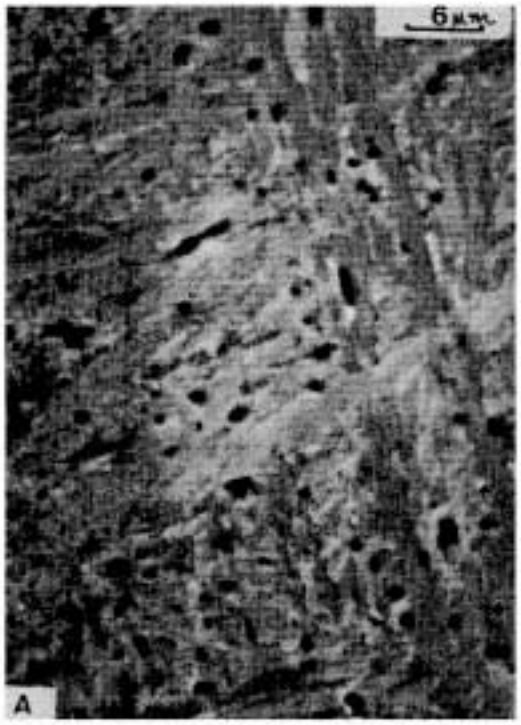
6 μm
A


0.5 μm
G(1$\bar{2}$10)
B

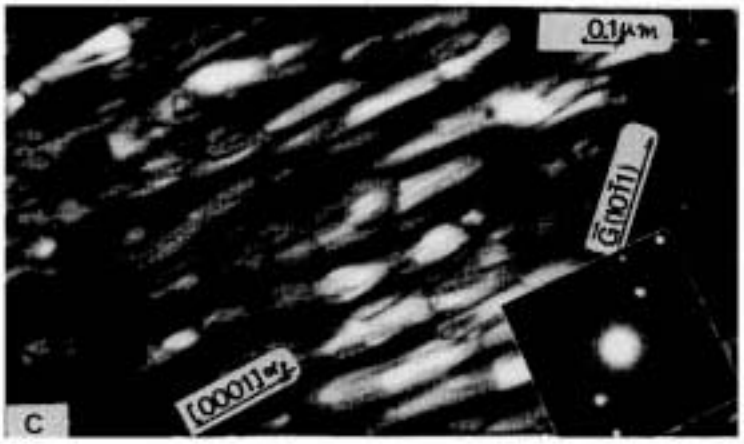
0.1 μm
G(10$\bar{1}$1)
[0001]
C

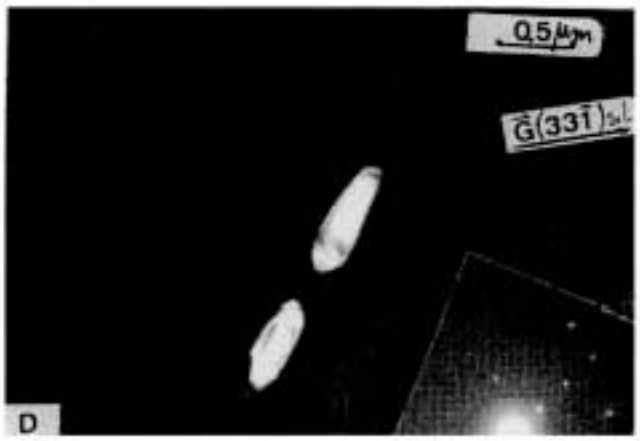
0.5 μm
G(33$\bar{1}$)
D

Figure 4.3.3.4. Isothermally Heat Treated Quaternary Alloys (Ti-14Al-1Si-1Zr - T=700°C for 36 days)

a) heterogeneous silicide precipitation (bright) at prior α/α boundaries; -SEM/SEI;

b) silicide precipitation; TEM-BFI;

c) detail of $\alpha 2$ precipitation: homogeneous and heterogeneous, the latter at the right ; TEM-DFI; $B=[10\bar{1}0]_{\alpha 2}$ and $g=(1\bar{2}10)_{\alpha 2}$

d) Ti_3Si particle; TEM-DFI; SADP: $g=(2\bar{1}0)_{Ti_3Si}$ and $B_{Ti_3Si}=[1\bar{2}1]$;


6 μm
A


1 μm
B

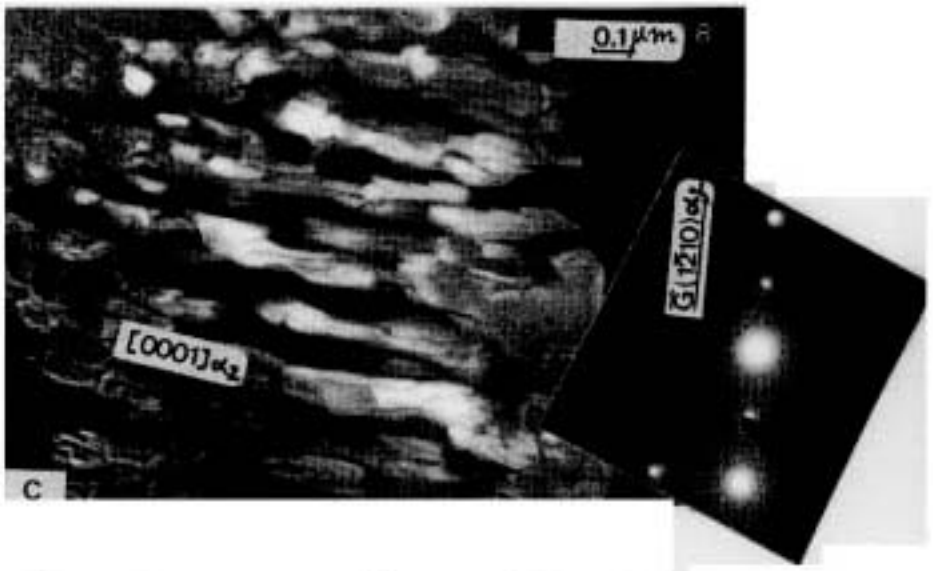
0.1 μm
[0001]α2
G(1$\bar{2}$10)α2
C

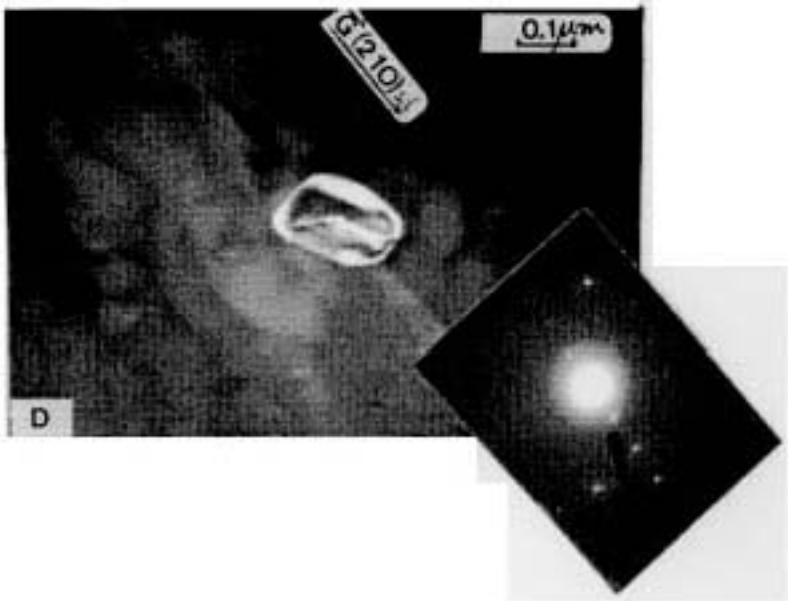
G(210)α2
0.1 μm
D

Figure 4.3.3.5. Isothermally Heat Treated Quaternary Alloys

a) sample 5NE (Ti-20Al-1Si-1Nb - T=900°C for 8 days) shows $\alpha 2$ microstructure developed from prior colony of parallel α plates; TEM-BFI;

b) sample 5NE (Ti-20Al-1Si-1Nb - T=900°C for 8 days) - presence of $\alpha 2$ subgrains suggest that the previous microstructure controls the morphology of the $\alpha 2$; TEM-DFI; $g=(11\bar{2}0)_{\alpha 2}$;

c) sample 5ZE (Ti-20Al-1Si-1Zr - T=900°C for 8 days) shows $\alpha 2$ subgrains; TEM-BFI;

d) sample 5ZE (Ti-20Al-1Si-1Zr - T=900°C for 8 days) shows additional presence of APD's, indicating a duplex $\alpha+\alpha 2$ microstructure; TEM-DFI, $g=(10\bar{1}1)_{\alpha 2}$.


1μm
A


1μm
G[1120]
B


0.5μm
C


0.5μm
G[0001]
D

Figure 4.3.3.6. Isothermally Heat Treated Quaternary Alloys

a) sample 5ZF (Ti-20Al-1Si-1Zr - T=800°C for 14 days,) shows α2 domains, developed from a previous massive α grain; TEM-DFI, g=$(11\bar{2}0)\alpha 2$;

b) sample 5NG (Ti-20Al-1Si-1Nb - T=700°C for 36 days) shows small α2 subgrains developed inside a prior α plate; TEM=BFI;

c) sample 5NG (Ti-20Al-1Si-1Nb - T=700°C for 36 days) shows small α2 subgrains developed inside a prior α plate; TEM-DFI, g=$(10\bar{1}1)\alpha 2$;

d) sample 5ZG (Ti-20Al-1Si-1Zr - T=700°C for 36 days) shows α2 domains developed from previous α plates: TEM-DFI, g=$(10\bar{1}1)\alpha 2$;

e) sample 5ZG (Ti-20Al-1Si-1Zr - T=700°C for 36 days) shows heterogeneous silicide precipitation (dark phase) along previous α/α boundaries.

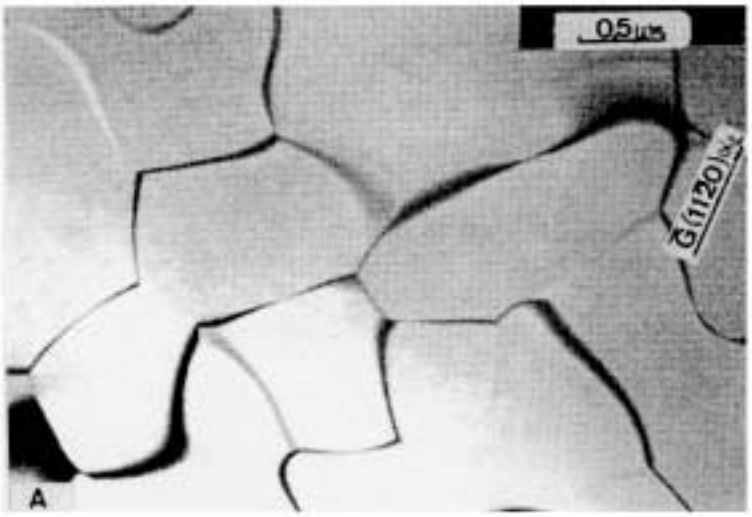
0.5μm
G(1120)α
A


0.1μm
B


0.1μm
G(1011)α
C

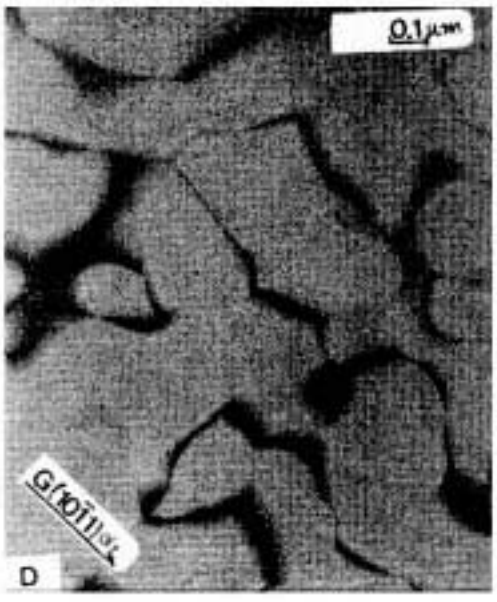
0.1μm
G(1011)α
D


0.5μm
E

4.3.4. Discussion

• α2 precipitation

The results from the mathematical modelling indicate that Si addition increases the driving force of the reaction: α–>α+α2 (see figures 4.3.4.4.a.-d.), so it could be expected that Si would promote a more homogeneous precipitation of α2. Figure 2.5.2.1. shows how ageing temperature and chemical composition affect the nucleation behaviour of α2 phase in Ti-Al system. Both parameters define the driving force available for the α2 nucleation, and higher temperature and lower Al content values promote heterogeneous nucleation. The present results for ternary alloys, however, suggest otherwise. Si addition promotes heterogeneous formation of α2 (see figures 4.3.1.4.e., 4.3.1.5.a-c., 4.3.1.6.b-c., 4.3.1.7.c. and 4.3.1.9.b.), where prior α/α boundaries and sub-boundaries were shown to be preferential nucleation sites. Concerning the homogeneous nucleation of α2 precipitates, the ternary alloys, despite presenting higher driving force for α–>α+α2 reaction, presented much larger precipitates.

The results showed that Si addition increased the α/α2 misfit. Table 4.3.1.3. shows that Ti-Al-Si alloy presents the highest values of α/α2 misfit values along both <a> and <c> directions. This increase in the interfacial α/α2 energy would alter the nucleation conditions by increasing $\Delta G^{*}_{\alpha->\alpha+\alpha 2}$ and, therefore, promoting the heterogeneous nucleation of α2 precipitates. Additionally, it has been shown that Si addition increases the area of α/α interfaces, so that Si addition would also promote an increase in the area of preferential nucleation sites, which would, therefore, enhance the heterogeneous character of α2 nucleation.

Quaternary alloys also presented heterogeneous nucleation behaviour. These alloys, however, present lower Al content, which would decrease the driving force for α2 precipitation and promote heterogeneous nucleation of α2. Nb addition does not appear to partition preferentially between α and α2, while Zr seems to partition preferentially into α2, reducing Al solubility in α2. This result agrees with previous investigation that Zr stabilisers α2 phase [SCA 84]

Additionally, both ternary and quaternary alloys presented in the as-quenched condition a much larger quantity of preferential nucleation sites such as dislocations and α/α boundaries and sub-boundaries. This increase in the amount of nucleation sites should accentuate the proportion of heterogeneous α2 precipitates.

The presence of the brittle α2 phase, which presents an insufficient number of independent slip systems to relieve the strain, at the grain

boundaries may lead to the earlier formation of microcracks at the adjoining grain. In this sense, a hypothetical microstructure presenting ductile β phase precipitated along prior α/α boundaries and sub-boundaries would allow the duplex (α+α2) matrix to be deformed to a greater extent before the formation of these microcracks. For the production of this hypothetical β+(α+α2) microstructure the following heat treatment procedure is suggested:

- isothermal heat treatment, following homogenisation heat treatment, between $T_{\beta/\alpha+\beta}$-20°C (to avoid formation of α GB allotriomorph [FUR 90]) and $T_{\alpha+\beta/\alpha}$ would produce a lamellar microstructure composed of α+β. The temperature of such isothermal heat-treatment would control the proportion of α and β phases, assuring continuity of ductile β phase along α/α plate boundaries;
- second isothermal heat treatment inside α+α2+β phase field would promote the precipitation of α2, whose size and particle distribution would be controlled by the temperature. Further investigation, however, on the effect of the heat treatment parameters on the thermal stability of retained β phase during the second isothermal heat treatment would be required, and the ideal alloy would preferentially present a ternary α+α2+β phase field around 14at%Al.

Ti-14Al-1Si-1Nb alloy, which presented β phase along α/α boundaries in the as-quenched condition, did not present any presence of retained β after heat treatment between 700 and 900°C, suggesting that Nb addition higher than 1at% should be necessary to stabilise β phase during isothermal heat treatment inside α+α2+β phase field.

Concerning the homogeneously nucleated α2 particles, ternary and quaternary additions did not change the preferential growth along <c>. This observation agrees with the calculated misfit values shown in tables 4.3.1.3. and 4.3.3.3.

The alloys with higher Al content presented either α2 domains, in the case of a prior microstructure of large massive grains, or α2 sub-grains. In this sense, the results have shown that the prior microstructure controls the presence of sub boundaries in α2 alloys. These sub-boundaries, thought to be the α/α plate sub-boundaries present in the as-quenched microstructure, do not just disappear after nucleation and growth of α2 phase and might play an important role on the deformation behaviour of α2 phase.

Comparing the two quaternary alloys with 20at%Al and heat treated at 900°C, the results may suggest that Nb addition is a stronger α2 stabiliser than Zr (see table 4.3.4.2). Oxygen content (see table 3.3.1.), however, is also an

α2 stabiliser [ARD 95], and these alloys present a large difference in this interstitial content (Ti-20Al-1Si-1Nb- 2150O versus Ti-20Al-1Si-1Zr- 1200O), so that no conclusion can be made.

• silicide precipitation

Tables 4.3.1.2. and 4.3.3.2. present a summary of the results of EDX analysis obtained for the silicide phase in the ternary and quaternary alloys investigated. The results for ternary alloys confirm previous result for as-quenched alloys:

- addition of Al increases the solubility of Al and decreases the solubility of Si in the silicide, in agreement with previous work [ZHA 91], suggesting that Al replaces Si in the sublattice(s) of Ti_5Si_3.
- addition of Al increases the ratio Ti/(Al+Si) of the silicide suggesting a possible change in the stoichiometry of the silicide.

Such observations were discussed previously, using the fact that Al presents a bigger atomic radius (table 4.2.1.2.); is less electronegative than Si (table 4.2.1.2.) and presents less electrons (+3) in the valence shell than Si (+4) [VAN 70], so that Al might have altered the site occupancy of Ti, Si and vacancies in the different sublattices of the Ti_5Si_3 crystal; decreasing the number of covalent (Ti-Si); and increasing the number of metallic-type bondings (Ti-Al) in the silicide crystal.

Additionally, it is observed (see table 4.3.3.2.) that the temperature of isothermal heat treatment also affects the solubility of Al in the silicide and, therefore, the ratio Ti/(Al+Si) of the silicide. Decreasing the temperature decreases the solubility of Al and increases the ratio Ti/(Al+Si).

Nb and Zr both promoted the formation of Ti_3Si, with no apparent solubility of Al (see table 4.3.3.2.), although the possible mechanism is still unknown. Pajunen et al.[PAJ 89] mentioned, however, that impurity contamination has a marked effect on the stability of Ti_3Si. They observed that a diffusion couple made of commercial purity Ti presented Ti_3Si precipitates after annealing at 1100°C for 32 hours, while the one made of high purity Ti did not present Ti_3Si precipitates after 100 hours at the same temperature. They suggest that oxygen may have promoted this precipitation. A calculated version of the Ti-Si-O system obtained via Thermocalc (figure 4.3.4.1.), however, shows that oxygen inhibits Ti_3Si formation. The present investigation did not establish a possible explanation, and it is suggested that a complete chemical analysis of interstitial elements and other possible contaminants should be carried out in the ternary and quaternary alloys investigated. Another approach would be that Nb and Zr catalyse themselves the precipitation of Ti_3Si.

Zr addition promoted a less heterogeneous silicide precipitation. Chemical analysis (see table 4.3.3.1.) show that solubility of Si in α and α2 is lower in Ti-Al-Si-Zr than Ti-Al-Si-Nb, suggesting that a higher supersaturation in Si in the former alloy is promoting such silicide distribution.

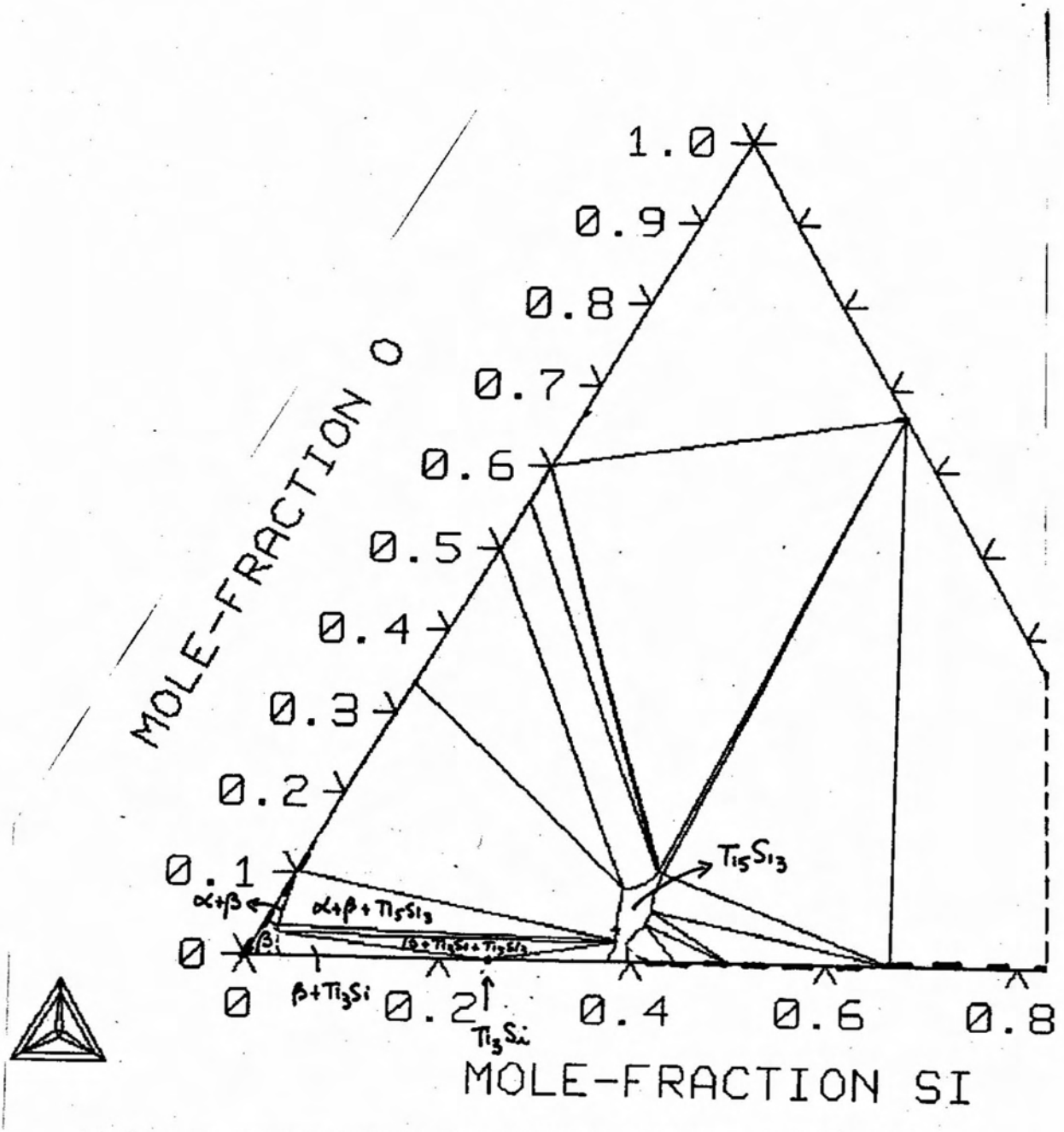

Figure 4.3.4.1. Calculated Ti-Si-O Phase Diagram obtained via Thermocalc: (Isothermal at 1100°C)

5. Conclusions and suggestions for further work

5.1. Conclusions

• as-cast samples

The angle between secondary and primary branches of the dendrites is very close to 90°, suggesting that the primary phase for ternary alloys containing between 16-22at%Al and 0-3.5at%Si is β(bcc).

XRD identified the interdendritic silicide as Ti_5Si_3, indicating the existence of an eutectic reaction given by ($L \rightarrow \beta + Ti_5Si_3$) between 16-22at%Al for alloys containing 3.5at%Si.

The addition of Al slightly increased the lattice parameters of Ti_5Si_3.

Al addition promoted coarser eutectic microstructure caused by a possible increase of the eutectic temperature with the increase in Al content from 16 to 22at%.

• as-quenched samples: allotropic transformation

Assuming a constant cooling rate and disregarding possible variations in the interstitial contents, it has been shown how variables such as $T_{\beta/\beta+\alpha}$, T_0, $T_{\beta+\alpha/\alpha}$, Ms temperature, which can be obtained through thermodynamic modelling of phase diagrams, and solute diffusivity control the morphology of α phase formed by the allotropic reaction β–>α.

The addition of Al promoted the massive-type transformation. This addition increased the T_0, $T_{\beta/\beta+\alpha}$, $T_{\beta+\alpha/\alpha}$ and Ms temperatures and these effects, especially on $T_{\beta+\alpha/\alpha}$ explain the favouring of massive products.

Si, Zr and Nb inhibited the massive-type transformation, especially in the alloys with lower Al content. All these alloying elements decreased $T_{\beta+\alpha/\alpha}$ and inhibited the formation of massive products.

Si is seen to be the weakest massive-type transformation inhibitor, and its addition was shown to decrease the massive grain size and increase the irregularity of the interface, producing a massive product typically formed at higher undercoolings. This addition promoted a much more faceted and acicular massive product interface, suggesting that at higher undercoolings the orientation relationship plays an important role on the growth of massive product.

Zr was very effective on inhibiting the formation of massive product, especially in the Ti-14Al-1Si-1Zr alloy, and promoting the formation

of martensitic microstructures. This result shows clearly the effect of the low diffusivity of Zr on inhibiting the diffusional formation of a typical massive product.

Nb addition drastically widened [$T_{\beta/\beta+\alpha}$ -$T_{\beta+\alpha/\alpha}$]. This effect indicates that the decomposition of β inside the two phase field would be promoted. The experimental work confirmed the solute partitioning and the presence of stabilised β, although no conclusive evidence concerning the mechanism of reaction could be established.

The present investigation observed for the massive products a few interesting morphological features such as the presence of: anisotropic growth; ledges of growth, "acicular" massive grains, dislocations, and transitional massive/primary plate morphologies. The latter feature (observed in some of the Ti-Al-Si-X alloys with higher Al content) indicates a very blurred transition between massive and primary α plates. It is suggested, therefore, that the transition between short-range diffusional and shear mechanisms is diffuse and might account for the transitional massive/primary plates morphologies observed. The model proposed by Aaronson and co-workers for the massive transformation was shown to be very useful to explain the formation of the transitional morphologies observed in the present investigation.

Concerning the roles of diffusion and shear on the formation of colonies of parallel α plates, the experimental results show that the colonies of parallel plates exhibited: moderate dislocation density; presence of low-angle α/α plate boundaries; presence of internal aligned subunits containing small angle sub-boundaries; and, in Ti-Al-Si-Nb alloys, presence of retained β (with solute partitioning) along α/α parallel plates boundaries.

The presence of subunits has been described in the literature as an example of sympathetic nucleation, but the results suggest that these subunits are supersaturated in solute, indicating either initial formation of subunits by shear or partitioning of solute under paraequilibrium conditions during sympathetic nucleation.

The presence of retained β and solute partitioning could not be used to identify the operative mechanism for the formation of parallel plates. Solute partitioning might be occurring after nucleation by shear. Also inconclusive is the fact that the extrapolated value of Ms for Ti-16Al-1Si-1Nb lies below $T_{\alpha+\beta/\alpha}$, suggesting that solute partitioning after nucleation by shear is not thermodynamically feasible for this alloy.

The presence of ledges of growth appeared to be the only evidence of diffusional growth of the colonies of parallel plates in quenched Ti-22Al-Si alloys. This evidence, however, does not refute the initial formation of the α

plate by shear and a change of mechanism during growth. Like the transition massive-> martensite, the transition martensite->colony of parallel plates appears to be diffuse. The high atomic diffusivity around Ms observed for Ti-Al alloys is likely to, at least, alter locally the thermodynamic conditions for further nucleation and growth of the α' phase via shear. In this sense it is suggested that a nucleus formed initially by shear may grow by a diffusion controlled mechanism, such as growth by ledges.

• as-quenched samples: APDs formation

The addition of 3.5 at% Si promoted the formation of α2 APDs in as-quenched alloys. The ternary sample Ti-22Al-3.5Si exhibited formation of columnar domains. In the present work, the elongated α2 domains where observed to grow along different directions such as $<11\bar{2}0>\alpha 2$, $<10\bar{1}0>\alpha 2$ and $<21\bar{3}\bar{1}>\alpha 2$. It is suggested that these elongated domains were heterogeneously nucleated at certain low-angle α/α boundaries, where by balance of interfacial energy an anisotropic nucleation and growth of α2 APDs can be expected .

Quaternary additions of Zr and Nb inhibited the growth of APD's as these elements diffuse more slowly than Ti or Al.

• isothermally heat treated samples

The growth of α2 particles along the **c** axis produces a misfit around 0.3% while the misfit for growth along **a** axis would be around 2%. This preferential growth along [0001] minimises the strain energy between α and α2, and produces extremely elongated α2 precipitates.

Heterogeneously nucleated α2 particles do not present a typical elongated morphology, stressing that the minimisation of strain energy is not a crucial process during the growth of heterogeneous precipitates.

These α2 particles in binary Ti-Al alloys are much smaller than the ones present in the ternary alloy indicating that Si addition alters the conditions of nucleation and growth of α2 particles.

The morphology of the α2 particles in the binary alloy was less elongated than the ternary one, suggesting that Si addition promotes more elongated particles. This observation is in agreement with the calculated misfit values, which showed that Si addition increases the misfit along a axis and decreases it along c axis.

Both ternary and quaternary alloys presented in the as-quenched condition a much larger quantity of preferential nucleation sites such as

dislocations and α/α boundaries and sub-boundaries. This increase in the amount of nucleation sites should accentuate the proportion of heterogeneous α2 precipitates, showing the role of the prior microstructure on the morphology of α+α2 microstructures.

The alloys with higher Al content presented either α2 domains, in case of large massive grains prior microstructure, or α2 sub-grains. In this sense, the results have shown that the prior microstructure also controls the presence of sub boundaries in α2 alloys.

Comparing the two quaternary alloys with 20at%Al and heat treated at 900°C, the results may suggest that Nb addition is a stronger α2 stabiliser than Zr. Oxygen, however, is also an α2 stabiliser, and these alloys present a large difference in this interstitial content (Ti-20Al-1Si-1Nb alloy presented 2150ppm O versus 1200ppm O for Ti-20Al-1Si-1Zr alloy), so that the α2 stabiliser effect might be due to larger amount of oxygen in the former alloy.

Nb and Zr additions both promoted the formation of Ti_3Si in Ti-14Al-1Si-1X alloys. The present investigation did not establish possible mechanisms to explain this formation.

Zr addition promoted a less heterogeneous silicide precipitation. EDX analyses show that solubility of Si in α and α2 is lower in Ti-Al-Si-Zr than Ti-Al-Si-Nb alloy, suggesting that a higher Si supersaturation in the former alloy is promoting a more homogeneous silicide distribution.

• experimental ternary phase diagram

Between 700 and 900°C, tie triangles containing α+α2+Ti_5Si_3 showed that the variation in Si content in both α and α2 phases with the heat treatment temperature is very small and presents a large relative error related to this measurement. The variation in Al content, especially in α phase, with heat treatment temperature is well defined and shows that both phases present less Al in solution than shown in the binary phase diagram, suggesting that Si reduces the solubility of Al in both phases.

Concerning Ti_5Si_3 analysis, some solid solution of Al is observed. The results confirm and complement previous observation of as-quenched alloys:

- Al addition promoted less widespread and coarser precipitation of silicide along α/α boundaries.
- addition of Al decreases the solubility of Si in the silicide suggesting that Al replaces Si in the sublattice(s) of Ti_5Si_3 crystal; and that Al increases the activity coefficient of Si in Ti_5Si_3. At higher Al contents, Al replaces more Si in the silicide.

- addition of Al increases the ratio Ti/(Al+Si) of the silicide from 1.64±0.14 to 2.02±0.32, suggesting a possible change in the stoichiometry of this phase.
- decreasing the temperature of isothermal heat treatment decreases the solubility of Al and increases the ratio Ti/(Al+Si).

The results for the equilibria (β+Ti_5Si_3) shows that increasing Al content reduces the solubility of Si in β phase, so that Al increases the activity coefficient of Si in β. The equilibrium (α+Ti_5Si_3) at 1000°C suggests that Al addition increases either the eutectoid (β->α+Ti_5Si_3) or the peritectoid (β+Ti_5Si_3->α) temperature.

The present results does not indicate the possible existence of the peritectoid reaction given by (β+Ti_5Si_3->α). For the alloy Ti-16Al-3.5Si the equilibria β+Ti_5Si_3 at 1100°C and α+Ti_5Si_3 at 1000°C show that the solubility of Si is higher in β than in α phase, indicating, therefore, the existence of an eutectoid (β->α+Ti_5Si_3) reaction instead.

The EDX-analyses of the three phase (β+α2+Ti_5Si_3 at 1100°C) and two phase (β+Ti_5Si_3 at 1200°C) fields indicate the existence of a peritectoid reaction given by (β+Ti_5Si_3->α2), as the solubility of Si in α2 is higher than β phase.

The existence of a two phase field (β+α2) at 1100°C in the ternary alloy along with the phase relationships shown in the Ti-Al phase diagram at 1100°C (which shows the presence of (β), (β+α), (α), (α+α2) and (α2) phase fields with increasing Al content), suggest the existence of a three phase field. This phase field is identified as (β+α+α2) and might exist for Al content around 22at% and Si content between 0 and 1at%. Its presence indicates the existence of a second peritectoid reaction in the ternary Ti-Al-Si given by (β+α2->α).

• calculated ternary phase diagram

The assessed ternary diagram indicates that:

- Si has a higher solubility in α2 than in α phase ;
- Si decreases the solubility of Al in α and α2 phases;
- the rather simple Ti_5Si_3 phase description, which does not include Al solid solubility, is responsible for some inconsistencies found in the calculated phase diagram;
- Al addition decreases the solubility of Si in both α and β phases;

- Si addition promotes a peritectoid reaction at 1100°C: ($\beta+\alpha2 \rightarrow \alpha$), in agreement with experimental work, which shows the presence of $\beta+\alpha2+Ti_5Si_3$ and $\beta+\alpha2$ phase fields;
- the solubility of Si in $\alpha2$ is higher than in β phase, indicating the existence of a second peritectoid reaction given by ($\beta+Ti_5Si_3 \rightarrow \alpha2$), in agreement with experimental work.

The comparison between experimental and calculated results shows that both results are qualitatively in good agreement. Quantitatively there are a few points that should be noted and regarded in case of future reassessment of the ternary system, such as the difference in the solubility of Si, and in some cases Al, in β phase; and the solubility of Al in $\alpha2$ phase. Such deviations, however, have been considered to be normal and the result of 0.289 for the reduced sum of squares obtained after the optimisation procedure is far below the advisable unity value.

The apparently weak effect of Si as an eutectoid β stabiliser was enough to promote the peritectoid reaction, given by $\alpha2+\beta \rightarrow \alpha$, around 22at%Al. The suggestion of this peritectoid reaction agrees qualitatively with previous observations in the Ti-Al system concerning the relative stability of α, $\alpha2$ and β phase.

The solution found for the present calculated ternary diagram resembles very much the ternary Ti-Al-Nb, bearing in mind the differences in solute solubility in α and β phases; and in the presence of eutectic/eutectoid products. This similarity indicates that the Ti-Al-Si system might become attractive for the production of low-cost $\alpha2+\beta$ alloys, with Si addition replacing Nb. For instance, low cost alpha 2 alloys could be produced by adding 1at%Si instead of 1½at%Nb, with savings of approximately 10% in weight and £2.12/g of alloy.

The thermodynamic calculation of the Ti-Al-Si phase diagram was considered to be a useful tool. It proposed two peritectoid reactions and produced a general description of the Ti-rich corner of the Ti-Al-Si system. Some of the isothermals do present uncertainties, which will, however, allow a more rational way of devising sets of critical experiments for a future and more accurate determination of the Ti-Al-Si phase diagram.

The effect of Nb on $T\beta/\alpha+\beta$; $T\alpha+\beta/\alpha$; and Ms in Ti-Al-Si-Nb alloys, so that the exact positioning of Ms in relation to the two phase field can be determined. If $Ms<T\alpha+\beta/\alpha$, the presence of retained β presenting solute partitioning defines the mechanism of formation of colonies of parallel α plates in Ti-14Al-1Si-1Nb as diffusional.

The mechanism of formation of sub-units in Ti-20Al-Si-X (X=Nb and Zr). Isothermal heat-treatments between $T\beta/\alpha+\beta$ and Ms following homogenisation heat treatment in single β field might produce useful insights on the mechanism of formation of sub-units. The system Ti-20Al-1Si-Nb is suggested for this study. This study might as well produce useful insights on the transition diffusional->shear.

There is room for optimising the assessed Ti-Al-Si phase diagram. The calculated version allow a more rational way of devising sets of critical experiments for a more accurate determination of the Ti-Al-Si phase diagram, especially in composition and temperature ranges not covered by the present investigation. A more realistic description of Ti_5Si_3 phase considering solubility range and solid solubility of Al would also provide a better basis for the calculation of the ternary diagram. Additionally, it is suggested that this optimisation should be carried on using a more updated database (COST).

The presence of the brittle α2 phase, which presents an insufficient number of independent slip systems to relieve the strain, at the grain boundaries may lead to the earlier formation of microcracks at the adjoining grain. In this sense, a hypothetical microstructure presenting ductile β phase precipitated along prior α/α boundaries and sub-boundaries would allow the duplex (α+α2) matrix to be deformed to a greater extent before the formation of these microcracks. For the production of this hypothetical β+(α+α2) microstructure the quaternary Ti-Al-Nb-Si system should be established.

The solution found for the present calculated ternary diagram resembles very much the ternary Ti-Al-Nb. This indicates that the Ti-Al-Si system might become attractive for the production of low-cost $\alpha 2+\beta$ alloys, with Si addition replacing Nb. Further investigation on the mechanical properties, thermal stability and oxidation resistance of Ti-Al-Si alpha 2 alloys should, therefore, be carried out.

The effect of Al on the stoichiometry of Ti_5Si_3 has been discussed very briefly using the fact that Al presents a bigger atomic radius; is less electronegative than Si and presents less electrons (+3) in the valence shell than Si (+4), so that Al might have altered the site occupancy of Ti, Si and vacancies in the different sublattices of the Ti_5Si_3 crystal; decreasing the number of covalent (Ti-Si); and increasing the number of metallic-type bondings (Ti-Al) in the silicide crystal. A more detailed model, however, should be used to account for all this variables in the balance of forces between atoms present in the $D8_8$ crystal.

Nb and Zr both promoted the formation of Ti_3Si. The present investigation did not establish any possible mechanism to explain this behaviour. It is suggested that a complete chemical analysis of interstitial elements and other possible contaminants should be carried out in the ternary and quaternary alloys investigated in order to determine a possible relationship between impurities and type of silicide. It would be also interesting to establish whether Ti_5Si_3 is the stable silicide phase in the Ti-Al-Si system.

I would like to thank: Capes-MEC/Brasil, for its financial support; and Prof. H.M.Flower, Imperial College, for his efficient supervision.

Further acknowledgments to:

• Prof. H.Goldestein, Escola Politécnica da Universidade de São Paulo;

• Prof. D.R.F.West, Imperial College;

• Dr.L.Mariotto and Dr.T.Cescom, IPT (Instituto de Pesquisas Tecnológicas do estado de São Paulo);

• Mr. M. Lindholm, Royal Institute of Technology;

• Mr. A.Palmer; Mr. D.Palmer; and Dr.R.V.Pinto,

• TRADE® and ff;

• my colleagues from E.M.Group (Alcan Fernandez, Graham Briers, Nalinda Salpatoru, Barbara Shollock, Kim Dyos, Rachel Tam, Saeed Hanesh, Shahid Ryas,...);

• the staff of the Department of Materials, Imperial College, in special to Mary Willes, Gill Hopkins, Norma Hikel, Richard Sweeney, Dan Walters, Shizu Inada-Kim;

• the staff from Charles Bell Ward, Middlessex Hospital;

• the staff from The London Lighthouse, London.

[AAN 71] H.B.Aanon and H.I.Aaronson, Metallurgical Transactions, v.2A, n.1, (1971), p.23.

[AAA 56] H.I.Aaronson and C.Wells, Journal of Metals, Trans. AIME, (1956), p.1216.

[AAR 77] H.I.Aaronson and K.R.Kinsman, Acta Metal., (1977), v.25, p.307.

[AAR 90] H.I.Aaronson, W.T.Reynolds Jr., G.J.Shiflet and G.Spanos, Metallurgical Transactions, v.21A, n.6, (1990), p.1343.

[AAR 94] H.I.Aaronson and M.G.Hall, Metallurgical Transactions, v.25A, n.9, (1994), p.1797.

[ABB 91] J.H.Aboud and D.R.F.West, Mat.Scie.Tech., (1991), v.7, p.827.

[AHM 92] T.Ahmed, PhD Thesis, University of London (Imperial College), 1992.

[AND 57] K. Anderko, K.Sagel and V.Zwicker, Zeit.Metallkunde, v.48, (1957), p.57.

[AND 86] J.-O.Andersson, A.Fernandez Guillermet, M.Hillert, B.Jansson and B.Sundman, Acta Metal., v.34, n.3, (1986), p.437.

[ANS 88] I.Ansara, B.Sundman and P.Willemin, Acta Metal, v.36, n.4, (1988), p.977.

[ARD 95] M.G.Ardakani, B.A.Shollock and H.M.Flower, 8th Conference on Ti, Birmingham, UK, 1995. to be published.

[ARR 92] D.J.Arrell, PhD Thesis, University of London (Imperial College), 1992.

[ARR 93] D.J.Arrell, H.M.Flower and S.Kerry, in Proc. 7th Conference on Ti, San Diego, California, Ed.F.H.Froes and I.L.Caplan, TMS, (1993), p.1003

[ASH 73] P.J.Ash, PhD Thesis, University of London (Imperial College), 1973.

[AST 93] M.Asta, D.de Fountaine, M.van Schilfgaarde, J.Mater.Res., v.8, n.10, (1993), p.2554.

[BAN 73] S.Banerjee, S.J.Vijayakar and R.Krishnan, in Proc. 2nd Int. Conf. "Titanium Science and Technology", Massachusets, USA, Ed.R.I.Jaffe and H.M.Burte, Plenum Press (1973), p.1597.

[BAN 88] D.Banerjee, C.G.Shelton, B.Ralph and J.C.Williams, Acta Metal., vol 36, n.1, (1988), p.125.

[BAN 93] P.J.Bania, in Proc. 7th Conference on Ti, San Diego, California, Ed.F.H.Froes and I.L.Caplan, TMS, (1993), p. 2227.

[BAR 93] A.Bartz, L.Rothenflue, M.Saqib, R.Omior and H.A.Lipsitt, in Proc. 7th Conference on Ti, San Diego, California, Ed.F.H.Froes and I.L.Caplan, TMS, (1993), p.1291.

[BHA 90] H.K.D.Bhadeshia and J.W.Christian, Metallurgical Transactions, v.21A, n.4, (1990), p.767.

[BHA 95] T.A.Bhaskaran, R.V.Krishnan and S.Ranganathan, Metallurgical Transactions, v.26A, (1995), p.1367.

[BIB 63] M.Bibby and G. Parr, J. Inst.Metals, v.92, (1963), p.341.

[BLA 67_a] M.J.Blackburn and J.C. Williams, Trans.AIME, v.239, (1967), p.287.

[BLA 67_b] M.J.Blackburn, Trans.AIME, v.239, (1967), p.1200.

[BLA 67_c] M.J.Blackburn, Trans.AIME, v.239, (1967), p.660.

[BLA 70] M.J.Blackburn, in Proc. Int. Conf. "The Science, Technology and Applications of Ti", London, Ed .R.I.Jaffe and N.E.Promisel, Pergamon Press, Oxford (1970), p.633.

[BRA 34] W.L.Bragg and E.J.Williams, Proc. R. Soc. A, v.145, (1934), p.699.

[BRA 35] W.L.Bragg and E.J.Williams, Proc. R. Soc. A, v.151, (1935), p.540.

[BUM 52] E.S.Bumps, H.D.Kessler and M.Hansen, J.Metals, (1952), p.609.

[CAH 79] J.W.Cahn and R.Kikuchi, Acta Metall., v.27, (1979), p.1329.

[CAR 86] J.C.Caretti, Acta Metal., v.34, (1986), p.385.

[CHA 93] R.A.Chave, S.Kerry, C.J.Beevers and P.Bowen, in Proc. 7th Conference on Ti, San Diego, California, Ed.F.H.Froes and I.L.Caplan, TMS, (1993), p.1179.

[CHO 88] W.Cho, J.W.Jones, J.E.Allison and W.T.Donlon, in Proc. 6th World Conference on Ti, Cannes, France, (1988), Ed. P.Lacombe, R.Tricot and G.Beranger, Les Editions de Physique, p.187.

[CLA 62] D.Clark, K.S.Jepson and G.I.Lewis, J.Inst.Metals, v.91, (1962–1963), p.197.

[CHR 94] J.W.Christian, Metallurgical Transactions, v.25A, (1994), p.1821.

[CHU 88] L.S.Chumbley, B.C.Muddle and H.L.Fraser, Act.Met., v.36, n.2, (1988), p.299.

[COH 84] M.Cohen, in Proc. Int. Conf. PhaseTransformation in Ferrous Alloys, Philadelphia, USA, TMS/AIME, (1984), p.403.

[COL 79] E.W.Collings, Metallurgical Transactions, v.10A, (1979), p.463.

[COL 84] E.W.Collings, in The Physical Metallurgy of Titanium Alloys, ASM, (1984).

[CRO 55] F.A.Crossley, W.F.Carew and A.D.Kessler, Ti-alloys for Elevated Temperature Application, Armour Research Foundation, WADC Technical Report 53–101, (1955), p.52.

[CRO 57] F.A.Crossley and W.F.Carew, J.Metals, (1957), p.43.

[CRO 58] F.A.Crossley and D.H.Turner, Trans.AIME, (1958), p.60.

[CRO 66] F.A.Crossley, Trans.AIME, v.236, (1966), p.1174.

[CRO 69] F.A.Crossley, Trans.AIME, v.245, (1969), p.1963.

[CUL 59] B.B.Cullity, in Elements of X-Ray Diffraction, Addison-Wesley Publishing Company, Inc; London, 2nd edition, (1959).

[DAH 94] U.Dahmen, Metallurgical Transactions, v.25A, (1994), p.1857.

[DAR 53] L.S.Darken and R.W.Gurry, in Physical Chemistry of Metals, (1953).

[DAV 79] R.Davis, H.M.Flower and D.R.F.West, J.Mat.Science, v.14, (1979), p.712.

[EHR 93] I.Ehrhart and A.Vassel, in Proc. 7th Conference on Ti, San Diego, California, Ed.F.H.Froes and I.L.Caplan, TMS, (1993), p.1009.

[ENC 57] E.Ence and H.Margolin, Trans.AIME, (1957), p.484.

[ENC 61] E.Ence and H.Margolin, Trans.AIME, v.221, (1961), p.151.

[ENO 90] M.Enomoto and MFujita, Metallurgical Transactions, v.21A, n.6, (1990), p.1547.

[ENO 91] M.Enomoto and T.Yoshida, ISIJ Intern., v.31, n.8, (1991), p.767.

[FIS 69] E.S.Fisher, Scrip.Metal., v.3, (1969), p.225.

[FLO 71] H.M.Flower, P.R.Swann and D.R.F.West, Metallurgical Transactions, v.2A, Dec.1971, p.3289.

[FLO 72] H.M.Flower, P.R.Swann and D.R.F.West, J.Mat.Science, v.7, (1972), p.929.

[FLO 74] H.M.Flower, S.D.Henry and D.R.F.West, J.Mat.Science, v.9, (1974), p.57.

[FLO 82] H.M.Flower, R.Davis and D.R.F.West, in Proc. 3rd Int. Conference on Ti, Moscow, Plenum Press, (1982), p.1703.

[FUR 90] T.Furuhara, H.J.Lee, E.S.K.Menon and H.I.Aaronson, Metallurgical Transactions, v.21A, n.6, (1990), p.1627.

[FUR 95] T.Furuhara, K.Wada and T.Maki, Metallurgical Transactions 26A, (1995), p.1971.

[GEH 70] P.C.Gehlen, in Proc. Int. Conf. "The Science, Technology and Applications of Ti", London, Ed .R.I.Jaffe and N.E.Promisel, Pergamon Press, Oxford (1970), p.349.

[GIL 95] T.Gill, MBM, (october 1995), p-56.

[GOL 61] A.J.Goldak and J.G.Parr, Trans.AIME, v.221, (1961), p.639.

[GRO 88] J.P.Gros, B.Sundman and I.Ansara, Scripta Metall., v.22, (1988), p.1587.

[HAL 94] M.G.Hall and H.I.Aaronson, Metallurgical Transactions, v.25A, (1994), p.1923.

[HAN 52] M.Hansen, H.D.Kessler and D.J.McPherson, Trans.ASM, v.44, (1952), p.518.

[HAW 70] E.B.Hawbolt and T.Massalki, Metallurgical Transactions, v.1A, n.8, (1970), p.2315.

[HEI 64] M. von Heimendahl, J.Applied Physics, v.35, n.2, (1964), p.457.

[HEL 92] A.Hellwig, G.Inden and M.Palm, Scripta Met.Mat., v.27, (1992), p.143.

[HEN 79] E.Th.Henig, H.L.Lukas, and G.Petzow, in Proc. Int. Conf. "Calculation of Phase Diagrams and Thermochemistry of Alloy Phases", Ed. Y.A.Chang and J.F.Smith, Wisconsin, AIME, (1979), p.207.

[HIL 79] M.Hillert, in Proc. Int. Conf. "Calculation of Phase Diagrams and Thermochemistry of Alloy Phases", Ed. Y.A.Chang and J.F.Smith, Wisconsin, AIME, (1979), p.1.

[HIL 84] M.Hillert, Metallurgical Transactions, v.15A, n.3, (1984), p.411.

[HIL 86] M.Hillert, in Proc. Int. Conf. "Computer Modeling of Phase Diagram", Toronto, Ed. L.H.Benett, AIME, (1986), p.1.

[HOC 73] M.Hoch, N.C.Birla, S.A.Cole and H.L.Gegel, in "The Development of Heat-Resistant Ti-Alloys", Tech.Report AFML-TR-73-297, Air Force Materials Lab., (1973).

[HOW 94] J.M.Howe, Metallurgical Transactions, v.25A, (1994), p.1917.

[HUA 70] Y.C.Huang, S.Suzuki, H.Kaneko and T.Sato, in Proc.Int.Conf."The Science, Technology and Applications of Ti", London, Ed.R.I.Jaffe and N.E.Promisel, Pergamon Press, Oxford (1970), p.691.

[HUH 90] J.Y.Huh, J.M.Howe and W.C.Johnson, Scripta Metall., v.24, (1990), p.2007.

[HUL 81] D.Hull, "Introduction to Dislocations", Pergamon Press Ed., 2nd Ed., (1975).

[JAN 84] B.Jansson, Thesis, Royal Institute of Technology, Stockholm, Sweden, 1984.

[JEP 70] K.S.Jepson, A.R.G.Brown and J.A.Gray, in Proc.Int.Conf."The Science, Technology and Applications of Ti", London, Ed.R.I.Jaffe and N.E.Promisel, Pergamon Press, Oxford (1970), p.677.

[JOU 87] C.Jourdan, J.Gastaldi and G.Grange, ActaMetal., v.36, (1987), p.2979.

[JOU 89] C.Jourdan, J.Gastaldi and G.Grange, Phase Transitions, v.14, (1989), p.201.

[JOU 91] C.Jourdan, J.Gastaldi, P.Marzo and G.Grange, J.Mat.Scie., v.26, (1991), p.4355.

[KAT 92] U.R.Kattner, J.-C.Lin and Y.A.Chang, Metallurgical Transactions, v.23A, (1992), p.2081.

[KAU 73] L.Kaufman and H.Nesor, in Proc. 2nd Int. Conf. "Titanium Science and Technology", Massachusets, USA, Ed.R.I.Jaffe and H.M.Burte, Plenum Press (1973), p.773.

[KAU 79] L.Kaufman, Calphad, v.3, n.1, (1979), p.45.

[KAU 92] L.Kaufman and M.Hillert, in "Martensite", edited by G.B.Olson and W.S.Owen, ASM international, USA, (1992), p. 41-58.

[KEL 75] P.M.Kelly, A.Jostsons, R.G.Blake and J.G.Napier, Phy.Stat.Sol.(a), v.31, p.771, (1975).

[KER 84] R.J.Kerans, Metallurgical Transactions, v.15A, (1984), p.1721.

[KHA 88] A.Khataee, H.M.Flower and D.R.F.West, in Proc. 6th World Conference on Ti, Cannes, France, (1988), Ed. P.Lacombe, R.Tricot and G.Beranger, Les Editions de Physique, p.991.

[KIK 51] R.Kikuchi, Phys.Rev., v.81, (1951), p.988.

[KIK 74] R.Kikuchi and C.M.vanBaal, Scripta Metall, v.8, (1974), p.425.

[KOR 70] I.I.Korlinov, in Proc. Int. Conf. "The Science, Technology and Applications of Ti", London, Ed.R.I.Jaffe and N.E.Promisel, Pergamon Press, Oxford (1970), p.407.

[KOT 72] P.S.Kotval and R.W.Calder, Metallurgical Transactions, v.3A, 1972, p.1308.

[LEE 88] H.Lee and H.I.Aaronson, Acta Metal., (1988), v.36, n-3, p.787.

[LEE 88] H.J.Lee and H.I.Aaronson, J.Mat.Science, v.23, (1988), p.150.

[LIP 80] H.A.Lipsitt, D.Shechtman and R.E.Schafrik, Metallurgical Transactions, v.11A, (1980), p.1369.

[LIP 85] H.A.Lipsitt, Mat.Res.Soc.Symp.Proc., v.39, (1984), p.351.

[LUK 77] H.L.Lukas, E.-Th.Henig, B.Zimmermann, CALPHAD, (1977), v.1, p 225.

[LUK 82] H.L.Lukas, J.Weiss and E.-Th.Henig, CALPHAD, (1982), v.6, p.229.

[LUP 83] C.H.P.Lupis, in "Chemical Thermodynamics of Materials", (1983), Elsevier Science Publishing Co.

[LUT 70] G.Lütjering and S.Weissman, Act.Met., v.18, (1970), p.785.

[MAN 94] S.H.Manesh and H.M.Flower, Mat.Sc.Tech., (1994), n.9. p.674

[MAR 68] H.Margolin and H.Portisch, Trans.AIME, v.242, (1968), p.1901.

[MAR 77] H.Margolin, E.Levine and M.Young, Metallurgical Transactions, v.8A, (1977), p.373.

[MAR 80] P.L.Martin, H.A.Lipsitt, N.T.Nuhfer and J.C.Williams, in Proc. 4th Conference on Ti, Kyoto, Japan, Ed.H.Kimura and O.Izumi, The Metallurgical Society of AIME, (1980), p.1246.

[MAS 84] T.B.Massalki, Metallurgical Transactions, v.15A, n.3, (1984), p.421.

[McC 88] C.McCullough, J.J.Valencia, H.Mateos, C.G.Levi and R.Mehrabian, Scrip.Met., v.22, (1987),p.1131.

[McC 89] C.McCullough, J.J.Valencia, C.G.Levi and R.Mehrabian, Act.Met., v.37, n.5, (1989), p.1321.

[McQ 63] M.K.McQuillan, Metal.Reviews, v.8, n.29, (1963), p.41.

[MEN 87] E.S.K.Menon and H.I.Aaronson, Acta Metal., v.35, n.3, (1987), p.549.

[MEN 88] E.S.K.Menon, M.R.Plichta and H.I.Aaronson, Act.Met., v.36, n.2, (1988), p.321

[MIS 89] J.C.Mishurda, J.C.Lin, Y.A.Chang and J.H.Perepezko, Mat. Res. Soc. Symp. Proc., v.133, (1989), p.57.

[MUR 87] J.L.Murray, Binary Phase Diagrams of Ti Alloys, ASM, (1987); p.12-24 (Al-Ti) , p.188-194 (Nb-Ti), p. 289-294 (Si-Ti) and p.340-345 (Ti-Zr); .

[MUR 88] J.L.Murray, Metallurgical Transactions, v.19A, (1988), p.243.

[NIC 73] R.G.Nichols, H.M.Flower and D.R.F.West, J.Mat.Science, v.8, (1973), 261.

[NIS 78] Z.Nishiyama, in Martensitic Transformation, Edited by M.E.Fine, M.Meshii and C.M.Wayman, Academic Press, London, (1978).

[NUR 95] M.Nurse, MBM, (october 1995), p.51

[OGD 51] H.R.Ogden, D.J.Maykuth, W.L.Finlay and R.I.Jaffee, J.Metals, (1951), p.1150.

[OKA 91] H.Okamoto, Journal of Phase Equilibria, v.12, n.6, (1991), p.623.

[ONO 94] H.Onodera, T.Abe and T.Yokokawa, Acta Metal., v.42, n.3, (1994), p.887.

[OUC 80] K.Ouchi; Y.Iijima and K.Hirano, in Proc. 4th Conference on Ti, Kyoto, Japan, Ed.H.Kimura and O.Izumi, The Metallurgical Society of AIME, (1980), p.559.

[OWE 92] M.Grujicic, H.C.Ling, D.M.Haezebrouck and W.S.Owen, in Martensite, edited by G.B.Olson and W.S.Owen, ASM international, USA, (1992), p. 175.

[PAJ 89] M.Pajunen, J.Kivilahti and J.Miettiness, in Proc. 1st Eur. Conf. on Advanced Materials and Processes, Ed. H.E.Exner and V.Schumacher, Deutsche Gesellschaft fur Metallkunde E.V., v.2, (1989), p.1055.

[PEA 95] D.Peacock, Ti World, (september 1995), p-28.

[PEA 95b] D.Peacock, personal communication.

[PEL 86] A.D.Pelton, in Proc. Int. Conf. "Computer Modeling of Phase Diagram", Toronto, Ed. L.H.Benett, AIME, (1986), p.19.

[PEN 93] R.Penelle and C.Servant, in Proc. 7th Conference on Ti, San Diego, California, Ed.F.H.Froes and I.L.Caplan, TMS, (1993), p.27.

[PER 84] J.H.Perepezko, Metallurgical Transactions, v.15A, n.3, (1984), p.437.

[PER 93] J.H.Perepezko and J.C.Mishurda, in Proc. 7th Conference on Ti, San Diego, California, Ed.F.H.Froes and I.L.Caplan, TMS, (1993), p.563.

[PET 95] M.Peters, Ti World, (september 1995), p-15.

[PLI 77] M.R.Plitcha, J.C.Williams and H.I.Aaronson, Metallurgical Transactions, v.8A, (1977), p.1885.

[PLI 78] M.R.Plitcha and H.I.Aaronson, Act.Met., v.26, (1978), p.1293.

[PLI 79] M.R.Plitcha, H.I.Aaronson, J.C.Williams and G.W.Franti, Scripta Metal., v.13, (1979), p.407.

[PLI 80] M.R.Plitcha, J.H.Perepezko, H.I.Aaronson and W.F.Lange, Acta Metal., v.28, (1980), p.1031.

[PLI 84] M.R.Plitcha, W.A.T.Clark and H.I.Aaronson, Metal.Trans., v.15A, n.3, (1984), p.427.

[POR 81] D.A.Porter and K.E.Easterling, in "Phase Transformations in Metals and Alloys", Chapman & Hall Ed., 1st ed., (1981).

[PRO 93] G.Proske, G.Lütjering, J.Albrecht, M.A.Däubler and D.Helm, in Proc. 7th Conference on Ti, San Diego, California, Ed.F.H.Froes and I.L.Caplan, TMS, (1993), p.1187.

[PUR 84] G.R.Purdy and M.Hillert, Acta Metal., v.32, n.6, (1984), p.823.

[RAM 65] A.Raman and K.Schubert, Zeit.Metallkunde, v.56, n.1, (1965), p.44.

[REE 73] R.E.Reed–Hill, in "Physical Metallurgy Principles", D.Van Nostrand Ed., 2nd ed., (1973).

[ROS 65] W.Roßteutscher and K.Schubert, Zeit.Metallkunde., v.56, n.11, (1965), p.813.

[RUC 90] M.Ruch and D.Arias, Scripta Metal., v.24, (1990), p.1577.

[SAL 96] N.H.Salpadoru and H.M.Flower, Metallurgical Transactions, v.26A, n.2, (1995), p-243.

[SAS 77] S.M.L.Sastry and H.A.Lipsitt, Metallurgical Transactions, v.8A, (1977), p.1543.

[SAT 60] T.Sato and Y.C.Huang, Trans.Jap.Inst.Metals, v.1, (1960), p.22.

[SAU 59] A.Saulnier and M.Croutzeilles, Mem.Sc.Rev.Met., LVI, n.4, (1959), p.379.

[SCA 84] G.K.Scarr, J.C.Williams, S.Ankem, H.B.Bomberger, in Proc. 5th Conf. on Titanium, Munich, FRG, (1984)., Ed. G.Lütjering, U.Zwicker and W.Bunk, Deutsche Gesellschaft fur Metallkunde E.V., p.1475.

[SCH 62] Von O.Schob, H.Nowotny and F.Benesovsky, Plan.Berichte fur Pulvermetallurgie, v.10, (1962), p.65.

[SHU 84] R.D.Shull, A.J.McAlister and R.C.Reno, in Proc. 5th Conf. on Titanium, Munich, FRG, (1984) , Ed. G.Lütjering, U.Zwicker and W.Bunk, Deutsche Gesellschaft fur Metallkunde E.V., p.1459.

[SMA 85] R.E.Smallman, in "Modern Physical Metallurgy", 4th edition, (1985), Butterworths & Co Publishers Ltd.

[SOU 90] M.EsSouni, P.A.Beaven and R.Wagner, Sript.Met., v.24, (1990), p.2175.

[STR 79] T.R.Strobridge, J.C.Moulder and F.Clarke, in "Titanium Combustion in Turbine Engines", FAA-RD-79-51, Federal Aviation Administration, Washington DC, (1979).

[SUN 81] B.Sundam and J.Agren, J.Phys.Chem.Solids, v,42, (1981), p-297.

[SUN 85] B.Sundman, B.Jansson and J.-O.Andersson, CALPHAD, 9, (1985), p.153.

[SUN 90] B.Sundman, Anales de Fisica, series B, v.86, 1990, p.69.

[SUN 95] B.Sundman, personal communication, bosse@prima.met.kth.se; (1995).

[SVE 70] V.N.Svechnikov, Yu.A.Kocherzhisky, L.M.Yupko, O.G.Kulik and E.A.Shishkin, Dokl.Akad.Navk.SSSR, v.193, n.2, (1970), p.393.

[SWA 81] L.J.Swartzendruber, L.H.Bennett, L.K.Ives and D.Shull, Mat.Sci.Eng., v.51, (1981), p.1.

[TER 82] S.Terauchi, H.Matsumoto, T.Sugimoto and K.Kamel, in Proc. 3rd Int. Conference on Ti, Moscow, Plenum Press, (1982), p.1335.

[THO 93] M.Thomas, S.Naka and T.Khan, in Proc. 7th Conference on Ti, San Diego, California, Ed.F.H.Froes and I.L.Caplan, TMS, (1993), p. 1243.

[TSU 66] T.Tsujimoto and M.Adachi, J.Inst.Metals, v.94, (1966), p.358.

[VAL 87] J.J.Valencia, C.McCullough, C.G.Levi and R.Mehrabian, Script.Met., v.21, (1987), p.1341.

[VAL 89] J.J.Valencia, C.McCullough, C.G.Levi and R.Mehrabian, Act.Met., v.37, n.9, (1989), p.2517.

[VAH 89] C.Vahlas, P.Y.Chevalier and E.Blanquet, CALPHAD, v.13, n.3, (1989), p.273.

[VAN 54] R.J.Van Thyne and H.D.Kessler, J.Metals, (1954), p.193.

[VAN 70] L.H. Van Vlack, in Princípio de Ciência dos Materiais, Ed. Edgard Blücher LTDA, São Paulo, 1970,.

[VER 93] R.Verma and A.K.Ghosh, in Proc. 7th Conference on Ti, San Diego, California, Ed.F.H.Froes and I.L.Caplan, TMS, (1993), p.995.

[WAN92] P.Wang, G.B.Viswanathan and V.K.Vasudevan, Metallurgical Transactions, v.23A, (1992), p.690.

[WAR 93] C.H.Ward, International Materials Review, v.38, n.2, (1993), p-79.

[WAY 94] C.M.Wayman, Metallurgical Transactions, v.25A, (1994), p.1787.

[WIL 70] J.C.Williams, B.S.Hickman and D.H.Leslie, Metallurgical Transactions, v.2, (1971), p.477.

[WIL 72] J.C.Williams, in Proc. 2nd Int. Conf. "Titanium Science and Technology", Massachusets, USA, Ed. R.I.Jaffe and H.M.Burte, Plenum Press (1973), p.1433.

[WIL 73] L.A.Willey and H.Margolin, in Metals Handbook, 8th Ed., v.8, ASM, Metals Park, (1973), p.264.

[WIL 85] J.C.Williams, in Titanium Technology: Present Status and Future Trends, Ed. F.H.Froes, D.Eylon and H.B.Bomberger, Publishe by The Titanium development Association, 1975, p. 75.

[WIL 79] E.A.Wilson, in Phase Transformations, Institute of Metals, London, v.2, (1979), p.67.

[WIN 73] M.R.Winstone, R.D.Rawlings and D.R.F.West, J.Less Comm.Met., v.31, (1973), p.143.

[WIN 75] M.R.Winstone, R.D.Rawlings and D.R.F.West, J.Less Comm.Met., v.39, (1975), p.205.

[WU 88] J.S.Wu, P.A.Beaven, R.Wagner, Ch.Hartig and J.Seeger, in "High Temperature Ordered Intermetallic Alloys III", Ed. C.T.Liu, A.I.Taub, N.S.Stollof and C.C.Koch, MRS (1989), p.761.

[WU 90] J.S.Wu, P.A.Beaven and R.Wagner, Script.Met., v.24, (1990), p.207.

[YAN 82] W.J.S.Yang, Metallurgical Transactions, v.13A, (1982), p.324.

[ZHA 91] Z.Zhang and H.M.Flower, Mat.Sci.Tech., v.7, n.9, (1991), p.812.